DEVELOPMENT OF A PLASMA FACILITY AND SPECTROGRAPHIC DETERMINATION OF PLASMA TEMPERATURES

By

DONALD ROBERT HAWORTH

Bachelor of Science in Mechanical Engineering
Purdue University
Lafayette, Indiana
1952

Master of Science in Mechanical Engineering
Purdue University
Lafayette, Indiana
1955

Submitted to the Faculty of the Graduate School of
the Oklahoma State University
in partial fulfillment of the requirements
for the degree of
DOCTOR OF PHILOSOPHY
May, 1961

DEVELOPMENT OF A PLASMA FACILITY AND SPECTROGRAPHIC

DETERMINATION OF PLASMA TEMPERATURES

Thesis Approved:

Milan K. Tomanovic

Thesis Adviser

J. W. Gryder

L. K. Norton

E. K. McLachlan

Harold Hinton

Dean of the Graduate School

ACKNOWLEDGEMENT

The author wishes to express his gratitude to the many persons and institutions for their moral, educational, and physical support during the conduct of this thesis work.

The financial support, without which this work could not have been undertaken, was provided by the National Science Foundation. The material presented in Chapters II, III, and IV of this thesis was taken primarily from the first annual report, "The Development of a Plasma Facility and a Survey of Spectroscopic Methods for Plasma Temperature Determination," submitted to the National Science Foundation. Acknowledgment is also given to the Chance Vought Research Center, Dallas, Texas, for permission to utilize their plasma facility in taking spectrographic data for plasma temperature calculations.

The general guidance of Dr. J. H. Boggs, Head of the School of Mechanical Engineering, and the individual instructive assistance of Dr. M. K. Jovanovic, Plasma Facility Project Leader, contributed significantly to the success of this work. The day to day help on all phases of the work by Mr. E. Pohlmann, a doctoral graduate student, was greatly appreciated.

The construction and operational problems were lightened considerably by the suggestions offered by Professor B. S. Davenport, Laboratory Supervisor, and by the services of J. A. McCandless and G. M. Cooper, Laboratory Technicians.

To my wife, Mimi, I give special thanks for the time she has spent raising the family without a husband and father.

TABLE OF CONTENTS

Chapter		Page
I.	INTRODUCTION	1
II.	PREVIOUS INVESTIGATIONS	4
	The Abel Integral Equation	9
	Saha Equation	17
	Spectral Line Emission	31
	The Broadening of the Spectral Lines	34
	Stark Effect Line Broadening	39
III.	METHODS AND PREVIOUS APPLICATIONS OF PLASMA TEMPERATURE DETERMINATION BY SPECTROSCOPIC ANALYSIS	41
	Relative Line Intensity Method	41
	Stark Broadening Method	48
	Recent Developments in Spectral Line Broadening Theory	62
IV.	DESIGN OF THE PLASMA FACILITY AND AUXILIARY EQUIPMENT	66
	Plasma Generator - Expansion Nozzle Assembly	66
	DC Power Supply and Controls	84
	Gas Supply and Controls	100
	Vacuum System	103
	Control Instrumentation	110
	Spectroscopic Equipment	115
V.	EXPERIMENTAL METHODS AND OBSERVATIONS	121
	Operational Procedure	121
	Operational Data Record	130
	Spectrographic Data Record	131
VI.	SPECTROGRAPHIC DETERMINATION OF PLASMA TEMPERATURES	137
	Emulsion Calibration	141
	Relative Intensities of Broadened Spectral Lines	144
	Transformation of $I_x(\Delta\lambda)$ to $i_r(\Delta\lambda)$	157
	Calculation of Plasma Temperature	164

Chapter Page

VII. RESULTS AND DISCUSSION 179

VIII. CONCLUSIONS AND RECOMMENDATIONS. 186

BIBLIOGRAPHY. 189

APPENDIX A. 192

APPENDIX B. 196

APPENDIX C. 219

APPENDIX D. 224

APPENDIX E. 228

LIST OF FIGURES

Figure		Page
1.	The Disc-Shaped Plasma Region	8
2.	Concentric Layers and Parallel Slices of a Disc-Shaped Plasma Region	13
3.	Definition of the Area $\triangle A'_{j,k}$	14
4.	Line Intensity Distribution Determined by the Densitometer.	16
5.	Intensity Profile for a Symmetrically Broadened Spectral Line	35
6.	The Functions $i^*_{T,p}$ for the Plasma Constituents I, II, III (24)	47
7.	Equilibrium Concentrations (n_i) for a Gerdien Arc Plasma (19)	49
8.	Distribution Function $W(\beta)$ Calculated by J. Holtsmark (26)(15)	52
9.	Theoretical Profile of the Broadened Spectral Line (3)	57
10.	Theoretical Intensity Ratio of the Broadened Spectral Line (3).	58
11.	Normal Field Strength versus Temperature (3).	60
12.	Plasma Facility - Plan View	67
13.	Plasma Generator - Expansion Nozzle Assembly.	72
14.	Comparison of McQuiston Nozzle With New Nozzle. . . .	75
15.	Plasma Starter Assembly	83
16.	Power Supply System Schematic Diagram	91
17.	Starting Resistance Schematic Diagram	95

Figure		Page
18.	DC Power Supply Volt-Ampere Characteristics I	101
19.	DC Power Supply Volt-Ampere Characteristics II. . . .	102
20.	Gas Supply System Schematic Diagram	104
21.	Cooling Water System Schematic Diagram.	111
22.	Instrument and Control Panel Schematic Diagram. . . .	116
23.	Optical System Schematic Diagram.	118
24.	Argon Flowmeter Calibration	126
25.	Hydrogen Flowmeter Calibration.	128
26.	Cooling Water Flowmeter Calibrations.	129
27.	Emulsion Calibration - Plate No. 12-19-60A.	145
28a-d.	Densitometer Reading versus Wave Length	150
29a-c.	Densitometer Reading versus Vertical Location	154
30a-b.	Relative Intensity $I_x(\Delta\lambda)$ for Exposure No. 4, H_γ .	160
31a-d.	Theoretical Relative Intensity Ratio for H_γ (38) . .	167
32.	Relative Intensity versus Wave Length	172
33.	Electron Concentration for an Argon Plasma.	175
34.	Normal Field Strength E_o for an Argon Plasma.	176
35.	Argon Plasma Jet Temperature Distribution I	183
36.	Argon Plasma Jet Temperature Distribution II.	184
37a-b.	Relative Intensity $I_x(\Delta\lambda)$ for Exposure No. 2, H_γ .	203
38a-b.	Relative Intensity $I_x(\Delta\lambda)$ for Exposure No. 3, H_γ .	205
39a-b.	Relative Intensity $I_x(\Delta\lambda)$ for Exposure No. 4, H_β .	207
40a-d.	Theoretical Relative Intensity Ratio for H_β (38). . .	215

LIST OF TABLES

Table		Page
I.	$\Delta A_{j,k}$ Coefficients for Calculating Radial Intensity Distribution (2)	18
II.	Temperature Instrumentation Locations	114
III.	Pressure Instrumentation Locations	114
IV.	OSU Plasma Facility Control Panel Data Sheet	132
V.	OSU Plasma Facility Spectrograph Data Sheet	135
VI.	Chance Vought Research Center Plasma Facility Data	138
VII.	Chance Vought Research Center Spectrograph Data	140
VIII.	Seven-Step Filter Calibration Data	142
IX.	Densitometer Readings - Emulsion Calibration	144
X.	Densitometer Readings - Exposure No. 4, H_γ	148
XI.	Corrected Densitometer Readings - Exposure No. 4, H_γ	158
XII.	Relative Intensity $I_x(\Delta\lambda)$ - Exposure No. 4, H_γ	159
XIII.	Computer Program Input Data $I_x(\Delta\lambda)$ - Exposure No. 4, H_γ	163
XIV.	Computer Program Output Data $i_r(\Delta\lambda)$ - Exposure No. 4, H_γ	165
XV.	Plasma Temperature Calculation - Exposure No. 4, H_γ for a Jet Radius of 6.13 mm	173
XVI.	OSU Plasma Facility Results	180
XVII.	CVRC Plasma Jet Temperatures	182
XVIII.	Densitometer Readings - Exposure No. 2, H_γ	193

Table		Page
XIX.	Densitometer Readings - Exposure No. 3, H_γ	194
XX.	Densitometer Readings - Exposure No. 4, H_β	195
XXI.	Corrected Densitometer Readings - Exposure No. 2, H_γ	197
XXII.	Corrected Densitometer Readings - Exposure No. 3, H_γ	198
XXIII.	Corrected Densitometer Readings - Exposure No. 4, H_β	199
XXIV.	Relative Intensity $I_x(\Delta\lambda)$ - Exposure No. 2, H_γ	200
XXV.	Relative Intensity $I_x(\Delta\lambda)$ - Exposure No. 3, H_γ	201
XXVI.	Relative Intensity $I_x(\Delta\lambda)$ - Exposure No. 4, H_β	202
XXVII.	Computer Program Input Data $I_x(\Delta\lambda)$ - Exposure No. 2, H_γ	209
XXVIII.	Computer Program Input Data $I_x(\Delta\lambda)$ - Exposure No. 3 H_γ	210
XXIX.	Computer Program Input Data $I_x(\Delta\lambda)$ - Exposure No. 4, H_β	211
XXX.	Computer Program Output Data $i_r(\Delta\lambda)$ - Exposure No. 2, H_γ	212
XXXI.	Computer Program Output Data $i_r(\Delta\lambda)$ - Exposure No. 3, H_γ	213
XXXII.	Computer Program Output Data $i_r(\Delta\lambda)$ - Exposure No. 4, H_β	214
XXXIII.	Plasma Temperature Calculation - Exposure No. 2, H_γ	220
XXXIV.	Plasma Temperature Calculation - Exposure No. 3, H_γ	221
XXXV.	Plasma Temperature Calculation - Exposure No. 4, H_γ	222
XXXVI.	Plasma Temperature Calculation - Exposure No. 4, H_β	223

LIST OF PLATES

Plate		Page
I.	Plasma Facility - Control Area	68
II.	Plasma Facility - Test Area	69
III.	Plasma Facility - Vacuum Tank	70
IV.	Plasma Facility - Vacuum Pump	71
V.	Plasma Generator - Expansion Nozzle Assembly Installed in Test Section	81
VI.	Starting Resistance Unit	94
VII.	Ballast Resistance Unit and Cooling Fan	97
VIII.	Power Supply Motor-Generator	99
IX.	Densitometer	120
X.	OSU Plasma Facility Spectrographic Record Plate No. 3-22-61A	136
XI.	CVRC Plasma Facility Spectrographic Record Plate No. 12-19-60A	139

CHAPTER I

INTRODUCTION

Flight at hypersonic velocities and high altitudes creates low pressure, high temperature gas fields immediately behind strong shock waves and in the boundary layers near the leading edges of the aircraft or missile. The conversion of directed kinetic energy of the aircraft into internal energy of the air flowing over the vehicle in these areas causes dissociation and ionization. Thus, the gas field is composed of an electrically neutral mixture of molecules, free atoms, electrons, and ions. The name used to identify such a mixture is "plasma."

The presence of this plasma flowing over the vehicle surface has presented challenging problems to the aircraft designer. The prediction of lift and drag forces by analysis of the dynamics of the flow is restricted by a lack of experimental data on the physical transport properties of the plasma. The calculation of the transfer of energy from the plasma to the surface is complicated by the prescence of a multicomponent fluid with unknown thermal properties, by the distributed energy release resulting from de-ionization and re-association, by the surface material effect on these recombination rates, and by the radiation emission and absorption characteristics of the highly excited plasma. An allied problem for both aerodynamics and

aerothermodynamics is the control of drag and energy transfer by subjecting the plasma flow, which is electrically conductive because of ions and electrons in the field, to a properly oriented magnetic force field which would favorably deflect the flow to reduce skin friction effects.

The airframe design problems discussed above are caused by the plasma environment resulting from a desired flight capability. There are other areas where a plasma field may be desired to investigate a different set of problems. For example, electromagnetically accelerated plasma jets are being studied for space propulsion systems. Also plasmas are providing the environment for high temperature physics research associated with controlled thermonuclear fusion.

The solutions to these problems and others involving high temperature, ionized and dissociated gas fields require basic research studies of the physical and thermal properties of plasmas. A versatile plasma facility is necessary to provide controlled plasma fields capable of simulating the desired range of gas pressures, energy levels, size, flow velocities, and gas composition.

The purpose of the research program reported in this thesis was the development of a basic plasma test facility readily adaptable for research on the physical and transport properties of plasma fields, for studying the flow characteristics of a plasma with and without applied magnetic fields, and for providing simulated environments for material and design evaluation. Fabrication and installation of the facility equipment was planned to assure accessibility to replaceable

parts and instrumentation. Controls and instrumentation necessary for the operation of the facility was provided. Spectroscopic instrumentation was installed for the analysis of the internal structure of the plasma field, and the application of spectrographic analysis for the determination of plasma temperatures was further developed.

CHAPTER II

PREVIOUS INVESTIGATIONS

A Plasma facility is recognized today as a necessary research device for the investigation of the nature of high temperature, partially ionized gases and the problems of hypersonic flight, space propulsion and other areas as presented in Chapter I. The design of such a facility depends on the exact type of research study to be conducted. The purpose for the establishment of the Plasma Facility at Oklahoma State University was to provide a versatile research complex that could be adapted to the study of many of these problems.

The general configuration of the Plasma Facility was based on a similar system that was installed at the Chance Vought Research Center in Dallas, Texas. The complete system consists of a plasma generator and expansion nozzle, DC power supply, vacuum system, gas supply system, control and instrumentation components, and spectroscopic equipment. A detailed description of each of these components of the Plasma Facility is given in Chapter IV.

The Plasma Facility was designed around an existing plasma generator and a controlled DC power supply system that was available in the Mechanical Engineering Laboratory at Oklahoma State University. The plasma generator was designed, constructed and tested by Mr. F. McQuiston (1) in the spring and summer of 1959. A summary of the

early development of the high intensity arc plasma generator and the discussion of recent designs have been presented in Mr. McQuiston's thesis (1). Also included in his thesis is the detailed specification of the plasma generator. A summary of the design particulars for this plasma generator is given in Chapter IV.

The DC power supply system consisted of a 165-kva DC generator driven by a 200-hp synchronous AC motor. The voltage and amperage ratings of the generator were 250 volts and 700 amperes, respectively. Therefore, this system was capable of supplying up to 700 amperes at whatever arc voltage resulted due to the physical configuration of the anode and cathode. Operation of the existing generator using argon at nearly atmospheric pressure resulted in arc voltages from 30-40 volts. (1). With argon, higher arc voltages would be obtained by increasing the argon pressure. Also, higher arc voltages are required with nitrogen as the working fluid, using the same physical configuration.

The existing plasma generator had been operated at power inputs varying from 3 to 7 kw. (1). Under these conditions, more than adequate cooling was available, and no rapid eroding of any parts was detected even after continued operation for time periods up to two hours. Based on this information, it was estimated that the existing generator could be operated at power levels up to 20 kw or even higher. It was decided that the present generator would be used to gain additional experience for a future design for even higher power levels.

In order to provide a test environment for analytical work and to minimize the problems of making measurements on very small test areas,

an expansion of the argon after passing through the arc was required. To keep from working with very high pressures in the arc area, which increases the difficulty in stabilizing the arc; to attain the highest possible energy level with the available DC power supply system by keeping the gas flow rate low; and to provide a moderately high velocity jet (4000-6000 ft/sec) for possible material ablation testing, a converging-diverging nozzle, designed to discharge into a vacuum system, was added to the existing generator.

The inlet pressure for the vacuum pump was selected on the basis of several factors. Very low pressures (below 0.1 psia) were undesirable because of the large volume that would have to be handled to match the design mass flow rates. Also, the low densities that would be encountered in the test area would tend to enhance the possibility of thermodynamic non-equilibrium conditions and would therefore make the spectrographic analysis extremely difficult. Pressures higher than 5 psia at the converging-diverging nozzle outlet would result in a small jet diameter for the design flow rate and would require plasma generator chamber pressures over 100 psia to produce jet velocities of 4000-6000 feet per second.

The instrumentation requirements for control and operation of the plasma facility were essentially the same as those used in the initial operation of the plasma generator. These are described in detail in Reference 1. A control unit was required to permit operation of the DC power supply system from the plasma facility control panel. All of the instrumentation is described in Chapter IV.

Spectroscopic instrumentation was selected to provide high quality

equipment for the evaluation of the plasma emission characteristics. The requirements for this equipment were established by discussions with other organizations currently working in the plasma research field. Also, The Symposium on Optical Spectrometric Measurement of High Temperatures held at the University of Chicago in March, 1960, was attended and was particularly helpful in establishing the spectroscopic measurement requirements. The work done by Dr. W. J. Pearce of the General Electric Company (2), Dr. P. J. Dickerman of Midway Laboratories (3), and the Chance Vought Research Center was reviewed to determine the dispersion and resolution requirements for the spectrograph and the microdensitometer.

A literature investigation was made of some of the methods which have been used in the spectroscopic determination of temperature distributions in a cross section of a plasma jet. The observed cross section is perpendicular to the axis of the jet; the spectrograph receives the radiation emitted parallel to the y-direction from a disc-shaped, narrow plasma region of radius r_o, bounded by two planes at z and $z + \triangle z$, (Figure 1). A thorough report of this investigation was presented in Reference 4. The results of this investigation which relate particularly to the research work of this thesis are given in what follows.

The temperature distribution analysis for a cross section of the plasma jet is based on three assumptions. They are (1) the jet is axisymmetric, (2) the absorption of radiation within the plasma is negligible, and (3) local temperature equilibrium exists within the plasma, i.e., the energy distribution among individual particles

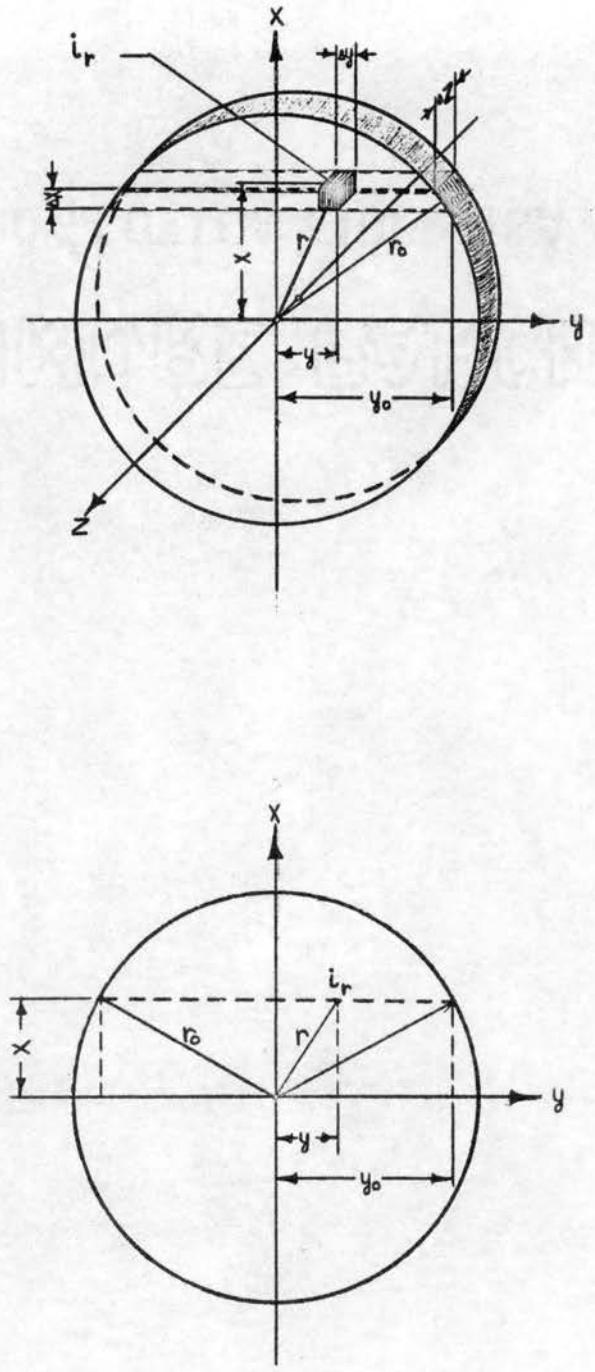

Figure 1. The Disc-Shaped Plasma Region

follows the Maxwell-Boltzmann Law. The first two assumptions combined with the concepts of electromagnetic radiation are the foundation of the first fundamental relationship to be used in the spectroscopic determination of plasma temperatures. This relation is referred to as the "Abel integral equation" because of its similarity to an integral equation solved by N. H. Abel in 1826 (5).

The Abel Integral Equation

Consider the radiation emitted from a plasma region, bounded by two cross sections; the distance between the cross sections is $\triangle z$. The radiation emitted in the y-direction is observed by the spectrograph; therefore, it is convenient to divide the disc-shaped plasma region into a number of horizontal columns by cutting it with horizontal planes parallel to the jet axis. The radiation emitted by a column, bounded by the planes z, $z + \triangle z$ and x, $x + \triangle x$ reaches the spectrograph and produces a part of a spectral line of intensity I_x. The spectroscopically observed line intensity, I_x, is proportional to the radiation emitted by a column, at a distance x from the jet axis, per unit projected area in the y-direction. If one divides a horizontal column into small volume elements, bounded by the planes x, $x + \triangle x$; y, $y + \triangle y$ and z, $z + \triangle z$, the radiation emitted by the column will be equal to the sum of radiations emitted by individual volume elements. Let u_r represent the radiation density (energy per unit volume) in the volume element $\triangle x \triangle y \triangle z$; the spectral line intensity produced by the radiation emitted by the volume element is

then proportional to

$$\frac{u_r \cdot \triangle x \triangle y \triangle z}{\triangle x \triangle z} = u_r \cdot \triangle y$$

or $$\triangle I_x = c' \cdot u_r \cdot \triangle y$$

where c' is a proportionality constant.

Summing up over all volume elements, one has

$$\sum \triangle I_x = I_x = \sum c' \cdot u_r \cdot \triangle y$$

When the size of the volume elements decreases, approaching zero in the limit, the preceding equation becomes

$$I_x = \int_{y=-y_o}^{y=+y_o} c' \cdot u_r \cdot dy \qquad (1)$$

With $r = \sqrt{x^2+y^2}$, $y_o = \sqrt{r_o^2-x^2}$ and due to the symmetrical distribution of the volume elements, one obtains

$$I_x = 2 \int_{y=o}^{y=\sqrt{r_o^2-x^2}} c' \cdot u_r \, dy \qquad (2)$$

The radiation density u_r can be eliminated by substituting for it the "specific normal intensity of radiation" i_r, where i_r represents the energy emitted perpendicular to the emitting surface in unit time, in unit solid angle, per unit area of the radiating surface. The two quantities, u_r and i_r, are related by the expression

$$i_r = \frac{c}{4\pi} u_r \,,$$

as shown for instance in the textbook by Hercus (6); in the above expression c is the speed of light.

The intensity of the spectral line is now

$$I_x = 2 \int_{y=o}^{y=\sqrt{r_o^2-x^2}} c' \cdot \frac{4\pi}{c} \cdot i_r \, dy$$

In further discussions, only ratios of spectral line intensities are of importance--relative intensities; therefore, the constant factor $4\pi\ c'/c$ will cancel, and one may consider the simplified expression

$$I_x = 2 \int_{y=o}^{y=\sqrt{r_o^2-x^2}} i_r \cdot dy \qquad (3)$$

Since $y = \sqrt{r^2-x^2}$ and x = const. for a column at distance x from the jet axis, one has

$$dy = \frac{r\,dr}{\sqrt{r^2 - x^2}}$$

Taking into consideration the changes of the limits of integration, one obtains finally, for the relative intensity of a spectral line, the following relation:

$$I_x = 2 \int_{r=x}^{r=r_o} \frac{r \cdot i_r}{\sqrt{r^2-x^2}} \, dr \qquad (4)$$

Relation (4) is an integral equation which can be transformed into an Abel integral equation of the general type,

$$I_x = \int_a^x \frac{i_r dr}{(x-r)^\lambda}, \quad 0<\lambda<1. \qquad (5)$$

According to G. Hamel (8), Abel was the first to solve an integral

equation when he was confronted with an equation of the same form as Equation (5) in his studies of the "tautochrone" problem.

According to H. Hörmann (9), Equation (4), which is of particular interest here, has as its solution

$$i_r = -\frac{1}{\pi} \int_{x=r}^{x=r_o} \frac{I'_x \, dx}{\sqrt{x^2-r^2}} \quad , \tag{6}$$

where

$$I'_x \equiv \frac{d}{dx} (I_x).$$

Unfortunately, the solution (6) generally cannot be expressed in a closed analytical form. It can be solved, however, by using graphical and numerical methods.

A direct numerical approach for determining the specific normal intensity distribution, i_r, was developed by W. J. Pearce (2); and this method is described briefly in the following lines.

The continuous radial intensity distribution is assumed to be stepwise, having constant values within an annular region between radii r_k and r_{k-1}. The axisymmetric jet is divided into a large number of concentric layers, and it is also cut into an equal number of "slices" parallel to the direction of observation y (see Figure 2). Depending on the slit width, a disc-shaped region of thickness $\triangle z$ will be observed (see Figure 1). If the thickness $\triangle z$ is set equal to unity, the volume of the observed regions will be proportional to the area bounded by the two circles r_k, r_{k-1} and by the two straight lines x_j, x_{j-1}. Making use of the existing geometrical relations (see Figure 3), one obtains an expression for the area bounding a volume

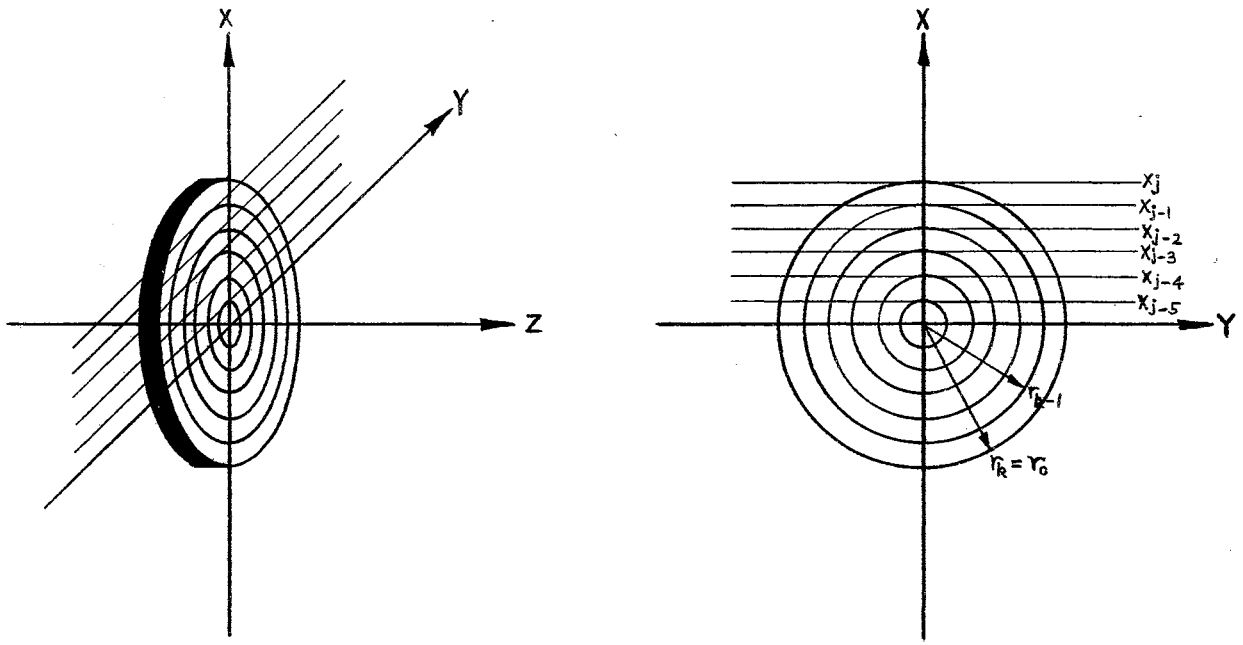

Figure 2. Concentric Layers and Parallel Slices of a Disc-Shaped Plasma Region

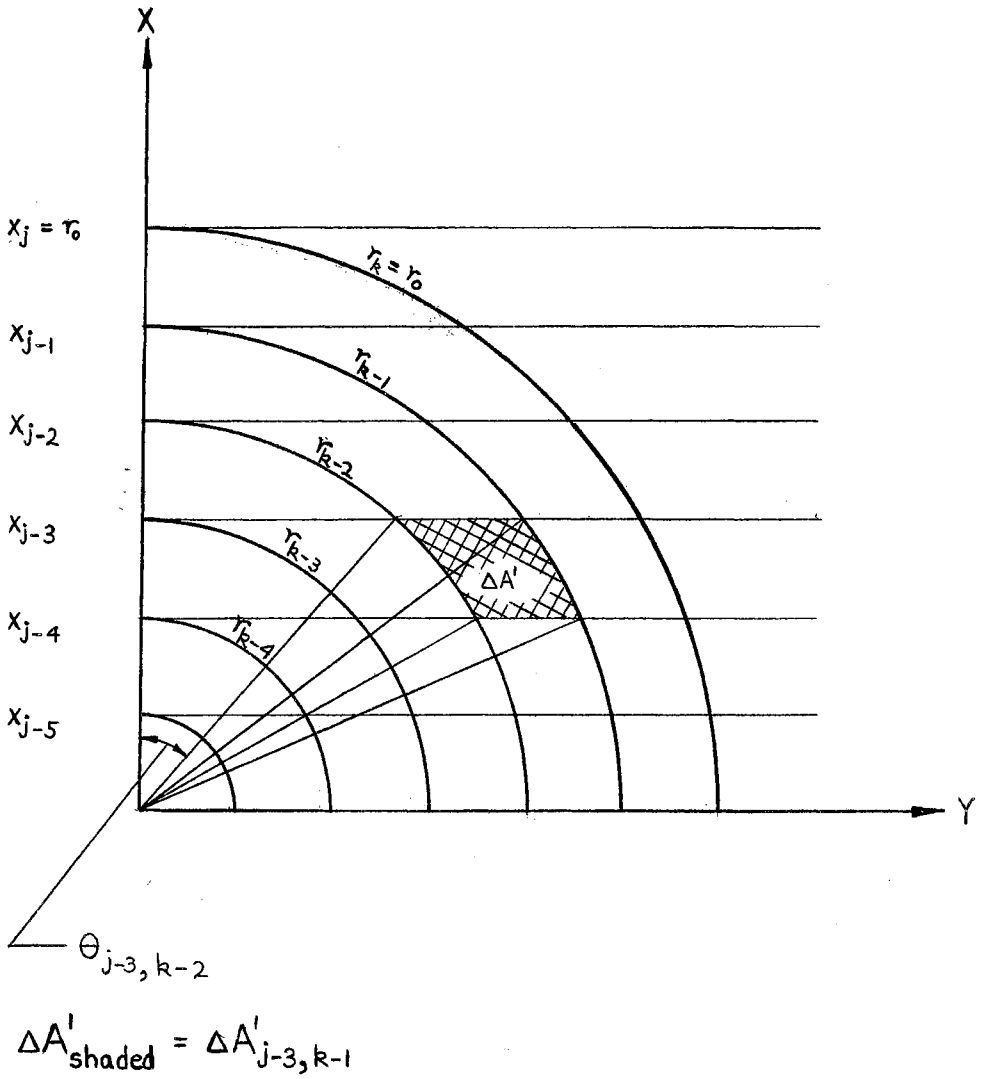

Figure 3. Definition of the Area $\Delta A'_{j,k}$

element:

$$\triangle A'_{j,k} = \frac{1}{2}\left[r_k^2 \,(\theta_{j-1,k} - \theta_{j,k}) - r_{k-1}^{\,2}\,(\theta_{j-1,k-1} - \theta_{j,k-1}) + x_j(y_{j,k} - y_{j,k-1}) - x_{j-1}(y_{j-1,k} - y_{j-1,k-1})\right] . \qquad (7)$$

The intensity of a spectral line, I_x, as recorded by the spectrograph, (see Figure 4), is proportional to the sum of the area weighted specific normal intensities of radiation from all the individual volume elements which constitute one horizontal column, e.g., the column bounded by the horizontal (parallel to y-direction) planes x_{j-4} and x_{j-3}. Since in each column a volume element with a base area $\triangle A'_{j,k}$ appears twice, it is convenient to define an area $\triangle A_{j,k}$ as

$$\triangle A_{j,k} = 2 \cdot \triangle A'_{j,k} . \qquad (8)$$

The intensity of a spectral line, I_x, of a column is then equal to the sum of the radiations of individual volume elements in a column; i.e., it is equal to the sum of terms of the form

$$i_{r,k} \cdot \triangle V_{j,k} = i_{r,k} \cdot \triangle A_{j,k} \cdot \triangle z$$

where $\triangle V_{j,k}$ is the volume of the element bounded by r_k and x_j. Having in mind that $\triangle z = 1$, one obtains a system of linear equations with respect to $i_{r,k}$ from which $i_{r,k}$ can be calculated starting with the first equation and proceeding toward the last one.

The mentioned system of equations is as follows:

$$\begin{aligned} I_{x,j} &= i_{r,k} \cdot \triangle A_{j,k} \\ I_{x,j-1} &= i_{r,k} \cdot \triangle A_{j-1,k} + i_{r,k-1} \cdot \triangle A_{j-1,k-1} \qquad (9) \\ I_{x,j-2} &= i_{r,k} \cdot \triangle A_{j-2,k} + i_{r,k-1} \cdot \triangle A_{j-2,k-1} + i_{r,k-2} \cdot \triangle A_{j-2,k-2} \\ &\cdots \\ &\cdots \end{aligned}$$

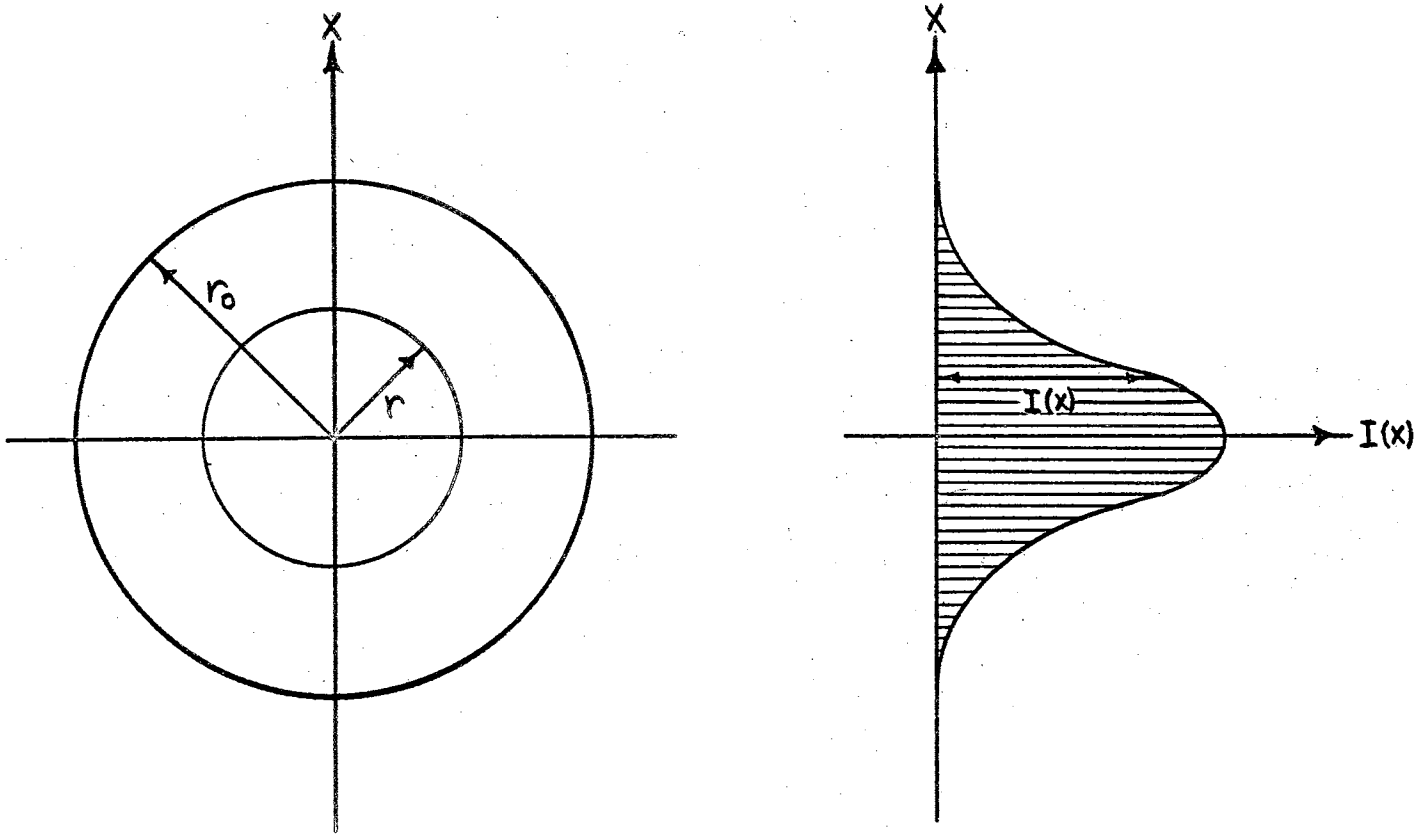

Figure 4. Line Intensity Distribution Determined by the Densitometer

Pearce has divided a disc-shaped region into 25 concentric layers and 50 horizontal slices (25 slices for one-half of the disc region) and tabulated the values of $\triangle A_{j,k}$. These are given in Table I. With values for $\triangle A_{j,k}$ and the system of equations given in equation (9), the measured intensity distribution, I_x, can be transformed into the radial intensity distribution, i_r.

Saha Equation

Another fundamental relation which is used in the evaluation of extremely high temperatures is based on the third assumption given previously. This relation originated in the field of astrophysics, and it refers to the weak ionization of atoms in the outer layers of fixed stars. It applies to an equilibrium mixture of neutral atoms, ions and electrons. The problem of weak ionization in the stars' atmosphere was first discussed by Sir Arthur S. Eddington in his theory of fixed stars, and then improved by John Eggert (10). The final solution and application of the theory developed by Eggert was made by Megh Nad Saha in 1920 (11).

Saha assumed that a mixture of neutral atoms, ions and electrons will behave similarly as a reactive mixture of monatomic gases and, thus, a fixed composition of such a mixture will correspond to each temperature T. He applied the concepts of chemical equilibrium to the thermal equilibrium of the mixture and obtained an expression for the equivalent "equilibrium constant."

For an ionization reaction of the general form

$$\nu_a A + \nu_b B + \ldots \rightleftarrows \nu_m M + \nu_n N + \ldots . - U,$$

TABLE I

$\triangle A_{j,k}$ COEFFICIENTS FOR CALCULATING RADIAL INTENSITY DISTRIBUTION (2)

j \ k	1	2	3	4	5	6	7	8	9	10	11	12	13	14	15	16	17	18	19	20	21	22	23	24	25	j
1	1.57080	2.25565	2.06051	2.02891	2.01706	2.01128	2.00802	2.00600	2.00466	2.00372	2.00304	2.00253	2.00214	2.00184	2.00159	2.00139	2.00123	2.00109	2.00098	2.00088	2.00079	2.00072	2.00066	2.00060	2.00056	1
2		2.45674	2.69599	2.23719	2.13023	2.08348	2.05838	2.04323	2.03334	2.02652	2.02161	2.01795	2.01515	2.01296	2.01122	2.00980	2.00864	2.00768	2.00686	2.00617	2.00558	2.00507	2.00463	2.00424	2.00390	2
3			3.09748	3.10298	2.43399	2.25572	2.17189	2.12445	2.09465	2.07457	2.06035	2.04989	2.04195	2.03579	2.03090	2.02695	2.02372	2.02104	2.01879	2.01689	2.01526	2.01386	2.01264	2.01158	2.01064	3
4				3.62649	3.46836	2.66587	2.38525	2.26717	2.19813	2.15358	2.12291	2.10078	2.08425	2.07153	2.06154	2.05352	2.04699	2.04160	2.03710	2.03329	2.03005	2.02726	2.02484	2.02274	2.02089	4
5					4.08753	3.80085	2.80879	2.51312	2.36390	2.27468	2.21602	2.17499	2.14498	2.12228	2.10464	2.09064	2.07932	2.07002	2.06230	2.05580	2.05028	2.04505	2.04146	2.03790	2.03479	5
6						4.50156	4.10745	2.98257	2.63750	2.45988	2.35192	2.27995	2.22699	2.19131	2.16254	2.14000	2.12196	2.10728	2.09516	2.08502	2.07644	2.06962	2.06282	2.05736	2.05258	6
7							4.88057	4.39322	3.14795	2.75790	2.55405	2.42875	2.34425	2.28384	2.23880	2.20414	2.17679	2.15477	2.13674	2.12178	2.10920	2.09852	2.08936	2.08145	2.07456	7
8								5.23219	4.66179	3.30579	2.87429	2.64631	2.50461	2.40830	2.33892	2.28682	2.24648	2.21446	2.18855	2.16784	2.14946	2.13446	2.12166	2.11066	2.10112	8
9									5.56162	4.91590	3.45690	2.98685	2.73622	2.57923	2.47176	2.39384	2.33500	2.28921	2.25266	2.22296	2.19842	2.17788	2.16048	2.14560	2.13275	9
10										5.87259	5.15763	3.60800	3.09580	2.82389	2.65846	2.53441	2.44836	2.38307	2.33200	2.29111	2.25773	2.23006	2.20682	2.18707	2.17012	10
11											6.16790	5.38861	3.74171	3.20140	2.90938	2.78425	2.59625	2.50234	2.43086	2.37473	2.32963	2.29269	2.26197	2.23609	2.21404	11
12												6.44971	5.61016	3.87655	3.30389	2.99877	2.79479	2.65662	2.55568	2.47826	2.41727	2.36809	2.32771	2.29402	2.26557	12
13													6.71970	5.82332	4.00699	3.40349	3.07415	2.86357	2.71667	2.60833	2.52580	2.45951	2.40641	2.36268	2.32612	13
14														6.97925	6.02899	4.13340	3.50043	3.15365	2.93115	2.77545	2.66025	2.57163	2.50141	2.44451	2.39753	14
15															7.22950	6.22790	4.25614	3.59486	3.23137	2.99741	2.83324	2.71145	2.61752	2.54893	2.48234	15
16																7.47136	6.42087	4.37550	3.68698	3.30740	3.06841	2.89006	2.76192	2.66286	2.58403	16
17																	7.70564	6.60783	4.49174	3.77693	3.38182	3.18619	2.94596	2.81166	2.70764	17
18																		7.93300	6.78985	4.60509	3.86486	3.45473	3.18882	3.00095	2.86069	18
19																			8.15402	6.96713	4.71574	3.95089	3.58621	3.25033	3.05506	19
20																				8.36921	7.14002	4.82389	4.03513	3.59634	3.31078	20
21																					8.57900	7.30882	4.98967	4.11768	3.65518	21
22																						8.78378	7.47383	5.03327	4.19869	22
23																							8.98390	7.63527	5.13479	23
24																								9.17965	7.79337	24
25																									9.37132	25

where U represents the energy released during the ionization reaction, the equivalent equilibrium constant is defined as

$$K = \frac{[n_M]^{\nu_m} [n_N]^{\nu_n} \cdots}{[n_A]^{\nu_a} [n_B]^{\nu_b} \cdots} ,$$

where $[n_M]$, $[n_N]$, . . . , $[n_A]$, $[n_B]$, . . . are the concentrations of the products and of the reactants, respectively, and ν_m, ν_n, . . ., ν_a, ν_b . . . are the corresponding stoichiometric coefficients. The energy U can be calculated from the measurements of the ionization potentials, e.g., by using the method of Franck and Hertz (12). The concentrations of the species involved are defined as the number of particles per unit volume. Since thermal ionization takes place at high temperatures, each constituent of the mixture can be considered as an ideal gas; and the kinetic theory expression for the pressure of a perfect gas, $p = nkT$, may be used. In the preceding expression p is the pressure of the gas, k is the Boltzmann constant, T is the absolute temperature and n is the gas concentration. The equivalent equilibrium constant is then

$$K = \frac{p_M^{\nu_m} p_N^{\nu_n} \cdots}{p_A^{\nu_a} p_B^{\nu_b} \cdots} = F(T) , \qquad (10)$$

where p_M, p_N, . . . , p_A, p_B, . . . are the partial pressures of the products and of the reactants, respectively.

Expression (10) is the definition of the equilibrium constant, and does not show the relationship between the constant K and the temperature T. This relationship can be obtained in many different ways. The

most commonly used is the one which considers the condition of a thermodynamic system when its free energy (Gibbs function) is a minimum (13). The relationship thus obtained contains, besides the ionization energy U, the so-called "entropy constant." The absolute entropy of an ideal gas can be expressed in the form

$$s = c_p \ln T - R \ln p + R \ln R + a,$$

where c_p and R are the molal specific heat at constant pressure and the universal gas constant, respectively; and a is the integration constant or the entropy constant.

At high temperatures the molecules of the species participating in the reaction are dissociated; therefore, all the constituents of the mixture behave as monatomic perfect gases. In such a case it is possible to calculate the entropy constant by using the formula of Sackur and Tetrode. The Sackur-Tetrode formula can be derived by applying the Bose-Einstein statistics to a monatomic perfect gas, e.g., see Hercus (6).

The entropy constant as obtained from the Sackur-Tetrode formula is given by the expression

$$a = R \ln \frac{(2\pi m)^{3/2} k^{5/2} e^{5/2}}{R h^3}, \qquad (11)$$

where m is the mass of the gas particle and h is the Planck constant; other symbols have the same meaning as before.

Assuming also that the specific heat at constant pressure of the free electrons in the mixture amounts to 5R/2--i.e., the same as for any monatomic perfect gas--Saha was able to derive an expression for

the function F(T) in the relation K = F(T), as indicated in equation (10).

The degree of ionization, x, is defined as the ratio of the concentration of the ions or electrons to the concentration of the particles from which these ions and electrons were produced. Thus, for a Ca-reaction, one has $Ca \rightleftarrows Ca^+ + e^- - U$, and

$$x = \frac{[n_{Ca^+}]}{[n_{Ca}] + [n_{Ca^+}]} = \frac{[n_{e^-}]}{[n_{Ca}] + [n_{Ca^+}]} \quad ,$$

since $[n_{Ca^+}] = [n_{e^-}]$, and $[n_{Ca}]$ is the Ca-concentration after ionization.

In a reactive mixture all the constituents are considered to be ideal gases; therefore, the relations valid for ideal gas mixtures may be applied. The partial pressures in relation (10) may be expressed in terms of the degree of ionization x, and the pressure p of the mixture. Thus, when the reaction includes one single specie, and when there is only one ionization step, expression (10) becomes

$$K = p \cdot \frac{x^2}{1-x^2} = F(T) \quad . \tag{12}$$

The function F(T) has an exponential form; therefore, the Saha equation is often written as a logarithmic expression. The final form of expression (12) as obtained by Saha is

$$\log K = \log \frac{x^2}{1-x^2} p = - \frac{U}{4.571T} + 2.5 \log T - 6.5 \quad . \tag{13}$$

In the above equation, the pressure p is in atmospheres, the temperature T is in degrees Kelvin, and the ionization energy is in

calories; the degree of ionization x is dimensionless.

Saha successfully applied equation (13) to the ionization of hydrogen, helium, calcium, strontium, barium and iron in his studies of the composition of the solar chromosphere.

The Saha equation appears in the literature in many various forms, some of which will be discussed in the following pages.

The theory of thermal ionization as developed by Eggert and by Saha was not satisfactory from a theoretical point of view. It combined the concepts of thermodynamics (chemical equilibrium) with the concepts of quantum statistics (entropy constant). R. H. Fowler and E. A. Milne (14) used a method previously developed by C. G. Darwin and R. H. Fowler in order to derive the Saha equation in an exclusively statistical way. The derivation of Fowler and Milne is far too complex, and simpler derivations, although quite rigorous, appeared in the literature. In the textbooks on astrophysics by A. Unsöld (15) and by M. Waldmeier (16), there appears a relatively simple derivation of the Saha equation. The derivations in the two textbooks are almost identical, and both are based on a derivation given by D. H. Menzel (17). The starting point in the derivation is the Boltzmann distribution law,

$$\frac{n_{r,s}}{n_r} = \frac{g_{r,s}}{u_r} \cdot e^{-\frac{w_{r,s}}{kT}} , \qquad (14)$$

where $n_{r,s}$ and n_r represent the concentrations of the r-times ionized atoms in the s-quantum state and all r-times ionized atoms, respectively. Other symbols need some additional explanation. The simple states--i.e., the energy levels of an atom--are determined by the azimuthal

quantum number k; in this case the atoms or ions occupy one and the same cell of phase space. When other quantum numbers (principal quantum number n, magnetic quantum number m and spin quantum number s) are considered, one obtains by combinations of quantum numbers n, m and s, many different s-quantum states with the same azimuthal quantum number k. The energy levels of the atom in such quantum states are slightly different (same k). These quantum states will occupy different cells in phase space, and the energy level (or atom state) is said to be "degenerate." The concept of degenerate and nondegenerate states originated in quantum mechanics, where it is possible to obtain many different eigenfunctions as the solutions of the Schrödinger Wave Equation, all corresponding to the same eigenvalue (total energy of the system). The number of eigenfunctions corresponding to the eigenvalue is called the degeneracy of this energy level. In statistical mechanics (and thermodynamics) the degeneracy is called the "statistical weight," and it is usually denoted by the symbol g. In expression (14), $g_{r,s}$ represents the statistical weight of an energy level s, of an r-times ionized atom, i.e., the number of quantum states corresponding approximately to the same energy level s; $w_{r,s}$ is the ionization energy of an r-times ionized atom in an s-state. The symbol u_r stands for the sum over all the states of an r-times ionized atom, and it is equal to

$$u_r(T) = \sum_{s=0}^{\infty} g_{r,s}\, e^{-\frac{w_{r,s}}{kT}} = g_{r,0} + g_{r,1}\, e^{\frac{w_{r,1}}{kT}} + g_{r,2}\, e^{-\frac{w_{r,2}}{kT}} + \ldots \quad (15)$$

The sum (15) is of great importance in statistical mechanics, and

it is called the "partition function" (German: Zustandssumme).

The derivation of the Boltzmann distribution law and the meaning of the partition function can be found in texts on statistical mechanics and on statistical thermodynamics.

In Maxwell-Boltzmann statistics, the extension of a cell in phase space is arbitrary. In order to derive the Saha equation it is necessary to assume a cell-size equal to h^f, where h is the Planck constant, and f is equal to one-half of the dimensions of phase space. For f=3 (the phase space is 6-dimensional: 3 spatial and 3 impulse coordinates), the extension of a unit cell is then h^3. This means the extension of a cell is assumed the same as in quantum statistics. The coordinates of an electron (spatial and impulse) are determined relative to its own atom nuclei, i.e., to the ion from which the electron was separated; with such coordinates the energy term of the Boltzmann Law is calculated. The number of electrons as well as the number of neutral atoms (the case of single ionized atoms is considered first) are counted per unit cell of phase space (i.e., nondegenerate quantum states are assumed); the ratio of these two numbers (concentrations per unit cell) is used in connection with the Boltzmann Law. An integration of the expression thus obtained over the average volume available to one free electron yields one form of the Saha equation. If the number of single ionized atoms per unit volume is denoted by n_1, then the average volume corresponding to a pair (ion + free electron) amounts to $1/n_1$. The ratio of the number of free electrons per unit cell to the number of neutral atoms per unit cell is equal to the ratio of the electron to

neutral atom concentrations per unit volume. Thus, the Saha equation obtained in the described manner relates the neutral atom, ion, and electron concentrations (per unit volume) with temperature, and can be written in the form:

$$\frac{n_1}{n_o}\, n_e = \frac{(2\pi mkT)^{3/2}}{h^3}\, e^{-\frac{w_o}{kT}} .$$

The neutral atom, ion, and electron concentrations are denoted by n_o, n_1, and n_e; m is the electron mass; and w_o is the ionization energy. The electron concentration n_e can be expressed in terms of the "electron pressure" p_e, since $p_e = n_e \cdot kT$. The preceding equation becomes then

$$\frac{n_1}{n_o}\, p_e = \frac{(2\pi m)^{3/2}\,(kT)^{5/2}}{h^3}\, e^{-\frac{w_o}{kT}} .$$

The above form of Saha equation holds for neutral and single ionized atoms when the atom-states are nondegenerate. If, however, one considers r-times ionized atoms which partially ionize and become r+1-times ionized, the same reasoning as before may be applied. It should be noticed that the coordinates of the separated electron are relative to the r+1-times ionized atom, and that the constituents, to start with, were the r-times ionized atoms. Therefore, the volume over which the integration of the Boltzmann Law is performed has the extension $1/n_{r+1}$. This yields the left-hand side of the Saha equation in a more general form: $(n_e/n_r)\cdot(n_{r+1})$, where n_r, n_{r+1} and n_e are the concentrations (per unit volume) of the r and r+1-times ionized atoms and of the electrons. When the degeneracy of the atom states (energy levels) is taken into

consideration, the partition functions u_r and u_{r+1} will appear in the Saha equation. Again, one may set $n_e = p_e/kT$, and thus obtain the Saha equation in the most general form

$$\frac{n_{r+1}}{n_r} p_e = 2 \frac{u_{r+1}}{u_r} \frac{(2\pi m)^{3/2} (kT)^{5/2}}{h^3} e^{-\frac{w_r}{kT}} . \qquad (16)$$

The factor 2, in equation (16), is the statistical weight, g_e, of a free electron, since each electron may have two orientations of its spin, when exposed to an external magnetic field. The r- and r+1-times ionized atoms may be in different atom states; therefore, when all the r- and r+1-times ionized atoms are considered, the sums over all states appear--i.e., the partition functions u_r and u_{r+1}, respectively--instead of the individual statistical weights $g_{r,s}$ and $g_{r+1,s}$. In cases when the first excited state is high above the ground state of the atom, the great majority of atoms are in the ground state and the partition functions u_r and u_{r+1} can be replaced with the first terms $g_{r,o}$ and $g_{r+1,o}$, the corresponding statistical weights of the ground states.

Another point to be emphasized is the fact that equation (16) is independent of the presence of other species in the mixture and that the same electron pressure p_e appears in the equation no matter which two consecutive species r and r+1 are considered. This is the consequence of the derivation of the Saha equation, namely, that always the ratio of the electron concentration n_e (of all elctrons in the mixture) to the concentration of a particular specie n_r is substituted in the

Boltzmann equation (14). The concentration n_{r+1} appears as a consequence of the extension of the volume over which the integration, of the expression thus obtained, is performed.

From the preceding discussion it is obvious that the Saha equation may be written in many different forms. In order to make its practical application more convenient, the most frequently encountered forms of it are summarized below:

1. $$\frac{n_{r+1}}{n_r} p_e = 2 \frac{u_{r+1}}{u_r} \frac{(2\pi m)^{3/2} (kT)^{5/2}}{h^3} e^{-\frac{w_r}{kT}} ; \qquad (17)$$

2. $$\frac{p_{r+1}}{p_r} p_e = 2 \frac{u_{r+1}}{u_r} \frac{(2\pi m)^{3/2} (kT)^{5/2}}{h^3} e^{-\frac{w_r}{kT}} , \qquad (18)$$

where p_{r+1} and p_r are the "partial" pressures of the r- and r+1-times ionized atoms, respectively;

3. $$\frac{x^2}{1-x^2} p = 2 \frac{u_{r+1}}{u_r} \frac{(2\pi m)^{3/2} (kT)^{5/2}}{h^3} e^{-\frac{w_r}{kT}} , \qquad (19)$$

where x represents the degree of ionization; therefore, $p_r=p_o(1-x)$, $p_{r+1}=p_o x$ and $p_e=p_o x$, where p_o is the pressure of the gas before ionization takes place. The total pressure of the gas, after the ionization process is then $p=p_r+p_{r+1}+p_e=p_o(1+x)$ and $p_o=p/1+x$; $p_e=p_o x=p(x/1+x)$. The left hand side of equation (18) becomes therefore

$$\frac{p_o x}{p_o(1-x)} \cdot p \frac{x}{1+x} = \frac{x^2}{1-x^2} p \quad .$$

4. $$\log \frac{x^2}{1-x^2} p = -\frac{U}{4.571T} + 2.5 \log T - 6.5 , \qquad (20)$$

U being the ionization energy in calories and p the total pressure in

atmospheres.

5. Waldmeier (16) recommends for practical use the following form:

$$\log \frac{n_{r+1}}{n_r} p_e = - w_r \frac{5040}{T} + \frac{5}{2} \log T - 0.48 + \log \left(2 \frac{u_{r+1}}{u_r}\right) , \qquad (21)$$

in which the pressure p_e is in bars $(\frac{\text{dyne}}{\text{cm}^2})$ and the ionization energy w_r is in electron-volts.

6. Meek and Craggs (18) use the relation $p_e = n_e kT$ and write the Saha equation in the form

$$\log \frac{n_i}{n_a} n_e = -w_r \frac{5040}{T} + \frac{3}{2} \log T + 15.38 \qquad (22)$$

where w_r is the ionization potential in electron-volts, and n_a, n_i and n_e are the concentrations of neutral atoms, ions and electrons, respectively.

In practical applications there appears, usually, a system of Saha equations, since in most cases there are more than one specie in the gaseous mixture, or the ionization is double, triple, etc. So, for example, P. H. Dickerman (3) analyzes a plasma consisting of neutral and ionized hydrogen as well as neutral and singly ionized oxygen and electrons. The corresponding system of Saha equations, equation (22), is then

$$\log \frac{n_H^+}{n_H} n_e = - w_H \frac{5040}{T} + \frac{3}{2} \log T + 15.38$$

and

$$\log \frac{n_O^+}{n_O} n_e = - w_O \frac{5040}{T} + \frac{3}{2} \log T + 15.38 .$$

A similar situation is found in the paper by F. Burhorn, H. Maecker and T. Peters (19) for the analysis of a hydrogen-oxygen plasma in which single, double and triple ionized oxygen atoms appear. The system of Saha equations, equation (18), is then

$$\frac{p_H^+}{p_H} p_e = 2\frac{u_H^+}{u_H}\frac{(2\pi m)^{3/2}(kT)^{5/2}}{h^3} e^{-\frac{w_H}{kT}}$$

$$\frac{p_O^+}{p_O} p_e = 2\frac{u_O^+}{u_O}\frac{(2\pi m)^{3/2}(kT)^{5/2}}{h^3} e^{-\frac{w_O}{kT}}$$

$$\frac{p_O^{++}}{p_O^+} p_e = 2\frac{u_O^{++}}{u_O^+}\frac{(2\pi m)^{3/2}(kT)^{5/2}}{h^3} e^{-\frac{w_O^+}{kT}}$$

and

$$\frac{p_O^{+++}}{p_O^{++}} p_e = 2\frac{u_O^{+++}}{u_O^{++}}\frac{(2\pi m)^{3/2}(kT)^{5/2}}{h^3} e^{-\frac{w_O^{++}}{kT}} .$$

In addition to the Saha equations there are some other relations which are generally used.

$$n=(n_1+n_2+n_3+\ldots)+2(n_1^+ +n_2^+ +n_3^+ \ldots)+3(n_1^{++}+n_2^{++}+n_3^{++}+\ldots)+\ldots \quad (23)$$

where n_1, n_2, n_3, . . . are the concentrations of neutral atoms of the species 1, 2, 3, . . . ; n_1^+, n_2^+, n_3^+ . . . and n_1^{++}, n_2^{++}, n_3^{++}, . . . are the concentrations of single and double ionized atoms of the species 1, 2, 3, . . . , respectively. Since p=nkT, one obtains

$$p = [(n_1+ n_2+ n_3+ \ldots) + 2(n_1^+ + n_2^+ + n_3^+ + \ldots) + 3(n_1^{++}+ n_2^{++}+ n_3^{++} + \ldots) + \ldots]kT \quad . \quad (24)$$

The Dalton Law of partial pressures also holds, and therefore

$$p = p_e + \sum_{i=1}^{z} p_{n_i} + \sum_{i=1}^{z} p_{n_i^+} + \sum_{i=1}^{z} p_{n_i^{++}} + \ldots \qquad (25)$$

where i = 1, 2, 3, . . . , z, refers to the constituents and their ions in the mixture.

The electron pressure p_e can be calculated from

$$p_e = \left[\sum_{i=1}^{z} n_i^+ + 2 \sum_{i=1}^{z} n_i^{++} + 3 \sum_{i=1}^{z} n_i^{+++} + \ldots \right] kT \qquad (26)$$

where n_i, n_i^{++}, n_i^{++} , . . . are ion-concentrations of the species i = 1, 2, 3, . . . , z. Expression (26) is based on the assumption that the plasma is electrically neutral, and therefore

$$n_e = \sum_{i=1}^{z} n_i^+ + 2 \sum_{i=1}^{z} n_i^{++} + 3 \sum_{i=1}^{z} n_i^{+++} + \ldots \qquad (27)$$

Expression (26) may be written also in the form

$$p_e = \sum_{i=1}^{z} p_i^+ + 2 \sum_{i=1}^{z} p_i^{++} + 3 \sum_{i=1}^{z} p_i^{+++} + \ldots \qquad (28)$$

where p_i^+, p_i^{++}, p_i^{+++}, . . . are the partial pressures of the single, double, triple, . . . ionized atoms of the species i=1, 2, 3, . . . , z.

The composition of a chemical compound from which the plasma was obtained yields also additional relationships. For example, the plasma investigated by Burhorn, Maecker and Peters (19) yields

$$\frac{n_H + n_H^+}{n_O + n_O^+ + n_O^{++} + n_O^{+++}} = 2 \qquad (29)$$

or

$$\frac{p_H + p_H^+}{p_O + p_O^+ + p_O^{++} + p_O^{+++}} = 2 \qquad (30)$$

The two relations discussed above are common to all spectroscopic determinations of equilibrium plasma temperatures that were presented in the literature. The remaining steps in the analyses were based on additional relations which varied with the particular method to be used. One method is based on relative line intensities. Another method considers the broadening of the emitted spectral line due to the varying electric field that exists in the plasma. The characteristics of spectral line emission and line broadening are presented in what follows.

Spectral Line Emission

In general, the intensity of a spectral line emitted by the transition from a state s' to a state s", of an r-times ionized atom, is proportional to the number of photon emitters, i.e., to the number of particles $N_{r,s'}$ responsible for the emission of the radiation, to the so-called "transition probability" $a_{s's"}$, and to the fourth power of the frequency of radiation $\nu_{s's"}$ of the emitted spectral line (the so-called "Einstein's ν^4 correction") (20) (21):

$$I_{s's"} = c \cdot a_{s's"} \nu^4_{s's"} \cdot N_{r,s'} \quad ,$$

where c is the proportionality constant. The transition probability $a_{s's"}$ represents the probability that, under given conditions, a change of state from s' to s" will take place. It can be calculated from the known structure of the atom, or it can be determined experimentally.

In relatively few cases, the transition probability is reliably known. (22).

The intensity of a spectral line, due to radiation per unit volume of the emitting plasma, is proportional to the concentration of the emitting atoms, i.e.:

$$I'_{s's''} = c \cdot a_{s's''} \cdot \nu^4_{s's''} \cdot n_{r,s'} \quad , \tag{31}$$

where c is a constant depending upon the units of intensity and the optical system, and $n_{r,s'}$ is the concentration of emitting r-times ionized atoms in state s'.

It was assumed previously that the plasma is in thermal equilibrium; therefore, the concentration $n_{r,s'}$ can be calculated from the Boltzmann Law, equation (14):

$$n_{r,s'} = n_r \cdot \frac{g_{r,s'}}{u_r} \cdot e^{-\frac{w_{r,s'}}{kT}} \quad .$$

Therefore,

$$I'_{s's''} = c \cdot a_{s's''} \cdot \nu^4_{s's''} \cdot n_r \cdot \frac{g_{r,s'}}{u_r} \cdot e^{-\frac{w_{r,s'}}{kT}}$$

or

$$I'_{s's''} = c \cdot a_{s's''} \cdot \frac{\nu^3_{s's''}}{h} \cdot h\nu_{s's''} \, n_r \, \frac{g_{r,s'}}{u_r} \, e^{-\frac{w_{r,s'}}{kT}} \quad .$$

The above expression can be written in the form (28)

$$I'_{s's''} = A_{s's''} \cdot \frac{g_{r,s'}}{u_r} \cdot n_r \, e^{-\frac{w_{r,s'}}{kT}} \cdot h\nu_{s's''} \quad ,$$

where

$$A_{s's''} = c \cdot a_{s's''} \cdot \frac{\nu^3_{s's''}}{h}$$

is proportional to the transition probability for the states s' and s".

The spectral line intensity I' is proportional to the intensity of radiation emitted by the plasma. One may write, therefore, for the intensity of the radiation, i'_o, emitted in all directions from the surface of a radiating gas

$$i'_o = A \cdot \frac{g_{r,s}}{u_r} \cdot n_r \cdot e^{-\frac{w_{r,s}}{kT}} h\nu \ .$$

In the above expression, A is proportional to the transition probability for the states s(s' and s") of the r-times ionized atom, ν is the frequency of radiation, n_r is the concentration of the r-times ionized atoms, $g_{r,s}$ is the statistical weight of the initial, upper state s (state s') and $w_{r,s}$ is its ionization energy (state s'). The partition function, u_r, refers to all the states s of the r-times ionized atom; k and h are the Boltzmann and the Planck constants and T is the absolute temperature.

The specific normal intensity of radiation, i, is now

$$i = \frac{A}{4\pi} \cdot \frac{g_{r,s}}{u_r} \cdot n_r \cdot e^{-\frac{w_{r,s}}{kT}} \cdot h\nu \ . \qquad (32)$$

The concentration $n_{r,s'}$ in equation (31) can be substituted by the concentration $n_{r,s''}$ of the r-times ionized atoms in the state s".

By applying the Boltzmann Law, one has

$$\frac{\frac{n_{r,s'}}{n_r}}{\frac{n_{r,s''}}{n_r}} = \frac{(\frac{g_{r,s'}}{u_r}) \cdot e^{-\frac{w_{r,s'}}{kT}}}{(\frac{g_{r,s''}}{u_r}) \cdot e^{-\frac{w_{r,s''}}{kT}}} = \frac{g_{r,s'}}{g_{r,s''}} e^{-\frac{(w_{r,s'} - w_{r,s''})}{kT}} \ .$$

Since $w_{r,s'} - w_{r,s''} = h\nu_{s's''}$, where $\nu_{s's''}$ is the frequency of the emitted radiation, the above expression becomes

$$n_{r,s'} = n_{r,s''} \cdot \frac{g_{r,s'}}{g_{r,s''}} \cdot e^{-\frac{h\nu_{s's''}}{kT}} \quad ;$$

thus, equation (31) can be written as

$$I'_{s's''} = c \cdot a_{s's''} \cdot \nu^4_{s's''} \cdot n_{r,s''} \cdot \frac{g_{r,s'}}{g_{r,s''}} \; e^{-\frac{h\nu_{s's''}}{kT}} \quad .$$

Proceeding in the same manner as in the derivation of equation (32), one obtains, finally, the following expression:

$$i_{s's''} = \frac{A}{4\pi} \cdot \frac{g_{r,s'}}{g_{r,s''}} \cdot n_{r,s''} \cdot e^{-\frac{h\nu_{s's''}}{kT}} \cdot h\nu_{s's''} \quad . \qquad (33)$$

The Broadening of the Spectral Lines

Some spectral lines are very sharp; others are diffused. Any spectral line is spread over a frequency range $\nu_o + \Delta\nu'$ and $\nu_o - \Delta\nu''$ where the broadening may be symmetrical $\Delta\nu' = \Delta\nu''$ or asymmetrical $\Delta\nu' + \Delta\nu''$. The line intensity profile of a symmetrically broadened spectral line is shown in Figure 5. The frequency ν_o corresponds to the maximum intensity of the line; $\Delta\nu'$ and $\Delta\nu''$ are the deviations on both sides from the frequency ν_o. The "half-intensity breadth" δ of a spectral line is defined as the sum of the absolute values of the deviations $\Delta\nu'$ and $\Delta\nu''$, when the deviations are measured at the points of the intensity profile where the intensity $I(\nu)$ amounts to one half of its maximum value. (See Figure 5).

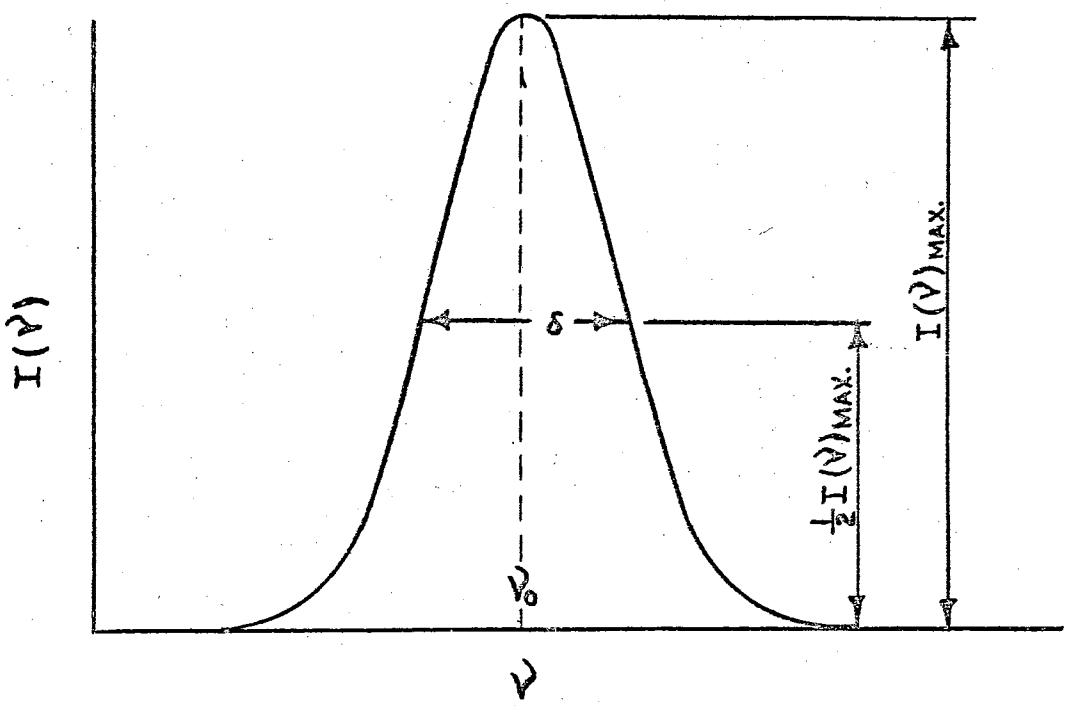

Figure 5. Intensity Profile for a Symmetrically Broadened Spectral Line

According to H. E. White (20), the causes for the broadening of spectral lines may be classified as follows:

1. Natural breadth
2. Doppler effect
3. External effects
   a. Collision damping
   b. Asymmetry and pressure shift
   c. Stark effect.

The "natural breadth" is the least significant. According to the concepts of quantum mechanics, the energy levels of an atom are not discrete levels; they are, more or less, composed of a continuum of energy levels. The observed energy levels, which are shown in an energy level diagram (term scheme), are those for which the probability distribution is the greatest. It is not possible to assign unique term values to either the initial or final states for a transition from one atom state to another one. The frequency of the emitted radiation, will, therefore, vary slightly and the spectral line will be broadened to some extent. The half-intensity breadth is extremely small.

The "Doppler broadening" is much larger than the previously described one. It is caused by the high, random speeds of the emitting atoms. Some of them will be approaching the observer (entrance slit of the spectrograph), whereas some others will be receding. According to the Doppler principle the frequency of radiation emitted by the approaching atoms will increase (violet shift); the frequency of radiation emitted by the receding atoms will decrease (red shift).

The relative change of the frequency is

$$\frac{\Delta\nu}{\nu_0} = \frac{u}{c} \quad ,$$

where u is the relative velocity of the approaching atom in the direction of observation. Doppler broadening increases with an increase in temperature and a decrease in the atomic (or molecular) weight of the gas. The half-intensity breadth due to Doppler broadening is about 10^2 as large as the natural breadth.

Collision damping is the name given for the effects produced by the collision of two atoms, one of which is emitting or absorbing radiation. In the analysis of such effects it is assumed that the collision time is very short as compared to the time between two collisions. It is also assumed that the emission of radiation is interrupted during the impact. After the impact the radiation is resumed with a change in phase and amplitude but with the same frequency.

For the collision damping the half-intensity breadth can be expressed in the form,

$$\delta = \frac{1}{\pi \tau_0} \quad ,$$

where τ_0 is the "mean flight time," i.e., the average time between two collisions. The mean flight time τ_0 is related to the mean free path and to the average velocity of motion $\bar{v}$ by the relation

$$\lambda = \bar{v}\,\tau_0$$

For a Maxwellian distribution of the velocities,

$$\bar{v} = \left(\frac{8kT}{\pi m}\right)^{\frac{1}{2}} \quad \text{and} \quad \lambda = \frac{kT}{\sqrt{2}\, p\pi\, \rho^2} \quad .$$

In the above expressions k is the Boltzmann constant, m is the mass of the atom (or molecule), p is the pressure of the gas and ρ is the so-called "collision diameter" (the average distance between the atom centers at closest approach). Since the mean free path λ depends on the gas pressure p, it follows that the half-intensity breadth increases as the pressure increases.

At very low pressures the Doppler broadening is predominant; at high pressures, however, the collision damping is the main cause for an observed change in the line profile. For visible light and room temperatures the two effects produce, approximately, the same line broadening (same half-intensity breadths). At high pressures the collision time becomes large as compared with the time between two collisions, since the mean free path decreases. In this case one speaks of "asymmetry and pressure shift."

According to Franck and Condon (15), one may consider the potential curves of the radiating atom, for the initial and final terms, as functions of the distance r between the radiating and the perturbing atom. At smaller distances the depression of the upper term will be greater than the depression of the lower one. This will reduce the energy of the emitted photon and a consequence of this will be a decrease of the frequency of radiation. During the collision the emitted spectral line will be shifted toward larger wave lengths (red shift), and the line intensity curve, $I(\nu)$, will be asymmetrical. It was found that the shift of a line is approximately proportional to the density of the radiating gas.

The number of modified oscillations is not so small despite the very short collision time. Thus, at normal temperatures the collision time is of the order 10^{-13} sec; the period of oscillation for visible light is about 10^{-15} sec. Therefore, some 10^{2} oscillations will be modified during the impact. (20).

Stark Effect Line Broadening

When a radiating gas is placed in an electric field, the spectral lines emitted by the gas atoms will be split into a number of components.* This phenomenon was discovered by J. Stark (23) in 1913, when he observed the splitting of hydrogen lines of the Balmer series in electric fields of over 100,000 volt/cm strength.

When exposed to the electric field, the energy levels of different atom states will change slightly. Therefore, in an energy level diagram of a hydrogen-like atom, the term value T will change. The change of the term value can be expressed by the series

$$T = AE + BE^2 + CE^3 + \ldots , \qquad (34)$$

where A, B, C, . . . are constants, E is the electric field strength in electrostatic units and T is the term value in wave numbers ($n_\nu = \frac{\nu}{c}$, cm^{-1}).

The first term of equation (34) is called the "first-order Stark effect." The second term is called the "second-order Stark effect."

---

* A similar effect, the splitting of spectral lines in magnetic fields, was discovered in 1897 by Zeeman.

For small electric field strengths ($E < 100{,}000$ volt/cm) only the first-order Stark effect will be observed for lower states (small principal quantum number n) of hydrogen. The splitting of energy levels (terms) will be symmetrical about the term, for which the electric field is zero.

When the electric field strengths are large ($E > 100{,}000$ volt/cm), the spectral lines of hydrogen, in higher states, will show the second-order Stark effect. In this case, there occurs a unidirectional displacement of each Stark component to the red or to the violet.

In general, the first-order Stark effect will be predominant in hydrogen and hydrogen-like atoms. For atoms which are not hydrogen-like, the first and second-order Stark effects are called the "linear" and "quadratic" Stark effects; usually the quadratic Stark effect will be more often encountered in weak electric fields; whereas the linear Stark effect will appear in strong electric fields.

CHAPTER III

METHODS AND PREVIOUS APPLICATIONS OF PLASMA TEMPERATURE DETERMINATION BY SPECTROSCOPIC ANALYSIS

Two methods which have been developed for plasma temperature determination are described in this chapter. The application of these methods by previous investigators to a hydrogen-oxygen plasma is reviewed briefly to illustrate the analytical technique.

Relative Line Intensity Method

R. W. Larenz (24) developed a method for the determination of temperature distributions in a plasma based on relative intensity measurements. The Abel integral equation is written in the form

$$I_x = 2 \int_{y=o}^{y=\sqrt{r_o^2-x^2}} i_r \, dy$$

which is identical to equation (4), and where $\sqrt{x^2+y^2} = r$, $\sqrt{r_o^2-x^2} = y_o$ (see Figure 1). Instead of solving the preceding equation in this form Larenz introduces the ratio I_x/I_o, where I_o is the measured intensity at x=0, and thus obtains

$$\frac{I_x}{I_o} = 2 \int_{y=o}^{y=\sqrt{r_o^2-x^2}} \frac{i_r}{I_o} \, dy = 2 \int_{y=o}^{y=\sqrt{r_o^2-x^2}} i_r' \, dy$$

where $$i'_r = \frac{i_r}{I_o}$$

From the above equation one obtains the function i'_r. When the function i'_r is plotted versus r, it will show a maximum which does not have to be at r=o. If one denotes the radius r for which $i'_r = (i'_r)_{max}$ by $\bar{r}$, then $(i'_r)_{max} = i'_{\bar{r}}$. Dividing the function i'_r by $i'_{\bar{r}}$ one obtains a new function denoted by i^*_r;

$$i^*_r = \frac{i'_r}{i'_{\bar{r}}} \tag{35}$$

The function i^*_r has the same characteristics as the functions i_r and i'_r; besides that, it is "normalized," since

$$i^*_{\bar{r}} = \frac{i'_{\bar{r}}}{i'_{\bar{r}}} = 1.0$$

The specific normal intensity of radiation, i_r, is a function of the radius r; at the same time, however, it is a function of the pressure and of the temperature at a particular point of interest (the cylindrical layer of radius r).

When the upper state of the r-times ionized atoms emitting the observed radiation is denoted by s, and when the changes of atom states take place from the state s to any state of the r-times ionized atom, equation (32) can be used

$$i = \frac{A}{4\pi} \cdot \frac{g_{r,s}}{u_r} \cdot n_r \cdot e^{-\frac{w_{r,s}}{kT}} \cdot h\nu$$

From the Boltzmann Law

$$\frac{g_{r,s}}{u_r} \cdot n_r \cdot e^{-\frac{w_{r,s}}{kT}} = n_{r,s} \; ;$$

therefore,

$$i = \frac{A}{4\pi} \cdot h\nu \cdot n_{r,s} \quad ,$$

or

$$i = \frac{A}{4\pi} \cdot h\nu \cdot \frac{n_{r,s}}{n_{r,o}} \cdot n_{r,o} \tag{36}$$

where the concentration of the r-times ionized atoms in the ground state is denoted by $n_{r,o}$.

The variations of the ratio $n_{r,s}/n_{r,o}$ and of the concentration $n_{r,o}$ with temperature can be evaluated from the equilibrium (Saha) equations. The ratio $n_{r,s}/n_{r,o}$ increases monotonically with increasing temperature; the concentration $n_{r,o}$, however, increases faster when the temperature increases; and after reaching a maximum, it gradually decreases. This is due to the fact that initially the formation of new ions, $n_{r,o}$, causes an increase in concentration. Further increases of temperature reduce the number of r-times ionized atoms by causing further ionization (to r+1-times ionized atoms); the decrease of the gas density also helps to reduce the concentration $n_{r,o}$. Thus, the product $(n_{r,s}/n_{r,o}) \cdot n_{r,o}$ will first increase as the temperature increases, reach a maximum value, and then gradually decrease.

The specific normal intensity of radiation, $(i_{T,p})$, where

$$i_{T,p} = \frac{A}{4\pi} \cdot h\nu \cdot \frac{n_{r,s}}{n_{r,o}} \cdot n_{r,o} \quad ,$$

when plotted versus temperature, at p=const., will reach a maximum value at a certain temperature. The temperature T, for which $i_{T,p}$ is a maximum is denoted as $\bar{T}$ which corresponds to the radius $\bar{r}$, as

previously defined.

The evaluation of the function $i_{T,p}$ is difficult because it requires the knowledge of the constant A. As mentioned before, the constant A is proportional to the transition probability $a_{s's''}$, which is seldom reliably known. It is convenient, therefore, to normalize the function $i_{T,p}$ by dividing it by the maximum value now denoted as $i_{\overline{T},p}$. The normalized function thus obtained is designated by $i^*_{T,p}$; therefore,

$$i^*_{T,p} = \frac{i_{T,p}}{i_{\overline{T},p}} \quad ; \quad i^*_{\overline{T},p} = 1.0 \ .$$

Both functions, i^*_r and $i^*_{T,p}$, are normalized to 1.0, i.e., $i^*_{\overline{r}} = i^*_{\overline{T},p} = 1.0$; therefore, the curves i^*_r and $i^*_{T,p}$ are similar. For an arbitrarily selected radius r, the value of i^*_r is obtained from the curve i^*_r versus r; the corresponding temperature is obtained from the graph of $i^*_{T,p}$ to satisfy the equality

$$i^*_r = i^*_{T,p} \ .$$

Therefore, once the function $i^*_{T,p}$ is calculated and plotted versus T for the desired values of p, it is possible to obtain the radial temperature distribution.

In order to calculate the function $i^*_{T,p}$, Larenz used the following relations:

1. The expression for the specific normal intensity of radiation, equation (32);

$$i = \frac{A}{4\pi} \cdot \frac{g_{r,s}}{u_r} \cdot n_r \cdot e^{-\frac{w_{r,s}}{kT}} \cdot h\nu$$

2. A system of Saha equations of the form (17)

$$\frac{n_{r+1}}{n_r} \cdot p_e = 2 \frac{u_{r+1}}{u_r} \cdot \frac{(2\pi m)^{3/2} (kT)^{5/2}}{h^3} \cdot e^{-\frac{w_r}{kT}} = F_r(T)$$

where F (T) is a function of temperature denoting the right-hand side of the above equation, and r = 0, 1, 2, . . . , z-1.

3. The gas equations (24) and (26):

$$p = [n_o + 2n^{+} + 3n^{++} + \ldots + (z+1)n^{z(+)}]kT$$

$$p_e = [n^{+} + 2n^{++} + 3n^{+++} + \ldots + zn^{z(+)}]kT$$

where n_o is the concentration of all nautral atoms, n^{+} the concentration of all single ionized atoms, . . . and $n^{z(+)}$ is the concentration of all z-times ionized atoms.

Larenz has solved the preceding systems of equations and thus obtained expressions for the electron pressure p_e, as well as for the neutral atom and ion concentrations n_o, n^{+}, n^{++}, . . . , which are all functions of pressure and temperature (in the analysis it was assumed p = const.). The expressions obtained by Larenz are very involved and cumbersome. For the simple case of neutral and single ionized atoms, the expression for p_e can be approximated by a quadratic equation; the expressions for the concentrations n_o and n^{+} are then obtained in a closed analytical form. In other cases graphical or iteration methods must be used in order to calculate p_e. Having obtained the electron pressure, p_e, it is possible to calculate the necessary ion concentration, n_r. Then equation (32) can be used for

the calculation of the function $i_{T,p}$. In calculating $i_{T,p}$ any arbitrary value for the constant A may be used. When, afterwards, the function $i^*_{T,p}$ is being plotted, the constant A will cancel, and its assumed value will have no effect on $i^*_{T,p}$.

The maximum specific normal intensity of radiation, for a particular spectral line, generally occurs in a cylindrical plasma layer for which $r > 0$. When more than one ionized specie are present in the plasma, there will correspond a different temperature $\overline{T}$ to each specie. The higher the level of ionization (r-1, r, r+1, . . .) of a specie, the higher the temperature $\overline{T}$ will be. Thus, for a plasma which contains neutral, single and double ionized atoms of a specie (e.g., oxygen) the functions $i^*_{T,p}$ will appear as shown in Figure 6, where the curves I, II, and III represent the functions $i^*_{T,p}$ for neutral, single and double ionized atoms. It should be noticed that all three curves have a maximum equal to unity.

The curves in Figure 6 indicate that certain spectral lines are convenient for temperature measurements only in limited ranges of temperature. However, the curves are close to each other and overlap partly; thus, a wide range of temperature can be measured by observing spectral lines corresponding to different levels of ionization of one and the same specie. As an example, Larenz has encompassed a range from 10,000 to 60,000°K by observing three spectral lines produced by neutral and ionized oxygen atoms (0, 0^+ and 0^{++}) in a so-called "Gerdien arc," which burns in a mixture of hydrogen and oxygen atoms, the hydrogen and oxygen atoms being in the same

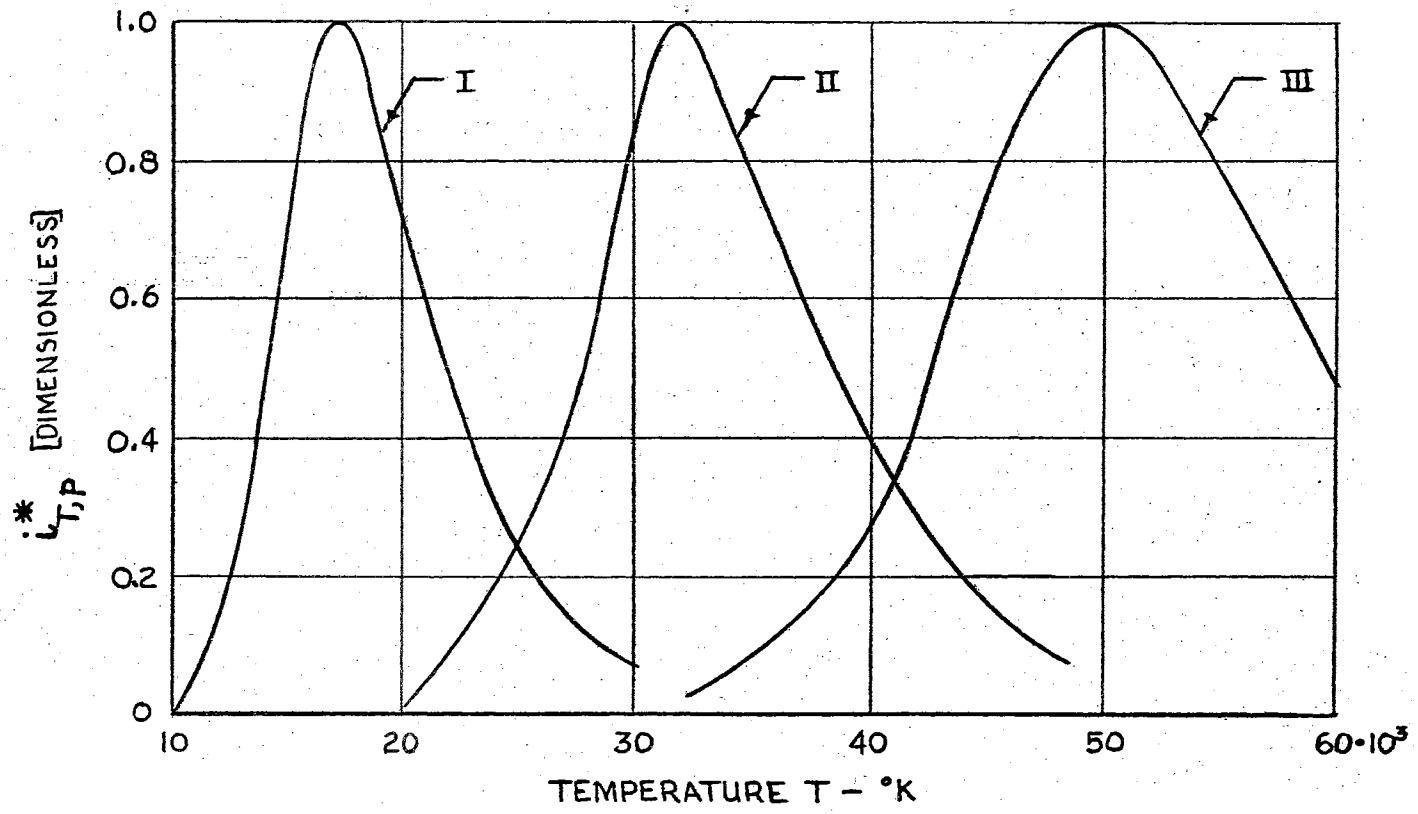

Figure 6. The Functions $i^*_{T,p}$ for the Plasma Constituents I,II,III (24)

proportion as in water.

Burhorn, Maecker and Peters have used Larenz's method to determine the temperatures in Gerdien arcs having current intensities from 100 to 1500 amperes. The set of Saha equations which they used in their work was given previously in Chapter II where the general aspects of the Saha equation were discussed. The solution of this set of Saha equations is shown in Figure 7, which is a plot of the concentrations n (total number of particles per cm^3), n_H, n_H^+, n_o, n_o^+, n_o^{++}, n_o^{+++} versus temperature.

The observed spectral lines were the following: H_β, $\lambda = 4861$ Å; 0^+, $\lambda = 4651$ Å, and 0^{++}, $\lambda = 3447$ Å. For these three lines the functions i_r^* and $i_{T,p}^*$ were calculated and plotted thus obtaining three pairs of values $\bar{T}$ and $\bar{r}$. These three pairs were used for the temperature distribution curve.

Stark Broadening Method

Strong local electric fields exist in a plasma. The consequences of such fields are the linear and quadratic Stark effects described in Chapter II. The electric fields are produced not only by the charged particles, ions and electrons; strong intermolecular electric fields can also be produced by the gas atoms and molecules in the case where they possess a "dipole" or "quadrupole" electric moment. In such molecules and atoms, the electric charges are separated so that a net electric moment results even in the absence of external electric fields. (25).

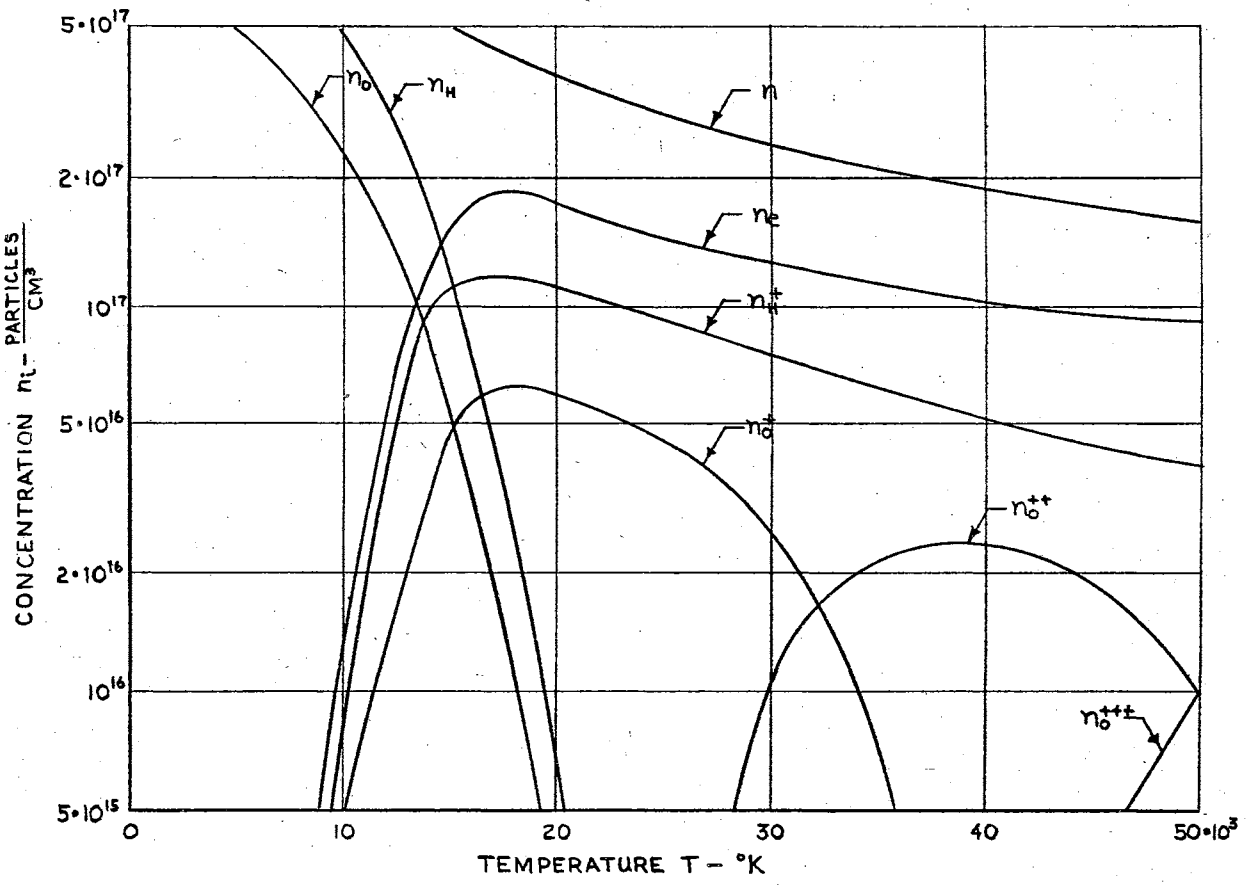

Figure 7. Equilibrium Concentrations (n_i) for a Gerdien Arc Plasma (19)

The local electric fields, thus produced, are inhomogeneous and continually changing. The variation of the electric fields is caused by the thermal motion of plasma particles. The above facts make the problem very complex, and the statistical distribution of electric fields produced by charged particles had to be evaluated. Such calculations were made by J. Holtsmark (26) and by P. Debye (27).

Holtsmark (26) investigated the probability that an electric field of strength E would exist at the location of an emitting atom or ion. In order to evaluate the distribution function for the field E, a new variable β was defined as

$$\beta = \frac{E}{E_o} , \tag{37}$$

where E_o is called the normal field strength. The normal field strength depends on the source of the electric field; i. e., whether it is produced by ions, dipoles or quadrupoles. The corresponding expressions for the normal field strength are

$$\begin{aligned} E_o &= a.en^{2/3} \quad \ldots\ldots\ldots\ldots \text{ ions} \\ E_o &= b.\mu n \quad \ldots\ldots\ldots\ldots \text{ dipoles} \\ E_o &= c.qn^{4/3} \quad \ldots\ldots\ldots\ldots \text{ quadrupoles.} \end{aligned} \tag{38}$$

In the above expressions a, b, and c are constants, e is the ionic charge, μ is the dipole moment, and q is the quadrupole moment. In all three relations n is the particle (ions, dipoles, quadrupoles) concentration.

For electric fields produced by ions the normal field strength is given by

$$E_o = 2.61 \cdot en^{2/3} ; \tag{39}$$

i.e., the constant a in equation (38) is equal to 2.61. It is interesting to note here than an electric field E_o', produced by an ionic charge e at a distance $r = r_o$ from the center of the charge, amounts to

$$E_o' = \frac{e}{r_o^2} = e \cdot \left(\frac{4\pi n}{3}\right)^{2/3} = \left(\frac{4\pi}{3}\right)^{2/3} \cdot e \cdot n^{2/3} ,$$

or

$$E_o' = 2.60\ e\ n^{2/3} .$$

This indicates that the effect of multiple ions on the electric field at some point is not significantly different than the field produced as if each ion acted independently.

Holtsmark's theoretical calculations for the probability distribution of the electric field E resulted in the following relations:

$$W(\beta)d\beta = \frac{4}{3\pi}\beta^2 \left[1-0.4628\beta^2 + 0.1227\beta^4 - 0.02325\beta^6 + \ldots\right] d\beta \qquad (40)$$

for small values of $\beta (0 < \beta < 1.7)$, and

$$W(\beta)d\beta = \frac{2.350}{\pi\beta^{5/2}} \left[1 + \frac{5.106}{\beta^{3/2}} - \frac{7.4375}{\beta^3} + \ldots\right] d\beta \qquad (41)$$

for large values of $\beta (1.7 < \beta < \infty)$. In the above equations $W(\beta)$ is the distribution function and $W(\beta)d\beta$ represents the probability that the field strength ratio $\frac{E}{E_o}$ will exist. The distribution functions, $W(\beta)$, have been normalized; i.e.,

$$\int_o^\infty W(\beta)d\beta = 1.0$$

A plot of equations (40) and (41) showing the variation of the distribution function with β is given in Figure 8.

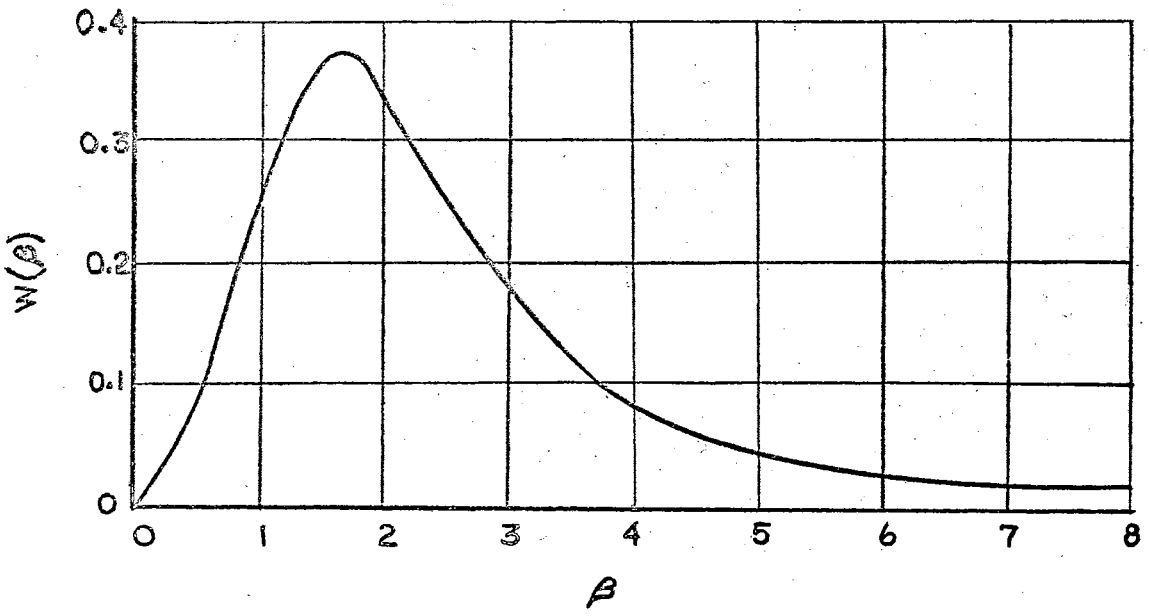

Figure 8. Distribution Function W(β) Calculated by J. Holtsmark (26)(15)

The existence of an electric field at the center of an emitting particle results in a change of frequency of the emitted radiation. A. Unsöld (15) suggested that a "perturbing particle" at a distance r from the radiating atom changed the frequency ν of the emitted radiation according to the relation.

$$\Delta\nu = \frac{C}{r^m} ,$$

where m depends on the interaction among the perturbing particles and C is a constant which accounts for the interaction between the atom and the perturbing particle.

The frequency change of emitted radiation caused by the existence of the electric field can be obtained from the above expression by considering again the field E' produced by an ionic charge e at a distance r from the charge,

$$E' = \frac{e}{r^2} .$$

Solving for $\frac{1}{r^2}$ gives

$$\frac{1}{r^2} = \frac{E'}{e} ;$$

therefore, the frequency change becomes

$$\Delta\nu = \frac{C}{r^m} = C \left(\frac{E'}{e}\right)^{m/2} = C' \left(\frac{E_o\beta}{e}\right)^{m/2} . \qquad (42)$$

The constant C becomes C' due to the change from the single ionic charge electric field E' to the multiple charge field E. The parameter m may have different values. For m = 2, the change in frequency is proportional to β, hence E, and thus corresponds to the linear Stark effect. When

$m = 4$, the frequency change varies with β^2 corresponding to the quadratic Stark effect. The distribution functions $W(\beta)$, as given by equations (40) and (41), were calculated for $m = 2$; therefore, they are valid for the linear Stark effect only.

A homogeneous electric field will cause a splitting of a spectral line into a number of discrete components. Let $\Delta\lambda$ represent the wave length displacement of a component from the original spectral line. Then, in a continually varying electric field the displacement $\Delta\lambda$ of each component will not be constant; it will vary within some limits $\Delta\lambda$ and $\Delta\lambda + d(\Delta\lambda)$. The broadening of the spectral line will appear, therefore, to be continuous.

When the broadening is caused, primarily, by the linear Stark effect (e.g., the spectral lines of hydrogen), the displacement $\Delta\lambda$ is, according to K. Schwarzschild and P. S. Epstein (15), proportional to the electric field strength. For each component k of the spectral line there is a proportionality constant c_k. One may write, therefore

$$\Delta\lambda = c_k \cdot E \ .$$

Since $E = \beta E_o$, one has $\Delta\lambda = c_k \beta \cdot E_o$. For convenience, one defines a new variable α, for the electric field strength, by

$$\alpha = c_k \beta = \frac{\Delta\lambda}{E_o} \ ;$$

then

$$\Delta\lambda = \alpha E_o \quad \text{and} \quad \beta = \frac{\alpha}{c_k} \ .$$

The intensity of a spectral line in the range α, $\alpha + d\alpha$ will be determined by the contributions of the individual components k in this

range. If the relative intensity of component k in a constant electric field is denoted by I_k, then in a variable electric field, its contribution in the above range will be

$$I_k \cdot W(\beta)d\beta = I_k \cdot W\left(\frac{\alpha}{c_k}\right) d\left(\frac{\alpha}{c_k}\right) \quad . \tag{43}$$

In the same range all other components will have a similar contribution and the total line intensity for the range α, $\alpha + d\alpha$ becomes

$$\sum_k I_k \cdot W\left(\frac{\alpha}{c_k}\right) d\left(\frac{\alpha}{c_k}\right) = \sum_k \frac{I_k}{c_k} W\left(\frac{\alpha}{c_k}\right) d\alpha, k=1, 2, 3, \ldots .$$

The intensity distribution of the spectral line is given by

$$I(\alpha) = \sum_k \frac{I_k}{c_k} \cdot W\left(\frac{\alpha}{c_k}\right) = \sum_k \frac{I_k}{c_k} W(\beta_k) \ , \ k = 1, 2, 3, \ldots \tag{44}$$

Thus, in order to evaluate the intensity distribution, a value for α is selected and $\beta_k = \alpha/c_k$ is calculated for the known values of c_k of the components of the line. Then, performing the indicated multiplication and summation, the value $I(\alpha)$ is obtained. The process is then repeated for other values of α.

An application of the theory of Stark broadening was made by P. Dickerman (3). He investigated the plasma produced from water in a water-stabilized arc, and compared the experimentally obtained line profile, $I(\Delta\lambda)$, with the theoretically calculated curves $I(\alpha)$. He made parallel temperature determinations by using the lines H_β and H_γ of the hydrogen Balmer series. The discharge pressure of the plasma was 1 atm., which corresponds to a particle density of 10^{16} to 10^{17} particles per cm^3. The method showed good agreement between the

temperatures obtained by using either the line H_β or the line H_γ, in the range of temperatures from 10,000°K. to 20,000°K.

As mentioned previously, Dickerman used equations (43) and (44), and thus obtained the theoretical curve $I(\alpha)$ for the observed spectral line (H_β or H_γ), Figure 9.

By definition $\alpha = \frac{\Delta\lambda}{E_o}$; therefore

$$\frac{\alpha_1 - \alpha_2}{\alpha_1} = \frac{\Delta\lambda_1 - \Delta\lambda_2}{\Delta\lambda_1} = \Omega \quad ,$$

where Ω denotes the above ratios. A suitable value for Ω was selected making α_2 a function of α_1. To each couple (α_1, α_2) there corresponded a ratio $(I_2/I_1)_{th}$ as obtained from Figure 9. This ratio was plotted, then, versus α_1, Figure 10.

For an arbitrary value $\Delta\lambda_1$ and the selected ratio Ω, the value of $\Delta\lambda_2$ was obtained. The experimental profile, $I(\Delta\lambda)$, was used to obtain the ratio $(I_2/I_1)_{exp}$ for the displacements $\Delta\lambda_1$ and $\Delta\lambda_2$. The quantities α_1 and $\Delta\lambda_1$ corresponded one to the other when

$$\left(\frac{I_2}{I_1}\right)_{th} = \left(\frac{I_2}{I_1}\right)_{exp} \quad .$$

Therefore, the value of α_1 was obtained by using the ratio $(I_2/I_1)_{exp}$ in conjunction with Figure 10.

The "scaling factor" E_o (the normal electric field strength) was calculated from

$$E_o = \frac{\Delta\lambda_1}{\alpha_1} \quad .$$

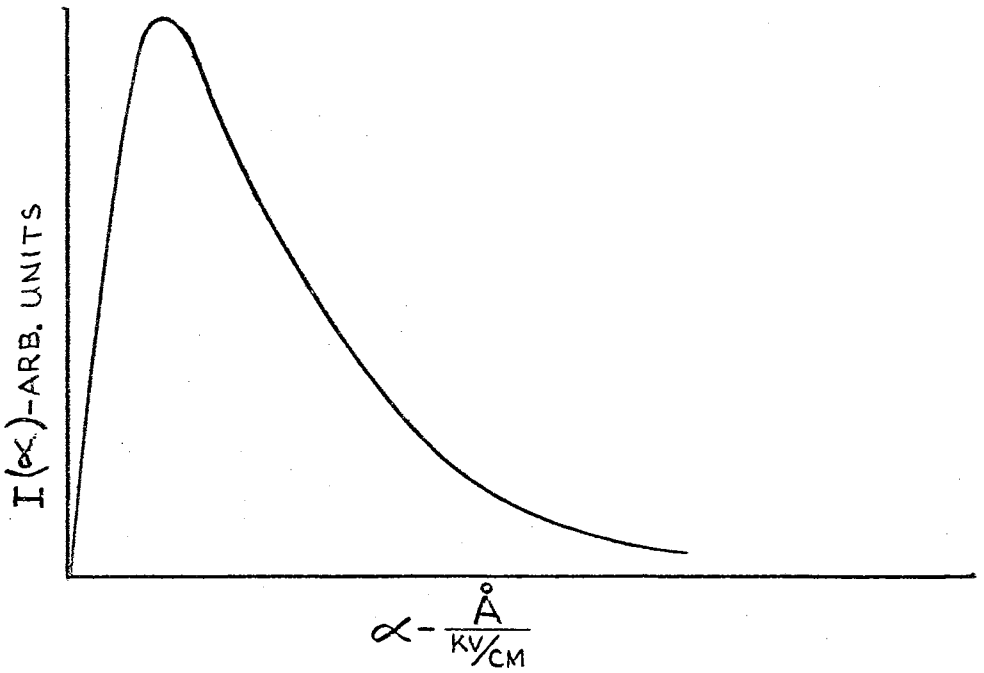

Figure 9. Theoretical Profile of the Broadened Spectral Line (3)

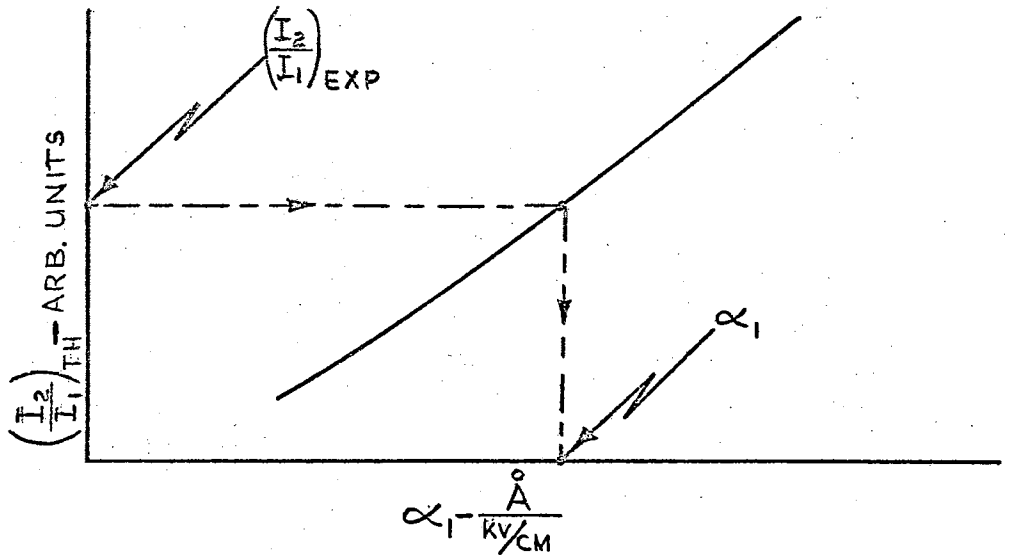

Figure 10. Theoretical Intensity Ratio of the Broadened Spectral Line (3)

The normal electric field strength is equal to $E_o = 2.61\ en^{2/3}$, where n is the ion concentration. This concentration, however, was calculated as a function of temperature, from a system of Saha equations. Then E_o was calculated as a function of temperature for a fixed pressure, Figure 11. With the calculated value of E_o, the temperature T was read directly from Figure 11.

According to Dickerman, the described method can be applied to any plasma which contains some hydrogen. The amounts of hydrogen need not be large, the partial pressure of hydrogen being only one percent of the total plasma pressure. The total pressure, however, must be large enough to provide the necessary conditions for thermal equilibrium.

Both methods described above were based on the assumption that local temperature equilibrium existed within the plasma. Strictly speaking, spectroscopic measurements give indication about the "electron excitation temperature" only. If there is thermal equilibrium among all the particles of a plasma (molecules, neutral atoms, ions and free electrons), any temperature, which can be measured, will indicate the correct plasma temperature. However, if thermal equilibrium does not exist, the measurement of electron excitation temperatures will not serve the above-mentioned purpose. It is, therefore, necessary to check under which conditions thermal equilibrium exists.

The calculations given by Busz and Finkelnburg (28) concerning thermal equilibrium in a plasma are summarized in the following lines:

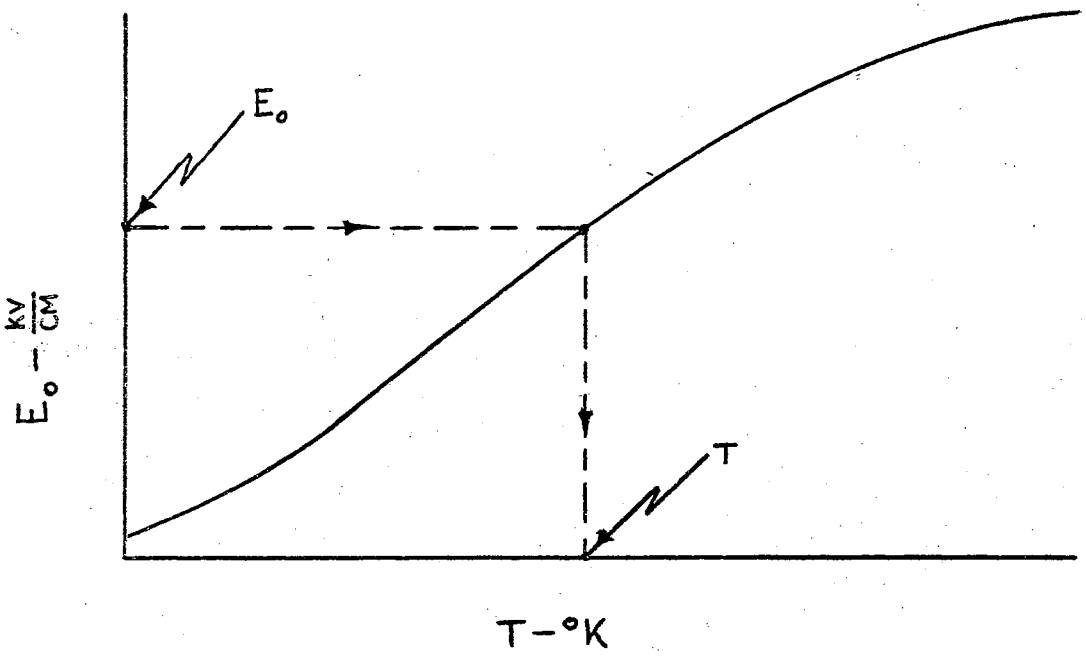

Figure 11. Normal Field Strength versus Temperature (3)

For a Maxwellian velocity distribution the "root-mean-square" speed, v_{th}, of the electrons, due to the random thermal motion, is given by

$$v_{th} = \left(\frac{3kT}{m}\right)^{\frac{1}{2}} ,$$

where m is the electron mass. In addition to the random thermal motion there exists, also, a drift motion caused by the presence of the electric field created by the charged particles in the plasma. The drift-velocity, v_e, is proportional to the electric field strength E, and to the electron mobility k_e; therefore, one may write, assuming a proportionality constant equal to unity,

$$v_e = k_e \cdot E \quad .$$

Knowing the plasma composition (from Saha equations), as well as the collision cross sections of the positive ions, Busz and Finkelnburg have calculated the electron mean free path, λ_e, as a function of temperature. With λ_e known they were able to calculate the electron mobilities and thus obtain the drift-velocity, v_e. Their calculations show that the thermal velocity is, about, one thousand times higher than the drift-velocity, at 30,000°K. This means that in order to cover a distance λ_e, in the direction of the electric field, an electron must suffer about one thousand collisions. Along this distance the electron takes from the electric field the energy $\lambda_e e_o E$, where e_o is the electron charge. According to Busz and Finkelnburg, during a collision an electron can transfer a fraction 2m/M of its own energy to the other particle of mass M, with which it collides.

They state that thermal equilibrium will exist if an electron transfers more energy to other heavier plasma particles, than it takes energy, during the same time interval, from the electric field. At 30,000°K. the average thermal energy of an electron is 4 electron-volt (eV); with the mass ratio $m/M = 1.4 \times 10^{-5}$, the energy transferred in one collision is $4 \times (2 \times 1.4 \times 10^{-5}) = 1.1 \times 10^{-4}$eV. The energy transferred in one thousand collisions is therefore equal to 0.11 eV.

The condition for equilibrium is now

$$\lambda_e e_o E < 0.11 \text{ eV} .$$

At 30,000°K. they have obtained $\lambda_e = 3 \times 10^{-4}$ cm; thus, with $e_o = 4.8024 \times 10^{-10}$ e.s.u.,

$$E < \frac{0.11 \text{ eV}}{\lambda_e \cdot e_o} = \frac{0.11 \times (4.8024 \times 10^{-10} \text{ e.s.u. volt})}{(3 \times 10^{-4} \text{cm})(4.8024 \times 10^{-10} \text{e.s.u.})}$$

or

$$E < 366 \text{ volt/cm.}$$

At lower temperatures the upper limit for the electric field strength increases. Since the electric field strength is usually below this limit, the conditions for thermal equilibrium are satisfied.

Recent Developments in Spectral Line Broadening Theory

The theory of Stark broadening presented in this chapter was developed by Holtsmark early in the twentieth century and published in 1919. (26). In his analysis he considered only the resultant electric field, at the center of the emitting atom, produced by the ions in the plasma. In calculating the distribution function $W(\beta)$ he included the neighboring ions as well as the distant ones. However, the electric

field and the corresponding line broadening produced by the fast moving electrons were not taken into consideration. Also, no interaction among ions and no shielding of ion fields by electron clouds, surrounding the ions, were taken into account. Therefore, many modifications of the Holtsmark theory have been made since. Recently, a theory was developed by H. R. Griem, A. C. Kolb and K. Y. Shen (29).

Griem et al. have developed first the theory of electron broadening; they have used the generalized impact theory taking into consideration the line splitting caused by the Stark effect due to the fields produced by ions.

For the ion interactions and the electron shielding, they used the distribution functions previously developed by G. Ecker (30).

In their impact theory, Griem et al. have classified the electron-emitting atom collisions into the strong, weak and screened ones; the first two classes apply to the electrons within the Debye sphere, and the third one refers to electrons outside of it. They also found the electric field produced by perturbing electrons to be practically hono-geneous and constant at the location of the emitting atom.

Next, they analyzed the fields produced by ions. For the case of strong electric fields, they considered the effects produced only by the ion very close to the emitting atom. Therefore, the distribution function will be proportional to the probability of finding a perturbing ion within a spherical shell, formed by the spheres of radii r and r+dr. In the case of weak fields they used the Debye screened fields instead of Coulomb fields as Holtsmark did. This was done because the

ionic fields are partially shielded by electron clouds around the ions. The interaction between the ions was accounted for by using the method developed by Ecker.

Finally, Griem et al. developed relations for the spectral distribution of combined fields produced by ions and electrons. Since the ions are moving relatively slowly, as compared to the high electron speeds, they assumed that many electron collisions will take place until the electric field, produced by ions, will change. They gave a very vivid description of the electric field around the emitting atom by stating that the electric field will behave "like a random function having rapid variations superimposed on a slowly varying component of comparable amplitude."

As an example, Griem et al. gave a comparison of the results obtained by their theory with the results yielded by the theories of Holtsmark and Ecker. The hydrogen line H_β of the Balmer series was selected for this purpose. As mentioned before, Ecker improved the Holtsmark theory by taking into account the ionic interactions as well as the screening effects; Griem et al. added to this the impact theory of electron broadening. The latter theory is more complete than the preceding ones. A comparison of the calculated H_β-profiles by the theory of Griem et al. and the profiles of the same line, obtained experimentally by P. Bogen (31), showed that the results of theory and of experiment agreed within 10 percent. The results obtained from Holtsmark's theory show much larger deviations.

Stark effect broadening is notably pronounced in the case of the

spectral lines of hydrogen. Also, only small amounts of hydrogen need be present in a plasma to produce measurably broadened lines on a spectrographic plate. For the analysis presented in this thesis small quantities of hydrogen "tracer" were added to an argon plasma jet and the broadened hydrogen lines used for plasma temperature determination. The recent contribution to line broadening theory made by Griem et al. (29) was used in the analysis of the spectrographic results. The details of the analysis applied to specific data is given in Chapter VI.

CHAPTER IV

DESIGN OF THE PLASMA FACILITY AND AUXILIARY EQUIPMENT

A plan view of the OSU Plasma Facility is given in Figure 12. The major components of the facility are the plasma generator and expansion nozzle; power supply; gas supply; vacuum system consisting of test section, tank, heat exchanger, expansion pipe and pump; control and instrumentation panel; and the spectroscopic equipment. Photographs showing the complete facility are given in Plates I, II, III, and IV. All of the equipment except the motor-generator set, the electronic control cabinet for the DC power supply, and a ballast resistor for the power circuit are located in an air-conditioned room of the Mechanical Engineering Laboratory. The area is furnished with storage cabinets and serviced with compressed air, cooling water and 110- and 220-volt 3-phase AC power.

Plasma Generator - Expansion Nozzle Assembly

The plasma generator - expansion nozzle assembly is composed of two separately designed components. A drawing of the complete assembly indicating the two components is shown in Figure 13. The plasma generator was designed and built at Oklahoma State University in the spring of 1959 by Mr. F. McQuiston, a graduate student (1). The expansion nozzle was designed and built in the spring and summer of 1960 by

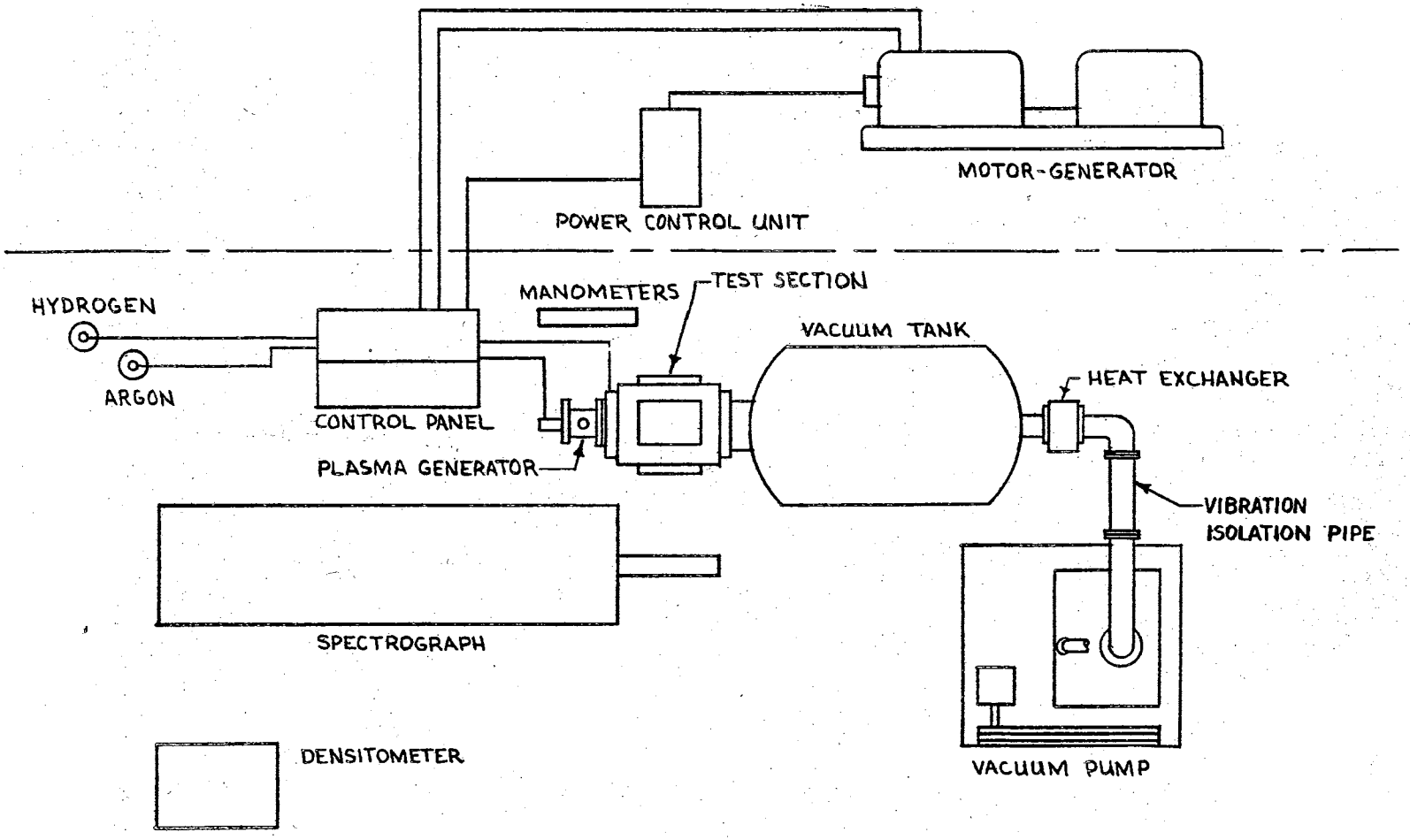

Figure 12. Plasma Facility--Plan View

Plate I

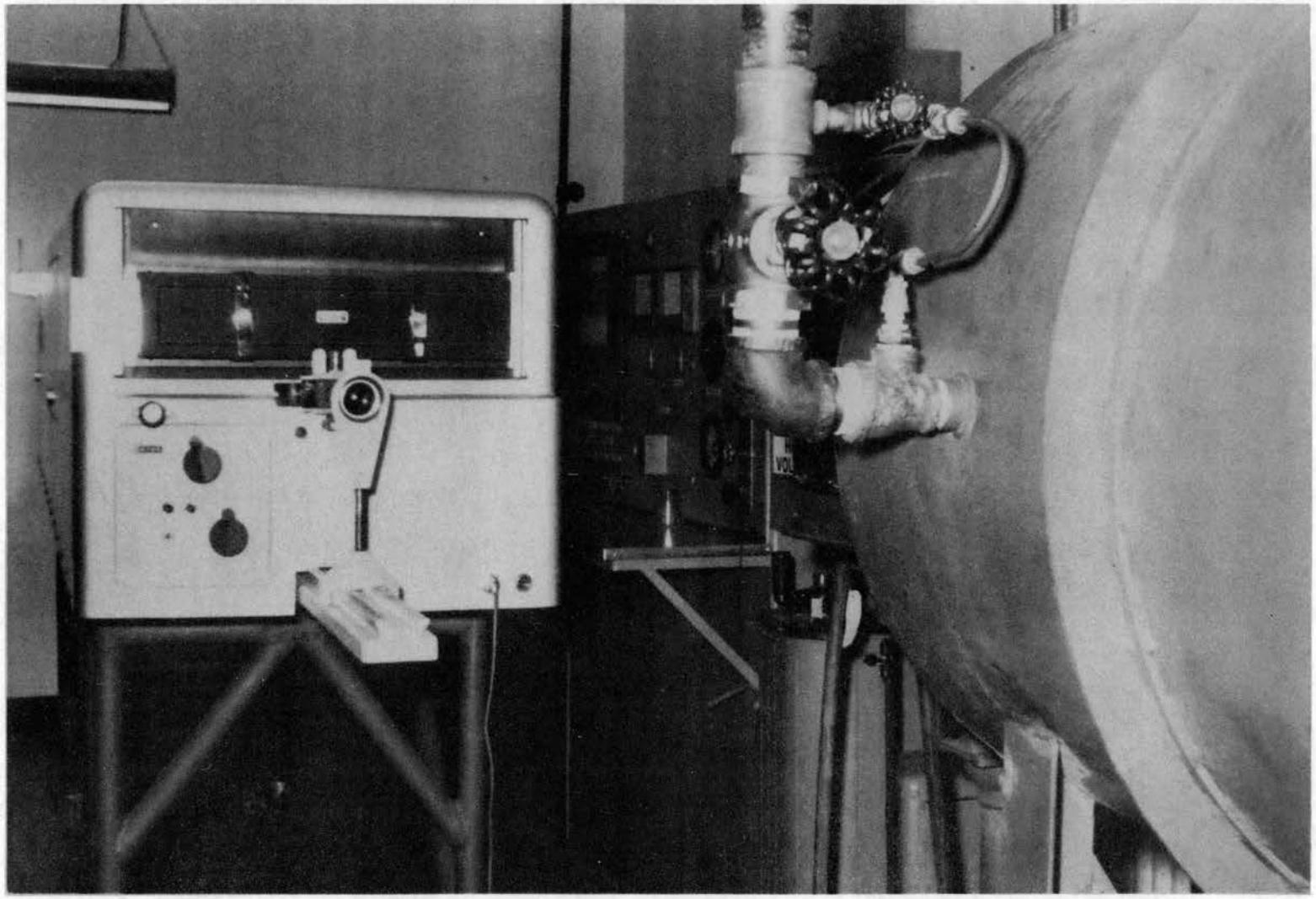

Plasma Facility-Control Area

Plate II

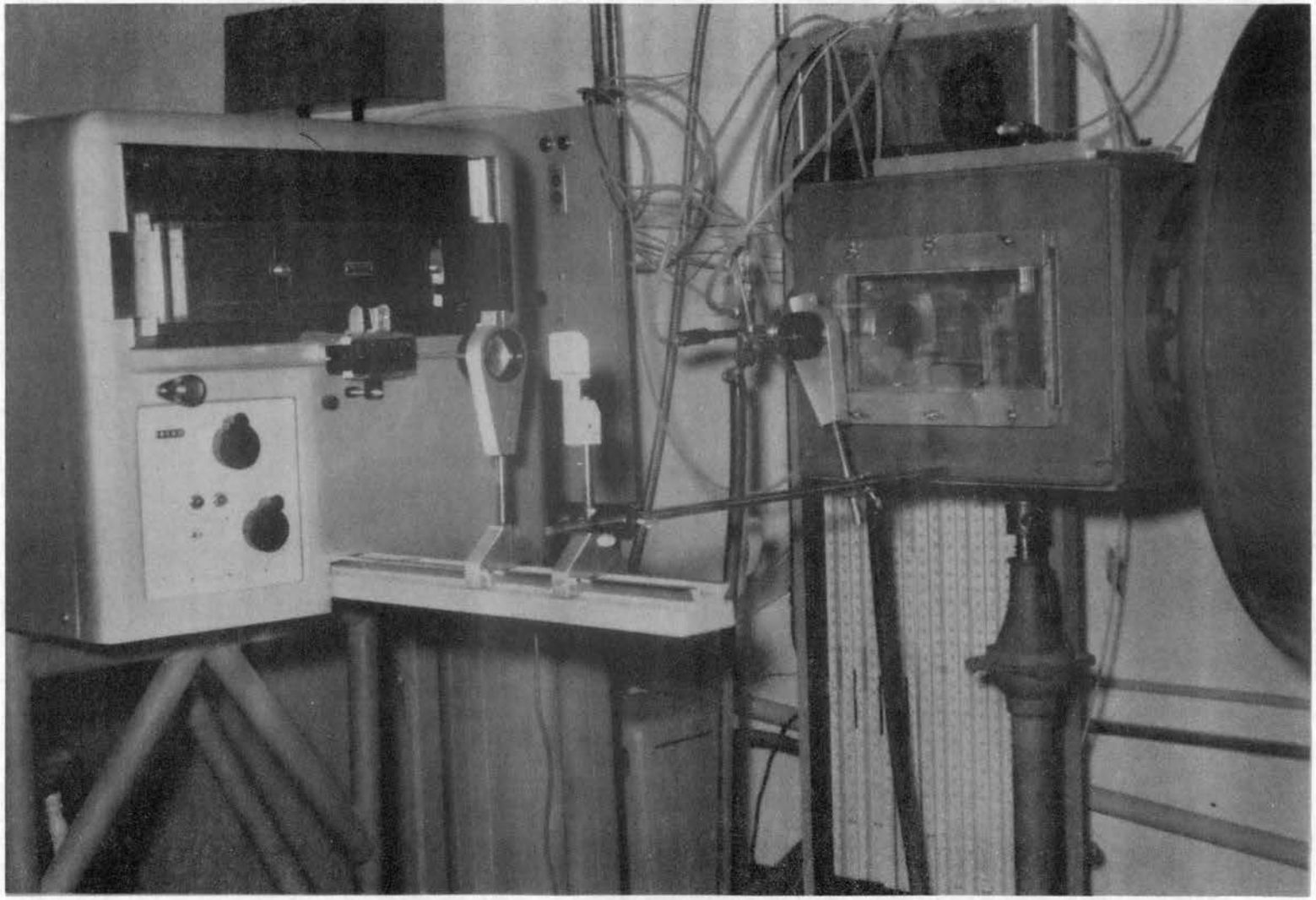

Plasma Facility-Test Area

Plate III

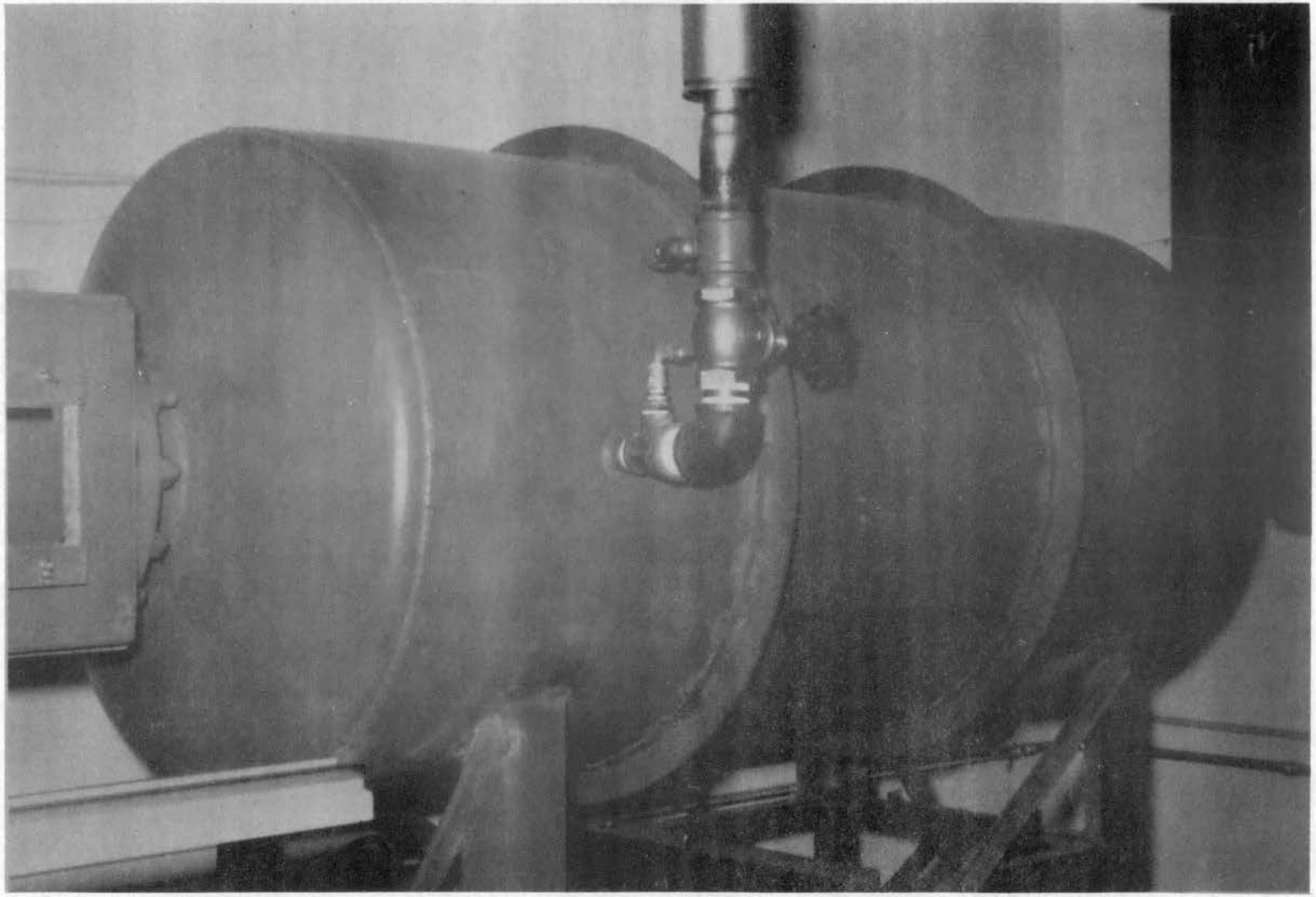

Plasma Facility-Vacuum Tank

Plate IV

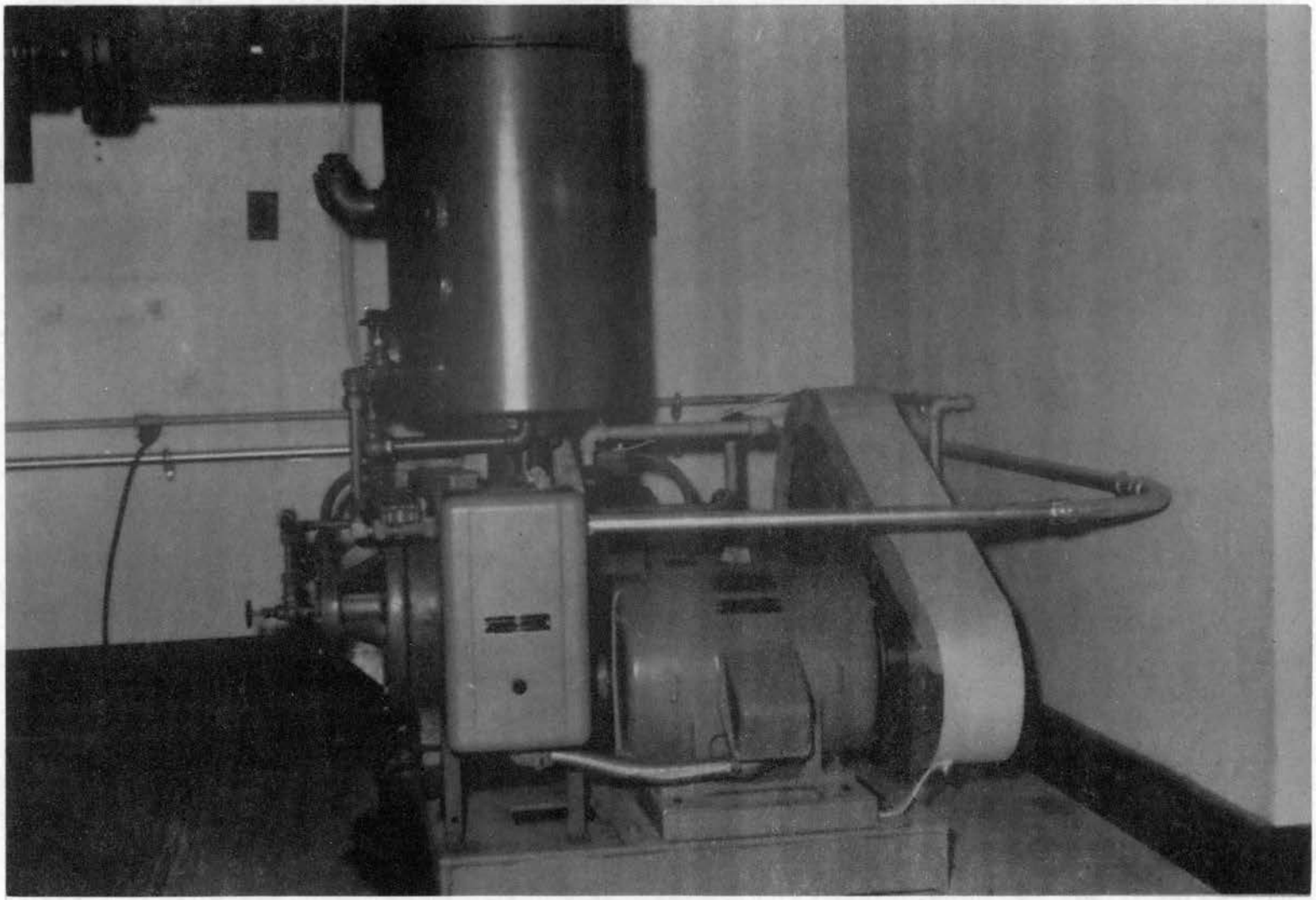

Plasma Facility-Vacuum Pump

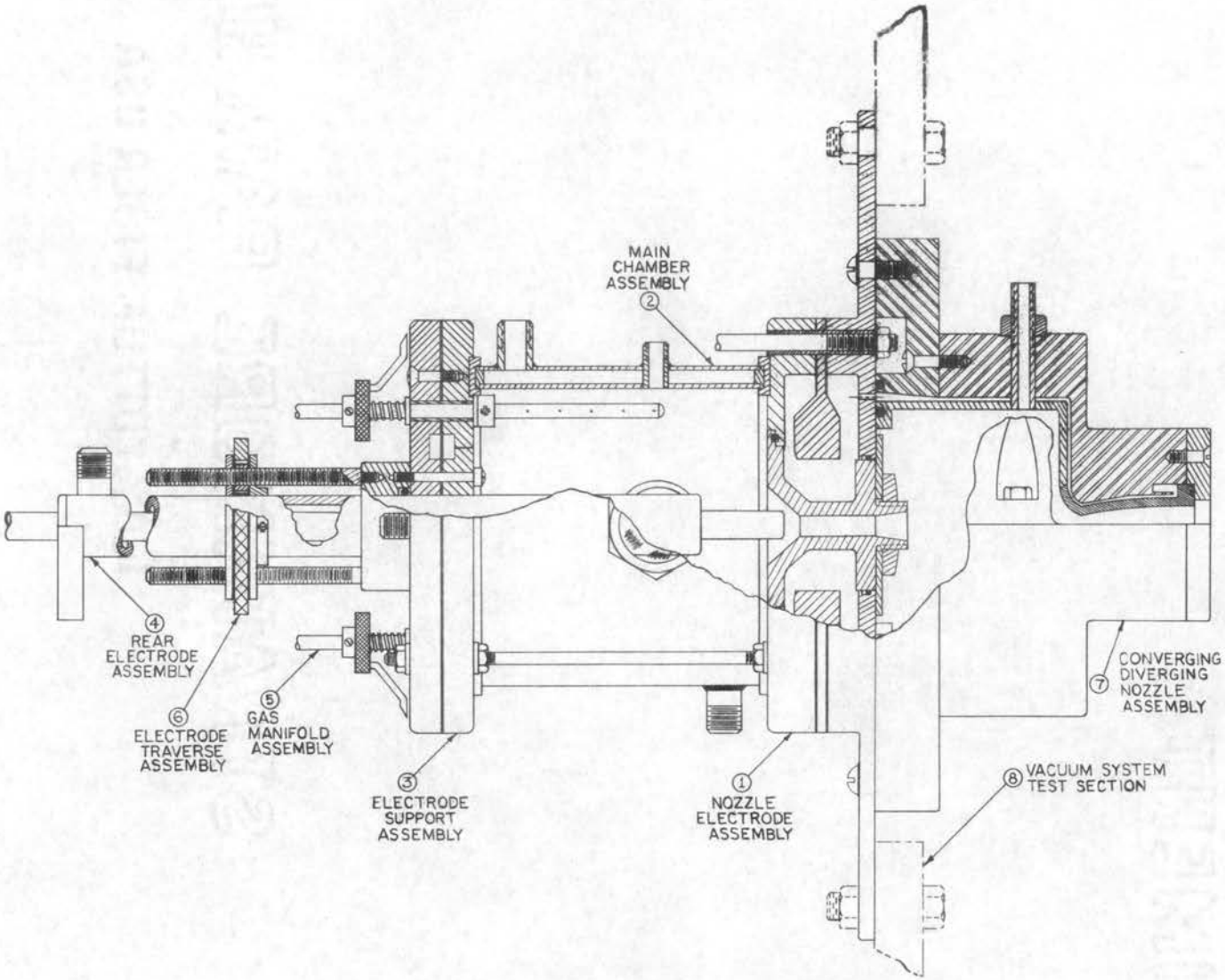

Figure 13. Plasma Generator-Expansion Nozzle Assembly

Mr. M. Burkhart, an honors fellowship graduate student (32). As a part of the expansion nozzle assembly Mr. Burkhart designed a new generator nozzle plate that would connect the plasma generator to the expansion nozzle, and also allow the attachment of the complete assembly to the test section of the vacuum system.

The design of the plasma generator was based primarily on the experience of other investigators in this field. Particularly useful was the design work reported by Messrs. W. Lai, J. Gustavson, and L. Talbot (33). The plasma generator is composed of six assemblies. They are as follows: the main chamber, nozzle, electrode support, gas manifolds, and traversing mechanism. These assemblies are indicated in Figure 13.

The principal function of the chamber is to contain the stabilizing gas. A double-walled cylinder made from steel pipe and tubing was used for the chamber. The annular area at each end was closed by welding and then faced on a lathe to provide a flat smooth surface. The annular space was designed for cooling of the chamber by circulation of water. Accordingly, water inlet and outlet openings were provided in the bottom and top of the chamber. For visual inspection of the rear electrode position, two observation ports were located in the sides of the chamber. A pressure tap into the chamber was provided to allow the measurement of chamber pressure during operation. The ends of the chamber were fitted with phenolic insulating rings to isolate electrically the oppositely charged parts of the plasma generator.

The nozzle assembly consists of a converging nozzle, nozzle support, flow divider, and generator nozzle plate. The nozzle has two functions. It serves as the anode for the arc, and it provides the flow path for the gas through the arc. Serving as one electrode in the power circuit, the nozzle had to be capable of carrying large currents (100-700 amperes) without experiencing electrical resistance heating. Also, the nozzle would be subjected to large heating rates by radiation and convection from the heated gases and would have to be cooled by the circulation of water around the outside of the nozzle. Copper was selected for the nozzle because of its high electrical and thermal conductivity. The original nozzle design by Mr. McQuiston was difficult to machine and the water sealing O-ring at the nozzle exit was damaged by excessive temperatures during preliminary operation of the facility. For these reasons a new nozzle design was made. A comparison of the two nozzles is shown in Figure 14. The nozzle support, flow divider, and generator nozzle plate were made of aluminum. They provide the support for the nozzle, direct the cooling water flow around the nozzle, support the expansion nozzle assembly and provide for the attachment of the plasma generator- expansion nozzle assembly to the test section.

For the electrode assembly a one-percent thoriated tungsten tip was silver-soldered to the end of two concentric copper tubes. This assembly serves as the cathode in the power circuit. Thoriated tungsten was selected for the electrode tip because of its high melting point and its low work function. Again copper was chosen for

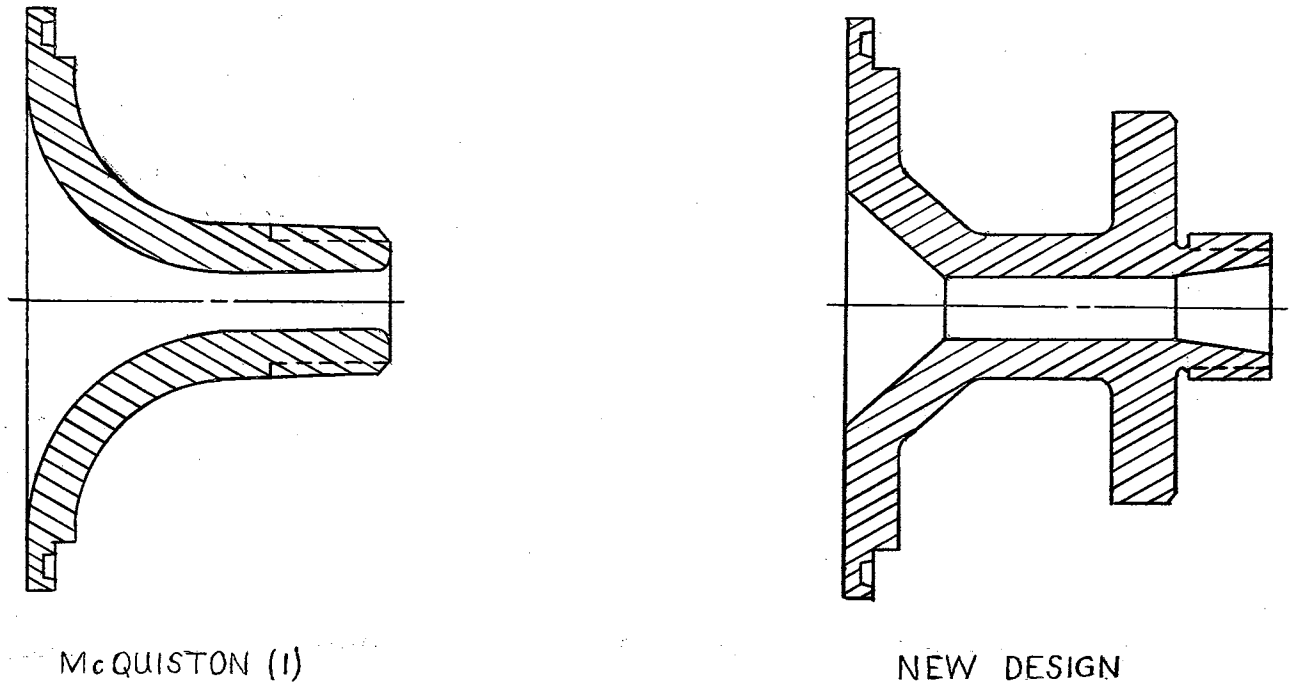

Figure 14. Comparison of McQuiston Nozzle with New Nozzle

the electrode body because its good electrical properties particularly suited it for conducting high current from the tungsten tip out to the power lug which was fastened on the opposite end of the copper tubes. A cooling water passage was formed by the concentric tubes allowing flow of coolant through the inner tube, impingement on the back of the tungsten tip, and thence flow out through the annular area between the two tubes.

The electrode support assembly positions the electrode and guides it along the geometric axis of the plasma generator. This assembly also provides a gas manifold for the injection of gas axially into the chamber, supports two manifolds for tangential flow of gas into the chamber, and closes one end of the chamber. Brass was selected as the material for this assembly because of its excellent machining property. No internal cooling is provided for the electrode support assembly other than the flow of gas through the axial gas manifold. An O-ring seal between the electrode and electrode support prevents gas leakage axially along the electrode into or out of the main chamber.

In addition to the axial gas manifold, which is an integral part of the electrode support assembly, two gas manifolds located diametrically opposite one another are mounted near the periphery of the main chamber. Each manifold consists of a straight steel tube (¼ in. O. D.) into which five small holes (No. 76 drill) are drilled radially with one-half inch spacing along the axis and near one end of the tube. A knurled brass collar is fastened to the other end of the tube and the assembly mounted in the electrode support assembly through a polyethylene bushing. A gas seal was achieved by use of an O-ring seal and a collar

spring arrangement shown in Figure 13. These manifold assemblies were designed such that the injection of gas through the small holes in the steel tube into the main chamber could be adjusted from a tangential to a radial direction with respect to the chamber.

An electrode traversing mechanism was designed to allow a slow, controlled movement of the electrode along the geometric axis of the plasma generator. The axial motion is accomplished by turning the knurled ring (actually an internal gear) which meshes with two small pinions threaded on traversing shafts. The threaded traversing shafts are mounted on the electrode support assembly.

Four ¼-in. diameter bolts were used to combine the six assemblies described above. The bolts were spaced 90 degrees apart around the plasma generator and passed through mating holes in the electrode support and nozzle assemblies. The bolts were electrically isolated from these assemblies by the use of polyethylene sleeves in the bolt holes and fiber washers beneath the nuts used to clamp the end assemblies against the main chamber assembly.

The expansion nozzle assembly was designed to receive the hot gas emerging from the plasma generator, provide a mixing area, and then to accelerate the gas to a high velocity. The components of the expansion nozzle assembly are as follows: the converging-diverging nozzle, mixing chamber, cooling water jacket, nozzle end plate, and the adaptor plate.

The converging-diverging nozzle was machined from a solid piece of copper to form the proper internal contour and to give a nozzle wall approximately 1/8 in. thick throughout. The contour of the nozzle

was determined by the method developed by K. Foelsch (34) using approximate nozzle throat and exit areas which were calculated based on one-dimensional flow relationships and a design Mach number of 3.4 at the nozzle exit. Copper was chosen as the material because of its high thermal conductivity which would make it feasible to cool the nozzle by the circulation of water around the outside of the nozzle. A groove for an O-ring seal was machined in the exit end of the nozzle to prevent water leakage from the cooling passage into the emerging plasma jet. Initially the nozzle was designed with a double press fit into the mixing chamber. However, it was found necessary later to silver-solder these two parts together to stop water leakage into the mixing chamber.

The mixing chamber was made of brass. It was designed to provide an area in which the swirling gas emerging from the converging nozzle of the plasma generator could be mixed before passing through the converging-diverging nozzle. The chamber is sealed against the plasma generator nozzle plate by an O-ring seated in the end of the chamber. The other end of the chamber was machined for a double press fit with the nozzle; but, as was noted above, silver-solder was used to seal positively the juncture of these two parts against water leakage. A pressure tap was provided at the top of the mixing chamber to measure the gas pressure prior to entry into the expansion nozzle. Three small spacers were soldered to the outside surface of the mixing chamber to center the chamber inside the cooling water jacket, thereby insuring the flow of cooling water on all sides of the mixing chamber.

The cooling water jacket is a two-piece aluminum assembly that is fastened together around the mixing chamber and expansion nozzle by four socket head bolts. When fastened together and with the mixing chamber centered by the spacers, a water passage approximately 1/16 inch in width is maintained around the chamber and nozzle. A 1/8-inch wide by 3/8-inch deep groove was cut into the nozzle exit end of the water jacket to allow the cooling water to flow freely from all points around the end of the nozzle. A water outlet tap is located on top of the jacket into this end groove. Four tapped holes were located on the nozzle exit end of the cooling jacket for attachment of the nozzle end plate. On the other end of the jacket six tapped holes were provided for fastening the adaptor plate.

The nozzle end plate was made of aluminum and fastens to the nozzle exit end of the cooling water jacket. A shoulder was machined on the inside face of the end plate to be used for centering the expansion nozzle. When screwed to the cooling water jacket, the end plate seats against the O-ring in the end of the expansion nozzle to prevent water leakage into the emerging plasma jet.

The adaptor plate connects the cooling water jacket to the plasma generator nozzle plate. A circular groove 7/8-inch wide by 1/2-inch deep was provided in the face of the adaptor plate that mates with the generator nozzle plate to allow clearance for the four 1/4-inch bolts used to fasten the plasma generator assembly together. The inside diameter surface of the adaptor plate forms the outer part of the cooling water passage at the beginning of the mixing chamber. O-rings

were located on both faces of the adaptor plate to provide seals against water leakage.

The complete plasma generator - expansion nozzle assembly is mounted on the end of the test section by placing the generator nozzle plate over the six studs welded into the test section. In this position the end of the converging-diverging nozzle extends approximately one-half inch past the back edge of the pyrex windows of the test section, thereby permitting spectroscopic measurements to be made of the plasma jet from the nozzle exit to a position 11½ inches downstream. A photograph of the complete plasma generator - expansion nozzle assembly as it is mounted in the test section is shown in Plate V.

All of the previous operating experience with the plasma generator had been restricted to the condition of atmospheric pressure at the converging nozzle exit and without the expansion nozzle attached. Mr. McQuiston in his work devised a very simple method for initiating the arc between the rear electrode and the converging nozzle. A graphite rod approximately 3/16 inch in diameter and 3½ inches long was connected electrically to one end of a heavy lead wire, and the other end of the wire was connected to the nozzle support. With an open circuit potential of 80-100 volts between the rear electrode and the converging nozzle, the graphite rod was inserted into the throat of the nozzle from the outside and momentarily placed in contact with the rear electrode. The graphite rod, being electrically connected to the nozzle support, was at the same potential level as the nozzle, and therefore an arc was established between the rear electrode and the graphite rod. The graphite rod was pulled slowly out of the nozzle lengthening the arc gradually.

Plate V

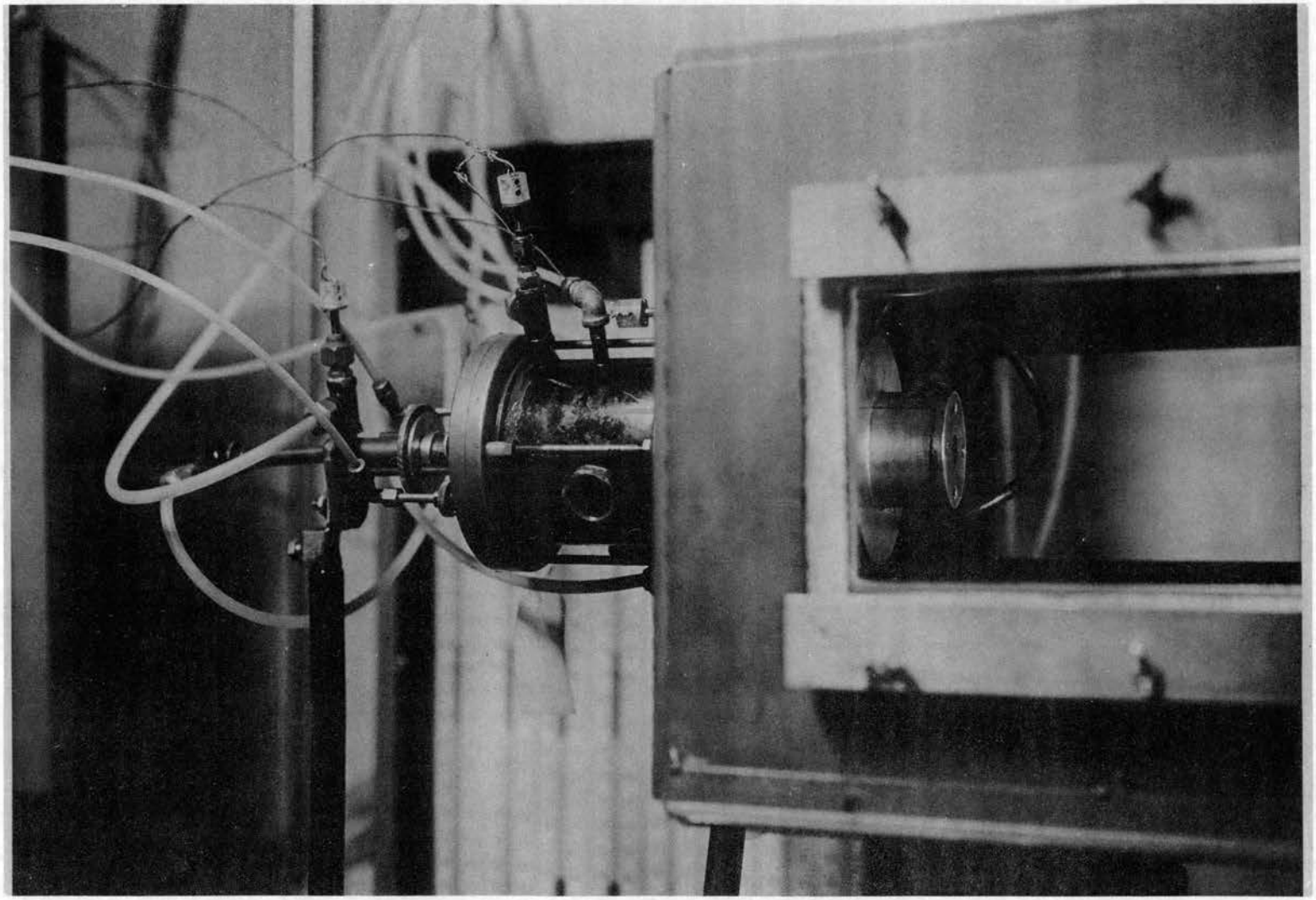

Plasma Generator-Expansion Nozzle Assembly
Installed in Test Section

As the rod was pulled out and away from the nozzle, the arc established itself to the nozzle, and the generator was then in its operational configuration.

With the design of the expansion nozzle and the adaptation of the plasma generator to a vacuum system it was no longer feasible to use the starting technique described above. A new starting system was designed by Mr. E. Killgore, a graduate student, in the summer of 1960. A drawing of the starter assembly is shown in Figure 15. Several starter concepts were considered with the final design being based on the successful results obtained at Northwestern University by Mr. R. Warder who has initiated some work on plasma research in the Department of Mechanical Engineering (35).

The starter assembly consists of a heavily insulated copper lead wire passing at an angle through a brass plug mounted on the lower left side of the main chamber of the plasma generator. A tungsten starter wire is fastened to the copper lead wire by a wire clamp. The brass plug can be rotated around an axis which is a radial line with respect to the main chamber. The insulated wire piece can be moved into and out of the chamber along its own axis with the gas seal being maintained by two O-rings in the brass plug. These motions permit the positioning of the starter electrode tip in relation to the two main electrodes (rear electrode tungsten tip and converging nozzle). The starter assembly is located on the far side of the plasma generator as shown in Plate V and hence cannot be seen. Starting the plasma generator - expansion nozzle assembly is accomplished by positioning

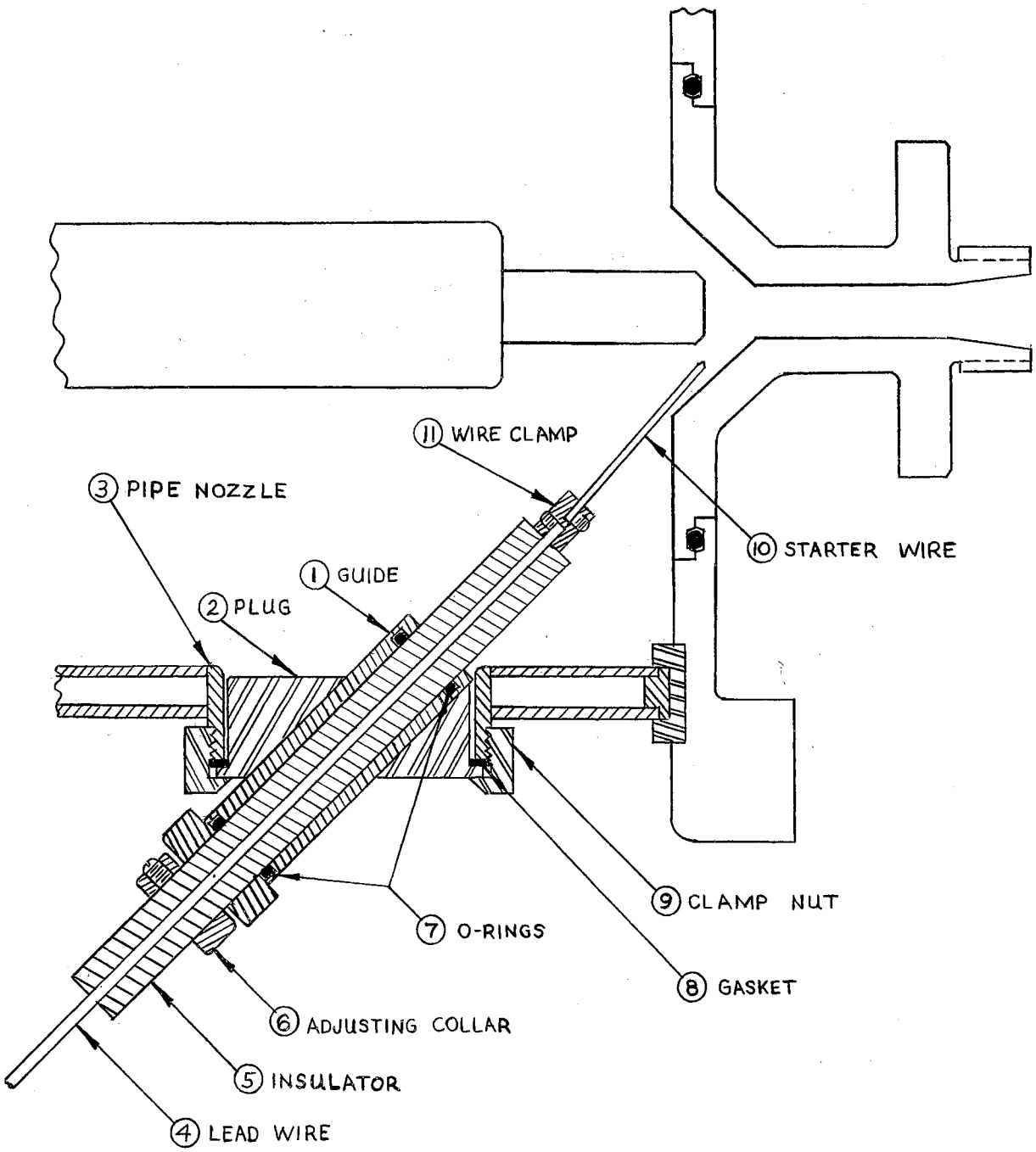

Figure 15. Plasma Starter Assembly

the starter tip close to both the rear electrode and the converging nozzle being careful not to make contact with either one, and then placing a high frequency, high voltage source (Tesla coil) in contact with the outside end of the copper wire of the starter. The high voltage causes breakdown of the gas in the chamber between the starter tip and the main electrodes. After the main arc is fired, the Tesla coil is removed and the starter assembly is pulled back along its own axis to remove the starter tip from the main arc area.

DC Power Supply and Controls

An important feature of the OSU Plasma Facility is the DC power supply system and its associated controls. For several years there has been available in the Mechanical Engineering Laboratory and elaborate General Electric DC dynamometer system for performance testing of internal combustion engines. This dynamometer system is comprised of a cradled DC dynamometer, a motor-generator set consisting of a synchronous motor and a DC generator, and an adjustable voltage control unit. The dynamometer can be used either to motor the test engine by receiving power from the DC generator being driven by the AC motor, or to absorb power from the test engine by delivering power back to the AC line in the reverse manner. In either case, the control unit is used to maintain the system at some fixed operating condition and to prevent overloading any part of the system by excessive current demands. Control of the generator and dynamometer is accomplished by field control of both machines using an amplidyne exciter for each.

The basic features of the control system as it applied to operation

of the dynamometer as a motor driving the test engine will be described. This mode of operation corresponds to the use of the system as a controlled DC power supply for the Plasma Facility. The two functions of the control system are to maintain a constant, selected speed of the engine and to limit the current flowing in the armature circuits of the generator and dynamometer during periods when rapid changes in engine speed are being made.

Consider first the steady condition when a fixed speed is desired. A tachometer-generator, mechanically connected to the dynamometer, supplies a voltage directly proportional to the speed of the dynamometer. This voltage is compared to a reference voltage set by a speed adjustment potentiometer (in reality a voltage selector) on the operator's panel. A closely regulated electronic power supply is used to provide the fixed voltage drop across the adjustment potentiometer, thereby insuring that the selected reference voltage will not vary with time. If the tachometer-generator voltage does not match the reference voltage, the resultant error voltage acts as the input to a four-stage electronic preamplifier. The output from the preamplifier is supplied to a high gain amplifier which controls the field current for the amplidyne exciters. Any change in amplidyne field current will change the output voltage of the amplidyne, and this in turn will change the field current for the main DC generator. In this way the output voltage of the generator is changed, and the effect on the dynamometer will be a change in speed in the proper sense to match the tachometer-generator voltage to the selected

reference voltage.

The high gain system used to maintain dynamometer speed within close limits as described above will result in large changes in generator armature voltage when rapid changes in selected speed settings (reference voltages) are made. Before the dynamometer and test engine can respond to these desired changes, the armature current could change rapidly and become so large that damage to the dynamometer and generator windings could result. Therefore, current limit circuits which continually monitor the armature current are included to protect the DC machines. This is accomplished by taking a voltage drop across a series resistor in the armature loop circuit and comparing it to a current limit reference voltage set by an adjustment potentiometer on the operator's panel. If the voltage drop across the series resistor should exceed the reference voltage (current excessive), the normal error signal voltage from the speed control will be overridden until the armature current is reduced and the series resistor voltage drop is equal to or below the current limit reference voltage. A second potentiometer located in the electronic control cabinet is in series with the current limit adjustment potentiometer on the operator's panel. This second control is set such that the maximum position on the operator's panel unit corresponds to a current limiting value equal to 125 to 140 percent of the rated armature current (700 amperes).

In addition to the speed (voltage) and current limit control aspects of the DC dynamometer system, many protective features are included. The following items will open the main contactor in the armature loop circuit:

1. Motor-generator set overspeed (centrifugal switch on end of generator).
2. Dynamometer overspeed (voltage sensitive relay operating from tachometer-generator).
3. Armature loop circuit instantaneous overcurrent relay.
4. Dynamometer field loss relay.
5. Dynamometer overvoltage relay.
6. Auxiliary starters or main motor-generator set starter.
7. Main contactor stop push button.

After analyzing the operation of the dynamometer control system described above and as a result of correspondence with the General Electric Company, it was decided that by breaking the armature circuit at the dynamometer, and with other small changes in the control circuitry, the power leads on the generator side of the break could be used for a controlled DC power supply system for the Plasma Facility. The changes that were made in the power system will be described in what immediately follows.

A large double-pole double-throw blade switch (LSW) was installed in its own cabinet on top of the electronic control cabinet in the motor-generator, dynamometer area. The power leads from the generator were disconnected from the dynamometer and brought to the center terminals of the LSW switch. New leads were run from the lower terminals back to the dynamometer and another set of leads were run from the upper terminals to the power terminal loop in the Plasma Facility area. With the LSW switch in the down position the motor-generator is connected to the dynamometer as in the original system, and with

it in the up position the dynamometer is out of the circuit and the system now acts as a controlled DC power supply with the power leads terminating in the Plasma Facility area. A safety interlock relay was installed and is operated by the door of the LSW switch cabinet to disconnect power to the amplidynes supplying the generator field voltage when the door is open. In this way, the LSW switch cannot be changed from one position to another while there is a potential on the generator leads to the LSW switch.

The current limit control feature is not affected by disconnecting the dynamometer. The series resistor which supplies the voltage signal to the current limit part of the electronic control of generator field current remains in the armature circuit. However, the voltage signal which came from the tachometer-generator on the dynamometer for use in speed control is no longer used in the power supply system. A new voltage feedback circuit had to be installed for the electronic control unit when the system was to be used as a DC power supply. The voltage to be set was the terminal voltage on the power leads to the Plasma Facility. As there are no resistances, only heavy power leads, from the Facility back to the upper terminals of the LSW switch and again only heavy power leads from the LSW switch back to the DC generator, the voltage feedback signal could be taken from across the DC generator leads in the electronic control unit area.

The actual circuitry is as follows: A small current is taken through two resistors--one fixed and one variable--connected in series across the DC generator leads. The variable resistor is only for initial

adjustment to match the voltage drop across the variable resistor at some value of generated voltage with the corresponding voltage that would come from the tachometer-generator on the dynamometer if the dynamometer were connected and operating at the same control settings. After this adjustment is made, the voltage drop across the variable resistor is always proportional to the generated voltage and is used for the voltage feedback signal.

One additional feature was added to the feedback voltage to insure that it corresponded to the tachometer-generator voltage signal of the dynamometer system. The latter signal was electrically isolated from the generated voltage, whereas the variable resistor voltage was not. Therefore, a signal isolation system was designed. The DC voltage signal from the variable resistor was changed to a proportional AC voltage. This AC voltage was connected to one side of a transformer. The isolated AC voltage from the other side of the transformer was rectified back to a DC voltage for the input signal to the electronic control circuits.

The operator's control panel which is used for dynamometer operation is physically located in the engine test area and could not be transferred easily to the Plasma Facility area. Also, it would have been undesirable to have to move the single control panel back and forth between the two test areas. Therefore, a duplicate of the dynamometer operator's control panel was designed for permanent installation in the Plasma Facility area. The controls that are common to both panels are as follows:

1. Motor-generator start-stop push buttons with indicator lights to show when generator is ready to start (green) and when generator is running (red).

2. Generator field switch to connect output of the generator amplidyne to the field windings.

3. Re-set push button to insure that all safety features are set.

4. Main circuit contactor start-stop push buttons with indicator lights to show when circuit is ready to be closed (green) and when circuit is closed (red).

5. Current limit control rheostat.

6. Coarse and fine voltage control rheostats.

The dynamometer panel has an emergency stop push button that is used to stop the dynamometer--hence, the test engine--very rapidly in case of a serious emergency. This feature is not required for plasma DC power supply operation and is not included in the new control panel. The Plasma Facility control panel has a control selector switch (CSW) that does not exist on the dynamometer control panel. This switch operates a set of relays that connect either the dynamometer panel controls (switch open) or the Plasma Facility controls (switch closed) to the electronic control unit so that only one panel can be used for control at any one time. This CSW switch is also connected to the LSW switch in such a way that with the LSW switch in the dynamometer position the relays cannot close, and only the dynamometer panel can be used for control. With the LSW switch in the plasma power supply position, either panel can be used depending on the position of the CSW switch. In this way, provision has been made for any future requirement for a DC power supply where the dynamometer control panel could be used.

A schematic diagram of the DC power supply system is shown in Figure 16.

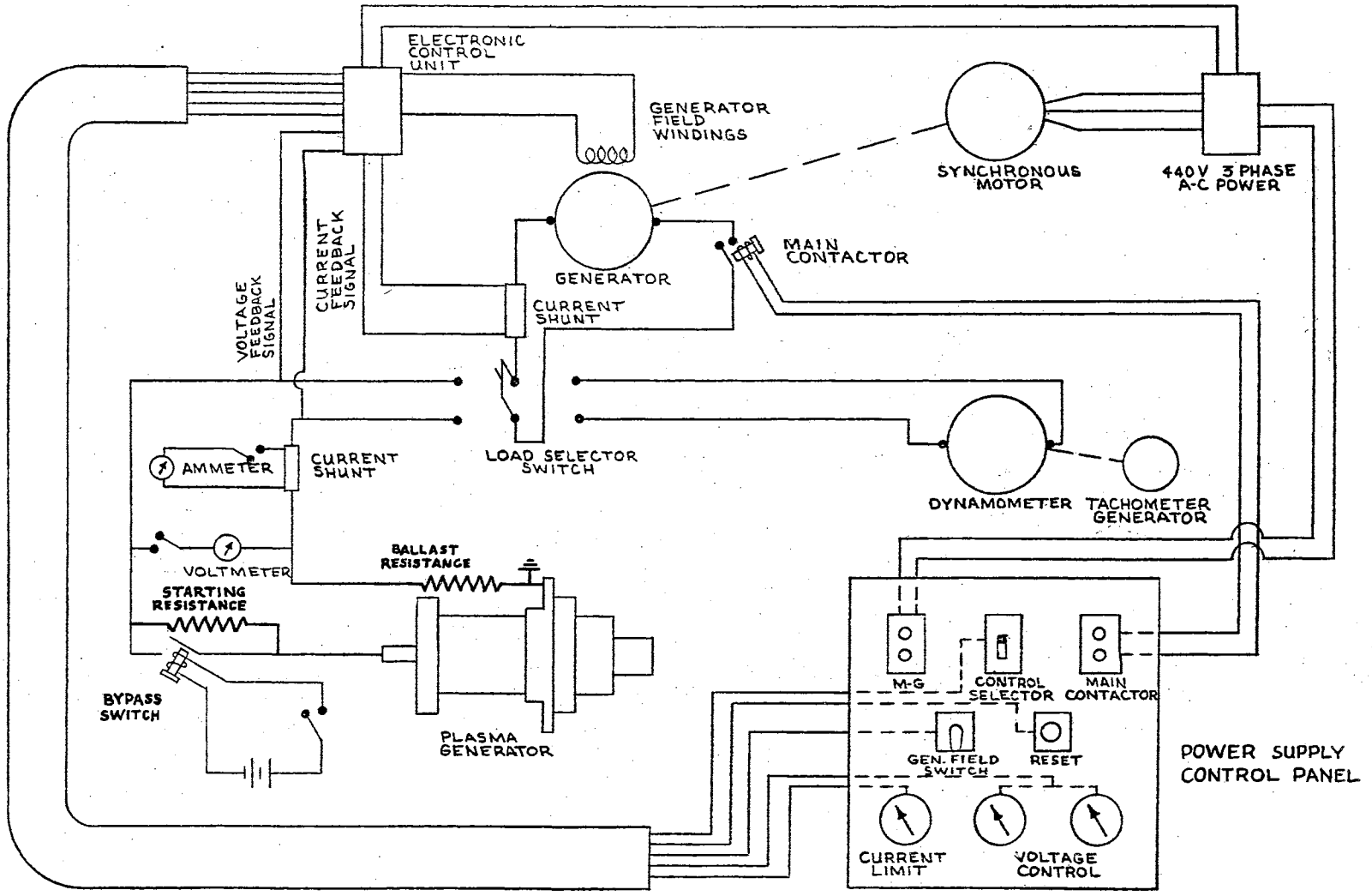

Figure 16. Power Supply System Schematic Diagram

The operator's panel with the respective location of the various controls is also shown in this diagram. The power leads from the generator run to the center terminals of the LSW switch after passing through the main contactor and the series resistor used for the current limit voltage signal. By positioning the LSW switch, the power circuit is connected either to the dynamometer (shown simply) or to the Plasma Facility (shown in detail). In the Plasma Facility the negative lead of the DC power supply is connected to both a starting resistance bank and one side of the starting resistance bypass switch. The variable position side of the starting resistance and the other side of the bypass switch are joined again and bolted to the rear electrode. The positive power lead passes through a current shunt used for the signal to an ammeter on the main plasma instrument and control panel and through a ballast resistor to the nozzle electrode. The nozzle electrode is grounded through the vacuum system.

Initial operation of the Plasma Facility using the DC power supply was attempted without either the starting or ballast resistances. The rapid change in arc voltage-amperage characteristics that occurs when the arc is initiated caused estimated current surges up to 2000 amperes before the electronic control unit could respond. Then the control would over-correct and the arc would go out. These current surges resulted in badly damaged nozzle electrodes. To correct this condition a starting resistance circuit was designed.

The starting resistance bank consists of five parallel resistance units with each unit being a series connection of cast iron grids from

a trolley car starting system. The resistance grids are mounted beneath the vacuum tank (Plate VI). The five units have resistance values of 1, 1, 1/2, 1/4, and 1/8 ohm respectively. The control box from a trolley car is used as a manual switch to connect in parallel each resistance unit as the arc is started. Each successive position of the switch connects the next resistance unit in parallel with the previous ones. Thus, as the switch is moved from off to the first position, the first one-ohm resistance unit is in the rear electrode circuit. The second position of the switch connects the second one-ohm resistance unit in parallel with the first giving an equivalent of one-half ohm in the circuit. The third position connects the one-half ohm resistance unit in parallel with the two one-ohm units giving an equivalent of one-fourth ohm in the circuit. Finally with all starting resistance units connected in parallel, the equivalent resistance in one-sixteenth ohm. A schematic diagram of the starting resistance system is given in Figure 17. With the arc now operating stably, its own resistance is approximately one-fifth ohm and the starting resistance is cut out completely by closing the bypass switch. With this starting system the initial current surges can be limited by selecting the correct equivalent starting resistance to be used with the chosen starting voltage. For example, if 125 volts is to be used for starting voltage and the current surge is to be limited to 250 amperes, the equivalent starting resistance is set at one-half ohm. After the arc is started, the starting resistance is gradually decreased as described above.

Plate VI

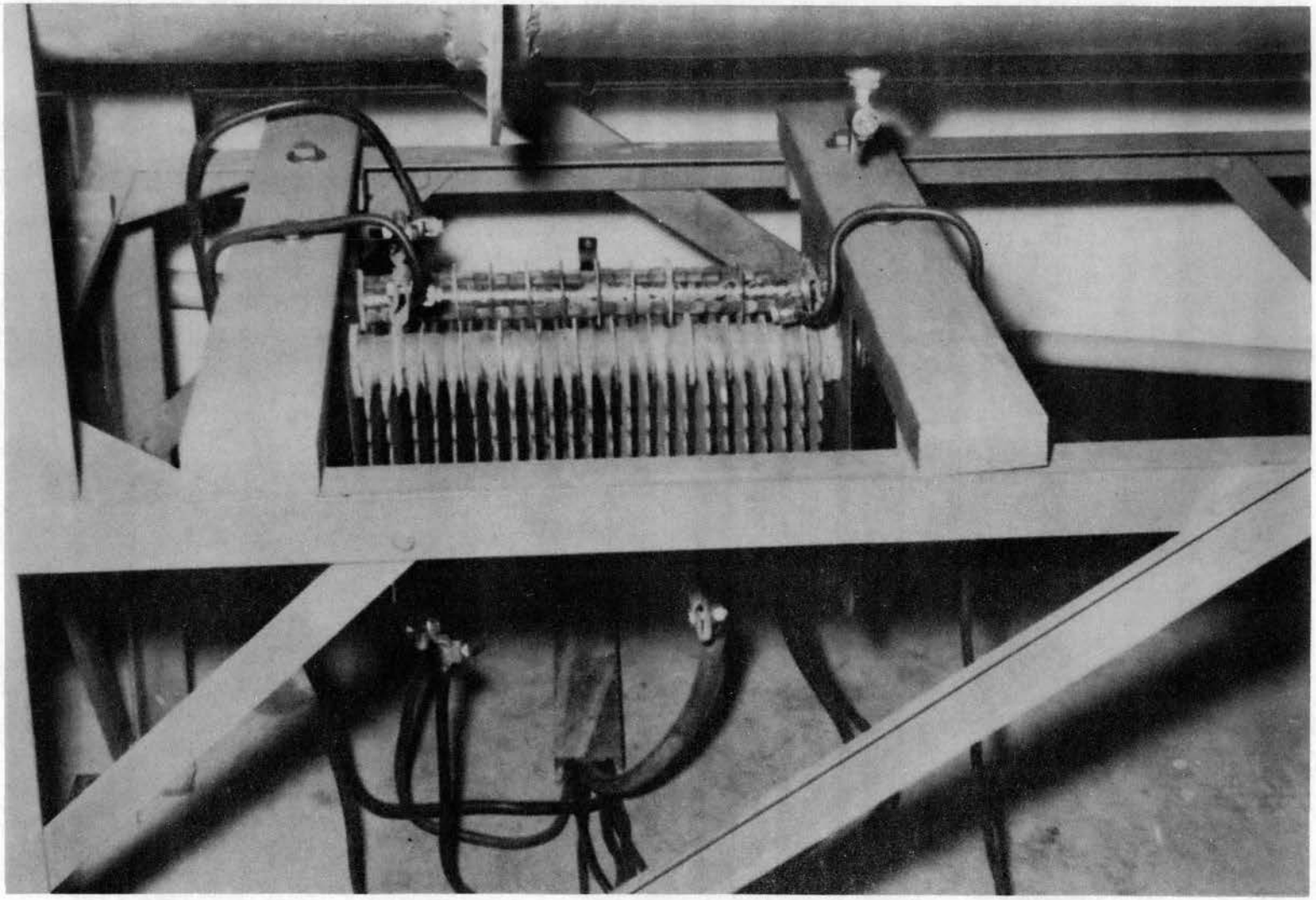

Starting Resistance Unit

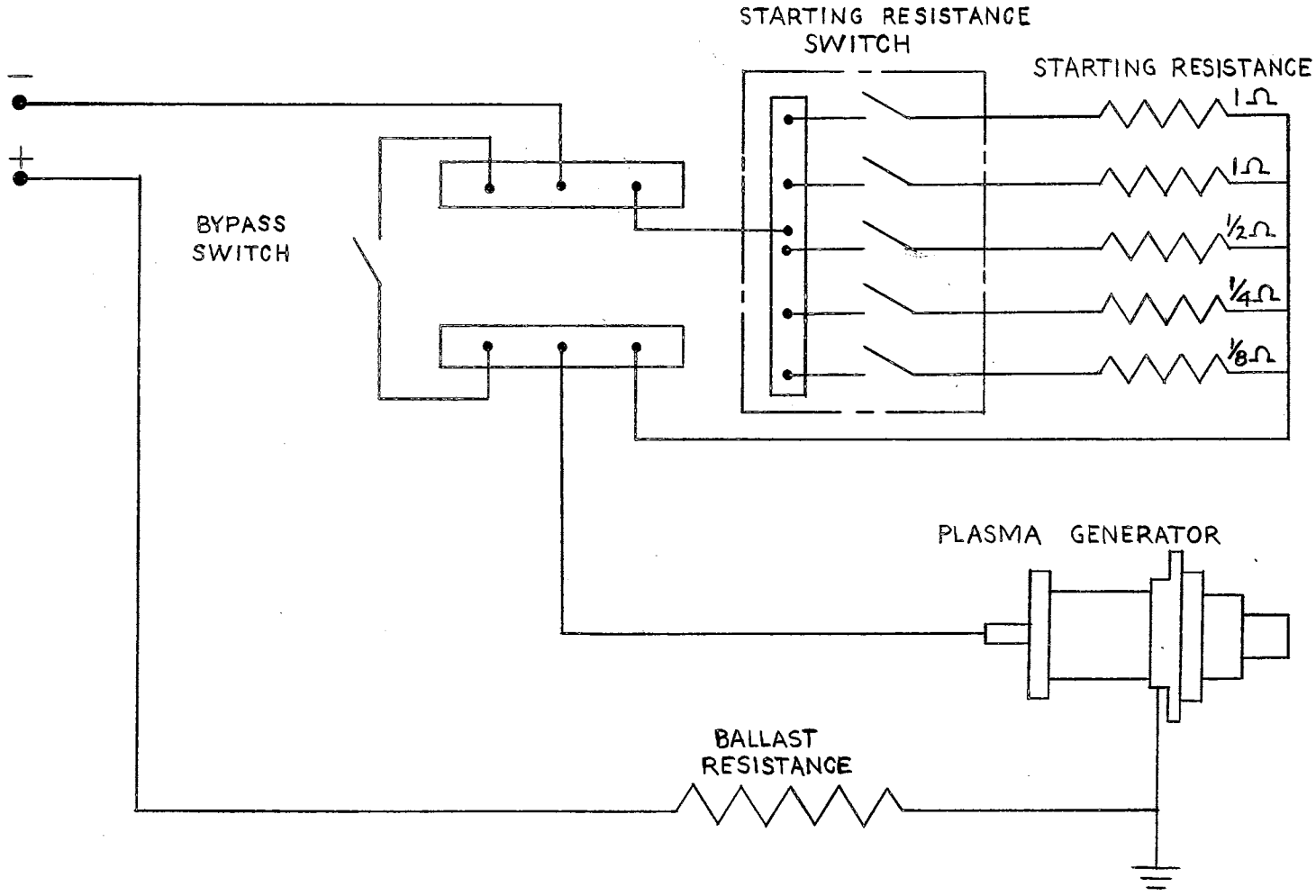

Figure 17. Starting Resistance Schematic Diagram

Prior to adding the ballast resistance to the circuit, the arc resistance was the only load on the DC generator after the starting resistance was bypassed. While operating the arc at atmospheric pressure, the arc fluctuations were small; and the electronic control could maintain a stable arc. However, when attempts were made to operate at reduced pressure, the fluctuations were large enough to result in unstable operation and the arc would not be maintained. Adding the ballast resistance increased the load, hence the voltage output, of the DC generator. Thus fluctuations in the arc voltage requirements were small compared to the total voltage output from the generator and stable operation was again achieved.

The ballast resistance is a parallel arrangement of three resistance units each being a series connection of cast iron grids. These grids are larger than those used for the starting resistance, and each grid is capable of carrying up to 300 amperes continuously depending on the amount of cooling air circulated over it. The equivalent resistance of the parallel arrangement is approximately 0.3 ohm. A large cooling fan is used to circulate air over the grids during operation. The ballast resistance is maintained in the power circuit at all times. The ballast resistance and cooling fan are shown in Plate VIII.

In Figure 16 control wiring is indicated schematically for starting the motor-generator set, closing the field circuit for the generator, closing the main contactor, and adjusting the current limit and voltage reference signals. The voltage feedback signals are also shown for both the voltage and current limit controls. A picture of the motor-generator

Plate VII

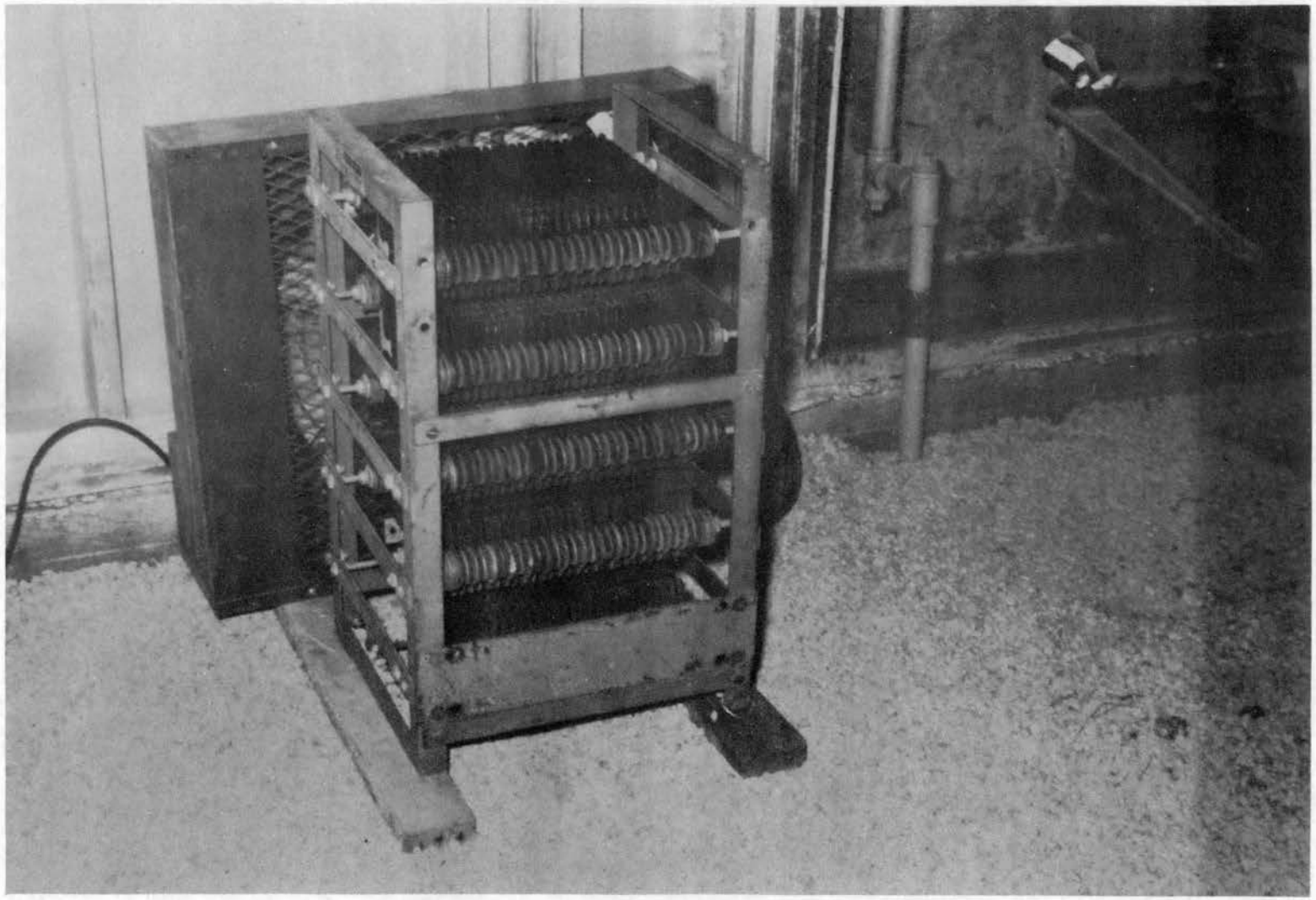

Ballast Resistance Unit and Cooling Fan

set and the main AC power junction box are shown in Plate VIII.

The operational sequence for the DC power supply system to establish the desired open circuit voltage on the plasma generator electrode prior to initiating the arc is as follows:

1. Place LSW switch in DC power supply position (switch up) and close cabinet door securely.

2. Close main 440-volt 3-phase AC power switch on junction box near motor-generator set.

The following operations are made in the Plasma Facility area using the control panel:

3. Close CSW switch on control panel to establish control operation in Plasma Facility area.

4. Start motor-generator set.

5. Put generator field switch in forward position.

6. Push re-set button.

7. If green indicator light is on above main contactor start-stop buttons, close main contactor by pushing the start button.

8. Set open circuit voltage with coarse and fine voltage controls.

9. Set current limit control in the desired position.

10. Making sure that the rear electrode and nozzle electrode of the plasma generator are not in contact, set starting resistance in the desired position.

Prior to utilizing the converted DC power supply system with the plasma generator, the volts-amperes characteristics of the system were determined experimentally for two fixed voltage control settings and variable current limit control settings. These tests were run with a variable resistance load in place of the plasma generator. The voltage control setting was adjusted to give open circuit voltages of

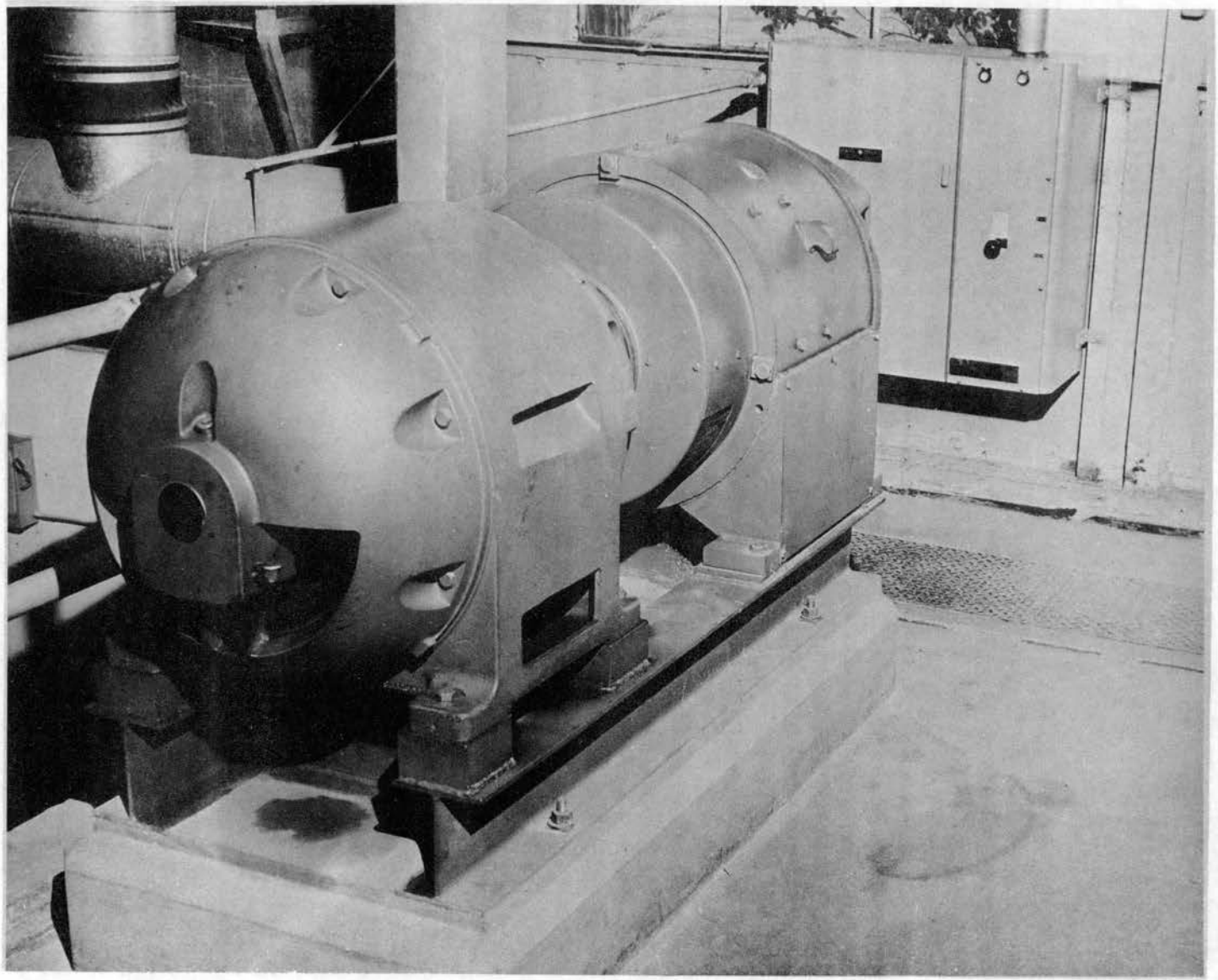

Power Supply Motor-Generator

230 volts and 120 volts. For each open circuit voltage setting, the current limit control was set at various positions from minimum to maximum (0-100 settings), and at each position the variation of load voltage with load current was determined by incrementally cutting out the load resistance to its minimum value. One final data point was taken for each test run by making the load resistance equal to zero. This was done by bypassing all of the load resistance with a fused short circuit.

The results of these tests were plotted and are shown in Figures 18 and 19. The dashed portions of the curves represent an area in which data were not taken. However, the points on the abcissa were actual observed values from the fused short circuit tests; therefore, the dashed lines are interpolations, not extrapolations. The effect of the current limit control can be noted from the sharp drop in load voltage with little change in load current. The strong effect of the current limit control is particularly evident by noting the small change in the short circuit current when the current limit control is fixed and the open circuit voltage changed from 120 to 230 volts. A slight effect on the open circuit voltage results with variation of the current limit control.

Gas Supply and Controls

A gas supply system was designed and constructed to control and measure the flow of gas into the plasma generator. Provision was made to handle three different gases either separately or in combination

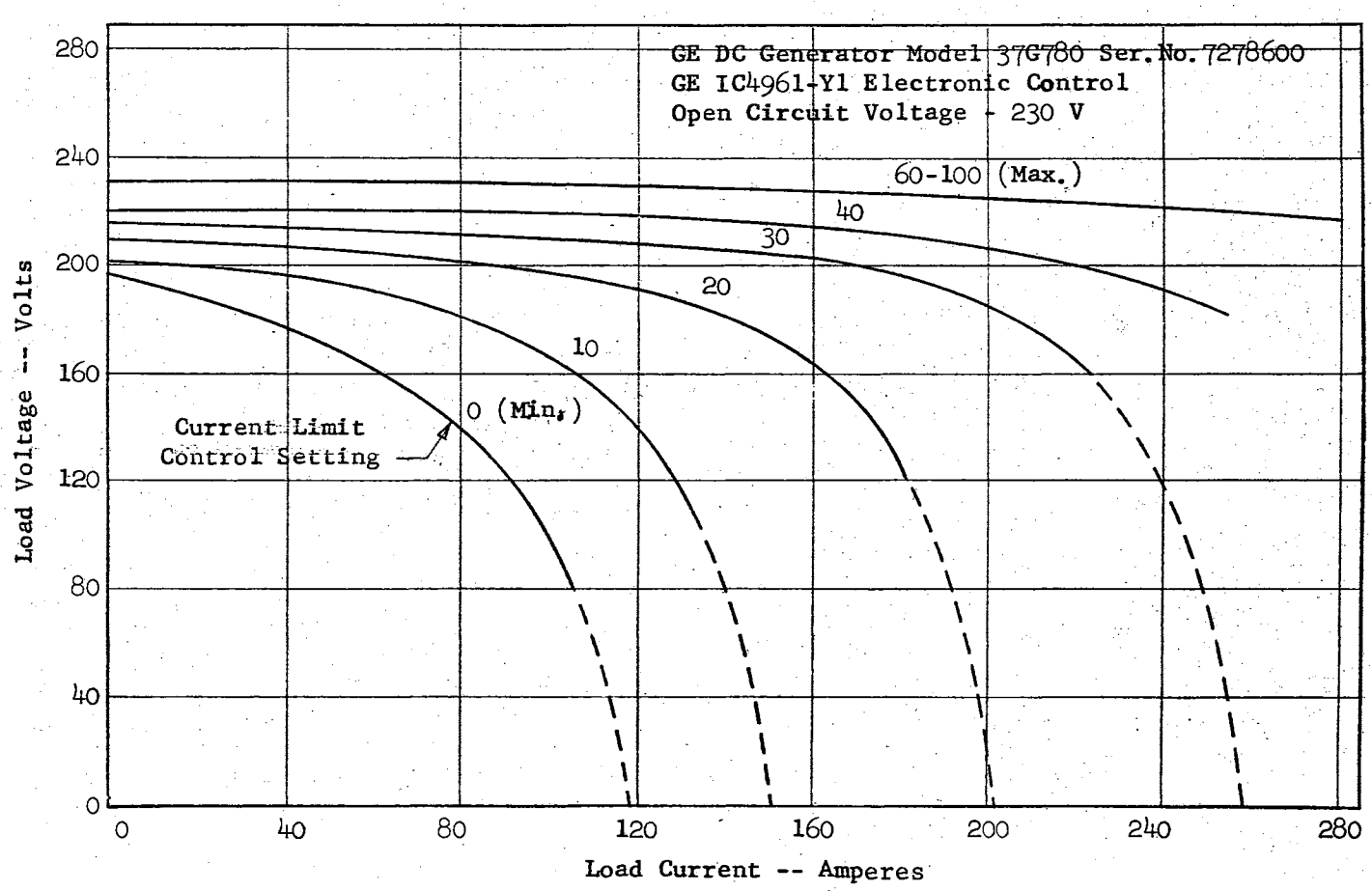

Figure 18. DC Power Supply Volt-Ampere Characteristics I

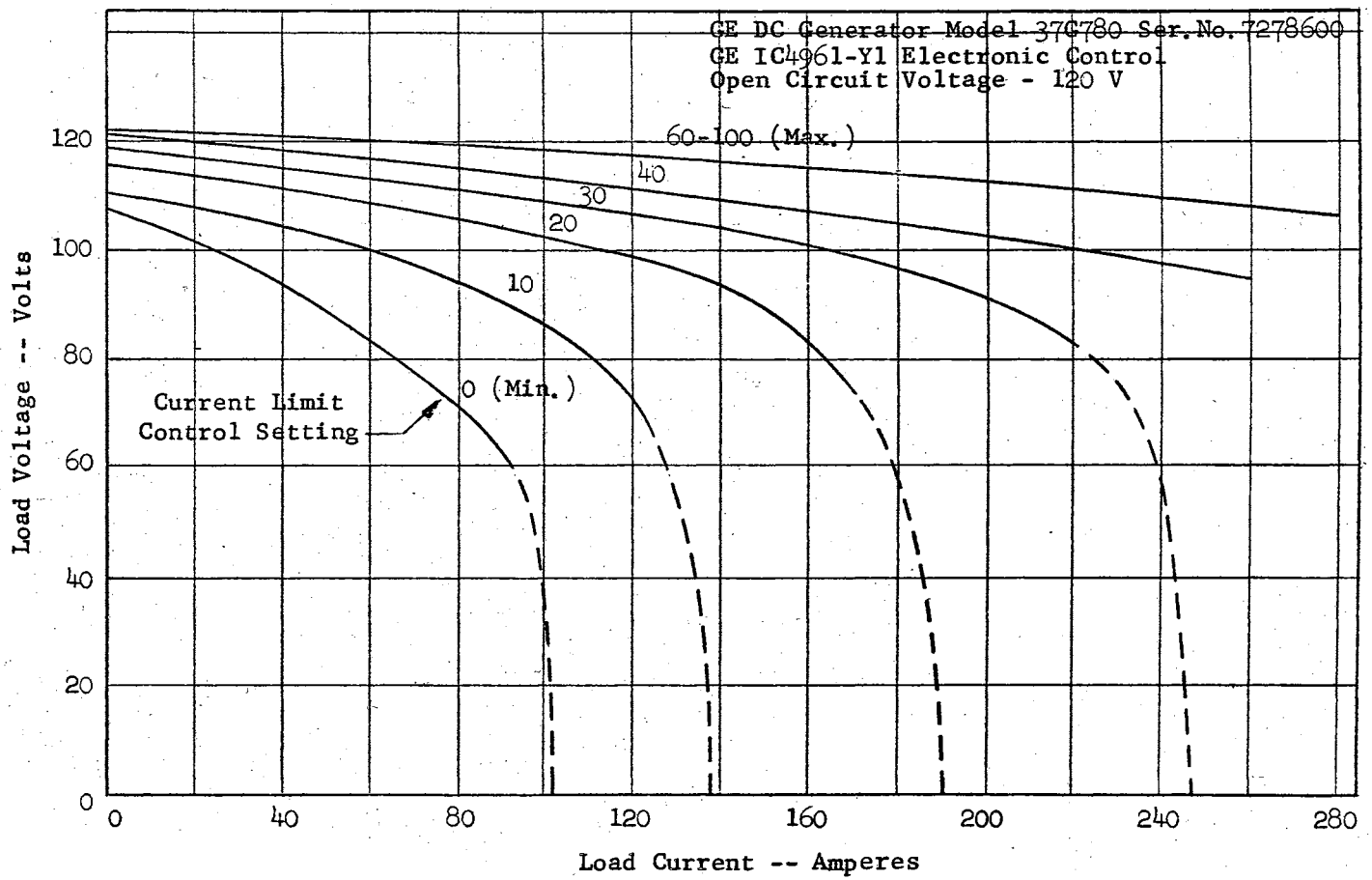

Figure 19. DC Power Supply Volt-Ampere Characteristics II

and to distribute the gas or gas mixture to the three inlet ports (two tangential and one axial) of the plasma generator. A schematic diagram of the system is shown in Figure 20. Only two gases--argon and hydrogen--are indicated in the diagram to correspond to the configuration used for the experimental work reported in this thesis. The flow pattern is from the high pressure gas cylinder through a pressure regulator to the main gas shut-off valve. From the shut-off valve the gas flows through a flow measurement sensing element (a sharp-edged orifice for argon and a Fischer Porter Tri-Flat Variable-Area Flowmeter for hydrogen) and into a gas-mixing manifold. After mixing, the gas then flows to a distribution manifold. There are three needle valves that control the flow from the distribution manifold to the two tangential and one axial gas inlet ports on the plasma generator.

Instrumentation is provided with the gas supply system for the following measurements:

1. Gas supply cylinder pressures.
2. Pressure regulator outlet pressures.
3. Gas pressure and temperature immediately upstream of the flow measurement sensing elements.
4. Differential pressure from flow measurement sensing elements.

Vacuum System

The vacuum system for the Plasma Facility was designed to serve several functions. The principal function of the system is to maintain a constant, low absolute pressure (1-3 psia) at the exit of the plasma

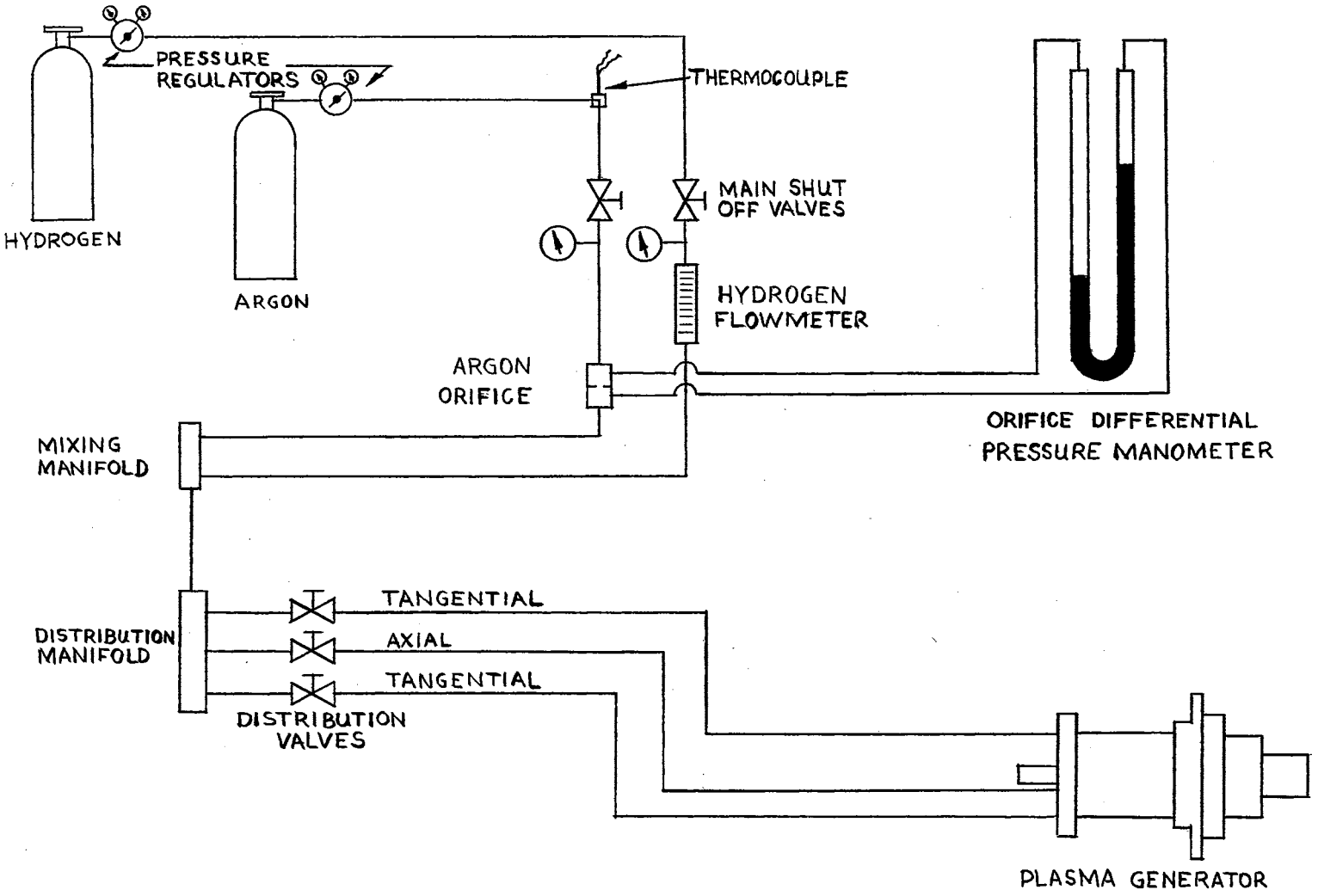

Figure 20. Gas Supply System Schematic Diagram

generator - expansion nozzle assembly. Other requirements are: to provide a test area for experimental work, to cool the plasma before it enters the vacuum pump, and to isolate the test area from the mechanical vibrations of the pump. Included in the vacuum system are a test section, a 45-ft^3 cylindrical tank, a heat exchanger, a 40-in. long section of expansion and vibration isolation pipe, and a vacuum pump. Figure 12, the Plasma Facility plan view, and Plates III and IV show the physical arrangement of the vacuum system equipment.

The test section is a rectangular steel box measuring 16 inches high, 16 inches wide, and 20 inches long. The end plates are 1 inch thick and the top, bottom, and side plates are one-half inch thick. Openings 10 inches in diameter were cut in both end plates and bolts seal-welded into both plates with the thread portion extending outward. At one end the bolts matched the 10-in. diameter flange on the vacuum tank; at the other end the bolts matched the pattern on the plasma generator nozzle plate and were used to fasten the plasma generator - expansion nozzle assembly to the test section. Rectangular openings 6 inches by 12 inches were cut in the top and two side plates for observation windows. Six stud-bolts were located on each of these plates to be used for window mounting brackets. Four 1 x 1 x 1/4 angles were welded into the corners formed at the junctions of the top and bottom plates to the side plates. The end plates were then positioned and the entire assembly was seal-welded along each edge.

Pyrex glass plates 8 inches by 14 inches and 5/8-inch thick were chosen for the observation windows. They are held in place by aluminum window brackets which extend along the long edge of the windows. Rubber

gaskets seat between the window and the test section plate and also between the window and the bracket. By mounting the bracket on the stud-bolts provided on the test section plate and hand tightening the wing-nuts, the bracket clamps the window against the test section. An additional sealing force on the window exists when the test section is under vacuum due to the pressure difference on the window.

A pressure tap is provided on top of the test section and located approximately at the plane of the expansion nozzle exit.

The vacuum tank is a steel cylinder with elliptical end plates. It was available from the Mechanical Engineering Laboratory and had been used previously as a compressed air receiver tank. The tank diameter is 3 feet and the overall length is 7 feet. Two stiffening flanges were welded to the outside of the tank to insure an adequate safety margin for operations under vacuum conditions. The flanges were made by first welding 1/4-in. thick, 2-in. wide steel straps around the tank, and then welding to the straps quarter sections of circular rings cut from 1/4-in. steel plate to extend 2 inches out from the straps. The resulting flange section was in the form of a "T" with the top of the section against the tank. A 10-in. diameter hole was cut in one end of the tank and a 10-in. steel pipe flange was welded to this end. This flange matched the bolt pattern on the end of the test section and was used to fasten the test section to the tank. A 6-in. diameter hole was cut and a 6-in. steel pipe flange was attached to the other end of the tank. The heat exchanger enclosure mounts on this flange.

On one side of the tank, provision was made to adjust the pressure in the test section by controlling the amount of air bleeding into the tank. A 2-in. and a 1/2-in. globe valve were connected in a parallel circuit to an opening in the tank. For rapid changes in pressure or bleeding down the system, the 2-in. valve is used. The 1/2-in. valve is used to make small adjustments in the test section pressure. A muffler was installed on the bleed line to reduce the noise level during bleed down operation. Another opening at the bottom of the tank was fitted with a small valve to be used as a drain outlet.

The vacuum tank is supported on a steel frame stand which is bolted to the concrete floor. The stand was adapted from an available table frame. Heavy 4 x 4-in. angles were welded to each corner of the frame extending upward to support the tank. The tank was welded to these angles. Stiffening braces of channel section were added to the sides and ends of the stand to help dampen any tank vibration caused by the vacuum pump and not eliminated by the vibration isolation pipe. The tank stand and pump were mounted on separate concrete floors to help reduce the transmission of pump vibrations through the building foundation. A single pedestal support having a hand-adjustable jack as its top member was used to support the weight of the test section.

The hot gas from the plasma generator - expansion nozzle assembly is partially cooled as it passes through the vacuum tank by radiation and convection to the tank walls. To provide additional cooling and insure that the gas entering the vacuum pump is nearly at room temperature, a finned-tube heat exchanger was mounted on the outlet side of

the vacuum tank. Cooling water is circulated through the tubes and the gas flows over the fins. Other plasma installations have been operated without this additional cooling device; therefore, no attempt was made to base the design on theoretical analysis. Instead, the condensing heat exchanger from a refrigerator was used. The face dimensions of the unit are approximately 8 inches by 11 inches and its depth in the flow direction is approximately 3 inches. There are two water circuits in the unit. One circuit consists of eight passes of a single copper tube all in one plane. The other circuit has twelve passes of a single copper tube in a staggered arrangement in two planes. The water inlet and outlet connections were made such that either or both of the circuits can be used depending on the amount of cooling required.

The heat exchanger is enclosed in a rectangular steel box measuring 11 inches wide, 11 inches high, and 4 inches thick in the gas flow direction. Six-inch diameter holes were cut in both end plates, which are one-half inch thick. These holes match the outlet flange on the vacuum tank and the flange on the pipe from the heat exchanger to the pump. Again, as with the test section, bolts were seal-welded in the end plates to match the mounting holes on these flanges. The top, bottom and side plates were made from 1/4-in. steel plate. The bottom and sides were seal-welded to the end plates. The heat exchanger was fastened to the top plate by extending the cooling water inlet and outlet tubes through the plate and soldering them in place. The top plate-heat exchanger assembly then was placed in the open top box, and the top plate secured in place by 1/4-in. machine bolts. A gasket

seal was used between the top plate and the mating surface of the box. A drain hole with plug was provided on the bottom plate of the enclosure.

Nominal 6-in. steel pipe was used from the heat exchanger to the vacuum pump. A 40-in. long section of this piping was of a bellows type construction. This section of flexible pipe was chosen to take up any misalignment between the tank and pump, to allow for expansion of the system, and to damp out the pump vibrations from the tank and test section. This last function was particularly important so that spectroscopic measurements could be made of the plasma jet at a known, fixed location with respect to the expansion nozzle exit plane.

The vacuum pump selected for the Plasma Facility was a Model KDH-220 Single Stage - Duplex Design, High Vacuum Pump made by the Kinney Manufacturing Company. Two eccentric rotary pistons acting 180° apart draw the low pressure gas into the compression area, compress it to a pressure above atmospheric and discharge it through a valve deck into the oil reservoir on top of the pump. The gas rises through the oil tank and passes out the top through a standard 3-in. steel pipe to the atmosphere outside the building. A swirling passage for the gas to escape the oil tank provides a centrifugal separation of the entrained oil so that it falls back into the tank.

Two small openings are provided at the pump inlet. One of these is used for a pressure tap and the other is used for a thermocouple station to check the gas temperature entering the pump. This measurement of gas temperature provides a check on the cooling capacity of the heat exchanger and prevents damage to the vacuum pump from excessive operating temperatures.

Control Instrumentation

The Plasma Facility has been provided with instrumentation for the following measurements: Power input to the plasma generator; cooling water inlet and outlet temperatures and flow rates for each cooling circuit; gas inlet temperature and flow rate for each gas being used; gas temperature entering the vacuum pump; and gas pressures in the main plasma generator chamber, the expansion nozzle mixing chamber, the test section, and the vacuum pump inlet. These instruments are used in the control of the Plasma Facility.

The DC power input to the system is calculated from the measurement of arc voltage and arc current. A Weston meter with a range from 0-250 volts is used to measure the generator output voltage. A Triplett meter with a range from 0-50 volts is used to measure the arc voltage. This latter meter is the one indicated in Figure 16. Also shown schematically in Figure 16 is the ammeter. An 800 ampere-50 millivolt shunt is used in conjunction with a Triplett ammeter to measure the current.

The cooling water circuits are shown in Figure 21. Those circuits passing through the plasma generator - expansion nozzle assembly were traced previously in the description of that assembly. Cooling water is supplied to the heat exchanger and distributed to the two internal circuits by a manifold arrangement on the inlet side. Control of the water flow through each of the internal circuits is accomplished by manual valves in the outlet lines from the heat exchanger. After passing through these valves the two lines are again brought together and a single line returns to the control panel and thence to the drain.

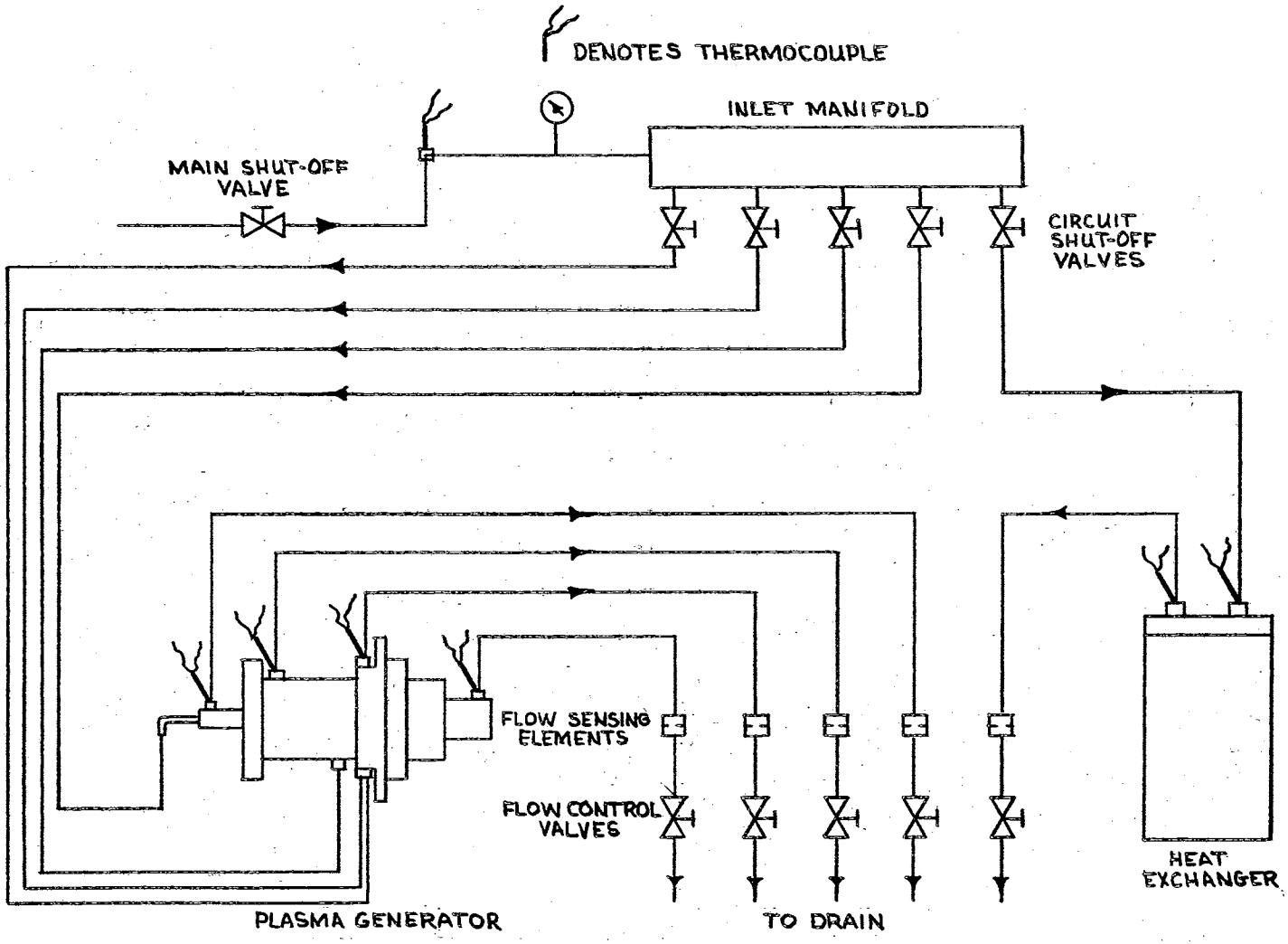

Figure 21. Cooling Water System Schematic Drawing

The flow pattern through each of the five main cooling water circuits is essentially the same. The water flows from the building supply line through the main shut-off valve to a manifold assembly behind the control panel. A thermocouple is located in the manifold to measure the inlet water temperature to all circuits. The water pressure in the manifold is also measured to insure a positive water supply during operation. From the manifold the water passes through a circuit shut-off valve and thence to the inlet ports on the equipment to be cooled. An additional thermocouple is provided at the heat exchanger inlet port to check the water inlet temperature at this location. After flowing through the cooling passages of the equipment, the water returns to the back of the control panel. The water outlet temperature is measured for each circuit by thermocouples located in the flow as it leaves the cooling passages.

The return water flow from the cooled equipment passes through an orifice meter for flow rate measurement and then to a needle valve used for controlling the flow rate. From the needle valve the water flows to the drain. A sharp-edged orifice is used in each circuit as the primary element for measuring the water flow rate. The pressure differential across the orifice is measured by a U-tube manometer using Meriam Blue Indicating Fluid which has a specific gravity of 1.75.

Positive water pressure is maintained in the cooling passages of each circuit by fully opening the main water shut-off and circuit shut-off valves and controlling the flow by the needle valves which are located on the outlet side of the cooled equipment.

Instrumentation is provided for the measurement of the gas flow rates and inlet temperatures into the plasma generator. The schematic diagram of the gas supply system shown in Figure 20 indicates the location of this instrumentation. For the argon gas supply a sharp-edged orifice was chosen as the primary element with a well-type manometer filled with Meriam Unity Fluid (specific gravity of 1.0) used to measure the orifice differential pressure. Argon temperature and static pressure were measured just upstream of the orifice to be used in determining the density of the argon at the orifice. This orifice had been used by Mr. McQuiston, and a description of its construction and calibration is given in Reference 1.

The hydrogen flow rate is designed to be approximately one to three percent by volume of the argon flow rate. A Fischer Porter Tri-Flat Variable Area Flowmeter is used for flow measurement. The hydrogen gas inlet temperature is assumed to be equal to room temperature since the flow rate is very low.

All of the temperature measurements were made using iron-constantan thermocouples and a Brown, Type 153 x 65, Electronik Multipoint Recorder. This instrument has provision for ten thermocouples, has an automatic standardization cycle every thirty minutes, and has automatic reference junction compensation. A summary of the recorded temperatures is given in Table II.

Pressure instrumentation was provided to measure all differential pressures across the flow measurement primary elements and to measure the gas and water static pressures throughout the system. A summary of the location where the pressure measurements are taken is given in Table III.

TABLE II

TEMPERATURE INSTRUMENTATION LOCATIONS

Thermocouple Number	Thermocouple Location
1	Water Inlet Manifold
2	Open
3	Rear Electrode Water Outlet
4	Open
5	Converging Nozzle Water Outlet
6	Converging-Diverging Nozzle Water Outlet
7	Heat Exchanger Water Outlet
8	Argon Gas Inlet
9	Main Chamber Water Outlet
10	Vacuum Pump Gas Inlet

TABLE III

PRESSURE INSTRUMENTATION LOCATIONS

Pressure Measurement Number	Pressure Measurement
1	Converging Nozzle Water Flow Rate Orifice Differential
2	Converging-Diverging Nozzle Water Flow Rate Orifice Differential
3	Main Chamber Water Flow Rate Orifice Differential
4	Rear Electrode Water Flow Rate Orifice Differential
5	Heat Exchanger Water Flow Rate Orifice Differential
6	Inlet Water Pressure
7	Argon Static Pressure at Flow Rate Orifice
8	Argon Gas Flow Rate Orifice Differential
9	Hydrogen Static Pressure at Flowmeter
10	Main Chamber Pressure
11	Expansion Nozzle Mixing Chamber Pressure
12	Test Section Pressure
13	Vacuum Pump Inlet Pressure

A schematic diagram of the complete instrument and control panel is given in Figure 22. At the left are the five U-tube manometers for the water flow rate orifice differential pressure measurements. Located to the right of these are the temperature recorder (top) and the circuit shut-off and needle control valves for the water circuits (bottom). Farther to the right at the center of the control panel are the power instruments--two voltmeters, ammeter, and starting resistance bypass switch. At the bottom center are the vacuum pump start-stop push buttons. Next to the right are the gas controls and the water and gas inlet pressure gages. The shut-off valves for the gases are at the bottom and the distribution valves to the plasma generator are at the top. To the right of the gas controls is the power control panel which was described earlier. Beneath the power control panel is the starting resistance switch. Finally there are at the extreme right the manometers for gas flow rate orifice differential pressure and the four static pressures from the plasma generator main chamber to the vacuum pump inlet.

Spectroscopic Equipment

Research work with the Plasma Facility requires spectroscopic analysis of the high velocity, high temperature gas emerging from the plasma generator - expansion nozzle assembly. A Jarrell-Ash, Model 71010, 3.4 meter, Ebert-mounted plane grating spectrograph was selected for this application. A semi-portable stand was fabricated of welded steel pipe construction to support the spectrograph

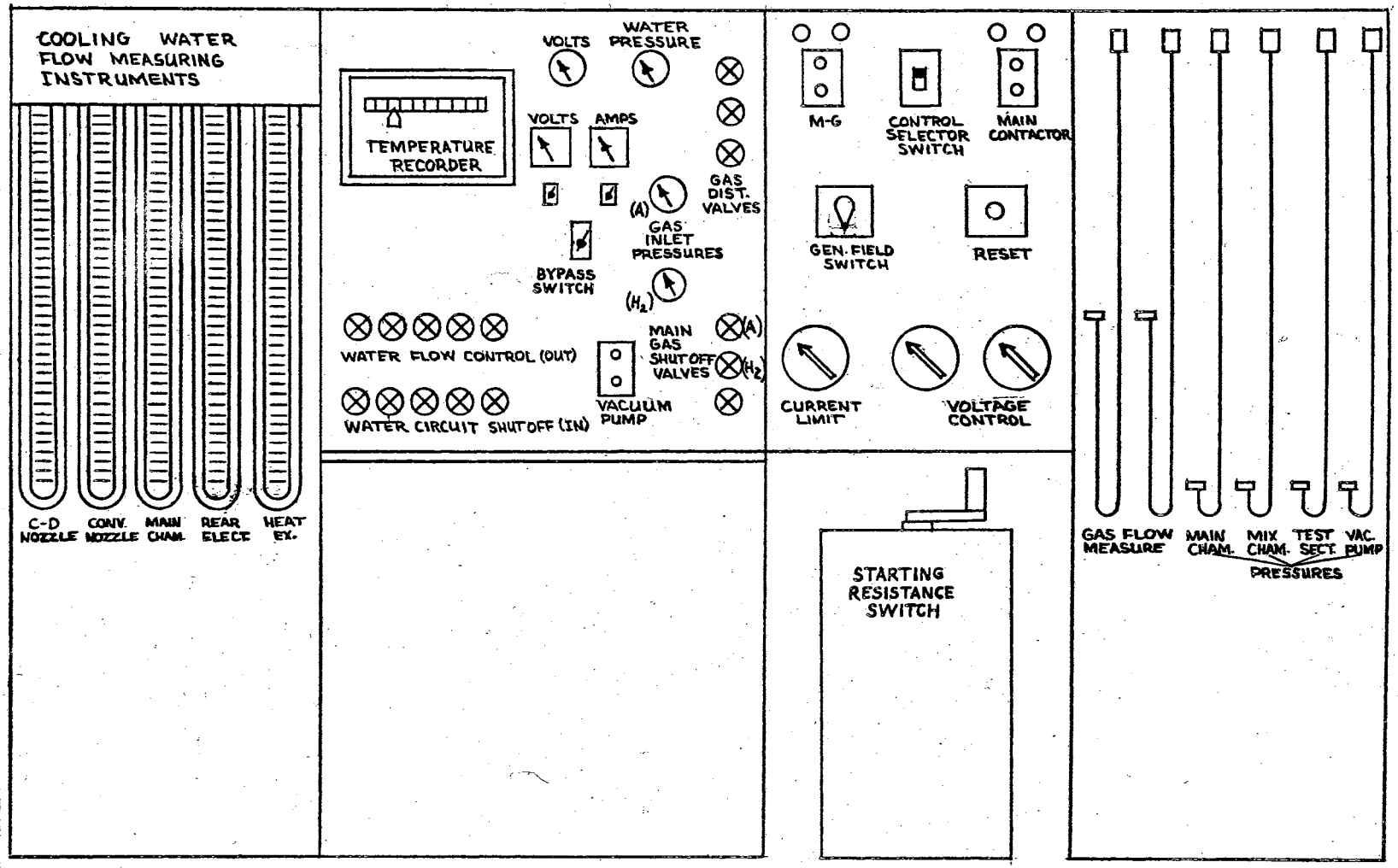

Figure 22. Instrument and Control Panel Schematic Diagram

and to place the center of the entrance slit at the same height as the centerline of the plasma jet. The spectrograph was located with respect to the plasma generator and test section as shown in Figure 12. With this arrangement, an image of a vertical section of the plasma jet can be focused on the entrance slit by suitable lenses and a right angle mirror.

A schematic diagram of the optical system is shown in Figure 23. Two lenses are used in the system. The lens nearest the test section is located such that the centerline of the jet is at the focal point of the lens. The emitted light from the jet is rendered into parallel rays by this lens. These parallel rays strike a right angle mirror mounted on the accessory bar of the spectrograph and are re-directed, still in parallel rays, toward the entrance slit. A second lens is located between the right angle mirror and the entrance slit with the slit at the focal point. This lens serves to focus the parallel rays into an image on the entrance slit. Both lenses used in the optical system are coated achromatic type lenses.

Figure 23 also indicates the internal optics of the spectrograph. The light entering the slit passes under the grating to a collimating mirror at the opposite end of the spectrograph. The light reflecting from this mirror strikes the grating (plane reflecting type) and the spectrally dispersed light returns to another mirror located just above the collimating mirror. This second mirror brings the spectrum into focus on a photographic plate located just above the entrance slit of the spectrograph.

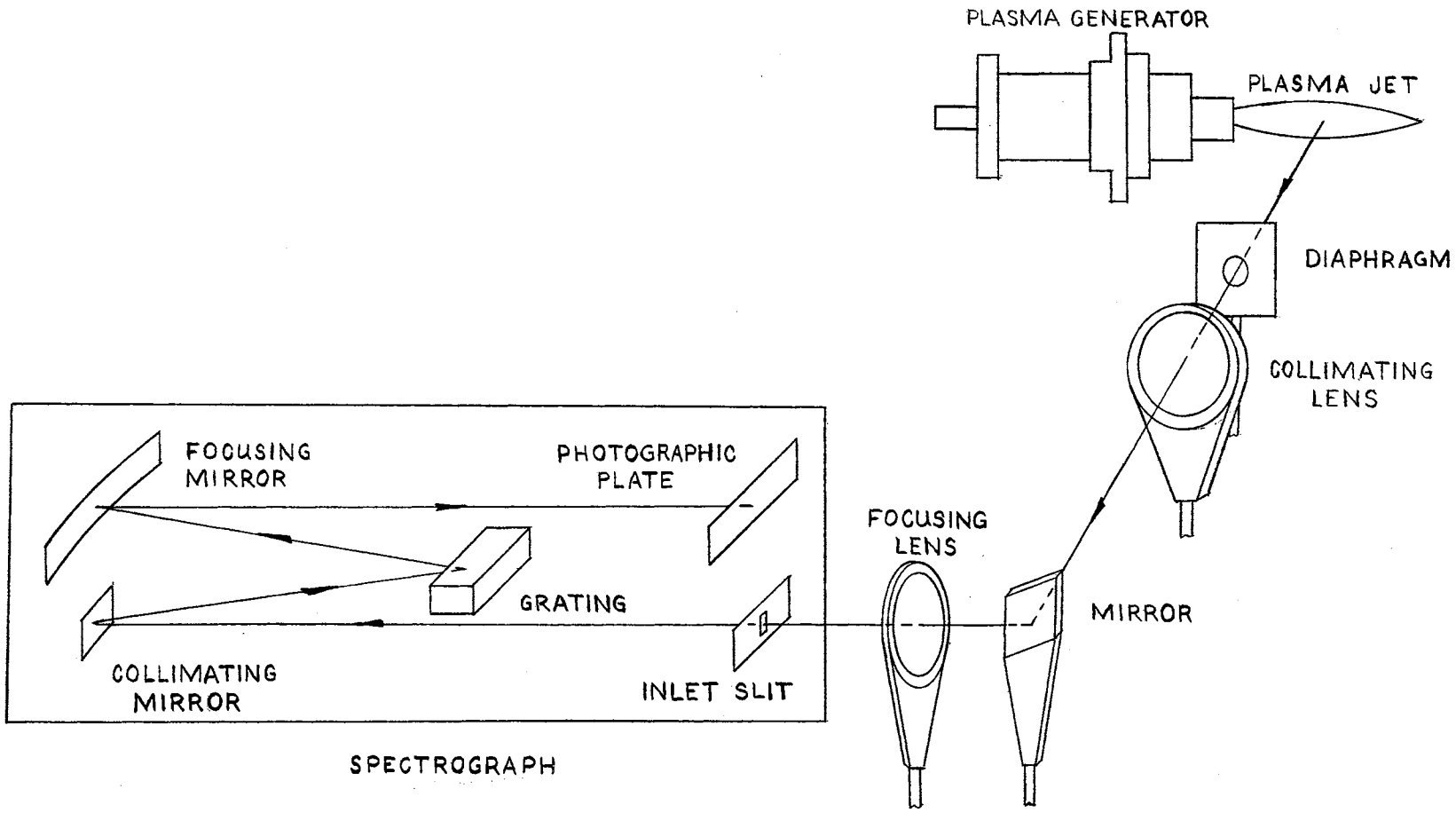

Figure 23. Optical System Schematic Diagram

Adjustments can be made by the controls on the front of the spectrograph to set the slit height and width, to position the photographic plates for multiple exposures, and to rotate the grating which will bring different areas of the spectrum into focus on the photographic plate. The front of the spectrograph can be seen in Plates I and II.

The photographic plates will be developed utilizing the equipment and darkroom available in the Mechanical Engineering Laboratory. After the plates are developed, a qualitative and quantitative evaluation of the exposures must be made. A Jarrell-Ash, Model JA200, direct-reading microdensitometer was chosen for this work. This instrument consists of a projection system to illuminate and focus the photographic plate on an observation screen. A sensitive photoelectric cell is mounted behind a slit arrangement on the screen. This cell is used to measure quantitatively the transmission of the projected light through exposed and unexposed portions of the plate. The output from the photoelectric cell actuates a sensitive galvanometer, and the galvanometer deflections, graded from zero to one hundred, are projected onto a small screen located just above the main viewing screen. A photograph of the densitometer is shown in Plate IX.

Plate IX

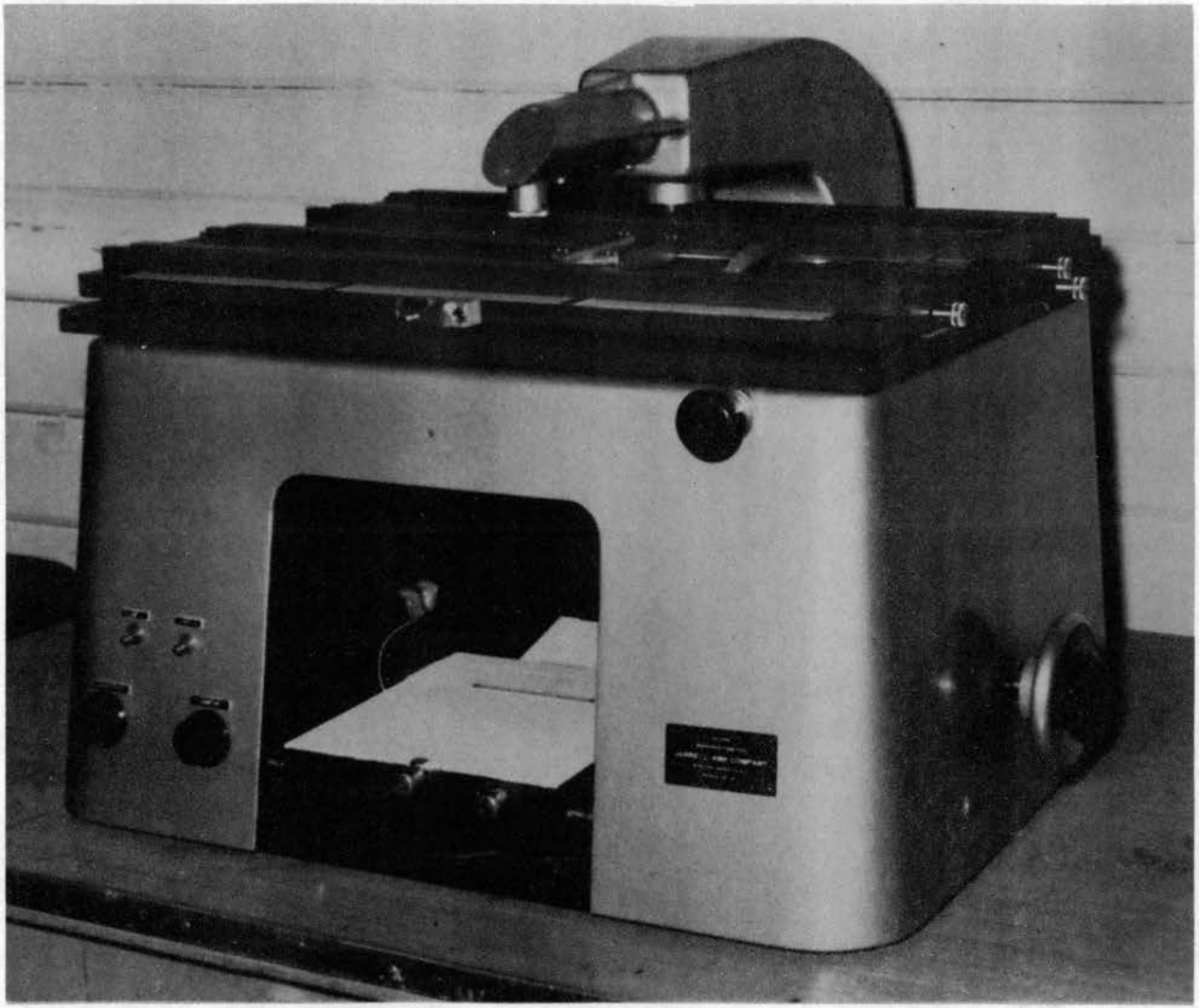

Densitometer

CHAPTER V

EXPERIMENTAL METHODS AND OBSERVATIONS

The material presented in this chapter describes the detailed procedure for starting the Plasma Facility and adjusting the operational parameters; namely, power level, gas flow rates, cooling water flow rates, and test section pressure. The techniques for recording operational and spectrographic data are given; and finally, sample data are shown for a typical run.

Operational Procedure

The operation of the Plasma Facility was divided into three separate phases; (1) pre-start preparations, (2) starting, and (3) operational adjustments. These steps are described in what follows.

Pre-Start Preparations

With the plasma generator assembly installed on the test section, all power, gas inlet, cooling water inlet and outlet, and pressure and temperature connections were made. Circulation of water through all cooling circuits was established. This included, in addition to the plasma generator assembly cooling circuits, the heat exchanger at the vacuum tank outlet and the vacuum pump cooling jacket. To insure maximum cooling, the initial water flow rates were set high.

The Brown Electronik temperature recorder was started.

The argon and hydrogen gas cylinder pressure regulators were set with the argon delivery pressure adjusted to 20 psig with flow, and the hydrogen delivery pressure brought to 25 psig without flow. The setting of the hydrogen pressure without flow was possible because the low flow rate used during operation results in a negligible drop in delivery pressure.

Several steps were necessary to prepare the DC power system for operation. The load selector switch (LSW) was placed in the up position thus connecting the DC generator power leads to the Plasma Facility terminal box. The control selector switch (CSW) was set in the closed position placing the Plasma Facility control panel in use. The voltage and current control rheostats on the control panel were set at their minimum positions. (This precautionary measure is taken to drive the DC generator output voltage to zero when the generator field switch is closed). The operation of the starting resistance bypass switch was checked and then set in the open position. The desired starting resistance (usually one-half ohm) was placed in the circuit by locating the hand switch on the starting resistance control box in the proper position. (Second position for one-half ohm).

The starter electrode was positioned by applying the Tesla coil to the copper lead wire, observing through the window in the main chamber the spark from the starter wire to the main electrodes, and adjusting the location of the starter wire until the spark jumped to both electrodes simultaneously.

Finally, the operation of the vacuum pump was checked. The pump was turned by hand for two or three revolutions to insure its freedom from foreign particles in the rotary pistons and valve mechanisms. The lubricating and sealing oil shutoff valve was opened. (A solenoid valve in the same oil line remains closed until the pump is started). The pump was started and run briefly to complete the check.

Starting

After the pre-start preparations were completed, the actual starting of the plasma generator system was accomplished according to the following steps:

1. Close main 440-volt, 3-phase AC power switch on junction box near the motor-generator set.
2. Start DC motor-generator.
3. Close DC generator field switch.
4. Push re-set button.
5. Close main contactor switch.
6. Set current control rheostat in maximum position and adjust voltage control rheostat to give an open circuit potential of 150 volts.
7. Start argon flow and adjust orifice differential pressure to 15.0 in. H_2O.
8. Apply Tesla coil to starter electrode until arc is established between the main electrodes.
9. Using the voltage control rheostat, adjust the arc current to 150 amperes.
10. Immediately after step 9, move the starting resistance control lever through its remaining positions, thus decreasing the starting resistance to 1/16 ohm.
11. Close starting resistance bypass switch.
12. Adjust voltage control rheostat to raise arc current to 250 amperes.

This starting procedure was used consistently to establish stable operation of the plasma generator with barometric pressure in the test section. Variations in argon flow rate and open circuit voltage still permitted successful starting of the system. The values given in the step by step procedure represent the best combination based on the results of many starting attempts.

Operational Adjustments

With the plasma generator system operating stably at barometric pressure, variations in the power level, gas flow rates, cooling water flow rates, and test section pressure can be made utilizing the available controls.

The power level depends directly on the arc voltage and current. Once stable operation of the plasma generator system is achieved for a fixed electrode configuration and argon flow rate, the arc voltage does not change appreciably. Therefore, changes in power level are effected by varying the arc current. Considering that the net load on the generator is a series combination of the arc resistance and the ballast resistance, the method for changing the current can be understood. With an increase in current, the arc resistance decreases slightly and the ballast resistance remains constant or increases slightly due to the higher temperature of the grid elements. The net load is then essentially a constant resistance. The current through this resistance is increased (decreased) by raising (lowering) the output voltage from the DC generator. Therefore, the voltage control rheostat is used to control the arc current. There are two limits on this control action; namely, the DC generator is rated at 250 volts

and 700 amperes. Visual monitoring of these parameters is provided by a Weston voltmeter measuring the DC generated voltage and the Triplett ammeter used for arc current. As pointed out in Chapter IV, protection is provided against both over-voltage and over-current by automatic opening of the main contactor if either parameter exceeds its rated value by approximately 40 percent.

The argon flow rate is a function of the orifice differential pressure measured on a well type manometer using a red indicating fluid having a specific gravity of 1.0. Variation of the argon flow rate is accomplished by adjusting the tangential and axial distribution valves and observing the indicated orifice differential pressure. By relative adjustment of these valves, the distribution of flow between tangential and axial can be varied. Operating experience has indicated that a large tangential component is desirable to maintain arc stability; hence, the tangential flow is set first and maintained to be at least 70 percent of the total flow. A calibration of the argon orifice flowmeter was made by Mr. McQuiston (1). The results of this calibration were used to plot the flow rate curves (standard cubic feet per hour, SCFH) shown in Figure 24.

The addition of hydrogen to the argon flow was carried out only after the system had reached stable operation. Only small quantities were required, and a suitable Fischer Porter Tri-Flat flowmeter was used for flow measurement. To add hydrogen flow to the system, a check was made first to make certain that the hydrogen line pressure was above the argon line pressure. The main shutoff valve in the

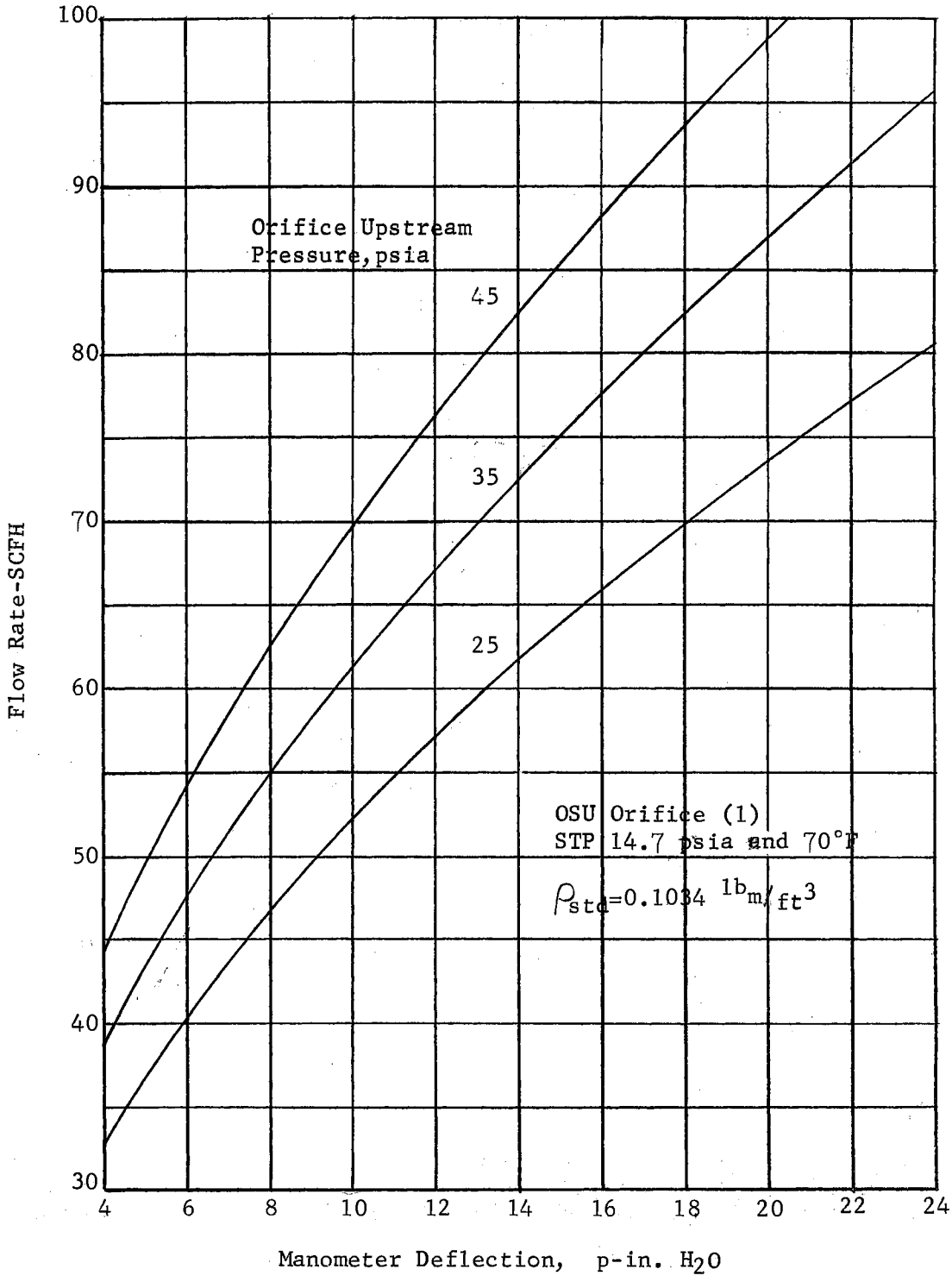

Figure 24. Argon Flowmeter Calibration

hydrogen line (a needle valve) was then opened carefully, and adjusted to position the stainless steel ball float in the flowmeter for the desired flow rate. Changes in hydrogen flow rate were made by regulation of the needle type shutoff valve. The actual flow rate corresponding to a given float position was obtained by reference to the flowmeter calibration curve calculated from data provided by the Fischer Porter Company for that particular meter, (36). This calibration curve is shown in Figure 25.

The flow of water through each cooling circuit is changed by opening or closing the needle valve in the outlet side of the circuit. By controlling the flow rate on the outlet side, a positive supply of water to the cooling passages is maintained at nearly line pressure. The flow rate through each circuit is indicated by its own orifice pressure differential which is measured by a simple U-tube manometer utilizing Meriam Indicating Fluid with a specific gravity of 1.75. Calibration runs were made on the rear electrode, converging nozzle, and main chamber orifice-manometer systems by collecting and weighing the cooling water over a measured period of time for various manometer deflections. The results of these calibrations are presented in Figure 26. The water outlet temperature for each cooling circuit is recorded, and care must be taken to keep the flow rate sufficiently high to maintain the water outlet temperatures safely below boiling temperature. A somewhat arbitrary value of 150°F was set as the maximum allowable water outlet temperature.

After the plasma generator system has been put into operation at barometric pressure, the test section pressure can be adjusted to values

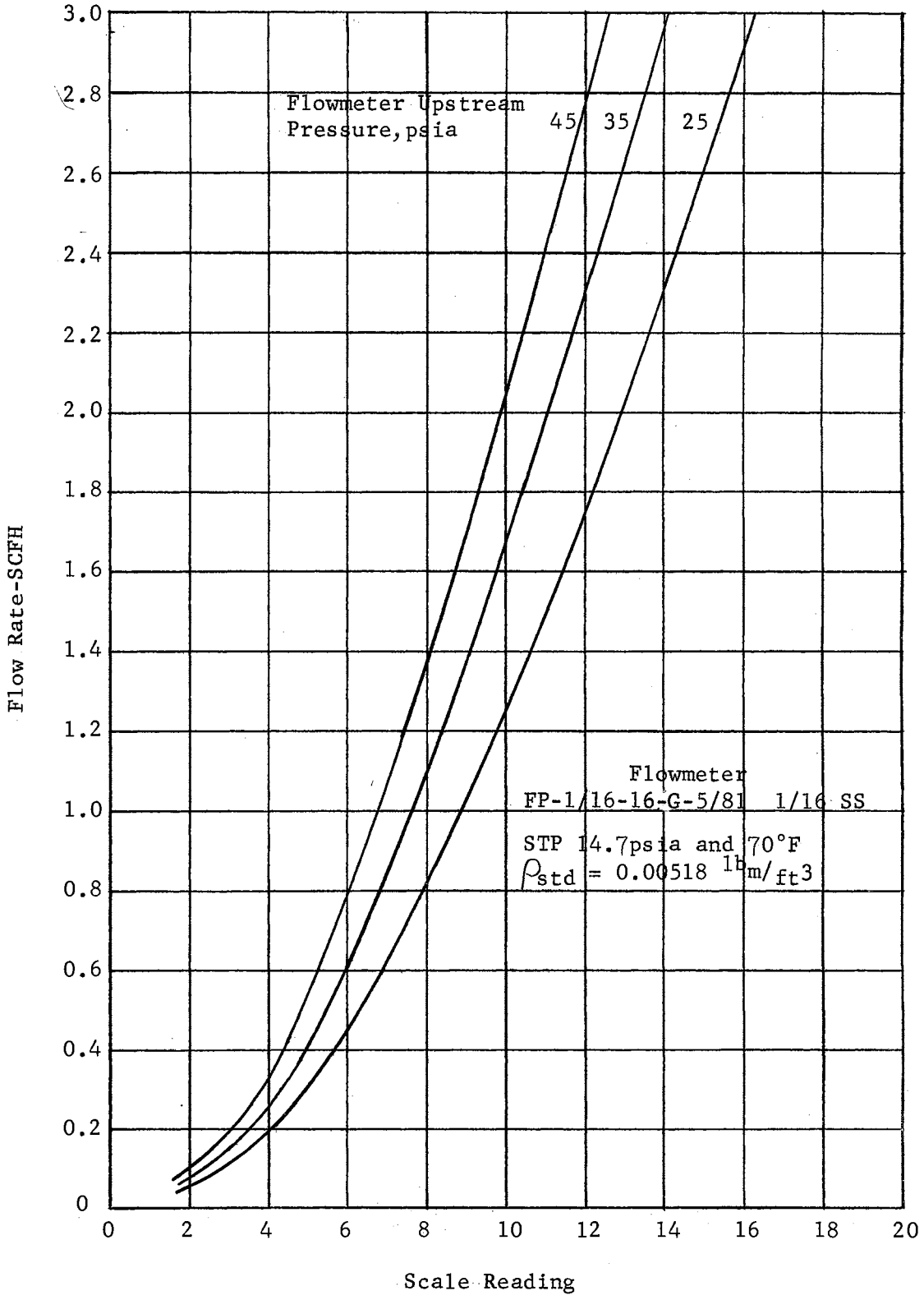

Figure 25. Hydrogen Flowmeter Calibration

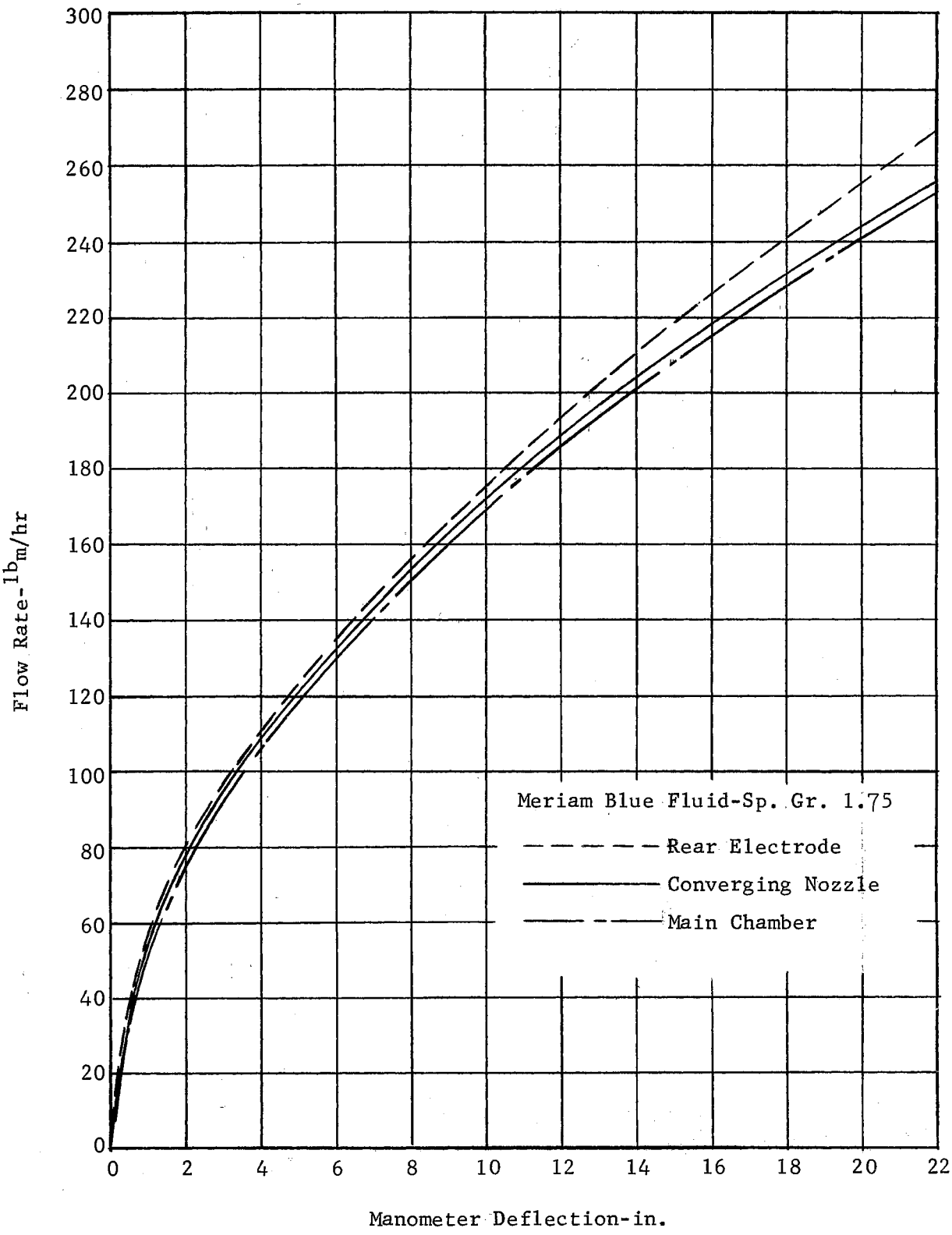

Figure 26. Cooling Water Flowmeter Calibrations

below atmospheric by use of the vacuum pump and the bleed down valves. Some difficulty of operation was encountered if the test section pressure was reduced when the arc current was below 250 amperes and the argon orifice differential pressure was below approximately 15 in. H_2O. Consequently, an arc current of about 300 amperes and argon flow manometer deflection of 20 in. H_2O were set prior to starting the vacuum pump. With these values set and the bleed down valves wide open, the vacuum pump was started and time was allowed (approximately 5 seconds) for the test section pressure to reach a new equilibrium value of about 4 in. Hg. Vac. Small adjustments were made if necessary to maintain the arc current at 300 amperes.

Adjustment of the test section pressure between this value of 4 in. Hg. Vac. and the maximum vacuum possible, which was below 1 in. Hg. absolute pressure, is accomplished by partially or fully closing the two bleed down valves mounted on the side of the tank. As the test section pressure decreases some small adjustments in arc current and argon flow rate may be necessary to maintain stable operation. As indicated above, 250-300 amperes was the lower limit for this facility and higher currents, 400-600 amperes, resulted in very stable operation.

Operational Data Record

The instrumentation provided for the Plasma Facility was described in Chapter IV. This instrumentation was used for operational control of the system during a test run. It also provided the data to be recorded during the run for later reduction to test results.

A data sheet was prepared for the Plasma Facility to be used for recording the necessary static pressures, temperatures, voltages, current, and flow rate pressure differentials for the data reduction process.

The temperature data was recorded automatically by the Brown Electronik instrument. The recorded values were isolated for each run by marking the beginning and end of the run on the recording paper. These values were then transcribed to the data sheet at the end of each set of runs. The remaining data on pressures, voltages and current were recorded on the data sheet during the run. A sample data sheet is given in Table IV.

Spectrographic Data Record

The description of the spectrographic equipment and the associated optical system was given in Chapter IV. With this arrangement any section of the plasma jet visible through the side window in the test section could be imaged on the spectrograph slit. This is accomplished by keeping the focusing lens fixed and moving the mounting bar, which holds the diaphragm, collimating lens and mirror, parallel to the jet axis. The technique used for obtaining the spectrographic data for a given cross section of the plasma jet is presented below.

With a selected cross section of the jet and its edge focussed on the entrance slit of the spectrograph, settings were made for the grating angle, the entrance slit height and width, the exposure time and the vertical location of the photographic plates. These data were listed on a data sheet prepared specifically for the spectrographic

TABLE IV

OSU PLASMA RESEARCH FACILITY

Control Panel Data Sheet

Operator E. C. Pohlmann
Gas Argon w/o Hydrogen
Electrode Position 5/16 in.
Bar. Pressure 29.14 in. Hg. @ 76°F

Date March 22, 1961
Starting Settings:
Open Cir. Volt 150 V
Current Control Max.

Item	Run No.	Zero Read.	1	2	3
Arc Volt.--Volts		0	36	35	33
Arc Current--Amps		0	400	500	420
Conv. Nozzle H_2O Flow--in. defl.		0	17.0	17.0	17.0
C-D Nozzle H_2O Flow--in. defl.		0	--	--	--
Main Chamber H_2O Flow--in. defl.		0	2.3	2.5	2.0
Rear Electrode H_2O Flow--in. defl.		0	6.6	7.0	7.0
Heat Exchanger H_2O Flow--in. defl.		0	19.5	19.5	18.8
Water Inlet Pressure--psig		0	56	55	55
Water Inlet Temp. #1--°F		--	58	58	58
Water Inlet Temp. #2--°F		--	--	--	--
Conv. Nozzle H_2O Out Temp.--°F		--	126	144	114
C-D Nozzle H_2O Out Temp.--°F		--	--	--	--
Main Chamber H_2O Out Temp.--°F		--	64	64	64
Rear Electrode H_2O Out Temp.--°F		--	130	147	130
Heat Exchanger H_2O Out Temp.--°F		--	85	86	86
Argon Gas Inlet Temp.--°F		--	76	76	76
H_2 Gas Inlet Temp.--°F		--	76	76	76
N_2 Gas Inlet Temp.--°F		--	--	--	--
Vac. Pump Gas Inlet Temp.--°F		--	85	86	87
Argon Press--psig		0	18	18	18
H_2 Press--psig		0	18.2	18.2	18
N_2 Press--psig		--	--	--	--
Main Chamber Press--in. Hg. Vac.		0	16.5	15.5	20.8
Mix. Chamber Press--in. Hg. Vac.		0	--	--	--
Test Section Press--in. Hg. Vac.		0	28.5	28.5	28.5
Vac. Pump Inlet Press--in. Hg. Vac.		0	28.5	28.5	28.5
Argon Flow Rate Δp--in. H_2O		30.0	9.9	9.9	9.2
Hydrogen Flow Rate-Flowmeter Reading		0	12.2	12.0	0

REMARKS: Expansion nozzle was not used during these runs.

record.

The grating angle was chosen such that the wave length for the particular spectral line to be analyzed was located near the center of the photographic record (two 4 x 10 inch plates placed end to end). A table giving the relation between grating angle and the wave length that would appear at the center of the photographic record was available for the Jarrel-Ash 3.4 meter Ebert Spectrograph in the Instruction Manual provided with the instrument. With a grating angle of 7.00°, both the H_β (4861.3A) and the H_γ(4340.5A) spectral lines appear on the left plate of the record.

The slit height depends on the vertical height of the jet image on the slit. Sufficient height was used to insure that the total image would be photographed. This varied from 10 to 20 millimeters depending on the power level of the plasma jet and the particular cross section being observed. The slit width was set at 10 microns as a compromise between sharp focus on the photographic plate which requires a narrow slit width and exposure time which could be decreased by using a wide slit opening.

An exposure time of 60 to 90 seconds was chosen based on previous experience with plasma jet spectrographic work conducted at Chance Vought Research Center.

The vertical location of the photographic plates was determined by taking the first exposure at the top of the plates and then indexing the camera through sufficient vertical movement to remove the exposed portion of the plates from the subsequent light path for the

next exposure. The vertical position of the plates in millimeters is indicated by the Veeder counter on the front of the spectrograph.

After the required exposures were obtained of the plasma jet cross section, a final exposure of a constant intensity source was taken through a Jarrell-Ash Model 16830 Seven-Step Filter Assembly mounted at the entrance slit. This exposure was used for emulsion calibration and for wave length identification. An argon ionization (Pluecker) tube was used for the light source. The grating angle and slit width settings were the same as were used for the plasma jet exposures. The slit height was set at 12 millimeters to cover the height of the filter coatings. The filter was calibrated by the Jarrel-Ash Company and values for the relative densities of the seven step coatings were supplied with the Filter Assembly Instruction Manual. The use of the seven-step filter emulsion calibration exposure is described in Chapter VII.

The development of the spectrographic plates was carried out according to standard technique. A four minute development in Kodak D-19 or D-11 developer was followed by a 15 second wash in water and a 15 minute fixing process in Kodak Acid Fix. After fixing, the plates were washed gently in cold water for 30 minutes. A final wash and stripping with distilled water followed by room air drying, readied the photographic record for analysis. The method of analysis for the spectrographic plates is given in Chapter VI. A spectrographic data sheet is shown in Table V, and the photographic record of the corresponding exposures is presented in Plate X. These spectrographic data for the plasma jet exposure correspond to the operational data given in Table IV.

TABLE V

OSU PLASMA RESEARCH FACILITY

Spectrograph Data Sheet

Operator D. R. Haworth Plate Type 103a-F Date March 22, 1961

PLATE NO. 3-22-61A

Exp. No	Vert. Plate Position mm	Grating Angle Degrees	Slit Height mm	Slit Width microns	Plate Subject	Exp. Time Sec.	Remarks
1	10	7.00	12	10	Argon + H_2 Plasma Jet	60	Run No. 1 Table IV
2	24	7.00	12	10	Argon + H_2 Plasma Jet	90	Run No. 1 Table IV
3	38	7.00	12	10	Argon + H_2 Plasma Jet	60	Run No. 2 Table IV
4	52	7.00	12	10	Argon Plasma Jet	60	Run No. 3 Table IV
5	66	7.00	12	10	Argon Ionization Tube	900	Emulsion Calibration and Wave Length Identification

Plate X

H_β - 4861.3A

H_γ - 4340.5A

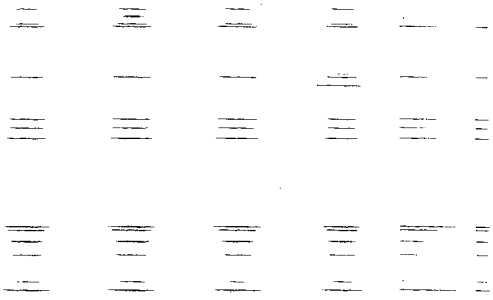

Exposure No. 1 2 3 4 5

OSU Plasma Facility Spectrographic Record
Plate No. 3-22-61A

CHAPTER VI

SPECTROGRAPHIC DETERMINATION OF PLASMA TEMPERATURES

A detailed method for the determination of the temperature distribution in a plasma jet is described in this chapter. The technique used in the analysis is based on Stark effect broadening of a spectral line of hydrogen which was added in small quantities to an argon plasma. The ratio of hydrogen flow to argon flow was from one to three percent by volume. The previous application of the Stark effect broadening theory, which was described in Chapter III, was made on a water stabilized plasma with the hydrogen being supplied by the stabilizing fluid. Also, in this analysis only one average temperature was calculated for the entire jet cross section; i. e., no attempt was made to determine the temperature distribution for the section.

The steps in the analysis are illustrated by actual calculations from specific data taken at the Chance Vought Research Center (CVRC). The use of spectrographic data taken from another plasma facility for the description of the analysis does not affect the procedure itself. The decision to use the CVRC data was based on two factors. First, the plasma facility at Chance Vought was available for use during the time the OSU facility was under development. For this reason the data was taken and analyzed at the same time the OSU facility was being completed. Second, the two facilities provide the same type of data required

for determining the temperature distribution in a plasma jet. For the above reasons all of the necessary measurements and calculations for the experimental data were made by the author at the Chance Vought Research Center.

The experimental data taken at CVRC was essentially the same as was recorded for the OSU facility as presented in the previous chapter. Operational data on power input (arc voltage and current), cooling water flow rate and temperature rise, argon and hydrogen flow rates, and test section static pressure were recorded. The final results for the runs are summarized in Table VI.

TABLE VI

CHANCE VOUGHT RESEARCH CENTER PLASMA FACILITY DATA

	Run Number		
	(1)	(2)	(3)
Arc Voltage - volts	36.5	36.5	36.5
Arc Current - amperes	1500	1500	1500
Argon Flow Rate - lb_m/hr	16.2	16.2	16.2
Hydrogen Flow Rate - lb_m/hr	0.0195	0.0141	0.0244
Hydrogen/Argon - by Vol.	0.023	0.016	0.029
Water Flow Rate - lb_m/hr	2250	2250	2250
Water temp. rise - °F	33	33	33
Test Section Press. - psia	0.364	0.364	0.364

The spectrographic record (Plate No. 12-19-60A) obtained for the corresponding runs of Table VI is shown in Plate XI. The optical system used to focus the edge of a cross section of the jet on the spectrograph slit has a magnification of 0.428; i.e., a vertical dimension in

Plate XI

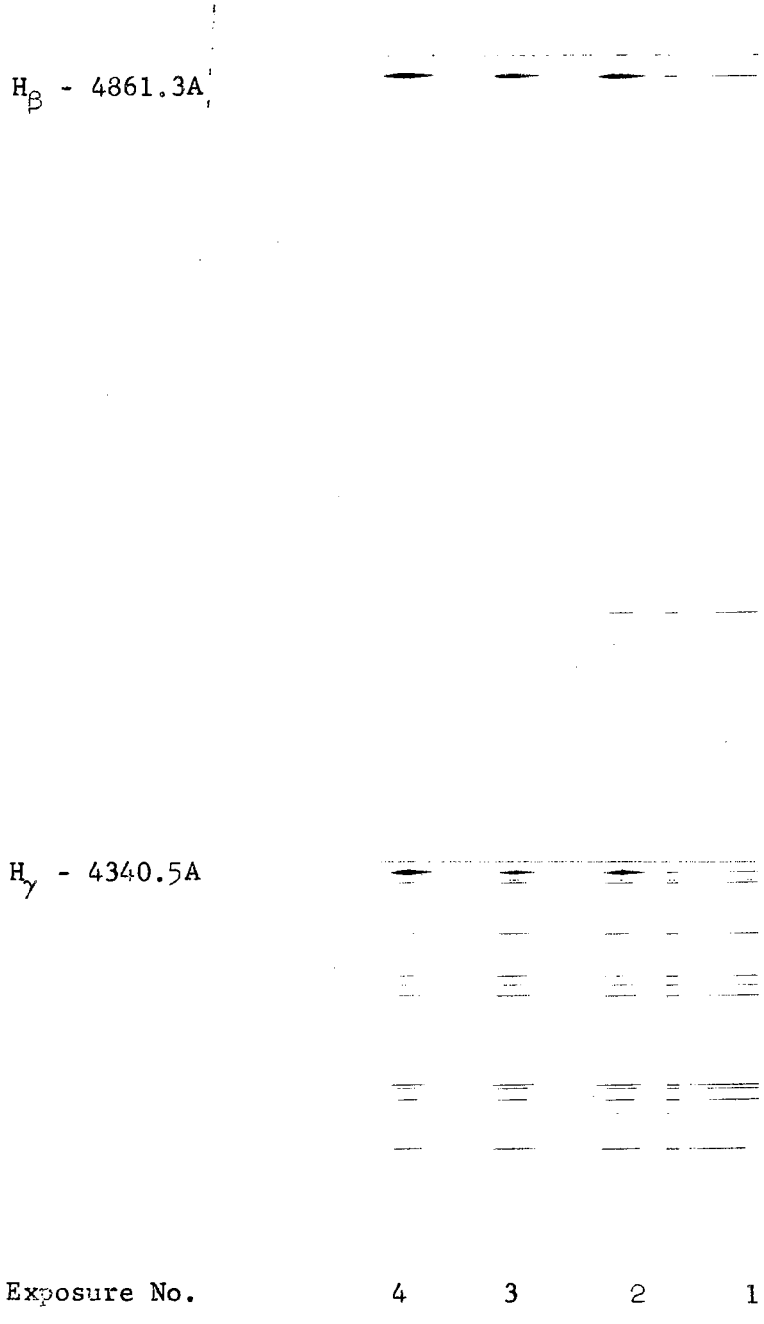

CVRC Plasma Facility Spectrographic Record
Plate No. 12-19-60A

the jet is multiplied by 0.428 to give the corresponding vertical dimension on the slit. Also, there is no further change in the vertical dimension within the spectrograph. The optical system was adjusted to locate the portion of the jet one diameter downstream of the nozzle exit on the slit of the spectrograph. The spectrograph settings for grating angle, slit width and height, vertical plate location (Veeder), and exposure time are given in Table VII.

TABLE VII

CHANCE VOUGHT RESEARCH CENTER SPECTROGRAPH DATA

PLATE NO. 12-19-60A

Exp. No.	Veeder mm	Grating Angle Degrees	Slit Height mm	Slit Width Microns	Exp. Time secs.	Source	Remarks
1	10	7.00	12	10	1800	Argon ionization tube	Emulsion calibration
2	24	7.00	12	10	60	Argon and hydrogen plasma jet	Run No. 1 Table VI
3	38	7.00	12	10	60	Argon and hydrogen plasma jet	Run No. 2 Table VI
4	52	7.00	12	10	60	Argon and hydrogen plasma jet	Run No. 3 Table VI

Only the left photographic plate is shown in Plate XI. With the grating angle of 7.00 degrees both the H_β (4861.3A) and the H_γ (4340.5A) lines appear on this plate. The analysis procedure is explained in this chapter using the H_γ line of Exposure No. 4. Temperature distributions

were obtained for each H_γ line to show the effect of the percent hydrogen tracer added at a fixed power input and argon flow rate. Also, the H_β line for Exposure No. 4 was analyzed to check for agreement with the results obtained for the H_γ line of the same exposure. The results of these comparisons are presented in Chapter VII.

Emulsion Calibration

The analysis of broadened hydrogen lines on a spectrographic record of the radiation from an argon-hydrogen plasma for calculating plasma temperatures requires the determination of the relative intensities of the radiation incident on the spectrograph slit. The response of the emulsion on the plate to incident light depends on the characteristic curve of the emulsion which is a relation between the density of the exposed and developed emulsion and the intensity of the incident light. The response also depends on the particular wave length being considered. A complete description of emulsion characteristics can be found in Reference 37.

Several methods for emulsion calibration are used. (37). For this work a seven-step filter was mounted at the spectrograph slit and a constant intensity source (an argon ionization tube) was focussed on the assembly. The seven-step filter was calibrated by the manufacturer, and data on the relative density of each step of the filter was supplied. From these values of relative density the relative amount of light transmitted through each step of the filter was calculated based on the definition of density, d; i. e.,

$$d = \log_{10} \frac{\text{incident light}}{\text{transmitted light}} = \log_{10} \frac{I}{T} \tag{45}$$

Letting 1.00 unit represent the incident light intensity from the source and solving for T from equation (45) gives

$$T = \frac{1.00}{10^d} \tag{46}$$

For the CVRC filter assembly the relative density values and the calculated values for transmitted light are given in Table VIII.

TABLE VIII

SEVEN-STEP FILTER CALIBRATION DATA

Step No.	Relative Density - d	Transmitted Light - T
1	0.000	1.000
2	0.213	0.612
3	0.400	0.398
4	0.606	0.248
5	0.801	0.158
6	1.000	0.100
7	1.194	0.064

The values given in Table VIII for the transmitted light become the relative incident light or relative intensities incident on the photographic emulsion through each step of the filter.

The emulsion calibration exposure for the photographic plate shown in Plate XI is Exposure No. 1. Although an argon ionization tube was used as the source, some hydrogen was present in the tube; therefore, spectral lines for H_β and H_γ appear in the calibration

exposure. This was advantageous since it is important to determine the emulsion response at or near the wave length being used in the subsequent analysis. Both the H_β and H_γ lines in the exposure were used for emulsion calibration since both H_β and H_γ lines from the plasma jet radiation were analyzed in the calculation of plasma temperatures. The calibration procedure is the same for both lines and is described for the H_γ line only.

The photographic plate was placed on the densitometer table and the plate region around the H_γ line was brought into view on the screen over the detecting photocell. The adjustable slit over the photocell was set to detect the light passing through an area of the plate 15 microns wide and 0.5 millimeters (mm) high. With a clear (unexposed but developed) portion of the plate near the H_γ line over the photocell slit, the galvanometer deflection was adjusted to give a scale reading of 100. Then the photocell slit height was set to zero, allowing no light to fall on the photocell, and the index line on the galvanometer scale viewing screen was set at the zero reading. The slit height was opened again to 0.5 mm and the 100 reading rechecked. This adjustment operation was repeated until no further movement of the index line and galvanometer was necessary.

The densitometer was used to determine the relative transmitted light through each step of the H_γ spectral line. With the adjustments described in the previous paragraph, the galvanometer deflections varied from zero (no light transmitted) to 100 (clear plate). The response of the photocell is essentially linear; therefore, the

recorded readings of galvanometer deflection gave a direct measure of the relative transmitted light through the exposure steps. The densitometer readings for the H_β and H_γ calibration lines are given in Table IX along with the relative intensities from Table VIII that correspond to each step.

TABLE IX

DENSITOMETER READINGS - EMULSION CALIBRATION

PLATE NO. 12-19-60A

Step No.	Relative Intensity	H_β - 4861.3A Densitometer Reading	H_γ - 4340.5A Densitometer Reading
1	1.000	3.1	15.7
2	0.612	6.4	25.9
3	0.398	11.6	37.3
4	0.248	22.0	53.7
5	0.158	38.0	71.3
6	0.100	61.6	86.2
7	0.064	78.2	94.4

The data from Table IX were plotted as shown in Figure 27.

Relative Intensities of Broadened Spectral Lines

After the data for the emulsion calibration were taken, the densitometer was used to measure the relative transmitted light through the broadened hydrogen spectral lines of the exposures obtained of the plasma radiation. The settings on the photocell slit were the same as for the readings for the emulsion calibration. To provide the data

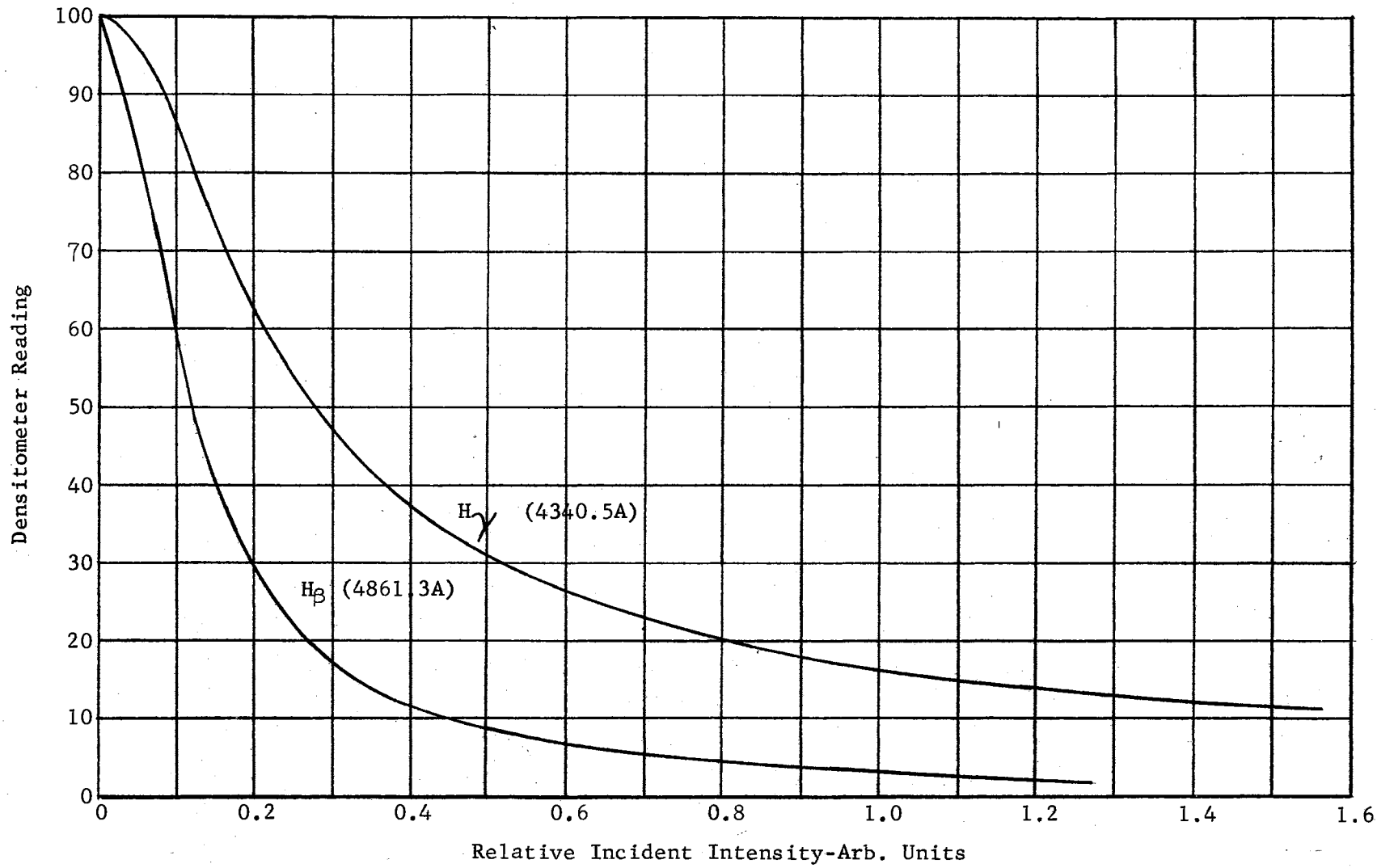

Figure 27. Emulsion Calibration - Plate No. 12-19-60A

necessary for the determination of plasma temperatures, densitometer readings were taken at each 0.5A across the spectral line and at each 0.5 mm vertical location* on the plate.

The vertical location was set by use of a millimeter scale mounted on the densitometer table next to the photographic plate with the length of the scale running in the "vertical" direction. One of the index marks on the viewing screen for the photocell slit height was selected as a reference. The table was moved laterally (left and right) until the scale was located over this index mark, and the scale value recorded. Then the table was moved back to bring the H_γ line over the screen. After the readings were taken for this vertical location, the table was moved laterally again bring the scale into view and a check made to insure that no transverse (in and out) motion had occurred. The table was then moved in or out until the reference mark coincided with a new scale value differing by 0.5 mm from the previous one. Another set of densitometer readings were taken and the above procedure repeated until the complete spectral line had been covered.

The wave length position was determined by first placing an index line on the photographic plate with a knife edge drawn across the emulsion side of the plate near the spectral line to be observed. These reference lines for the H_β and H_γ lines can be seen in Plate XI. Then for each vertical location the table was moved laterally until the argon spectral lines on either side of the broadened hydrogen line were

---

* The term "vertical location" is used to denote a corresponding position in the plasma jet. The jet is horizontal and its cross section edge imaged on the slit of the spectograph is a vertical line.

centered over the photocell slit. This was determined by obtaining the minimum reading for the galvanometer deflection. When the argon line was centered, the index line on the plate projected across a reference millimeter scale on the viewing screen and the scale reading was recorded. The argon lines that were used with the H_γ line were at 4333.6A and 4345.2A.

The dispersion of the plane grating spectrograph is nearly linear over the photographed spectrum of approximately 20 inches; therefore, with these two known wave lengths separated by less than 1/4 inch, linear interpolation was used to determine the corresponding wave lengths across the broadened hydrogen line. Densitometer readings were taken at each millimeter on the reference scale, and an additional value was recorded for the minimum galvanometer reading and its corresponding reference scale location.

With this arrangement and using a magnifying glass, it was relatively easy to estimate the reading on the viewing screen scale to 0.2 mm; and with the 10:1 magnification of the densitometer optics, this represents 0.02 mm on the plate. The approximate reciprocal dispersion of the spectrograph is 5A/mm; therefore, wave length location is known within 0.1A.

The densitometer readings obtained for the H_γ line of Exposure No. 4 are given in Table X. Data for the other spectral lines are given in Appendix A. The reference scale readings for the location of the argon lines varied with changes in the vertical location. This was caused by the inability to place the wave length index line on the

TABLE X

DENSITOMETER READINGS

PLATE NO. 12-19-60A EXPOSURE NO. 4 H_γ SPECTRAL LINE

Photocell Slit: Height-0.5 mm Width-15 microns

LATERAL LOCATION mm	VERTICAL LOCATION-mm 6.0	6.5	7.0	7.5	8.0	8.5	9.0	9.5	10.0	10.5	11.0	11.5	12.0	12.5	13.0	13.5	14.0
74.0							98.2	96.3	93.5	96.7	98.0	95.6	97.0				
73.0						100.0	96.5	98.0	93.8	93.6	93.5	96.0	97.2	100.0			
72.0						98.8	97.6	93.6	92.3	92.2	93.4	94.8	97.0	98.9			
71.0						96.4	96.2	91.3	87.3	86.7	89.8	91.4	92.8	97.4	100.0		
70.0					100.0	94.2	90.6	85.4	82.8	79.9	82.6	85.9	92.0	96.2	99.2		
69.0				100.0	95.6	94.0	86.2	77.3	71.6	68.3	74.4	78.6	88.6	93.6	96.6	100.0	
68.0			100.0	99.2	94.5	86.2	75.5	65.0	59.2	57.0	61.2	67.4	76.3	88.6	92.2	98.5	
67.0		100.0	98.2	96.0	84.4	72.1	57.7	52.0	43.4	43.4	49.1	52.7	62.4	76.9	89.3	96.8	100.0
66.0	100.0	99.1	97.4	86.5	69.7	48.8	41.9	33.6	31.0	31.2	34.5	38.7	47.5	62.2	71.8	89.0	98.5
65.0	97.2	94.0	76.1	45.2	31.2	22.7	19.5	17.1	15.8	16.4	19.2	22.0	28.4	39.1	52.0	71.2	87.4
64.0	90.4	65.3	42.7	25.6	21.0	18.7	18.8	19.0	17.8	22.0	26.4	30.6	43.6	56.5	76.8	88.7	97.7
63.0	98.2	97.0	91.1	81.1	63.5	51.8	42.0	39.2	37.0	38.0	44.0	49.8	62.8	76.6	90.3	97.9	99.4
62.0	100.0	100.0	99.4	96.0	80.7	69.0	60.4	54.8	47.2	50.2	55.1	61.1	74.6	86.4	93.5	99.5	100.0
61.0			100.0	98.6	90.0	84.6	75.8	69.5	60.7	64.0	67.4	72.7	83.7	94.5	97.5	100.0	
60.0				100.0	95.4	92.0	85.1	78.0	74.5	75.0	77.0	82.8	92.0	97.0	99.6		
59.0					98.4	93.8	89.3	84.4	82.8	82.0	85.7	91.2	94.0	100.0	100.0		
58.0					100.0	96.0	94.2	91.6	89.3	87.4	90.7	92.5	97.6				
57.0						99.2	97.0	94.0	94.5	91.0	94.3	99.6	99.1				
56.0						100.0	100.0	94.7		94.4	94.3	100.0	100.0				
55.0																	
Minimum Reading & Lateral Location	90.4 64.0	62.2 64.2	36.8 64.3	21.8 64.3	15.3 64.3	14.0 64.4	13.1 64.5	12.8 64.5	12.5 64.5	14.2 64.6	17.4 64.6	20.4 64.7	27.6 64.8	39.1 65.0	52.0 65.0	71.2 65.0	87.4 65.0
Argon Spectral Line @ 4333.6A Lateral Location	78.2	78.0	78.1	78.2	78.2	78.2	78.2	78.3	78.3	78.3	78.4	78.4	78.5	78.6	78.7	78.7	78.7
Argon Spectral Line @ 4345.2A Lateral Location	55.0	55.0	55.0	55.0	55.0	55.0	55.0	55.1	55.1	55.1	55.2	55.2	55.3	55.4	55.5	55.5	55.5

photographic plate exactly parallel to a constant wave length line on the plate. However, by recording the wave length scale reading of the argon lines for each vertical location, the effect of this discrepancy was eliminated.

The next step in the analysis was to plot the densitometer readings versus wave length for each vertical location and then to draw smooth curves through the data points. The assumption was made that the wave length broadening was symmetrical, and the data at 4340.0A and 4341.0A were plotted together. Likewise, the data at 4339.5A and 4341.5A were combined and so forth. These curves are shown in Figures 28a-28d.

From these figures a second set of curves were drawn of densitometer readings versus vertical location for fixed wave lengths starting at the center of the line (4340.5A) and using 0.5A increments. To satisfy the assumption of an axisymmetric plasma jet, the curves had to be symmetrical with respect to vertical location. This criterion was used as a guide in plotting the curves. First, an estimate was made of the vertical location value for the centerline of symmetry. Then the data on the left of the centerline was transferred to its corresponding location on the right side of the centerline. Finally a smooth curve was drawn to give the best fit for the combined data points.

The results of this second curve plotting are given in Figures 29a-29c. The centerline for the two curves of Figures 29a was at a vertical location (denoted by x) equal to 10.0 mm. Similarly the centerline for Figures 29b and 29c were at x = 10.25 mm and x = 10.50 mm respectively.

The location of the centerline varied with wave length as a result

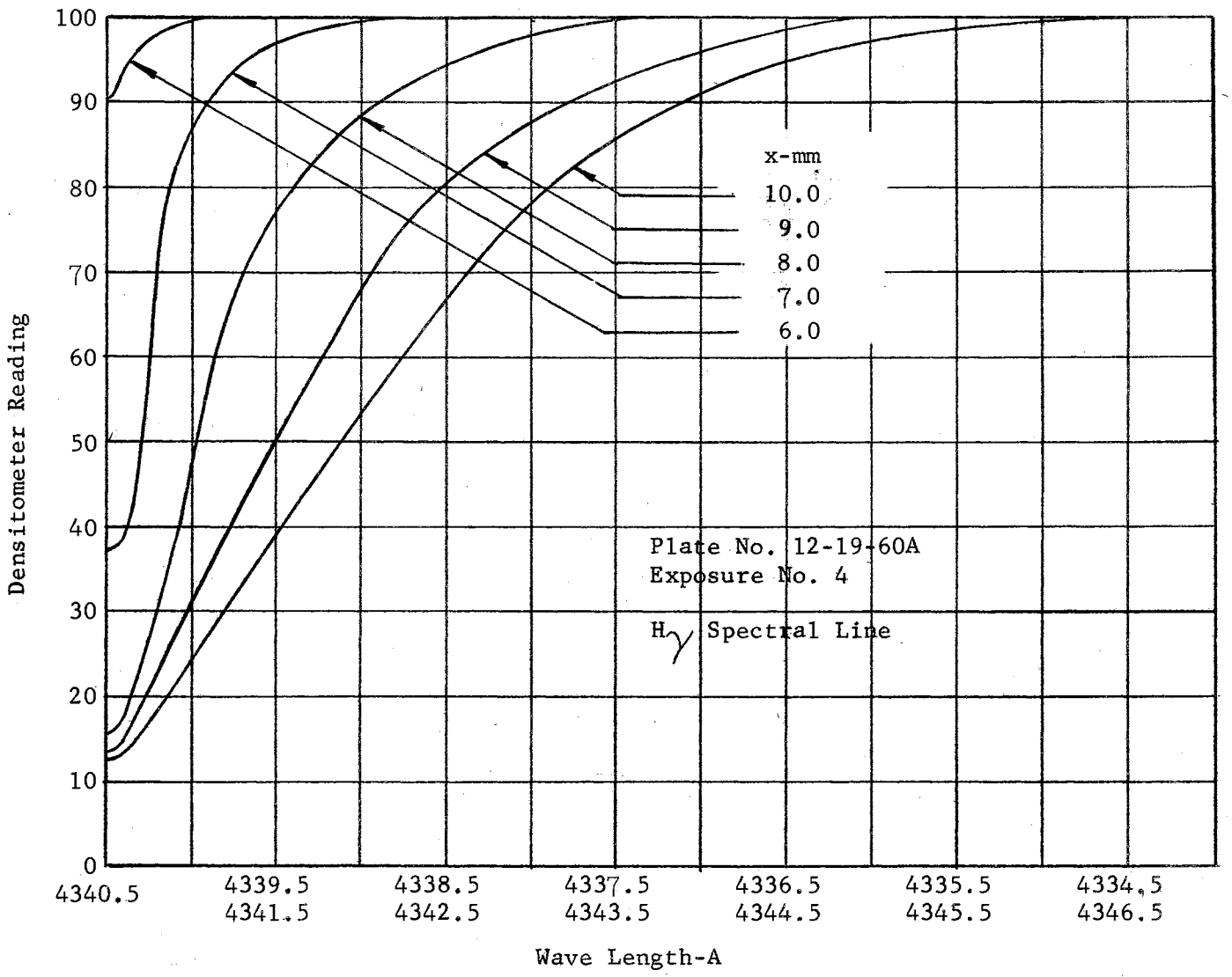

Figure 28a. Densitometer Reading versus Wave Length

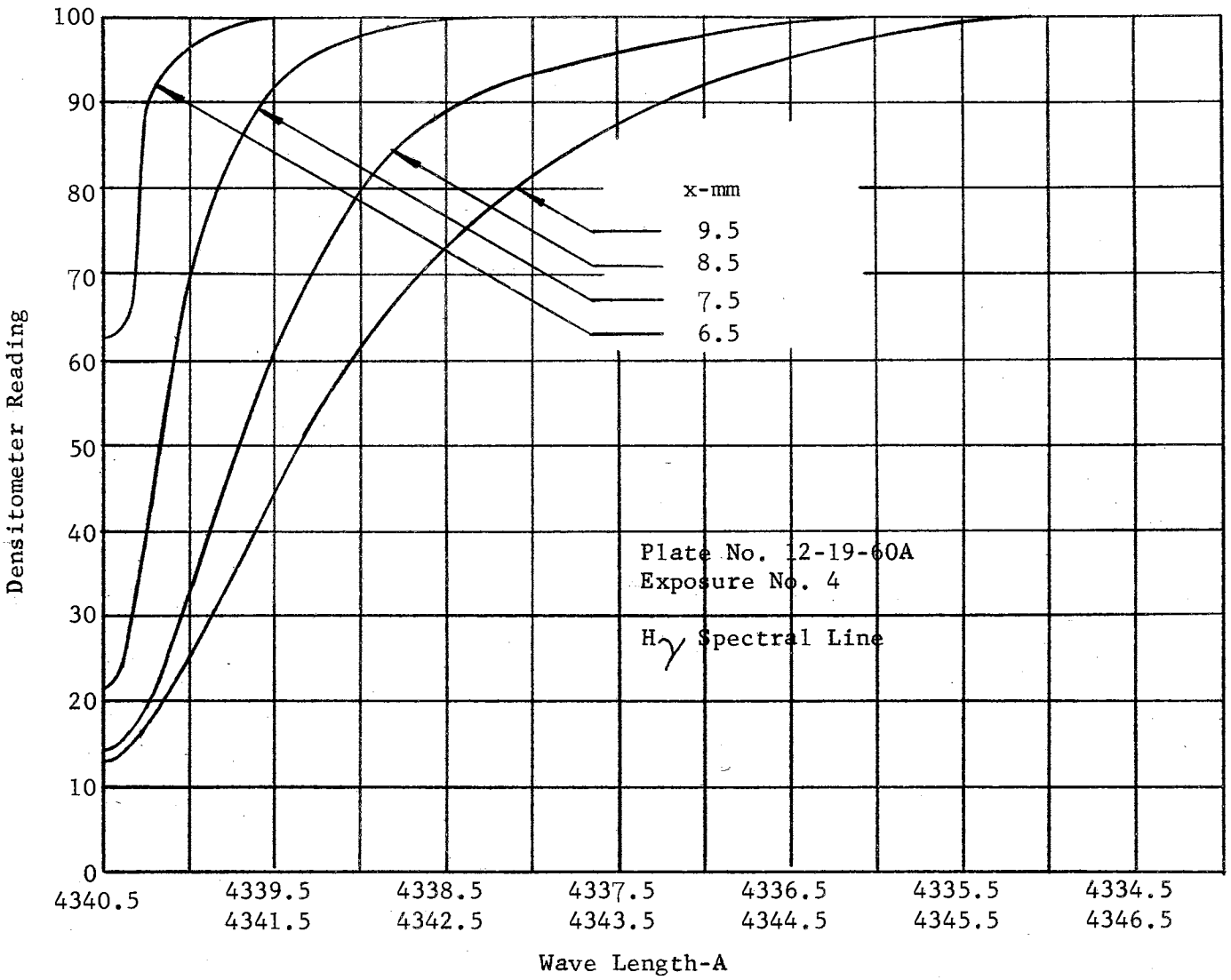

Figure 28b. Densitometer Reading versus Wave Length

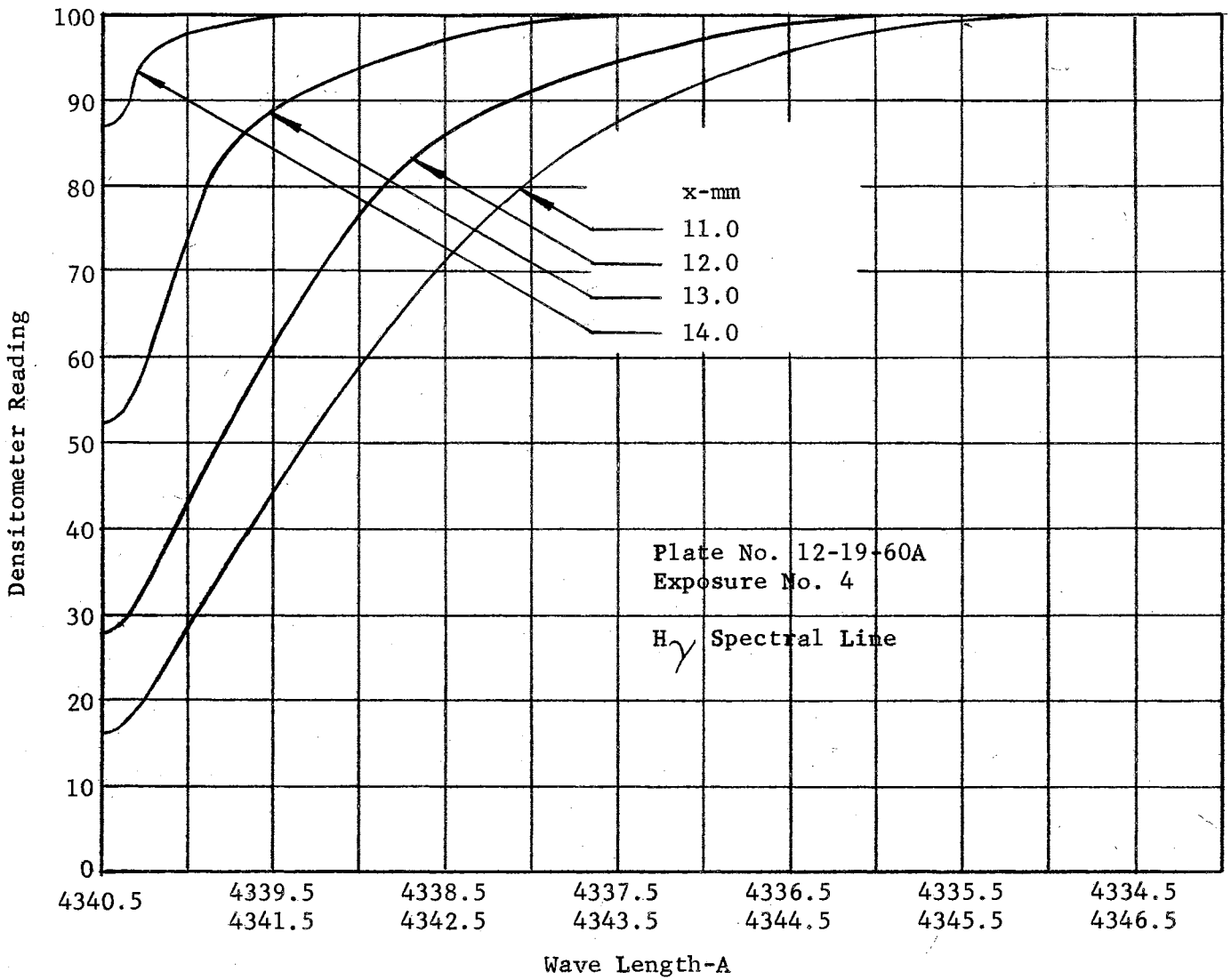

Figure 28c. Densitometer Reading versus Wave Length

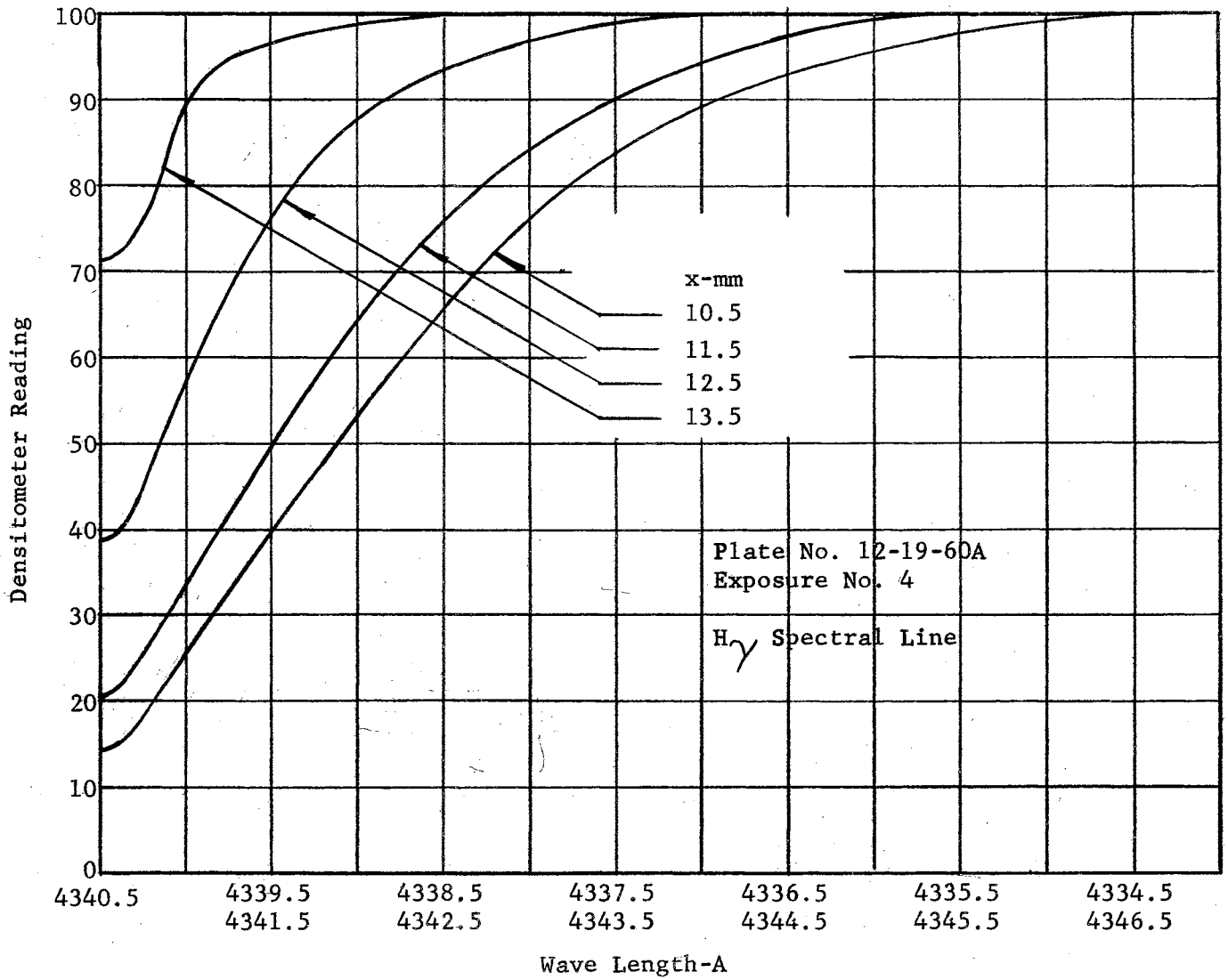

Figure 28d. Densitometer Reading versus Wave Length

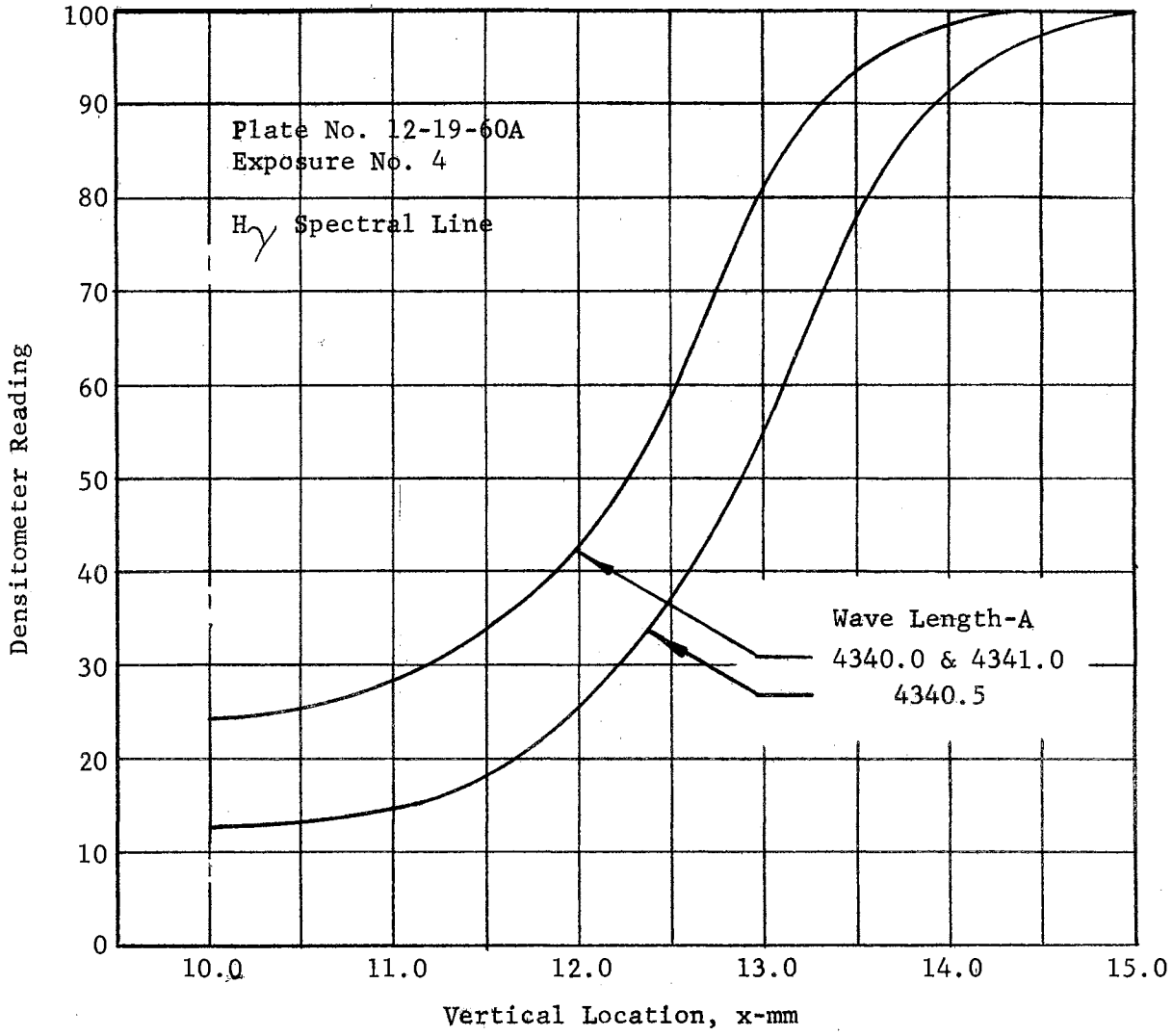

Figure 29a. Densitometer Reading versus Vertical Location

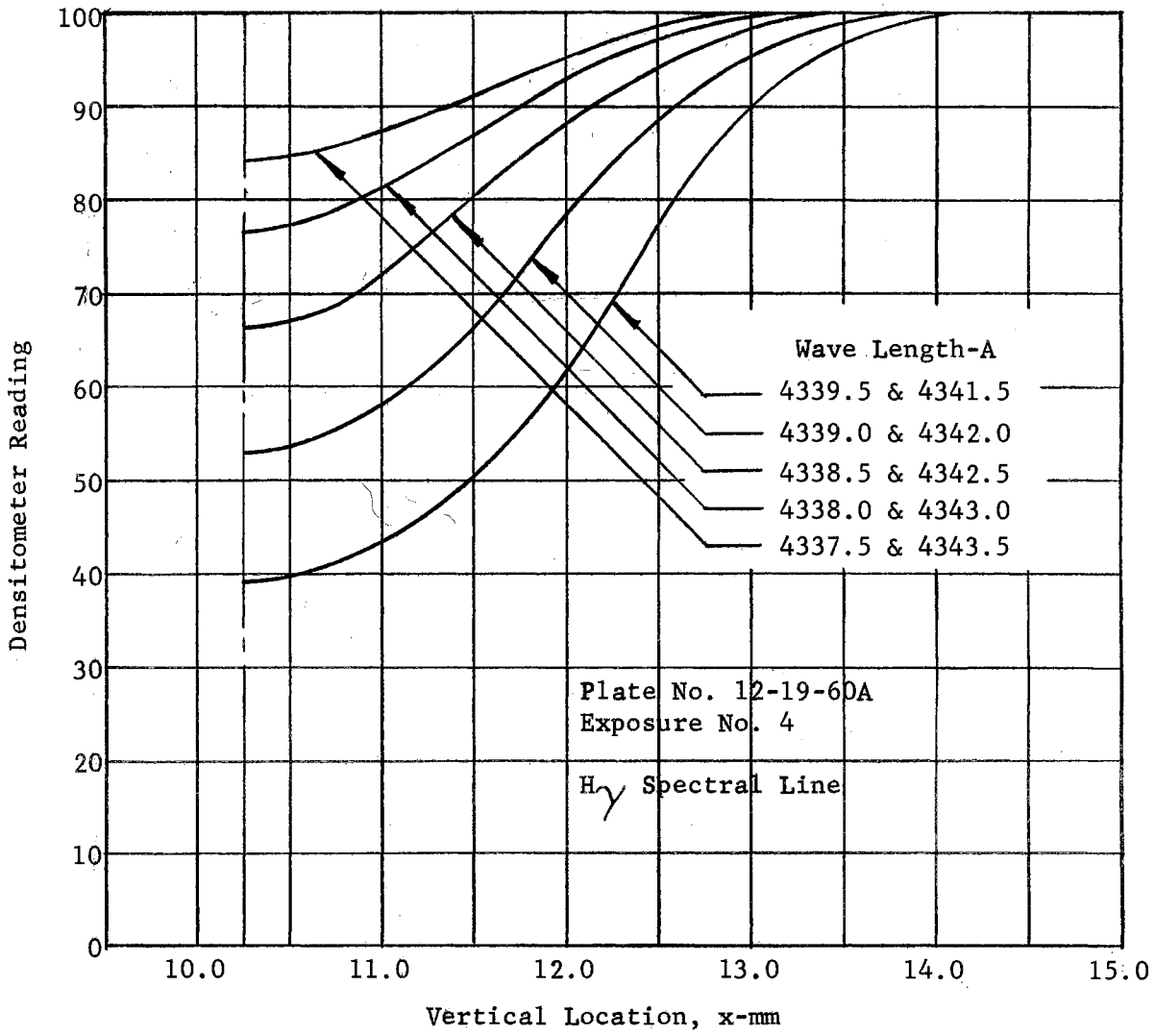

Figure 29b. Densitometer Reading versus Vertical Location

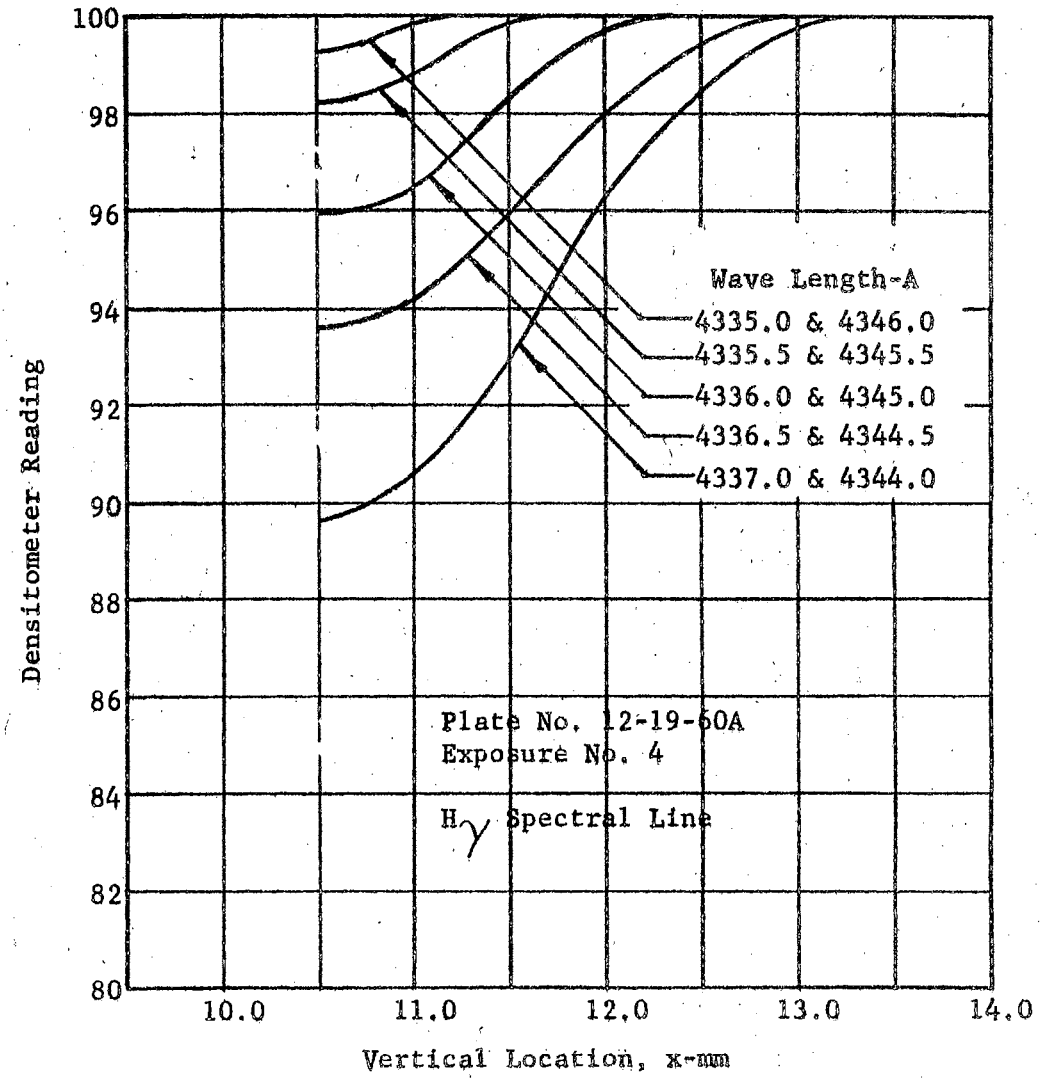

Figure 29c. Densitometer Reading versus Vertical Location

of small errors in aligning the vertical location scale along the true "vertical" direction. This variation was small ($\pm$0.25 mm), and it was decided that the condition of symmetry was the more important guide for establishing the centerline location.

The data given in Figures 29a-29c was used to tabulate the values of densitometer readings for values of change in wave length ($\Delta\lambda$) from the line center designated as $\Delta\lambda = 0$ to $\Delta\lambda = 5.5$A in increments of 0.5A. These densitometer readings are listed for vertical locations (x) on the photographic plate from the centerline (corresponding to the plasma jet centerline) designated as x = 0 out to x = $\pm$5.50 mm in increments of 0.25 mm. These data are given in Table XI. These same data for the other spectral lines that were analyzed are given in Appendix B.

For each densitometer reading in Table XI, the corresponding value of relative intensity that produced that portion of the exposure on the plate was obtained from the emulsion calibration given in Figure 27. The resulting values of relative intensities, $I(\Delta\lambda)$, for the same variations of wave length change ($\Delta\lambda$) and vertical plate location (x) are given in Table XII. Corresponding data for the other spectral lines are given in Appendix B.

Transformation of $I_x(\Delta\lambda)$ to $i_r(\Delta\lambda)$

A plot of the data in Table XII was made as $I_x(\Delta\lambda)$ versus plate location x with $\Delta\lambda$ as a parameter. These curves are shown in Figures 30a and 30b. These curves were made to insure consistent data

TABLE XI

CORRECTED DENSITOMETER READINGS

PLATE NO. 12-19-60A EXPOSURE NO. 4 H_γ SPECTRAL LINE

x mm	$\Delta\lambda$-A											
	0	0.5	1.0	1.5	2.0	2.5	3.0	3.5	4.0	4.5	5.0	5.5
0	12.5	24.2	39.0	53.0	66.2	76.5	84.0	89.6	93.6	96.0	98.2	99.3
±0.25	12.8	24.6	39.6	53.6	66.7	77.0	84.4	90.0	93.7	96.1	98.3	99.4
±0.50	13.2	25.6	41.0	55.3	68.5	78.8	85.5	90.6	94.2	96.4	98.7	99.8
±0.75	13.8	26.8	43.3	58.2	71.6	81.0	87.0	91.6	95.0	97.3	99.4	100.0
±1.00	14.8	28.4	46.3	62.0	76.0	83.8	89.0	92.8	95.9	98.2	99.8	
±1.25	16.0	31.0	50.2	66.0	80.2	87.0	91.0	94.7	97.0	99.1	100.0	
±1.50	18.0	34.0	55.4	72.0	84.4	90.0	93.0	96.3	98.0	99.6		
±1.75	21.0	37.8	61.6	78.6	88.0	92.8	95.0	97.5	98.8	99.9		
±2.00	25.4	42.8	69.0	84.0	91.3	95.3	96.9	98.4	99.4	100.0		
±2.25	31.0	49.4	77.0	88.5	94.0	97.0	98.5	99.2	99.9			
±2.50	37.4	58.6	84.4	92.3	96.4	98.5	99.5	99.7	100.0			
±2.75	45.6	70.4	90.0	95.3	98.1	99.5	100.0	100.0				
±3.00	55.0	81.0	94.0	97.5	99.4	100.0						
±3.25	66.4	88.6	96.8	98.8	100.0							
±3.50	77.8	93.6	98.2	99.8								
±3.75	86.0	97.0	99.4	100.0								
±4.00	91.2	98.8	100.0									
±4.25	95.0	99.8										
±4.50	97.6	100.0										
±4.75	99.0											

TABLE XII

RELATIVE INTENSITY, I_x ($\Delta\lambda$)

PLATE NO. 12-19-60A EXPOSURE NO. 4 H_γ SPECTRAL LINE

x mm	$\Delta\lambda$-A											
	0	0.5	1.0	1.5	2.0	2.5	3.0	3.5	4.0	4.5	5.0	5.5
0	1.330	.660	.378	.254	.180	.136	.110	.090	.068	.053	.034	.021
±0.25	1.285	.650	.372	.252	.178	.134	.108	.088	.067	.052	.033	.020
±0.50	1.240	.622	.356	.238	.170	.128	.103	.085	.065	.050	.030	.010
±0.75	1.180	.590	.334	.222	.157	.120	.098	.080	.060	.042	.020	
±1.00	1.100	.550	.306	.202	.140	.110	.092	.074	.053	.034	.010	
±1.25	1.005	.498	.275	.182	.128	.098	.084	.063	.045	.023		
±1.50	.887	.445	.238	.156	.108	.088	.073	.050	.036	.018		
±1.75	.766	.395	.205	.128	.096	.074	.060	.040	.028	.005		
±2.00	.626	.338	.168	.110	.082	.058	.045	.031	.020			
±2.25	.498	.282	.134	.093	.066	.045	.030	.022	.005			
±2.50	.398	.220	.108	.078	.050	.030	.020	.015				
±2.75	.312	.162	.088	.058	.035	.020						
±3.00	.240	.120	.066	.040	.020							
±3.25	.180	.092	.046	.028								
±3.50	.132	.068	.034	.010								
±3.75	.102	.045	.020									
±4.00	.084	.028										
±4.25	.060	.010										
±4.50	.038											
±4.75	.022											

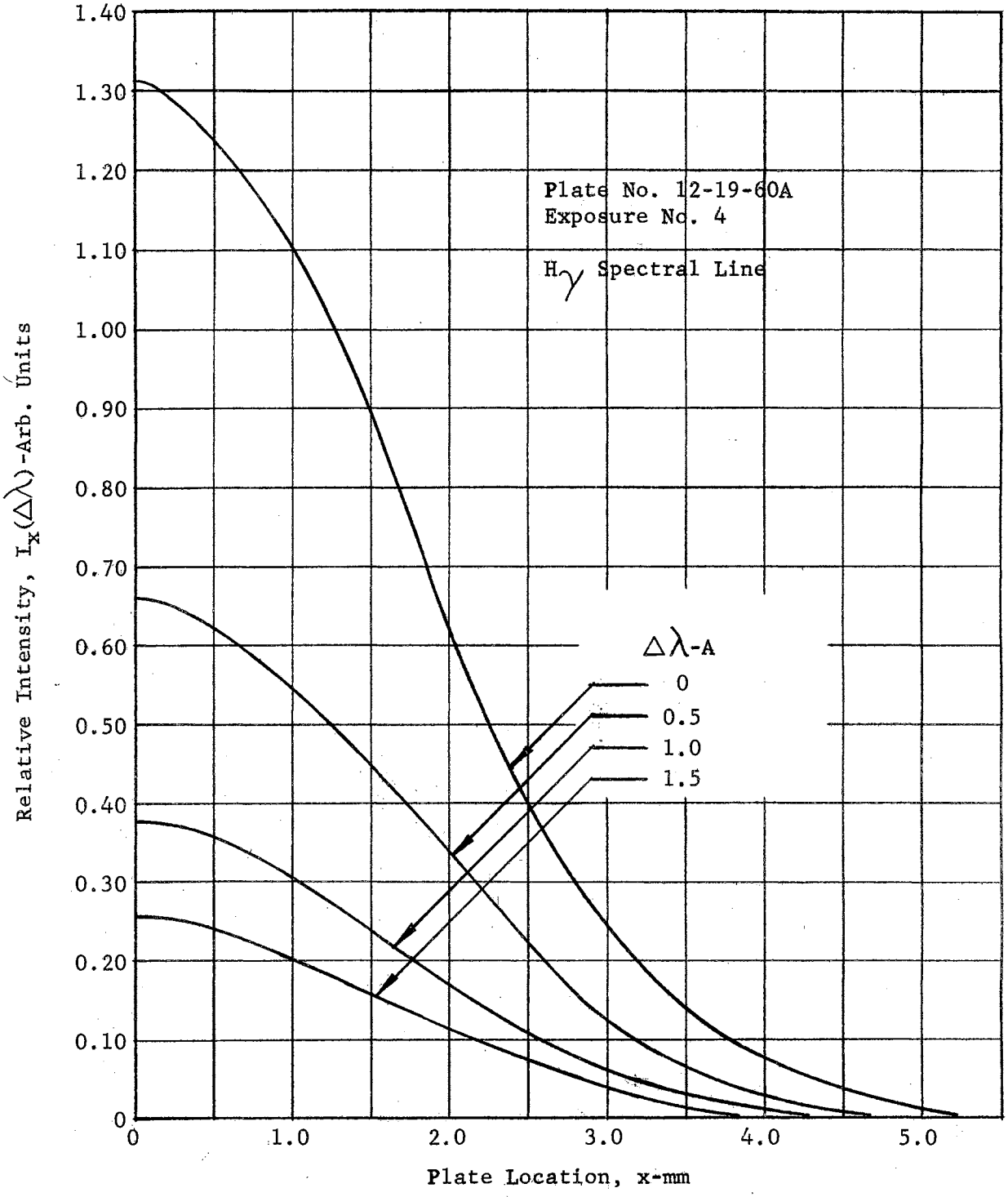

Figure 30a. Relative Intensity versus Plate Location

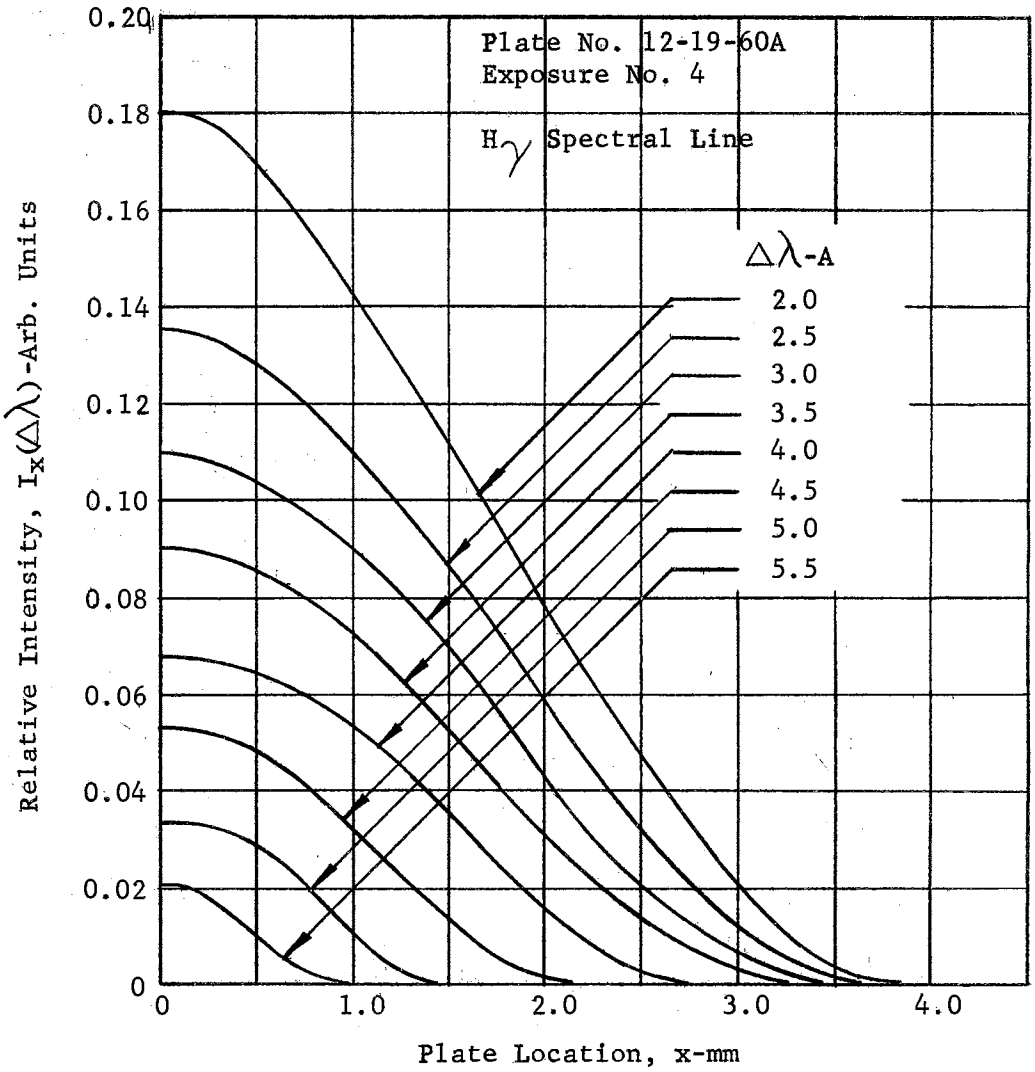

Figure 30b. Relative Intensity versus Plate Location

for relative intensities to be used in the calculation of the radial distribution of relative intensities, $i_r(\Delta\lambda)$. Also, the numerical procedure given by Pearce (2) and summarized in Chapter II was based on using the relative intensity value $I_x(\Delta\lambda)$ at the outer edge of the bounded area $\Delta A_{j,k}$ for that particular area. In this thesis the relative intensity at the center of the bounded area was used; therefore with equal increments in plate dimension x of 0.25, 0.50, 0.75, . . . mm defining the relative areas $\Delta A_{j,k}$, the values of $I_x(\Delta\lambda)$ to be used in the calculation were taken at x = 0.125, 0.375, 0.625, . . . mm. The $\pm$ signs have been omitted from Figures 30a and 30b and all subsequent references to the dimension x.

Table XIII was prepared from the curves of Figures 30a and 30b. The transformation of the relative intensities, $I_x(\Delta\lambda)$, given in Table XIII to relative intensities, $i_r(\Delta\lambda)$ was made according to the set of equations (9) given in Chapter II. The actual calculations were carried out on the IBM 650 computer at the OSU Computing Center. A check was made on the program results by re-computing the data on the IBM 704 computer at the Chance Vought Research Center. The results from both computers were in agreement to the sixth significant figure.

The computer program used with the IBM 650 machine was a standard matrix inversion program supplied by the International Business Machine Corporation. Its official name is Matrix Inversion III. The program write-up is given in Appendix D. The input data for the program was the triangular coefficient matrix given in Table I, which are the $\Delta A_{j,k}$ values for equations (9), and the relative intensities of Table XIII,

TABLE XIII

COMPUTER PROGRAM INPUT DATA, I_x ($\Delta\lambda$)

PLATE NO. 12-19-60A EXPOSURE NO. 4 H_γ SPECTRAL LINE

Row No.	x mm	$\Delta\lambda$-A											
		0	0.5	1.0	1.5	2.0	2.5	3.0	3.5	4.0	4.5	5.0	5.5
1	0.125	1.305	0.657	0.376	0.253	0.179	0.135	0.109	0.090	0.068	0.053	0.033	0.021
2	0.375	1.265	0.638	0.367	0.247	0.174	0.132	0.106	0.087	0.066	0.051	0.032	0.015
3	0.625	1.210	0.605	0.347	0.232	0.164	0.124	0.101	0.083	0.063	0.045	0.025	0.006
4	0.875	1.145	0.568	0.320	0.213	0.148	0.115	0.095	0.077	0.057	0.037	0.016	0.001
5	1.125	1.060	0.523	0.290	0.190	0.134	0.104	0.086	0.068	0.049	0.027	0.006	
6	1.375	0.954	0.475	0.256	0.168	0.118	0.093	0.076	0.057	0.039	0.018	0.001	
7	1.625	0.825	0.422	0.220	0.145	0.102	0.080	0.064	0.045	0.030	0.009		
8	1.875	0.685	0.366	0.185	0.123	0.087	0.067	0.050	0.035	0.021	0.003		
9	2.125	0.552	0.308	0.151	0.101	0.070	0.050	0.035	0.026	0.011			
10	2.375	0.442	0.250	0.120	0.081	0.054	0.037	0.024	0.017	0.005			
11	2.625	0.350	0.191	0.093	0.063	0.039	0.025	0.016	0.010	0.001			
12	2.875	0.276	0.141	0.070	0.045	0.026	0.016	0.009	0.005				
13	3.125	0.212	0.104	0.052	0.029	0.015	0.008	0.004	0.001				
14	3.375	0.158	0.075	0.038	0.018	0.007	0.002	0.001					
15	3.625	0.120	0.052	0.027	0.008	0.001							
16	3.875	0.088	0.034	0.018	0.002								
17	4.125	0.065	0.020	0.009									
18	4.375	0.046	0.010	0.003									
19	4.625	0.030	0.005										
20	4.875	0.017											
21	5.125	0.008											
22	5.375												
23	5.625												
24	5.875												
25	6.125												

which are the $I_{x,j}$ values for equations (9). The full table of coefficients $\Delta A_{j,k}$ was used although many of the values of $I_{k,j}$ were zero.

The problem was to solve 25 linear equations in 25 unknowns for each value of $\Delta\lambda$. This can be written in matrix form as

$$[\Delta A_{j,k}][i_k\ (\Delta\lambda)] = [I_j\ (\Delta\lambda)] \tag{47}$$

In equation (47) the subscripts r and x were replaced by k and j respectively. The values of $i_k\ (\Delta\lambda)$ obtained from the IBM computer program for the H_γ line of Exposure No. 4 are given in Table XIV. Similar results for the other spectral lines are given in Appendix B.

Calculation of Plasma Temperature

The determination of the temperature at one fixed radius (r_{plate} = 2.625 mm) from the radial distribution of relative intensities given in Table XIV is described in what follows. The basic procedure is that given in Chapter III as used by Dickerman (3). The profiles for the variation of the theoretical relative intensity of the broadened hydrogen lines, H_β and H_γ, used in this analysis were those presented by Griem (29)(38). In his work Griem (38) plotted the theoretical relative intensity, $S(\alpha)$, as a function of α, where α is defined as in Chapter III,

$$\alpha = \frac{\Delta\lambda}{E_o} \tag{48}$$

and E_o is the normal field strength as before.

TABLE XIV

COMPUTER PROGRAM OUTPUT DATA, i_r ($\Delta\lambda$)

PLATE NO. 12-19-60A EXPOSURE NO. 4 H_γ SPECTRAL LINE

Row No.	r_{plate} mm	$\Delta\lambda$-A											
		0	0.5	1.0	1.5	2.0	2.5	3.0	3.5	4.0	4.5	5.0	5.5
1	0.125	8.363	4.141	2.385	1.622	1.218	.850	.721	.654	.511	.483	.331	.504
2	0.375	7.532	3.954	2.400	1.694	1.169	.908	.690	.585	.467	.535	.473	.403
3	0.625	6.912	3.512	2.252	1.534	1.165	.798	.630	.567	.491	.474	.387	.166
4	0.875	6.656	3.293	2.017	1.415	.945	.750	.633	.560	.461	.426	.304	.028
5	1.125	6.328	2.979	1.834	1.198	.863	.654	.576	.521	.429	.310	.126	
6	1.375	5.949	2.739	1.628	1.063	.758	.620	.539	.437	.340	.241	.022	
7	1.625	5.294	2.468	1.388	.905	.640	.527	.486	.370	.273	.133		
8	1.875	4.415	2.199	1.178	.785	.588	.517	.421	.275	.236	.057		
9	2.125	3.418	1.895	.964	.650	.486	.371	.289	.227	.125			
10	2.375	2.676	1.629	.764	.528	.397	.297	.195	.157	.071			
11	2.625	2.051	1.261	.596	.444	.302	.203	.145	.097	.016			
12	2.875	1.619	.900	.443	.348	.222	.149	.090	.065				
13	3.125	1.265	.663	.327	.222	.138	.094	.047	.015				
14	3.375	.885	.488	.244	.166	.088	.029	.014					
15	3.625	.692	.351	.179	.088	.014							
16	3.875	.492	.244	.146	.027								
17	4.125	.377	.161	.084									
18	4.375	.284	.074	.038									
19	4.625	.208	.061										
20	4.875	.124											
21	5.125	.093											
22	5.375												
23	5.625												
24	5.875												
25	6.125												

Several curves of $S(\alpha)$ are given by Griem for values of temperature from 10,000 to 40,000°K and electron concentrations, n_e, of 10^{15} to 10^{17} particles per cubic centimeter. As a result of the slowly varying nature of the curves, interpolation and extrapolation of these curves is possible for a range of temperatures from 5,000 to 80,000°K and for electron concentrations from 10^{14} to 10^{19} particles per cm^3.

From the theoretical line profiles presented by Griem and for a value of Ω equal to 0.4, where

$$\Omega = \frac{\alpha_1 - \alpha_2}{\alpha_1} ,$$

calculations were made for the relative intensity ratio, $S(\alpha_2)/S(\alpha_1)$, as a function of α_1 for a range of temperatures and electron concentrations. The results of these calculations for the H_γ line are shown in Figures 31a-31d. The same calculations were made for the H_β line with the resulting curves given in Appendix B.

The data points from Table XIV for r_{plate} = 2.625 mm were plotted using a transparent sheet of log-log coordinate paper with the relative intensity $i_r(\Delta\lambda)$ as the ordinate and the wave length change $\Delta\lambda$ as the abscissa. As a guide in drawing a smooth curve through these data points, an estimate was made for the approximate plasma temperature (10,000°K) and electron concentration (10^{15} cm^{-3}); and the corresponding theoretical relative intensity curve from Griem (38) was drawn on another sheet of log-log coordinate paper. By placing the plotted experimental data points over the theoretical curve and adjusting the two sheets in relation to one another keeping the coordinate axes

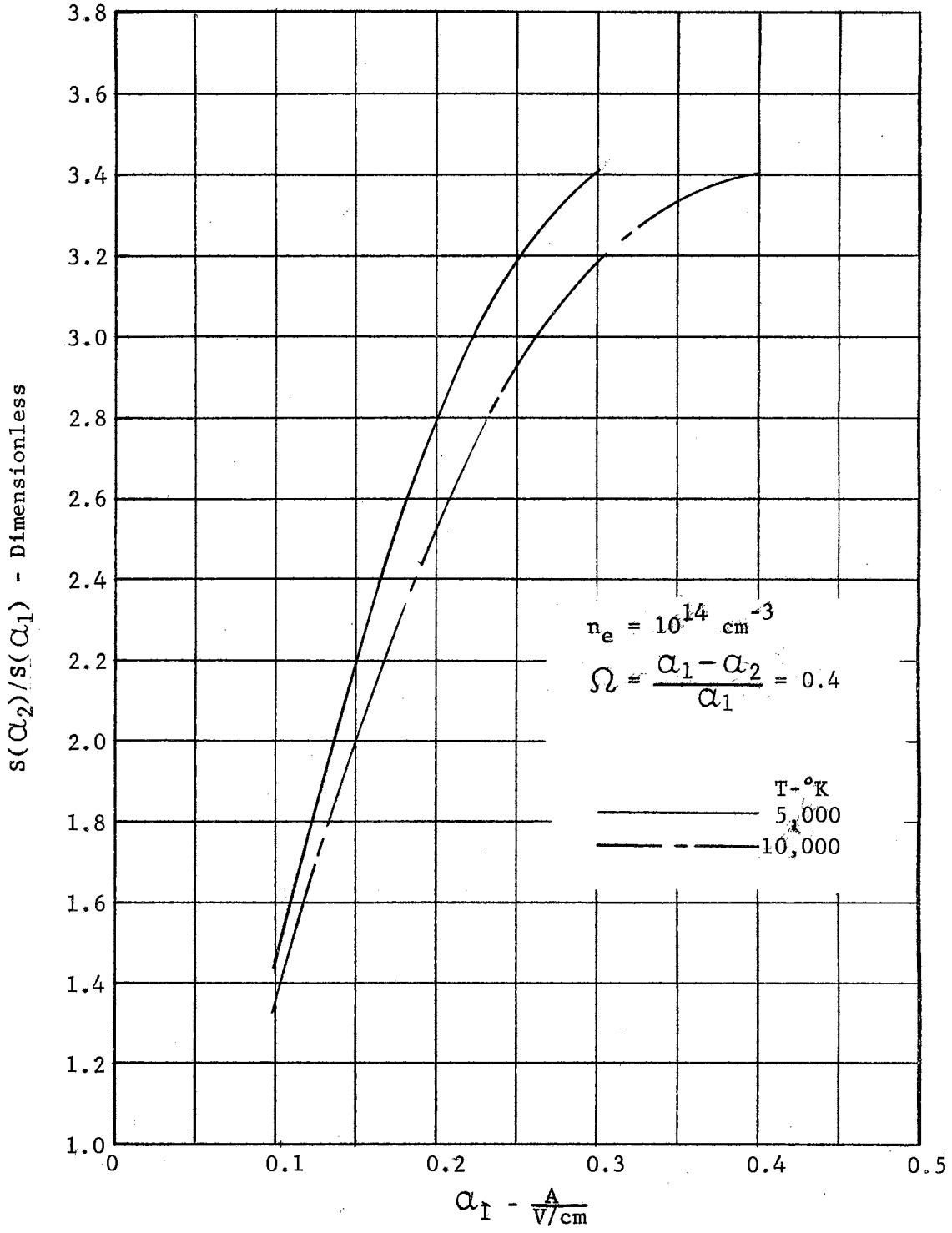

Figure 31a. Theoretical Relative Intensity Ratio for H_γ(38)

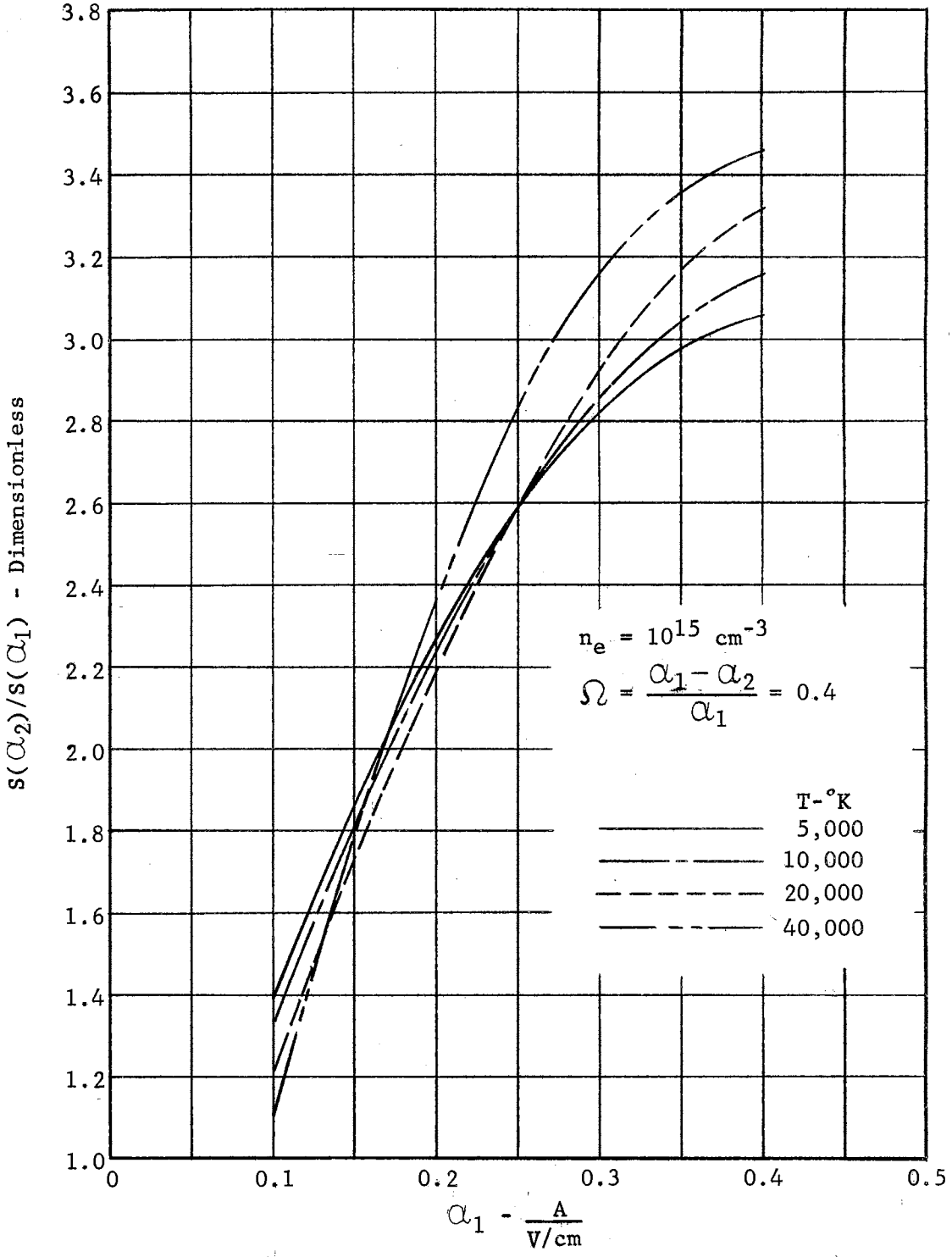

Figure 31b. Theoretical Relative Intensity Ratio for H_γ(38)

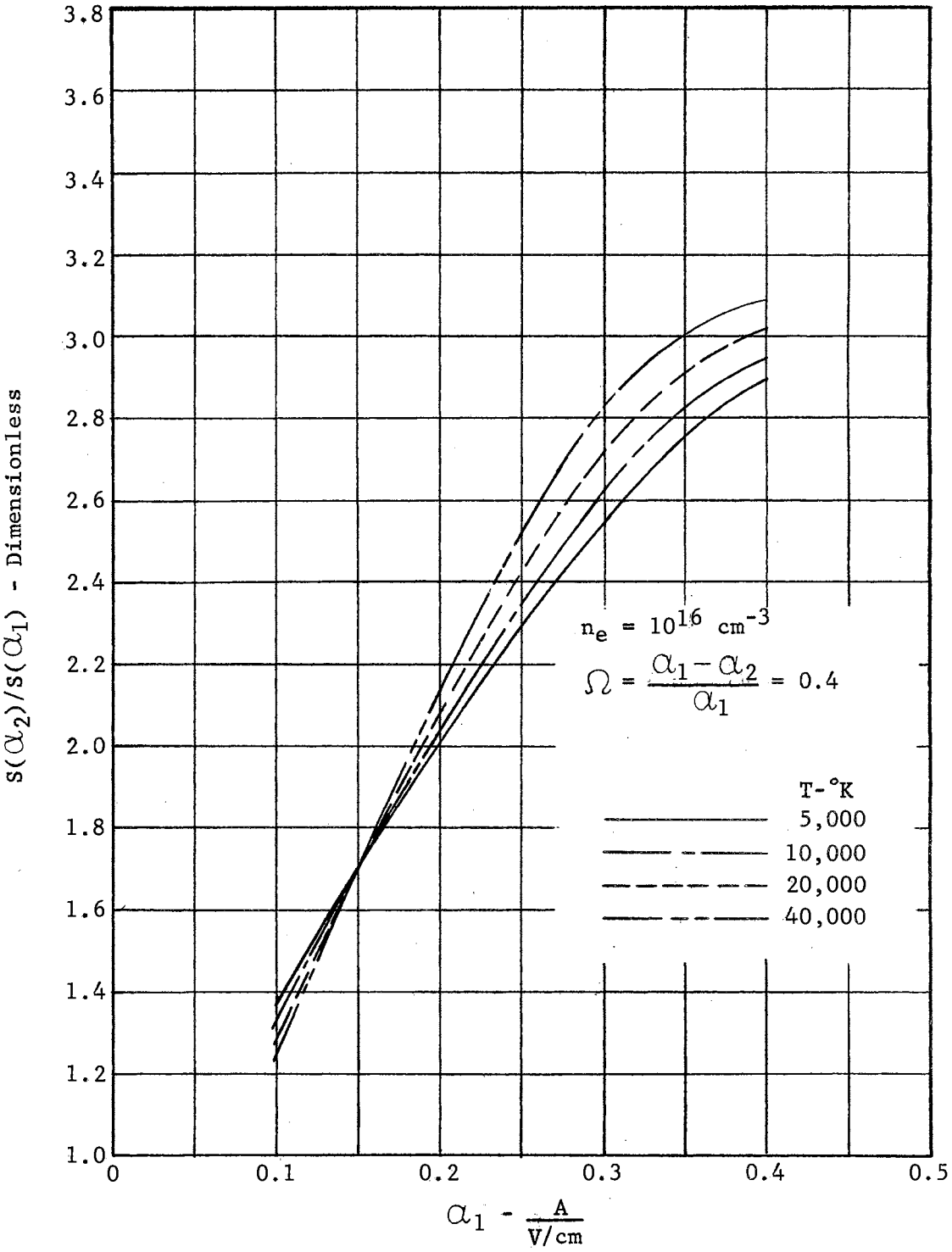

Figure 31c. Theoretical Relative Intensity Ratio for $H_\gamma(38)$

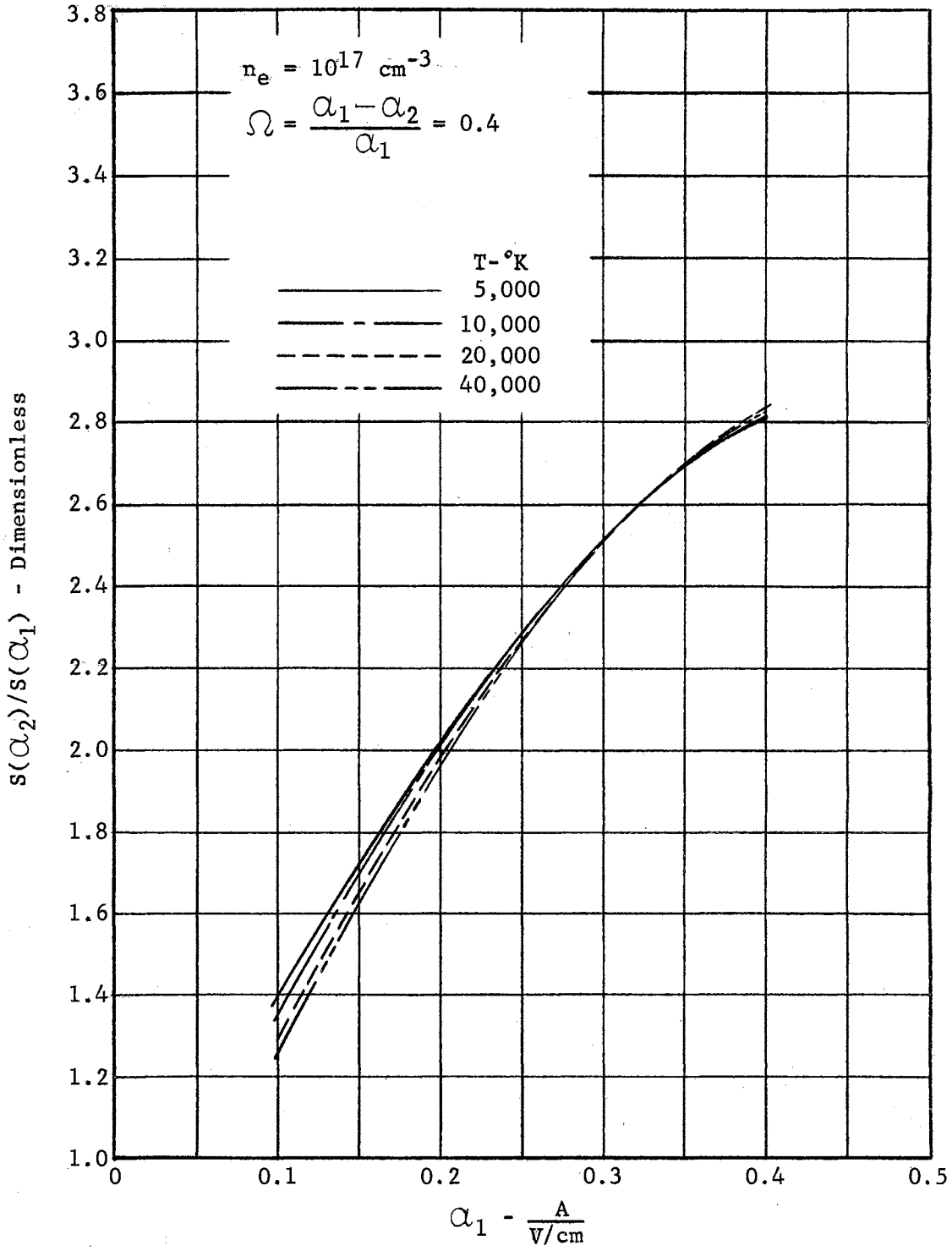

Figure 31d. Theoretical Relative Intensity Ratio for $H_\gamma(38)$

parallel, the experimental curve was drawn which provided the best fit for the experimental data points with the general form of the theoretical curve.

In Figure 32 the plotted data points and the experimental curve are shown with the coordinate axes labeled for the values of $i_r(\Delta\lambda)$ and $\Delta\lambda$. The theoretical relative intensity curve is also shown in Figure 32 as it would appear under the data points after the two sheets had been adjusted as described above. The coordinate axes for the theoretical curve are not given. They would be displaced with respect to the axes for the experimental data.

Noting that the data points coincided very closely with the theoretical curve for $\Delta\lambda$ between 1.5 and 3.0A, this region of the curve was used in the next step. With the same ratio Ω equal to 0.4 and recalling that

$$\Omega = \frac{\alpha_1 - \alpha_2}{\alpha_1} = \frac{\Delta\lambda_1 - \Delta\lambda_2}{\Delta\lambda_1},$$

values of $\Delta\lambda_1$ of 1.5, 2.0, 2.5, and 3.0A were selected and the corresponding values of $\Delta\lambda_2$ calculated. The experimental relative intensities for each couple $(\Delta\lambda_1, \Delta\lambda_2)$ were read from Figure 32, and the relative intensity ratios $i_r(\Delta\lambda_2)/i_r(\Delta\lambda_1)$ were calculated. Entering Figure 31b for T = 10,000°K and $n_e = 10^{15}$ cm^{-3} and for the calculated intensity ratios, the corresponding values for α_1 were obtained. From the definition of α_1, equation (48), and for each $\Delta\lambda_1$ a value for the normal field strength E_o was determined, i. e.,

$$E_o = \frac{\Delta\lambda_1}{\alpha_1} \qquad (49)$$

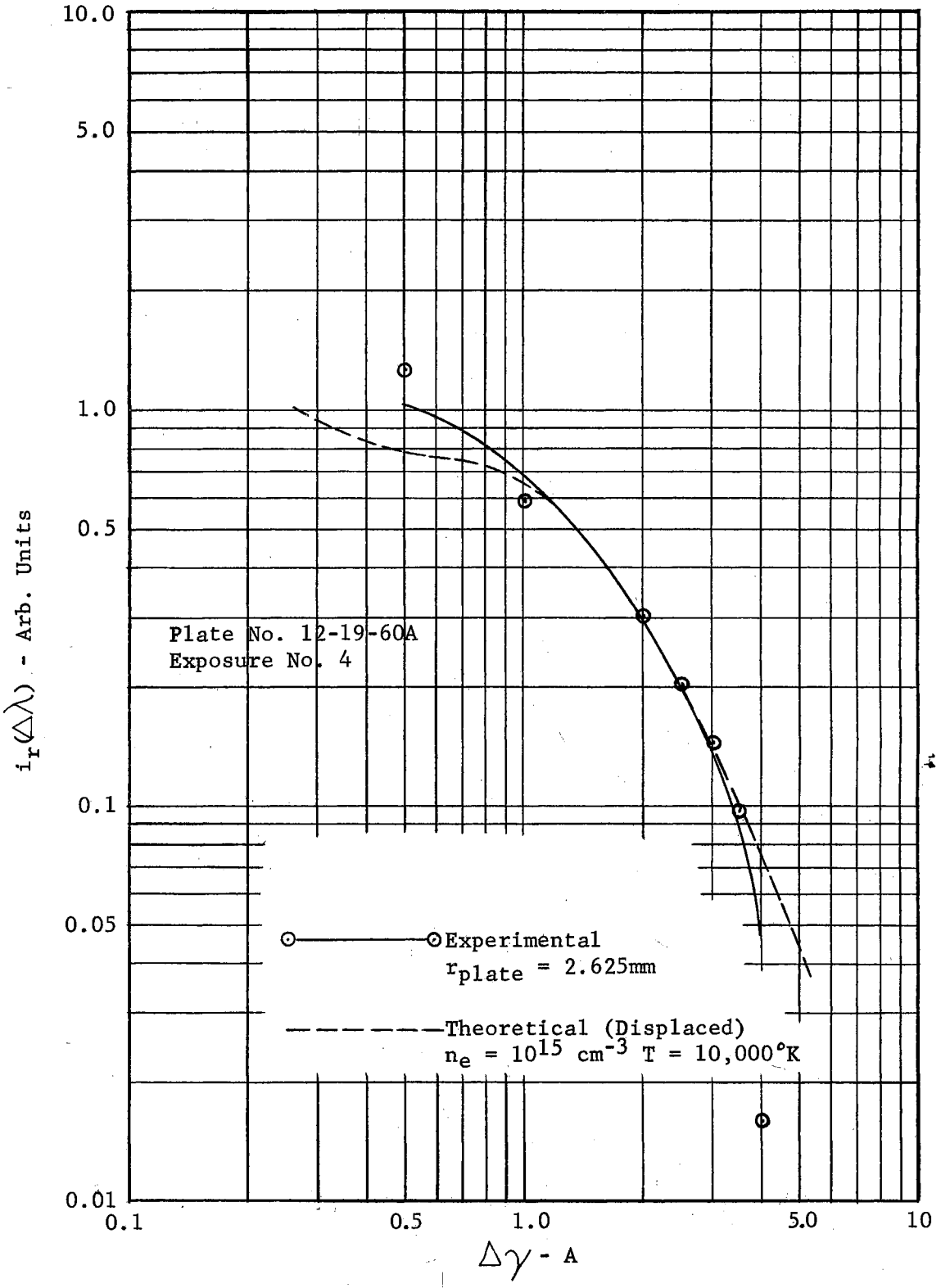

Figure 32. Experimental and Theoretical (Displaced) Relative Intensities for H_γ Spectral Line

Table XV shows the results of these last calculations.

TABLE XV

PLASMA TEMPERATURE CALCULATION

PLATE NO. 12-19-60A H_γ - 4340.5A EXP. No. 4

Plate Radius 2.625 mm Plasma Jet Radius 6.13 mm

$\Omega = \frac{\Delta\lambda_1 - \Delta\lambda_2}{\Delta\lambda_1}$ $n_e = 10^{15}/cm^3$ T = 10,000°K

$\Delta\lambda_1$	$\Delta\lambda_2$	$i(\Delta\lambda_1)$	$i(\Delta\lambda_2)$	$\frac{i(\Delta\lambda_2)}{i(\Delta\lambda_1)}$	α_1	E_o-$\frac{volt}{cm}$	T-°K
1.5	0.9	0.445	0.730	1.640	0.131	11.45	9090
2.0	1.2	0.296	0.572	1.932	0.162	12.35	9190
2.5	1.5	0.200	0.445	2.223	0.197	12.70	9200
3.0	1.8	0.138	0.340	2.465	0.231	13.00	9250

Average Temp = 9180°K

$n_e = 0.98 \cdot 10^{15}/cm^3$

The transformation from normal field strength, E_o, to plasma temperature was obtained by combining the relation between E_o and the ion concentration in the plasma given by equation (39),

$$E_o = 2.61 \cdot e \cdot n_i^{2/3} \quad , \tag{39}$$

with the equilibrium composition of the plasma. For this analysis an argon plasma was assumed neglecting the small percentage contribution of the hydrogen. The equilibrium composition of the plasma was calculated from the data given in Reference 39. For temperatures up to 14,000°K the concentration of doubly ionized argon is negligible

(less than one percent); therefore, the electron and singly ionized argon atom concentrations are equal. The variation of electron concentration with temperature and pressure is shown in Figure 33.

Using equation (39) with the data of Figure 33, the variation of normal field strength with temperature and pressure was calculated. These results are given in Figure 34.

Referring back to Table VI, the test section pressure for Run No. 3, which corresponds to Exposure No. 4 on the photographic plate was 0.364 psia. Based on standard atmospheric pressure of 14.696 psia, the pressure ratio P/P_o was calculated;

$$P/P_o = \frac{0.364}{14.696} = 0.0248 \ ,$$

and

$$\log_{10} \frac{P}{P_o} = \log_{10}(0.0248) = -1.606 \ .$$

Entering Figure 34 for the values of E_o given in Table XV and for $\log_{10} P/P_o = -1.606$, values for the plasma temperature were obtained. These values are listed in Table XV.

These temperatures represent the first approximations for one particular radius ($r_{plate} = 2.625$ mm). Two assumptions were made during the analysis which must be checked; namely, a plasma temperature of 10,000°K and an electron concentration of 10^{15} particles per cubic centimeter. The calculated average temperature was 9180 ± 90°K; and with the slowly varying nature of the theoretical profiles this checked with the assumed value. The electron concentration for the calculated

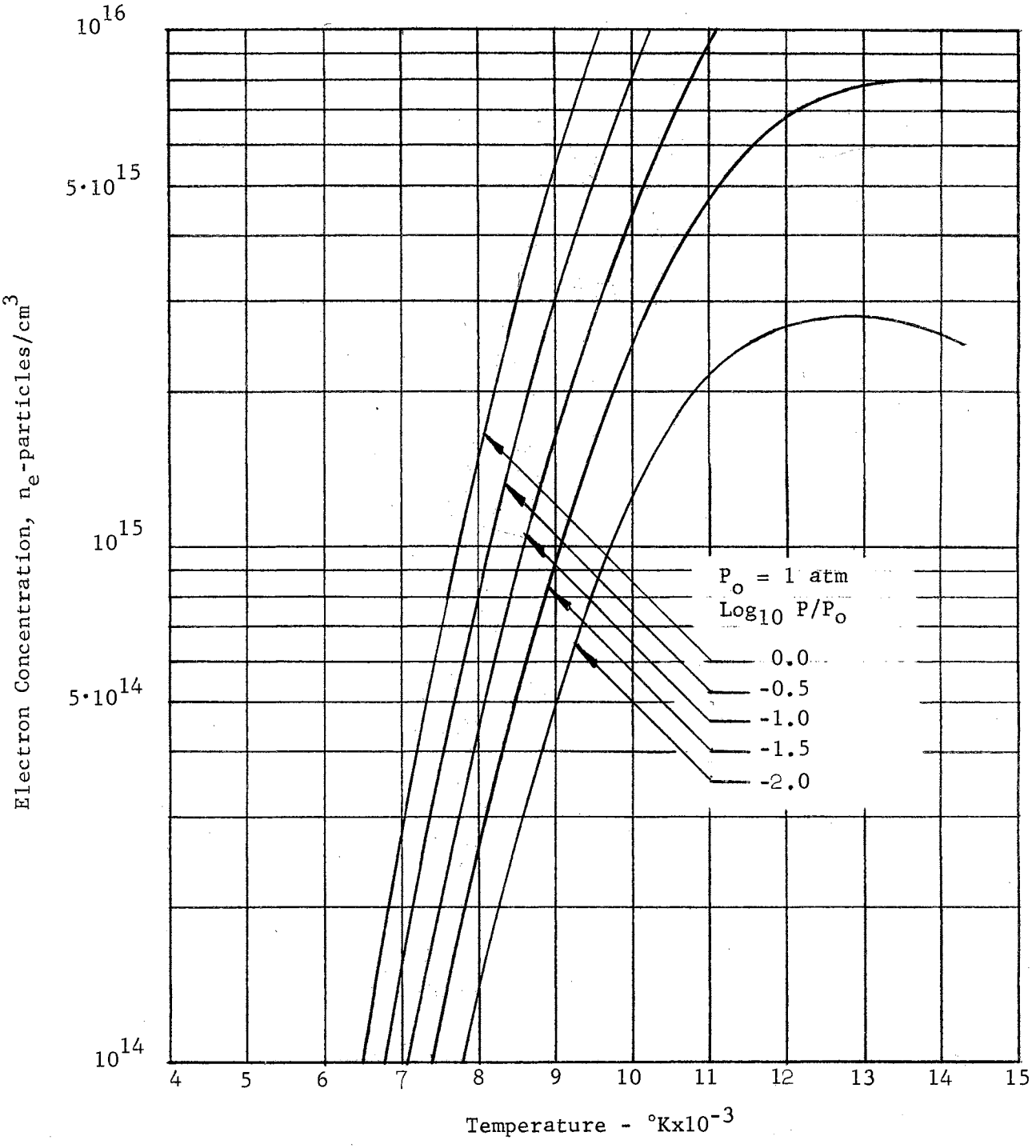

Figure 33. Argon Plasma Electron Concentration

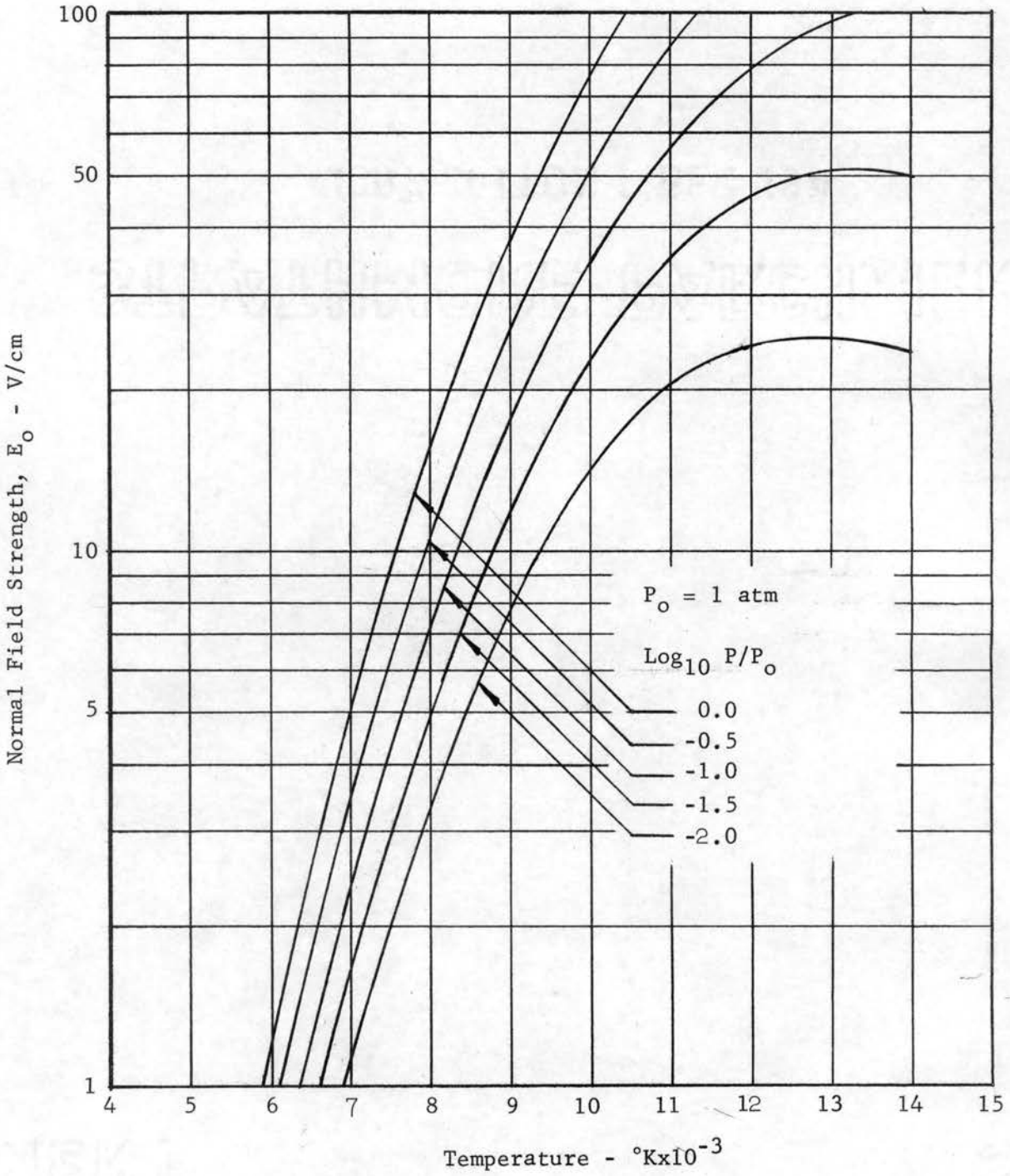

Figure 34. Normal Field Strength E_o for Argon Plasma

plasma temperature and pressure of 9180°K and 0.364 psia respectively was read from Figure 33. The value obtained was $n_e = 0.98 \cdot 10^{15}$ cm^{-3} which agreed with the assumed value of 10^{15} cm^{-3}.

If the calculated temperature and/or the electron concentration had varied appreciably from the assumed values, a second calculation would have to be made using the first calculated values as the new estimates. As a result of using relative intensity ratios in the procedure, a rapid convergence to the correct temperature was achieved.

As an example consider the data in the first line of Table XV. If the electron concentration were assumed to be 10^{17} cm^{-3} instead of 10^{15} cm^{-3}, the value of α_1 obtained from Figure 31d would have been 0.146. The new value of E_o would have been

$$E_o = \frac{\Delta\lambda_1}{\alpha_1} = \frac{1.5}{0.146} = 10.27 \ ,$$

and the resulting temperature read from Figure 34 would have been 8900°K. The electron concentration for this temperature read from Figure 33 would have been $0.74 \cdot 10^{15}$ cm^{-3}. The second iteration using $0.74 \cdot 10^{15}$ cm^{-3} for the electron concentration would then yield the same final temperature as shown in Table XV.

The above analysis was performed for several other radial locations to determine the radial temperature distribution. The change from plate radius to plasma jet radius was calculated from the known magnification of the external optics for the CVRC facility ($r_{plate} = 0.428\ r_{jet}$). Radial temperature distributions were obtained from the analysis of the H_γ lines of Exposures No. 2, 3, and 4 and of the H_β line of

Exposure No. 4. All of the data used in these calculations and not included in this chapter are given in Appendices A, B, and C. The results of these calculations are presented in Chapter VII.

CHAPTER VII

RESULTS AND DISCUSSION

The establishment of the OSU Plasma Facility was completed and preliminary runs gave satisfactory operation. The starting procedure and techniques for making operational adjustments in power input, gas flows, and test section pressure were determined. Using argon and argon with hydrogen tracer for the stabilizing gas, the system has been run successfully up to the present current limit for the power leads (400-500 amperes). A sample data sheet for operation at 400-500 amperes was given in Table IV.

Calculations were made for the data in Table IV to determine the net energy input to the stabilizing gas and the average gas temperature (based on assumed thermodynamic equilibrium) at the exit section of the plasma generator. These calculations are shown in Appendix E, and the results are given in Table XVI.

The spectrographic plate shown in Plate X was taken during Runs No. 1, 2, and 3 reported in Table IV. A comparison of the broadened hydrogen lines H_β and H_γ with those shown on the CVRC spectrographic plate (Plate XI) indicated that the analysis given in Chapter VI for determining plasma temperature distribution can be used with the OSU Plasma Facility data.

TABLE XVI

OSU PLASMA FACILITY RESULTS

Date: 3-22-61 — Recorded Data: Table IV

	Run Number (1)	(2)	(3)
Total Power Input, P_{in} - Btu/hr	49,200	59,800	47,300
Power Loss to Cooling Water, P_L - Btu/hr	26,000	32,900	23,550
Net Power to Gas, P_g - Btu/hr	23,200	26,900	23,750
Argon Flow Rate, $\dot{m}_A$ - lb_m/hr	8.68	8.68	8.78
Hydrogen Flow Rate, m_{H_2} - lb_m/hr	0.0114	0.0112	----
Hydrogen-Argon Ratio by Volume	0.026	0.026	----
Test Section Pressure, p_t - psia	0.314	0.314	0.314
Average Gas Temperature at Nozzle Exit, T_g - °K (Effect of Hydrogen neglected)	8950	9250	9000

The background radiation on the OSU spectrographic plate was more pronounced than on the CVRC plate. This was caused by the presence of air in the OSU plasma generator. The plasma generator assembly was not completely sealed; and during operation with test section pressures below atmospheric, the chamber pressure was also below atmospheric resulting in air leakage into the chamber. The oxygen in the air reacted with the high temperature tungsten tip and copper nozzle causing contamination of the main argon and hydrogen flow with additional radiation emitting components. These additional components were the source for the observed background radiation. The level of this background was not high enough to prohibit the use of the plate for plasma temperature determination. Care would have to be taken to subtract

this background level when the relative intensity distribution was obtained from the densitometer readings.

The results for the determination of plasma temperature distributions from the CVRC spectrographic plate (Plate XI) are given in Table XVII. The power input, argon gas flow rate, and cooling water flow rates were held constant throughout the test. Only the hydrogen flow rate was changed (see Table VI).

The data for Table XVII were obtained from the calculation tables given in Appendix C. The range shown with each temperature was the deviation of the maximum and minimum temperatures from the arithmetic average temperature calculated for each radius. Except for the first temperature in the H_β column the deviations were within the ± 5 percent accuracy predicted by Dickerman (3) for the analysis procedure. The consistency of the arithmetic mean temperatures for each radius as obtained for the four different lines was well within this limit of accuracy.

The arithmetic mean temperatures were plotted in Figures 35 and 36. Figure 35 shows a comparison of the plasma temperature distributions obtained from the H_γ lines. The negligible effect of the variation in hydrogen tracer from 1.6 to 2.9 percent is clearly shown. A comparison of the temperature distributions obtained for a fixed percentage of hydrogen (2.9 percent) and for two spectral lines, H_β and H_γ, was presented in Figure 36. Again the variation in temperature distribution was within the accuracy of the method used for the calculations.

Two additional observations were made from the data presented in

TABLE XVII

CVRC PLASMA JET TEMPERATURE DISTRIBUTION

ONE NOZZLE DIAMETER DOWNSTREAM OF NOZZLE EXIT

PLATE NO. 12-19-60A NOZZLE EXIT DIAMETER = 21.3 mm

Temperatures-°K

Exposure No.	2	3	4	4
Spectral Line	H_γ	H_γ	H_γ	H_β
Percent Hydrogen	2.3	1.6	2.9	2.9
r_{jet}-mm				
0.29	9460^{+170}_{-240}	9560^{+230}_{-260}	9640^{+180}_{-140}	9930^{+770}_{-530}
1.46	9470^{+180}_{-190}	9570^{+160}_{-220}	9560^{+210}_{-280}	9760^{+200}_{-360}
2.63	9460^{+110}_{-200}	9620^{+200}_{-250}	9490^{+230}_{-280}	9720^{+170}_{-320}
3.80	9430^{+150}_{-120}	9590^{+100}_{-180}	$9350^{+\ 50}_{-140}$	9630^{+140}_{-190}
4.96	$9320^{+\ 80}_{-140}$	$9450^{+\ 70}_{-100}$	$9260^{+\ 80}_{-140}$	9270^{+140}_{-120}
6.13	$9240^{+\ 80}_{-120}$	$9250^{+\ 70}_{-\ 70}$	$9180^{+\ 70}_{-\ 90}$	$9010^{+\ 40}_{-\ 50}$
7.30	$8830^{+\ 70}_{-100}$	8750^{+120}_{-250}	$8820^{+\ 80}_{-170}$	$8750^{+\ 80}_{-130}$
8.47	$8550^{+\ 70}_{-150}$	$8450^{+\ 70}_{-150}$	$8480^{+\ 80}_{-180}$	8560^{+110}_{-110}

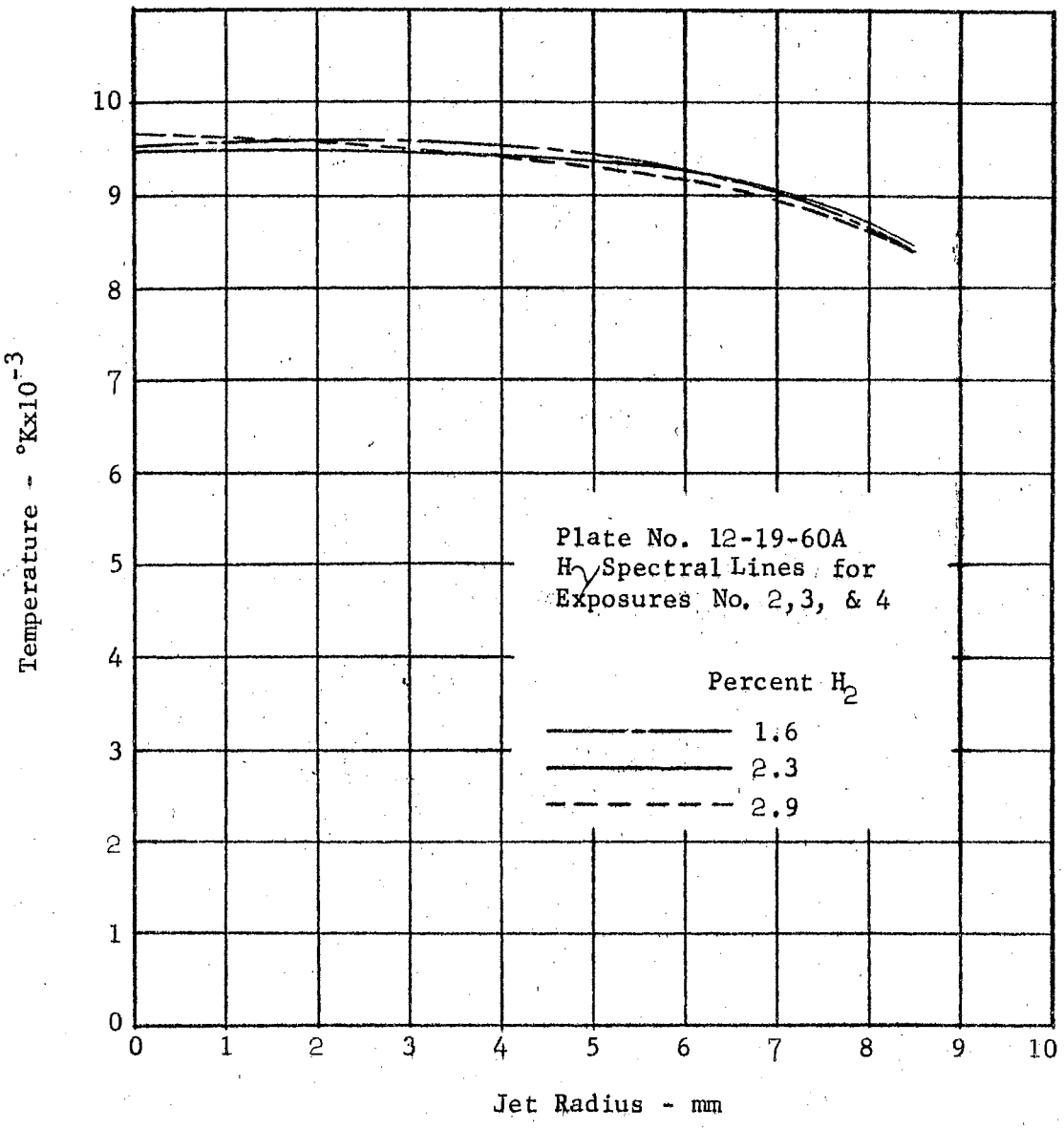

Figure 35. Comparison of Argon Plasma Jet Temperature Distributions With Variation in Percent Hydrogen Tracer

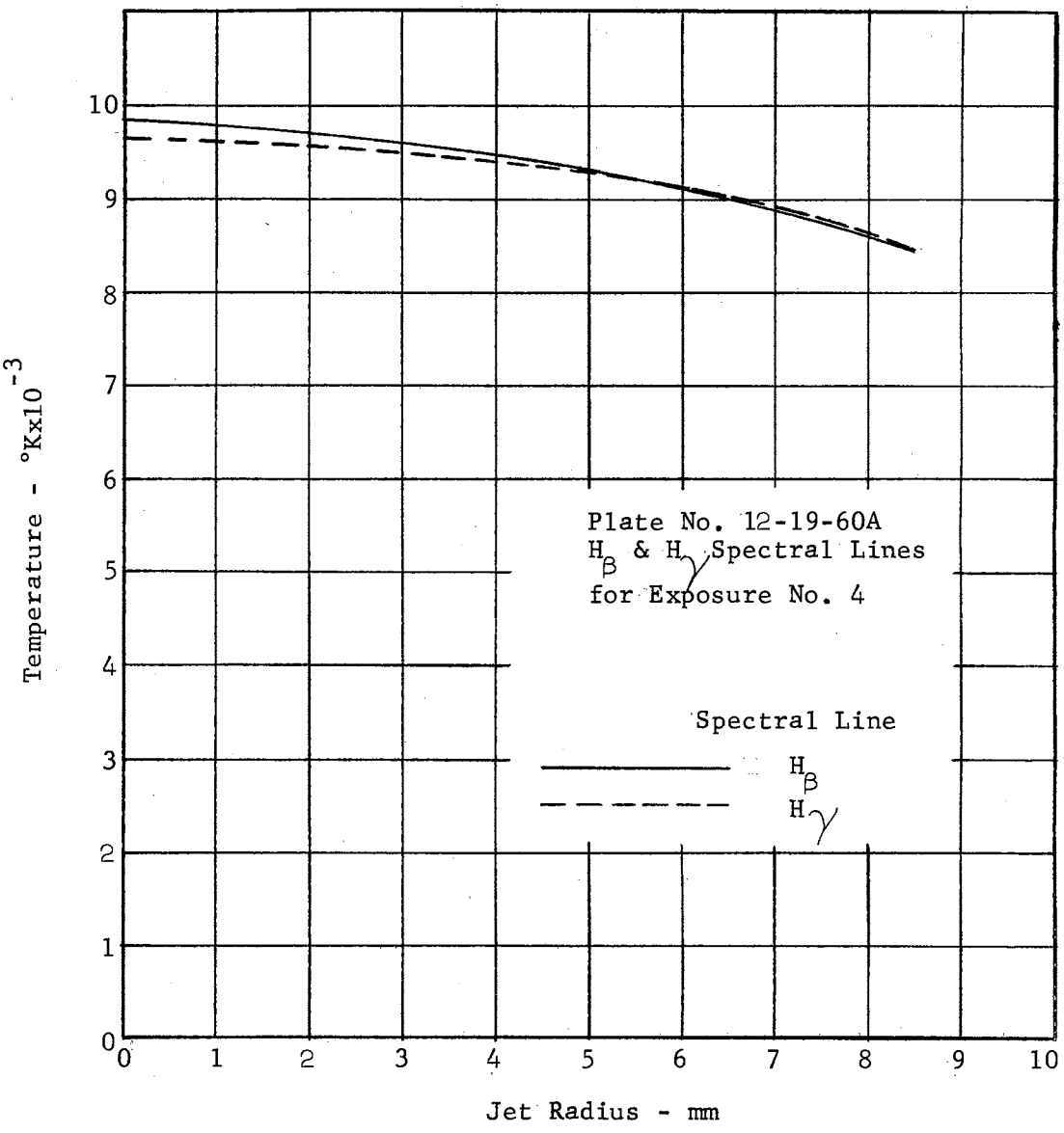

Figure 36. Comparison of Argon Plasma Jet Temperature Distributions for 2.9 Percent Hydrogen Tracer From Analysis of H_β and H_γ Spectral Lines

Table XVII. First, the deviations from the average temperatures were consistently larger near the center of the jet (small values of r_{jet}). This resulted from the method used for transformation of the observed relative intensities, $I_x(\Delta\lambda)$, into the radial relative intensities, $i_r(\Delta\lambda)$. The calculation for the relative intensity $i_r(\Delta\lambda)$ at radius r_k depended on the previously calculated relative intensities at r_{k+1}, r_{k+2}, ...; therefore, the calculated value $i_r(\Delta\lambda)$ for each successive layer moving inward toward the center contained the errors of all the calculated values of $i_r(\Delta\lambda)$ for the outside layers.

Second, the deviations for the H_β line calculations were larger, generally, than those for the H_γ line. The main cause for this was the difficulty in establishing the wave length location accurately while making the densitometer readings. There are no visible argon spectral lines located near either side of the H_β line. The wave length locations for the H_β line were determined by first finding the center of the line, as previously described in Chapter VI for the argon lines, and then using a constant value of 5A/mm for the reciprocal dispersion in this region. Also the H_β line does not broaden so much as the H_γ line; hence, even more accurate wave length determination was necessary but was not possible with the available equipment.

CHAPTER VIII

CONCLUSIONS AND RECOMMENDATIONS

The objectives of the work reported in this thesis were (1) to establish a versatile plasma facility readily adaptable to basic research on the nature of high temperature, partially ionized gases; and (2) to develop further a procedure for determining plasma temperatures based on the theory of Stark broadening of the spectral lines of hydrogen, which was added in small quantities to the main plasma gas flow.

The construction of the OSU Plasma Facility was completed and successful operation of the equipment was achieved. A starting procedure and the techniques for operational adjustments in power input, gas flow rates, and test section pressure were developed. The analytical procedure for the determination of plasma temperatures was presented in detail and illustrated by actual calculations.

The results of the preliminary operation of the OSU Plasma Facility using argon as the stabilizing gas indicated that the expected power input of 20 kilowatts was attainable. Also, the spectrographic results (Plate X) showed that a small hydrogen addition to the main argon flow could be used to produce broadened spectral lines for plasma temperature calculations.

The use of argon as the primary arc stabilizing gas limits the

power input with the present equipment. With the arc voltage nearly constant at approximately 35-40 volts and the current limited to 400-500 amperes by the power leads, the maximum power input is 20 kilowatts. Using nitrogen as the primary gas, the arc voltage would be doubled (70-80 volts) and up to 40 kilowatts could be used for the same current limit of 400-500 amperes. Modification of the power leads to carry 700 amperes would extend the available power input range up to the current limit of the DC power supply.

The consistency of the results of the plasma temperature calculations as shown in Table XVII and Figures 35 and 36 provided confirmation for the use of the Stark broadening theory. The effect of the small percentage of hydrogen on the equilibrium composition of the argon plasma was neglected in the analysis presented in this thesis. The fact that the calculated plasma temperatures did not vary significantly with a change in the percentage of hydrogen added to the flow indicated that this assumption was valid. A further check could be made on this assumption by recalculating the equilibrium compositions for mixtures of argon and hydrogen and replotting Figures 33 and 34 to show the electron concentration and normal field strength of the mixtures versus temperature and pressure.

An improvement in the mechanics of the analytical procedure could be gained by adding a constant speed drive to the lateral motion of the densitometer table and using a chart recorder to measure the output of the photocell as the plate is moved at constant speed over the photocell slit. These additions would give a continuous trace

of the densitometer readings versus lateral location (wave length) for each vertical location. This would eliminate the plotting and smoothing process shown in Figures 28a-28d.

In conclusion, suggestions for future plasma research are given in the following lines.

Research into the nature of plasmas and the determination of their basic physical and transport properties is necessary to provide the knowledge required for the successful solution of the problems associated with high temperature, partially ionized gases. The first important component of this knowledge is the ability to specify the temperature and composition at any particular location in a plasma. For plasmas in thermodynamic equilibrium one method that may be used was presented in this thesis. Other methods may have to be developed for non-equilibrium conditions.

Many of the problems that arise with plasmas result from the intense radiation from the highly excited components in the gas. An understanding of the radiative process and the determination of the macroscopic absorptivities and emissivities of plasma fields is required for the solution of these problems.

Another area for future research is the study of the use of electromagnetic fields on plasmas for containment, acceleration and deceleration. Associated with this work is the determination of velocity and pressure distributions in the plasma.

BIBLIOGRAPHY

1. McQuiston, F. C., "Design and Operation of a Plasma Generator Using Argon as the Stabilizing Gas," (unpub. M.S. thesis, Oklahoma State University, 1959).

2. Pearce, W. J., "Plasma Jet Temperature Study," Report No. R59SD440, Aerosciences Laboratory, Missile and Space Vehicle Department, General Electric Company.

3. Dickerman, P. H., "The Determination of Equilibrium Temperature of a Plasma," Conference on Extremely High Temperature, (H. Fischer and L. C. Mansur, Editors), John Wiley and Sons, New York, 1958.

4. Jovanovic, M. K. and Haworth, D. R., "The Development of a Plasma Facility and a Survey of Spectroscopic Methods for Plasma Temperature Determination," Annual Report to National Science Foundation on Grant No. G-10161, December, 1960.

5. Abel, N. H., "Solution de Quelques problèmes à l'aide d'intégrales définies," 1823, Oeuvres, Christiania, 1881, Tôme I, p. 11.

6. Hercus, E. O., Elements of Thermodynamics and Statistical Mechanics, Melbourne University Press (Australia), 1950.

7. Kowalewski, G., Integralgleichungen, Walter de Gruyter and Company, Berlin, 1930.

8. Hamel, G., Integralgleichungen, Julius Springer, Berlin, 1937.

9. Hörmann, H., "Temperaturverteilung und Elektronendichte in Frei Brennenden Lichtbögen," Zeitschrift für Physik, Bd. 97, 1935.

10. Eggert, J., "Über den Dissoziationszustand der Fixsterngase," Physik. Zeitschrift, 20, December, 1919.

11. Saha, M. N., "Ionization in the Solar Chromosphere," Phil. Mag. Vol. 40, October, 1920.

12. Franck, J. and Hertz, G., Verhandlungen d. Deutsch. Phys. Ges. 16, 1914 or Phys. Zeits. 17, 1916.

13. Fermi, E., Thermodynamics, Dover Publications, Inc., New York, 1956.

14. Fowler, R. H. and Milne, E. A., "Dissociation Equilibria by the Method of Partitions," Phil. Mag. 45, 1, 1923.

15. Unsöld, A., Physik der Sternatmosphären, Julius Springer, Berlin, 1948.

16. Waldmeier, M., Einführung in die Astrophysik, Birkhaüser Verlag, Basel, 1948.

17. Menzel, D. H., "A Simple Derivation of the Dissociation Formula," Proc. Nat. Acad. Sci. (Washington), 19, 40, 1933.

18. Meek, J. M. and Craggs, J. D., Electrical Breakdown of Gases, The Clarendon Press, Oxford, 1953.

19. Burhorn, F., Maecker, H., and Peters, T., "Temperaturmessungen am Wasserstabilisierten Hochleistungsbogen," Zeitschrift für Physik, Bd. 131, 1951.

20. White, H. E., Introduction to Atomic Spectra, McGraw-Hill, Inc., New York, 1934.

21. Broida, H. P., "Experimental Temperature Measurements in Flames and Hot Gases," Temperature, Its Measurement and Control in Science and Industry, Vol. II, (H. C. Wolfe, Editor), Reinhold Publishing Company, New York, 1955.

22. Dieke, G. H., "High Gas Temperatures," Temperature, Its Measurement and Control in Science and Industry, Vol. II, (H. C. Wolfe, Editor), Reinhold Publishing Company, New York, 1955.

23. Stark, J., Berl. Akad. Wiss., 40, 1913.

24. Larenz, R. W., "Über ein Verfahren zur Messung sehr hoher Temperaturen in nahezu durchlässingen Bogensaülen," Zeitschrift für Physik, Bd. 129, 1951.

25. Constant, F. W., Theoretical Physics -- Thermodynamics, Electromagnetism, Waves and Particles, Addison-Wesley, Inc. Reading, Mass., 1958.

26. Holtsmark, J., "Über die Verbreiterung von Spektrallinien," Annalen der Physik, 58, 1919.

27. Debye, P., "Das Molekulare Elektrische Feld in Gasen," Phys. Zeits., 20, 1919.

28. Busz, G. and Finkelnburg, W., "Thermische Lichtbogen hoher Temperature und niedriegen Brennspannung," Zeitschrift für Physik, Bd. 138, 1954.

29. Griem, H. R., Kolb, A. C., and Shen, K. Y., "Stark Broadening of Hydrogen Lines in a Plasma," Phys. Rev., Vol. 116, No. 1, Oct. 1959.

30. Ecker, G., "Das Mikrofeld in Gesamtheiten mit Coulombscher Wechselwirkung," Zeitschrift für Physik, 148, 1957.

31. Bogen, P., "Experimentelle Prüfung der Holtsmarkschen Theorie der Linienverbreiterung," Zeitschrift für Physik, 149, 1957.

32. Burkhart, M. K., "A Supersonic, Shock Free Nozzle for an Existing Plasma Generator and Its Facilities," (unpub. M.S. thesis, Oklahoma State University, 1960).

33. Lai, W., Gustavson, J. and Talbot, L., "Design Considerations and Initial Evaluation of Model B Plasma Generator," Institute of Engineering Research Technical Report HE-150-161, University of California.

34. Foelsch, K., "The Analytical Design of an Axially Symmetric Laval Nozzle for a Parallel and Uniform Jet," Journal of the Aeronautical Sciences, Vol. 16, No. 3, 1949, pp. 161-166, 188.

35. Warder, R. C., "Design Considerations and Development of a Plasma Research Facility," (unpub. M.S. Thesis, Northwestern University, 1960).

36. "The F & P Tri-Flat Variable-Area Flowmeter Handbook," Fischer and Porter Company, Hatboro, Pa.

37. Harrison, G. R., Lord, R. C., and Loofbourow, J. R., Practical Spectroscopy, Prentice-Hall, Inc., New York, 1948.

38. Griem, H. R., Kolb, A. C., and Shen, K. Y., "Stark Broadening of Hydrogen Lines in Plasma," Naval Research Laboratory Report 5455, USNRL, Washington, D. C., 1960.

39. Cann, G. L., "Argon Mollier Chart," Air Force Office of Scientific Research TN 59-247, Armed Services Technical Information Agency Document No. AD212227.

APPENDIX A

RECORDED DENSITOMETER READINGS FOR CVRC SPECTROGRAPHIC PLATE NO. 12-19-60A

TABLE XVIII

DENSITOMETER READINGS

PLATE NO. 12-19-60A EXPOSURE NO. 2 H_γ SPECTRAL LINE

Photocell Slit: Height-0.5 mm Width-15 microns

LATERAL LOCATION mm \ VERTICAL LOCATION-mm	2.0	2.5	3.0	3.5	4.0	4.5	5.0	5.5	6.0	6.5	7.0	7.5	8.0	8.5	9.0	9.5	10.0	10.5
74.0						100.0	100.0	92.1	92.6	92.0	96.6	94.4	99.6					
73.0						99.5	98.4	96.8	92.6	93.8	94.9	97.6	100.0	100.0				
72.0						98.6	96.4	92.7	94.0	90.2	93.6	95.4	97.8	97.9				
71.0				100.0	100.0	94.3	94.3	88.4	88.8	88.2	90.1	90.7	93.4	98.2	100.0			
70.0				99.2	98.8	94.2	90.4	85.1	81.8	79.8	81.8	85.0	90.9	95.6	97.8	100.0		
69.0				96.4	96.4	87.7	83.9	77.9	74.0	71.8	74.3	77.3	87.6	91.0	98.6	99.5		
68.0			100.0	95.8	90.1	84.0	75.6	65.4	60.3	60.0	63.8	69.8	76.0	86.7	90.1	96.4	100.0	
67.0		100.0	98.2	92.4	82.6	69.1	58.7	53.3	47.2	50.2	52.5	58.0	65.6	72.9	85.7	96.0	97.0	
66.0		97.4	91.6	82.6	68.6	53.3	44.2	37.8	36.0	35.7	39.5	44.5	53.0	59.9	76.8	89.2	95.7	100.0
65.0	100.0	90.0	68.9	47.6	35.5	29.4	23.3	20.9	19.8	20.9	23.2	26.0	34.1	41.4	56.8	74.7	87.2	95.7
64.0	93.0	64.3	43.4	32.0	26.0	22.8	24.4	22.4	22.5	25.6	29.2	35.4	47.6	59.4	76.5	91.3	94.8	100.0
63.0	100.0	96.2	88.4	75.0	65.1	52.1	44.9	41.8	39.0	41.2	46.8	51.5	63.2	75.4	89.4	95.0	97.6	
62.0		99.6	97.9	90.6	81.0	67.3	60.5	54.5	49.6	53.6	57.5	65.3	73.9	86.8	92.7	99.3	99.8	
61.0		100.0	100.0	98.4	92.5	80.4	73.0	66.2	61.9	64.6	70.6	75.9	82.0	92.4	96.3	100.0	100.0	
60.0				99.7	94.2	88.5	81.9	75.8	73.2	77.7	80.9	82.5	89.3	95.9	98.6			
59.0				100.0	97.5	92.6	89.6	85.9	83.8	83.4	84.0	90.1	92.6	98.0	100.0			
58.0					97.8	95.0	93.7	89.6	90.4	88.5	91.1	93.4	96.0	98.4				
57.0					100.0	98.8	96.2	92.2	94.6	91.6	96.4	96.2	97.6	100.0				
56.0						100.0	96.8	94.9	94.0		94.5	97.8	98.6					
55.0																		
Minimum Reading & Lateral Location	91.9 64.1	59.2 64.1	37.2 64.2	24.4 64.2	20.0 64.3	17.8 64.3	17.4 64.4	17.0 64.4	16.8 64.5	18.2 64.5	22.0 64.6	24.9 64.7	32.6 64.7	41.4 65.0	56.8 65.0	74.7 65.0	87.2 65.0	94.5 65.3
Argon Spectral Line @ 4333.6A Lateral Location	78.0	78.1	78.1	78.2	78.2	78.3	78.3	78.3	78.3	78.4	78.4	78.5	78.6	78.7	78.8	78.9	78.9	79.0
Argon Spectral Line @ 4345.2A Lateral Location	54.9	54.9	54.9	54.9	54.9	55.0	55.0	55.0	55.1	55.2	55.2	55.3	55.3	55.4	55.5	55.6	55.6	55.7

TABLE XIX

DENSITOMETER READINGS

PLATE NO. 12-19-60A EXPOSURE NO. 3 H_γ SPECTRAL LINE

Photocell Slit: Height-0.5 mm Width-15 microns

LATERAL LOCATION mm	VERTICAL LOCATION-mm 4.0	4.5	5.0	5.5	6.0	6.5	7.0	7.5	8.0	8.5	9.0	9.5	10.0	10.5	11.0	11.5	12.0	12.5
74.0								98.2	97.6	94.4	93.8	100.0						
73.0							100.0	98.5	97.2	94.2	93.0	97.5	100.0					
72.0						100.0	98.8	94.8	92.6	92.8	93.5	95.9	98.0	100.0				
71.0						97.4	98.0	92.0	89.9	91.0	90.6	92.6	96.1	98.3				
70.0					100.0	95.4	95.2	88.3	86.4	82.9	85.9	89.8	93.3	97.5	100.0	100.0		
69.0					96.5	95.0	87.5	83.1	79.3	78.8	77.4	82.5	87.5	94.3	97.6	98.3	100.0	
68.0				100.0	95.8	88.4	81.0	72.8	68.5	64.2	70.2	73.8	81.0	86.9	94.3	95.0	99.0	
67.0			100.0	95.6	89.8	75.8	69.6	62.5	56.2	55.0	58.8	61.4	70.2	79.2	88.7	94.3	98.7	100.0
66.0	100.0	100.0	97.6	91.6	77.1	61.7	55.6	49.4	42.7	44.0	47.4	48.8	58.7	68.2	80.8	91.4	96.5	97.5
65.0	97.0	96.3	89.6	66.1	47.9	40.5	33.3	31.5	26.7	27.0	31.0	35.2	40.6	52.1	61.4	72.8	89.0	95.3
64.0	93.8	78.2	56.8	38.9	32.4	28.4	27.5	26.4	26.4	28.7	34.4	41.8	49.2	63.4	77.0	87.4	96.5	100.0
63.0	96.5	100.0	95.5	82.6	67.6	57.9	50.9	46.2	44.4	46.4	48.9	58.9	64.2	77.9	87.0	94.1	97.5	
62.0	100.0		100.0	95.1	87.0	75.3	66.4	60.0	56.8	57.2	62.4	67.6	77.3	85.0	92.4	97.2	98.6	
61.0				100.0	93.5	86.6	77.9	73.6	69.0	66.3	70.4	77.6	85.1	92.3	98.0	98.2	100.0	
60.0					97.3	91.8	88.6	82.0	77.8	76.5	80.2	86.7	91.6	96.5	99.2	100.0		
59.0					100.0	95.2	91.5	88.9	84.4	85.3	87.1	92.3	94.8	100.0	100.0			
58.0						96.3	96.0	94.0	90.8	88.8	90.2	dark	97.2					
57.0						98.8	94.8	96.5	92.4	92.6	94.4	spot on plate	97.2					
56.0						100.0	100.0	98.4	95.8	95.0	95.6	98.2	99.0					
55.0																		
Minimum Reading & Lateral Location	93.6 64.1	77.6 64.1	55.2 64.2	36.3 64.2	27.2 64.2	24.7 64.3	22.9 64.4	21.9 64.4	21.3 64.5	22.9 64.6	27.0 64.6	31.1 64.6	37.7 64.7	47.6 64.8	60.6 64.9	71.5 64.9	89.0 65.0	92.1 65.1
Argon Spectral Line @ 4333.6A Lateral Location	77.9	77.9	78.0	78.0	78.1	78.1	78.2	78.2	78.3	78.3	78.4	78.4	78.5	78.5	78.7	78.7	78.8	78.8
Argon Spectral Line @ 4345.2A Lateral Location	54.6	54.6	54.7	54.8	54.9	54.9	55.0	55.0	55.0	55.0	55.1	55.2	55.2	55.3	55.4	55.4	55.5	55.6

TABLE XX

DENSITOMETER READINGS

PLATE NO. 12-19-60A EXPOSURE NO. 4 H_β SPECTRAL LINE

Photocell Slit: Height-0.5 mm Width-15 microns

LATERAL LOCATION mm	VERTICAL LOCATION-mm 2.0	2.5	3.0	3.5	4.0	4.5	5.0	5.5	6.0	6.5	7.0	7.5	8.0	8.5	9.0	9.5	10.0	10.5
85.0								100.0										
84.0						100.0	100.0	98.0	100.0	100.0	100.0	100.0						
83.0					100.0	99.0	98.6	96.4	98.2	96.6	97.0	98.0	100.0	100.0				
82.0					98.7	98.0	94.2	93.0	93.4	93.0	95.9	97.5	96.6	98.6	100.0			
81.0				100.0	97.2	94.2	86.5	85.2	85.6	85.8	88.5	90.9	96.0	97.2	98.9			
80.0	100.0	100.0	100.0	98.8	90.6	85.6	74.3	70.0	70.7	69.2	78.6	86.2	91.9	99.6	99.6			
79.0	98.6	99.0	97.6	92.2	79.1	67.8	56.8	53.0	47.4	49.6	56.6	63.7	83.7	92.9	96.1	100.0	100.0	
78.0	96.2	96.6	90.8	71.1	54.2	43.4	31.6	29.3	27.6	27.1	29.6	38.1	54.2	75.4	90.8	97.9	97.4	100.0
77.0	94.6	85.5	58.6	42.8	30.2	23.2	17.4	15.2	12.7	12.8	13.8	15.3	22.7	34.8	60.4	83.7	93.0	98.1
76.0	85.6	61.2	40.0	28.0	20.8	14.2	10.3	8.8	7.8	6.4	6.0	5.5	6.0	7.6	10.6	22.5	51.8	89.4
75.0	98.2	89.0	72.5	54.4	37.0	26.5	19.3	16.9	13.8	12.6	11.6	12.8	17.4	23.5	43.9	68.8	90.6	96.0
74.0	97.4	96.6	94.5	83.2	61.6	47.2	36.6	32.2	30.4	29.7	32.4	37.6	52.6	70.7	90.0	97.4	97.8	100.0
73.0	99.6	97.0	98.2	93.7	84.0	75.3	59.2	56.4	49.6	53.1	57.4	65.5	80.7	89.9	98.6	100.0	100.0	
72.0	100.0	100.0	100.0	98.0	97.8	87.2	79.2	74.8	74.2	76.9	76.9	84.1	94.1	97.8	96.7			
71.0				100.0	97.2	96.8	88.6	88.8	88.6	86.8	88.2	94.5	97.6	98.6	99.6			
70.0					100.0	98.5	94.6	95.2	96.7	95.6	95.8	98.0	99.0	100.0	100.0			
69.0						100.0	97.0	99.4	98.0	98.4	98.5	100.0	100.0					
68.0							100.0	98.0	99.0	100.0	100.0							
67.0								100.0	100.0									
Minimum Reading &	83.4	58.4	38.1	27.2	19.1	13.4	10.2	8.8	7.8	6.4	6.0	5.5	5.8	7.2	10.6	22.0	49.8	87.2
Lateral Location	76.3	76.3	76.2	76.2	76.2	76.2	76.1	76.0	76.0	76.0	76.0	76.0	75.8	75.8	75.8	75.8	75.8	75.7
Hydrogen Spectral Line @ 4861.3A																		
Lateral Location	76.3	76.3	76.2	76.2	76.2	76.2	76.1	76.0	76.0	76.0	76.0	76.0	75.8	75.8	75.8	75.8	75.8	75.7

APPENDIX B

INTERMEDIATE DATA FOR PLASMA TEMPERATURE CALCULATIONS FROM CVRC SPECTROGRAPHIC PLATE NO. 12-19-60A

TABLE XXI

RELATIVE Ddensitometer READINGS

PLATE NO. 12-19-60A EXPOSURE NO. 2 H_γ SPECTRAL LINE

x mm	$\Delta\lambda$ -A											
	0	0.5	1.0	1.5	2.0	2.5	3.0	3.5	4.0	4.5	5.0	5.5
0	18.1	28.8	42.7	56.0	68.0	77.6	85.5	90.4	93.6	96.4	98.2	99.2
±0.25	18.2	29.0	43.3	56.6	68.6	78.1	85.8	90.7	93.8	96.7	98.4	99.6
±0.50	18.6	30.0	44.9	58.2	70.3	79.7	86.4	91.4	94.4	97.4	99.0	100.0
±0.75	19.2	31.9	47.0	60.7	72.6	81.5	87.6	92.4	95.5	98.4	99.6	
±1.00	20.0	34.0	50.0	64.0	75.3	83.6	89.0	93.5	96.7	99.1	99.9	
±1.25	21.0	36.8	53.8	67.5	78.3	85.9	90.7	94.8	97.7	99.5	100.0	
±1.50	22.3	40.3	58.4	71.7	82.0	88.3	92.7	96.1	98.6	99.8		
±1.75	24.0	44.7	63.7	76.2	85.7	90.8	94.6	97.4	99.3	100.0		
±2.00	26.2	49.8	69.1	81.4	89.3	93.4	96.5	98.6	99.8			
±2.25	29.5	56.0	75.1	86.3	92.4	95.6	98.0	99.5	100.0			
±2.50	33.7	63.0	81.2	90.4	95.2	97.3	99.0	99.9				
±2.75	39.9	70.5	86.6	93.8	97.3	98.7	99.6	100.0				
±3.00	47.2	78.4	91.3	96.4	98.9	99.7	100.0					
±3.25	57.5	85.6	95.0	98.3	99.9	100.0						
±3.50	68.0	91.0	97.5	99.6	100.0							
±3.75	79.0	95.0	99.0	100.0								
±4.00	87.8	97.9	100.0									
±4.25	93.0	99.4										
±4.50	96.4	100.0										
±4.75	98.4											

TABLE XXII

RELATIVE DENSITOMETER READINGS

PLATE NO. 12-19-60A EXPOSURE NO. 3 H_γ SPECTRAL LINE

x mm	$\Delta\lambda$-A											
	0	0.5	1.0	1.5	2.0	2.5	3.0	3.5	4.0	4.5	5.0	5.5
0	20.7	33.3	48.4	61.1	73.0	80.8	87.4	91.5	94.2	96.2	97.8	99.0
±0.25	20.8	33.9	49.0	61.8	73.4	81.5	87.6	91.8	94.5	96.5	98.1	99.3
±0.50	21.4	35.3	51.0	63.5	74.6	82.7	88.5	92.5	95.3	97.1	98.7	99.8
±0.75	22.5	37.6	53.8	65.8	76.5	84.3	89.8	93.7	96.4	98.2	99.4	100.0
±1.00	24.0	40.3	57.0	69.0	79.2	86.5	91.6	95.1	97.6	99.1	99.8	
±1.25	25.8	43.7	60.7	72.6	82.2	88.9	93.6	96.6	98.5	99.6	100.0	
±1.50	28.0	47.3	65.0	76.6	85.3	91.6	95.6	97.9	99.2	99.9		
±1.75	30.4	51.3	69.4	80.7	88.5	94.1	97.4	98.9	99.6	100.0		
±2.00	33.4	56.2	74.4	85.0	91.6	96.2	98.4	99.5	99.9			
±2.25	37.2	62.0	79.8	89.0	94.5	97.8	99.2	99.9	100.0			
±2.50	41.9	69.0	85.5	92.7	97.1	98.9	99.7	100.0				
±2.75	48.2	77.0	90.2	96.0	98.8	99.6	100.0					
±3.00	56.0	84.6	94.2	98.1	99.7	99.9						
±3.25	65.5	90.2	97.0	99.3	100.0	100.0						
±3.50	74.3	94.2	98.8	100.0								
±3.75	82.5	96.8	99.8									
±4.00	88.5	98.7	100.0									
±4.25	92.0	99.4										
±4.50	94.6	100.0										
±4.75	96.6											

TABLE XXIII

RELATIVE DENSITOMETER READINGS

PLATE NO. 12-19-60A EXPOSURE NO. 4 H_β SPECTRAL LINE

x mm	$\Delta\lambda$ -A								
	0	0.5	1.0	1.5	2.0	2.5	3.0	3.5	4.0
0	7.0	12.3	27.4	48.8	71.5	86.4	93.7	97.4	99.0
±0.25	7.1	12.5	27.8	49.3	72.0	86.5	93.8	97.5	99.1
±0.50	7.3	13.0	28.8	50.8	73.0	86.9	94.1	97.7	99.5
±0.75	7.7	13.8	30.0	53.4	74.6	87.5	94.7	98.1	99.9
±1.00	8.1	14.7	32.1	57.2	77.0	88.6	95.6	98.7	100.0
±1.25	8.9	16.1	35.2	61.7	80.8	90.6	96.7	99.3	
±1.50	9.9	18.0	40.0	67.3	84.7	93.2	98.0	99.8	
±1.75	11.0	20.7	47.3	73.9	88.8	95.5	99.0	100.0	
±2.00	12.6	24.7	56.8	81.3	92.5	97.7	99.6		
±2.25	14.4	31.0	66.0	88.0	95.5	99.2	99.9		
±2.50	16.9	39.2	75.4	92.9	97.7	99.9	100.0		
±2.75	19.9	48.3	84.7	96.3	99.1	100.0			
±3.00	24.0	58.6	90.3	98.2	99.8				
±3.25	30.2	70.0	93.6	99.4	100.0				
±3.50	41.5	81.5	96.0	99.9					
±3.75	54.5	89.6	97.6	100.0					
±4.00	69.0	94.2	98.8						
±4.25	84.6	97.1	99.5						
±4.50	93.7	98.9	99.9						
±4.75	96.6	99.5	100.0						
±5.00	97.7	100.0							
±5.25	98.3								

TABLE XXIV

RELATIVE INTENSITY, I_x ($\Delta\lambda$)

PLATE NO. 12-19-60A EXPOSURE NO. 2 H_γ SPECTRAL LINE

x mm	$\Delta\lambda$-A											
	0	0.5	1.0	1.5	2.0	2.5	3.0	3.5	4.0	4.5	5.0	5.5
0	.880	.542	.340	.235	.172	.133	.103	.086	.069	.050	.034	.021
±0.25	.877	.540	.332	.231	.170	.131	.102	.084	.067	.046	.031	.018
±0.50	.859	.517	.319	.222	.162	.126	.100	.081	.066	.041	.024	
±0.75	.838	.480	.300	.209	.153	.118	.097	.077	.057	.031	.018	
±1.00	.803	.446	.277	.191	.141	.111	.092	.070	.046	.022	.005	
±1.25	.767	.404	.250	.176	.129	.102	.084	.060	.038	.019		
±1.50	.721	.364	.221	.156	.117	.094	.075	.051	.030	.010		
±1.75	.665	.320	.192	.138	.103	.084	.064	.041	.021			
±2.00	.606	.279	.168	.118	.090	.070	.050	.030	.010			
±2.25	.528	.235	.141	.100	.077	.055	.036	.019				
±2.50	.450	.196	.119	.086	.059	.041	.024	.005				
±2.75	.369	.161	.099	.067	.041	.029	.018					
±3.00	.300	.129	.081	.050	.026	.018						
±3.25	.226	.103	.059	.032	.005							
±3.50	.172	.083	.040	.018								
±3.75	.127	.059	.024									
±4.00	.097	.037										
±4.25	.072	.020										
±4.50	.050											
±4.75	.031											

TABLE XXV

RELATIVE INTENSITY, I_x ($\Delta\lambda$)

PLATE NO. 12-19-60A EXPOSURE NO. 3 H_γ SPECTRAL LINE

x mm	$\Delta\lambda$-A											
	0	0.5	1.0	1.5	2.0	2.5	3.0	3.5	4.0	4.5	5.0	5.5
0	.780	.455	.289	.206	.151	.120	.099	.080	.066	.051	.038	.024
±0.25	.775	.449	.284	.202	.149	.118	.097	.079	.063	.050	.035	.021
±0.50	.750	.423	.270	.193	.144	.113	.093	.076	.058	.044	.029	.010
±0.75	.715	.398	.250	.183	.137	.109	.089	.070	.050	.035	.020	
±1.00	.677	.363	.229	.169	.127	.100	.080	.058	.039	.022	.010	
±1.25	.618	.329	.208	.153	.115	.092	.070	.049	.031	.018		
±1.50	.560	.298	.187	.137	.104	.080	.057	.037	.021	.005		
±1.75	.507	.267	.167	.120	.093	.067	.040	.026	.018			
±2.00	.455	.234	.146	.106	.080	.051	.032	.019	.005			
±2.25	.400	.202	.124	.091	.063	.038	.021	.005				
±2.50	.349	.169	.104	.074	.044	.026	.015					
±2.75	.290	.134	.087	.053	.026	.018						
±3.00	.236	.107	.066	.035	.015	.005						
±3.25	.183	.087	.047	.021								
±3.50	.146	.066	.026									
±3.75	.113	.045	.010									
±4.00	.093	.029										
±4.25	.078	.020										
±4.50	.063											
±4.75	.049											

TABLE XXVI

RELATIVE INTENSITY, I_x ($\Delta\lambda$)

PLATE NO. 12-19-60A EXPOSURE NO. 4 H_β SPECTRAL LINE

x mm	$\Delta\lambda$ -A								
	0	0.5	1.0	1.5	2.0	2.5	3.0	3.5	4.0
0	.580	.380	.211	.123	.077	.043	.021	.010	.003
±0.25	.572	.375	.208	.122	.076	.042	.021	.009	.003
±0.50	.565	.368	.203	.119	.074	.040	.020	.009	.002
±0.75	.545	.351	.196	.113	.070	.039	.019	.007	.001
±1.00	.520	.334	.185	.105	.065	.037	.015	.004	
±1.25	.490	.314	.170	.097	.056	.030	.011	.002	
±1.50	.450	.290	.150	.086	.047	.022	.007	.001	
±1.75	.413	.261	.128	.072	.036	.015	.003		
±2.00	.374	.229	.106	.056	.025	.009	.002		
±2.25	.340	.190	.088	.038	.015	.003	.001		
±2.50	.303	.153	.069	.023	.009	.001			
±2.75	.270	.125	.047	.013	.003				
±3.00	.233	.101	.031	.007	.001				
±3.25	.194	.080	.021	.002					
±3.50	.145	.055	.014	.001					
±3.75	.111	.033	.009						
±4.00	.082	.020	.004						
±4.25	.047	.010	.002						
±4.50	.021	.004	.001						
±4.75	.012	.002							
±5.00	.009								
±5.25	.007								

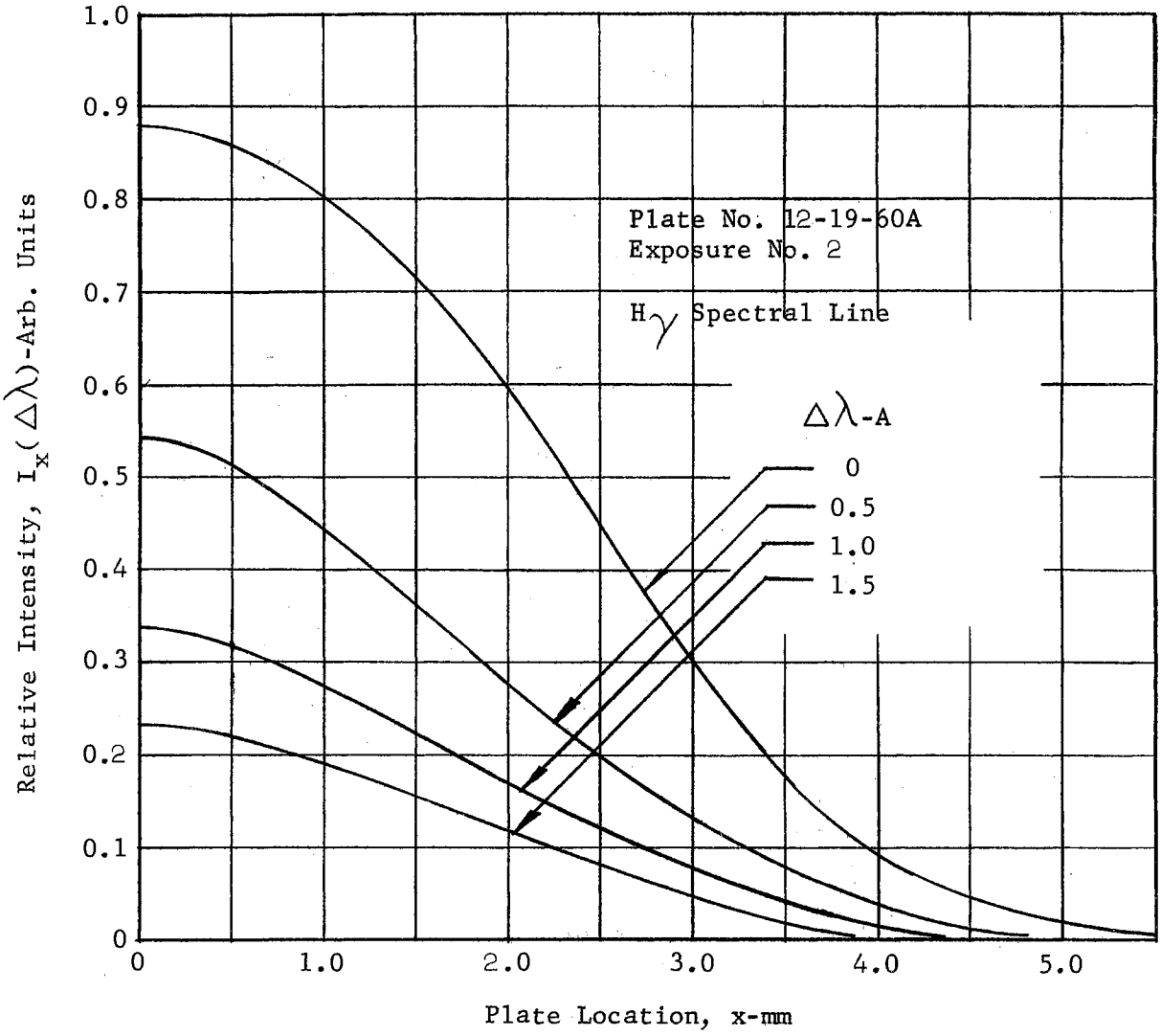

Figure 37a. Relative Intensity versus Plate Location

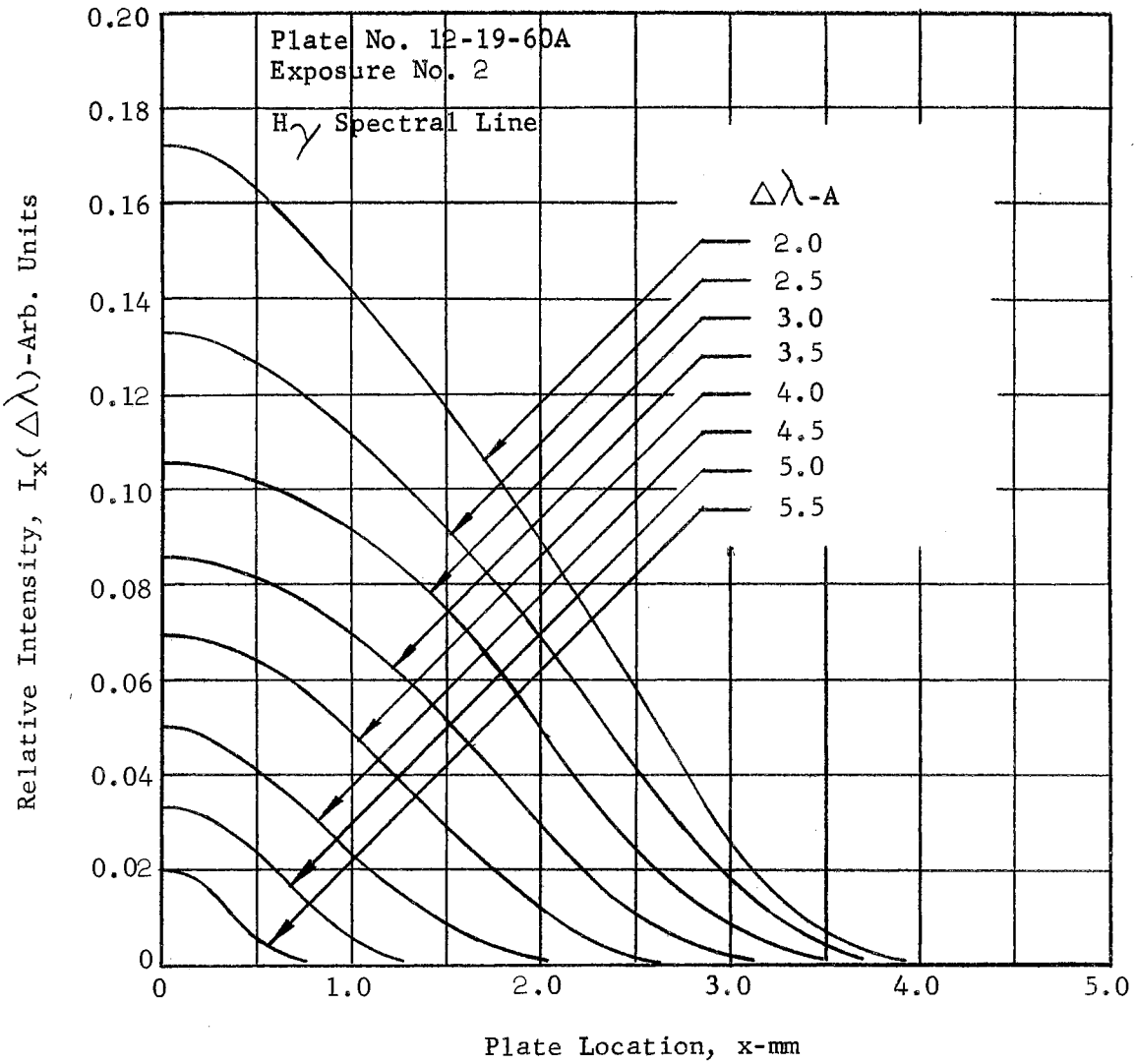

Figure 37b. Relative Intensity versus Plate Location

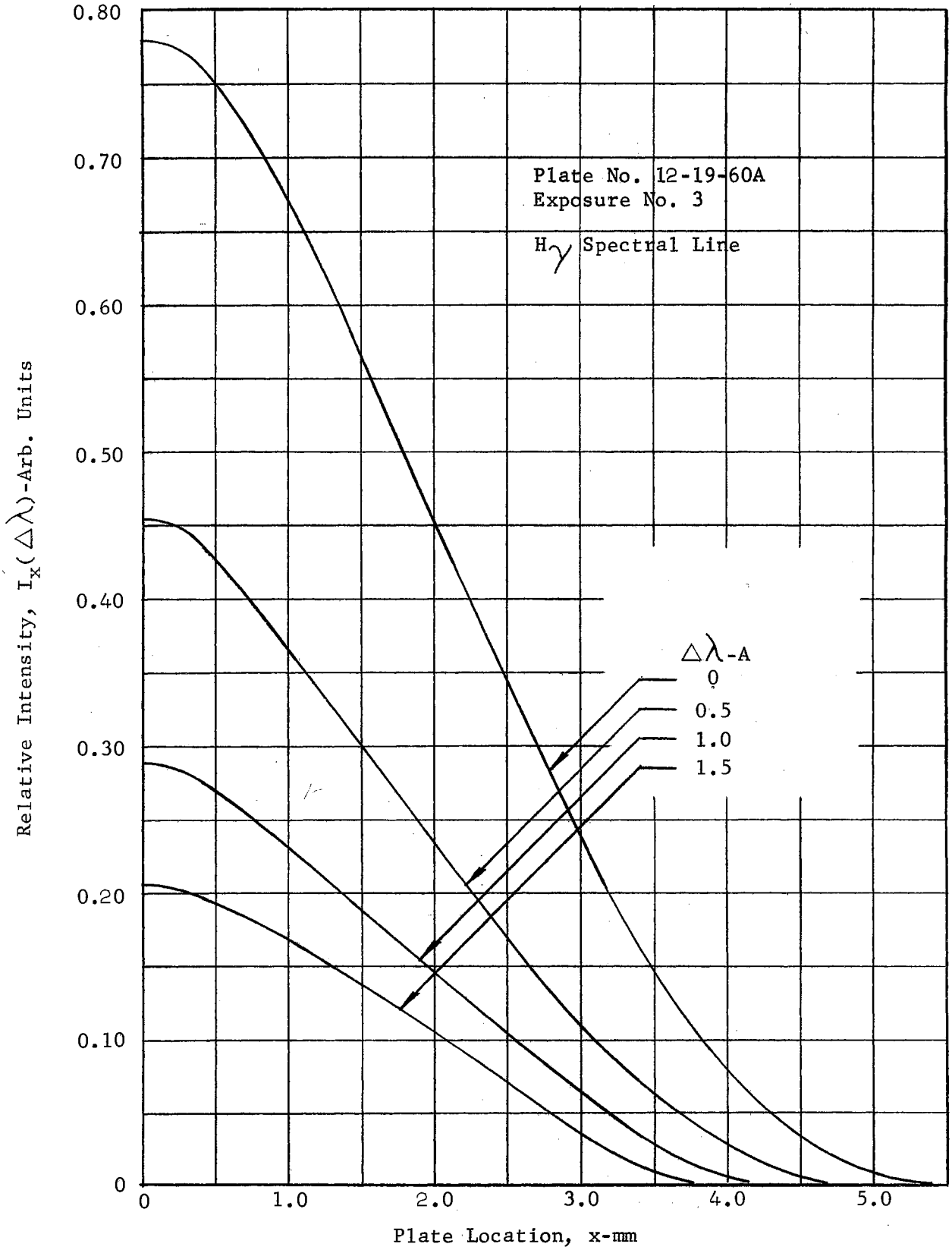

Figure 38a. Relative Intensity versus Plate Location

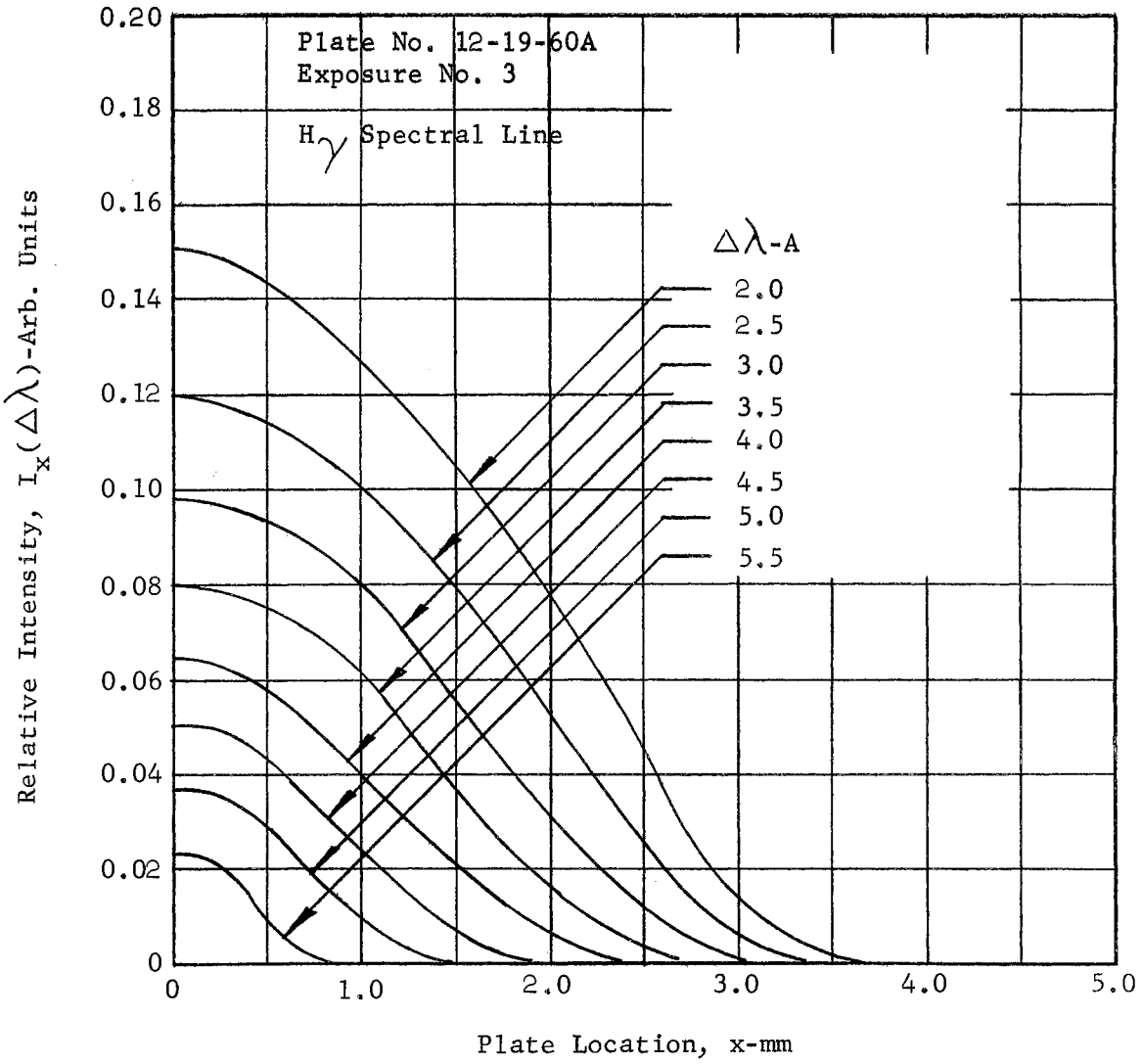

Figure 38b. Relative Intensity versus Plate Location

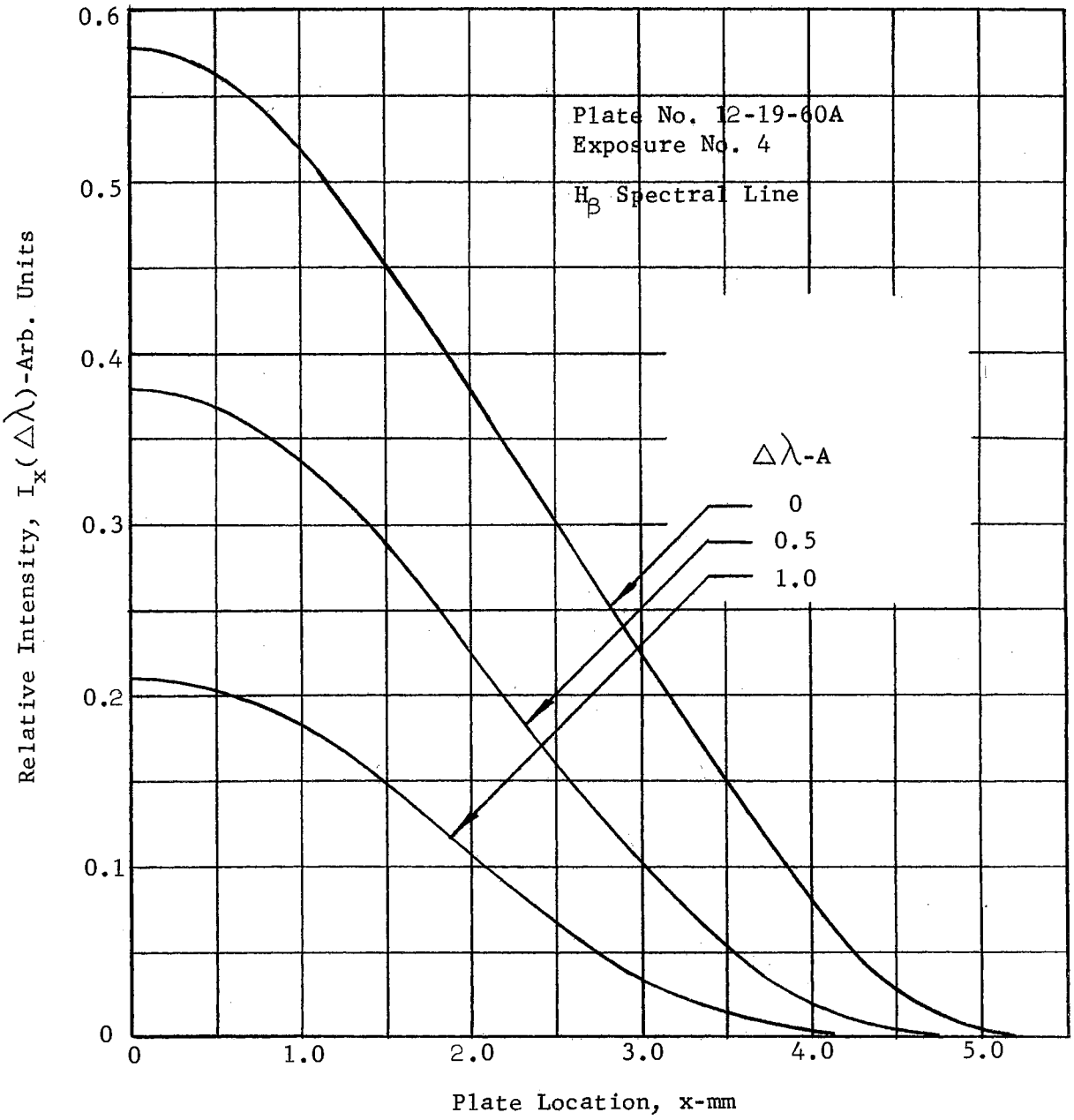

Figure 39a. Relative Intensity versus Plate Location

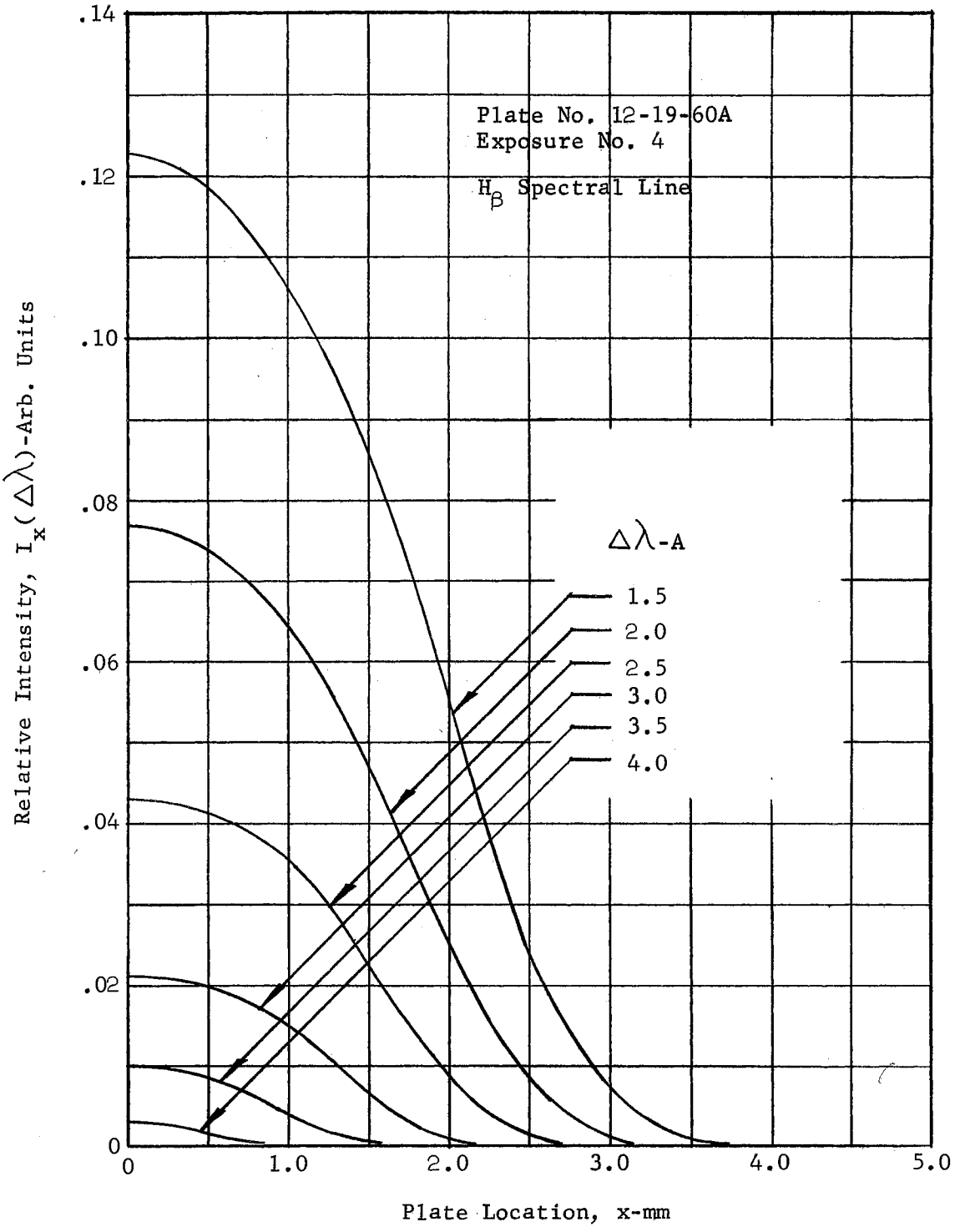

Figure 39b. Relative Intensity versus Plate Location

TABLE XXVII

COMPUTER PROGRAM INPUT DATA, I_x ($\Delta\lambda$)

PLATE NO. 12-19-60A EXPOSURE NO. 2 H_γ SPECTRAL LINE

Row No.	x mm	$\Delta\lambda$-A											
		0	0.5	1.0	1.5	2.0	2.5	3.0	3.5	4.0	4.5	5.0	5.5
1	0.125	0.878	0.542	0.336	0.233	0.172	0.132	0.106	0.085	0.069	0.050	0.033	0.019
2	0.375	0.868	0.528	0.327	0.227	0.167	0.129	0.103	0.083	0.066	0.045	0.028	0.010
3	0.625	0.848	0.500	0.310	0.216	0.158	0.123	0.100	0.079	0.061	0.037	0.019	0.003
4	0.875	0.822	0.464	0.289	0.202	0.147	0.116	0.095	0.073	0.054	0.028	0.009	
5	1.125	0.787	0.425	0.264	0.187	0.136	0.107	0.088	0.066	0.044	0.020	0.003	
6	1.375	0.745	0.386	0.236	0.169	0.124	0.097	0.080	0.057	0.034	0.012		
7	1.625	0.692	0.344	0.208	0.150	0.111	0.087	0.070	0.046	0.025	0.006		
8	1.875	0.634	0.300	0.180	0.132	0.097	0.075	0.058	0.035	0.016	0.002		
9	2.125	0.567	0.257	0.154	0.112	0.082	0.062	0.043	0.024	0.008			
10	2.375	0.493	0.216	0.130	0.093	0.066	0.049	0.030	0.014	0.003			
11	2.625	0.412	0.178	0.107	0.074	0.049	0.034	0.019	0.007				
12	2.875	0.333	0.145	0.086	0.056	0.033	0.022	0.011	0.002				
13	3.125	0.261	0.115	0.066	0.040	0.020	0.012	0.006					
14	3.375	0.200	0.089	0.048	0.025	0.010	0.006	0.002					
15	3.625	0.148	0.065	0.032	0.013	0.004	0.001						
16	3.875	0.111	0.046	0.019	0.005	0.001							
17	4.125	0.081	0.030	0.010									
18	4.375	0.058	0.017	0.004									
19	4.625	0.041	0.008										
20	4.875	0.026	0.002										
21	5.125	0.015											
22	5.375	0.006											
23	5.625												
24	5.875												
25	6.125												

TABLE XXVIII

COMPUTER PROGRAM INPUT DATA, I_x ($\Delta\lambda$)

PLATE NO. 12-19-60A EXPOSURE NO. 3 H_γ SPECTRAL LINE

Row No.	x mm	$\Delta\lambda$ -A											
		0	0.5	1.0	1.5	2.0	2.5	3.0	3.5	4.0	4.5	5.0	5.5
1	0.125	0.778	0.454	0.287	0.204	0.150	0.119	0.098	0.079	0.064	0.050	0.037	0.023
2	0.375	0.764	0.440	0.278	0.198	0.147	0.116	0.096	0.077	0.061	0.047	0.035	0.017
3	0.625	0.733	0.412	0.260	0.187	0.140	0.112	0.091	0.073	0.054	0.039	0.024	0.005
4	0.875	0.694	0.381	0.240	0.175	0.132	0.105	0.085	0.066	0.045	0.029	0.014	0.001
5	1.125	0.647	0.348	0.220	0.161	0.122	0.096	0.075	0.056	0.035	0.019	0.006	
6	1.375	0.592	0.316	0.198	0.146	0.111	0.085	0.062	0.043	0.025	0.011	0.001	
7	1.625	0.534	0.282	0.176	0.130	0.099	0.074	0.049	0.031	0.017	0.004		
8	1.875	0.478	0.250	0.155	0.113	0.086	0.060	0.038	0.020	0.010	0.001		
9	2.125	0.423	0.216	0.134	0.097	0.071	0.045	0.026	0.012	0.004			
10	2.375	0.369	0.183	0.113	0.079	0.054	0.032	0.016	0.006				
11	2.625	0.315	0.150	0.093	0.061	0.035	0.019	0.008	0.001				
12	2.875	0.261	0.120	0.073	0.043	0.019	0.009	0.002					
13	3.125	0.211	0.095	0.054	0.027	0.009	0.003						
14	3.375	0.165	0.073	0.036	0.014	0.003							
15	3.625	0.126	0.053	0.021	0.005								
16	3.875	0.093	0.035	0.010									
17	4.125	0.065	0.020	0.002									
18	4.375	0.043	0.010										
19	4.625	0.025	0.002										
20	4.875	0.013											
21	5.125	0.005											
22	5.375												
23	5.625												
24	5.875												
25	6.125												

TABLE XXIX

COMPUTER PROGRAM INPUT DATA, I_x $(\Delta\lambda)$

PLATE NO. 12-19-60A EXPOSURE NO. 4 H_β SPECTRAL LINE

Row No.	x mm	$\Delta\lambda$-A								
		0	0.5	1.0	1.5	2.0	2.5	3.0	3.5	4.0
1	0.125	.577	.378	.210	.1225	.0767	.0430	.0209	.0099	.0030
2	0.375	.570	.373	.205	.1205	.0752	.0420	.0201	.0092	.0024
3	0.625	.555	.362	.199	.1160	.0721	.0402	.0189	.0077	.0010
4	0.875	.533	.346	.190	.1097	.0671	.0373	.0164	.0052	
5	1.125	.504	.325	.175	.1017	.0606	.0329	.0129	.0029	
6	1.375	.471	.302	.158	.0917	.0520	.0263	.0087	.0010	
7	1.625	.434	.275	.138	.0790	.0416	.0185	.0046	.0001	
8	1.875	.397	.243	.117	.0640	.0299	.0115	.0017		
9	2.125	.358	.207	.095	.0462	.0196	.0060	.0003		
10	2.375	.320	.174	.075	.0302	.0115	.0022			
11	2.625	.281	.142	.055	.0180	.0056	.0004			
12	2.875	.242	.115	.039	.0100	.0020				
13	3.125	.205	.088	.027	.0046	.0002				
14	3.375	.167	.063	.018	.0018					
15	3.625	.131	.042	.011	.0003					
16	3.875	.096	.025	.007						
17	4.125	.063	.015	.003						
18	4.375	.036	.008							
19	4.625	.019	.003							
20	4.875	.008								
21	5.125	.001								
22	5.375									
23	5.625									
24	5.875									
25	6.125									

TABLE XXX

COMPUTER PROGRAM OUTPUT DATA, i_r ($\Delta\lambda$)

PLATE NO. 12-19-60A EXPOSURE NO. 2 H_γ SPECTRAL LINE

Row No.	r_{plate} mm	$\Delta\lambda$ -A											
		0	0.5	1.0	1.5	2.0	2.5	3.0	3.5	4.0	4.5	5.0	5.5
1	0.125	3.9063	3.3339	2.1008	1.4278	1.1006	.7882	.6746	.5670	.5954	.6494	.5839	.6506
2	0.375	3.8972	3.2727	2.0420	1.3720	1.0491	.7836	.5744	.5565	.5566	.5648	.4998	.3008
3	0.625	3.7385	3.0101	1.8639	1.2753	.9576	.7112	.5752	.5444	.5149	.4586	.3774	.0969
4	0.875	3.6903	2.6907	1.7139	1.1436	.8411	.6780	.5696	.5015	.4963	.3292	.1780	
5	1.125	3.5552	2.3662	1.5610	1.0731	.7719	.6284	.5326	.4764	.4093	.2557	.0734	
6	1.375	3.4978	2.1455	1.3631	.9738	.7100	.5612	.5154	.4455	.3161	.1605		
7	1.625	3.2890	1.9246	1.1946	.8418	.6508	.5325	.4779	.3739	.2527	.0885		
8	1.875	3.1392	1.6731	1.0171	.7782	.5920	.4865	.4535	.3063	.1856	.0382		
9	2.125	2.9139	1.4319	.8620	.6659	.5292	.4137	.3455	.2343	.0987			
10	2.375	2.6718	1.2097	.7426	.5777	.4637	.3788	.2549	.1439	.0511			
11	2.625	2.2963	.9847	.6190	.4837	.3741	.2696	.1691	.0864				
12	2.875	1.8950	.8196	.5220	.3822	.2676	.1972	.0973	.0310				
13	3.125	1.4819	.6555	.4196	.3039	.1802	.1062	.0645					
14	3.375	1.1644	.5393	.3277	.2130	.0975	.0740	.0287					
15	3.625	.8207	.4002	.2370	.1222	.0438	.0138						
16	3.875	.6235	.3014	.1504	.0669	.0134							
17	4.125	.4595	.2175	.0865									
18	4.375	.3262	.1339	.0504									
19	4.625	.2555	.0777										
20	4.875	.1718	.0239										
21	5.125	.1167											
22	5.375	.0683											
23	5.625												
24	5.875												
25	6.125												

TABLE XXXI

COMPUTER PROGRAM OUTPUT DATA, i_r ($\Delta\lambda$)

PLATE NO. 12-19-60A EXPOSURE NO. 3 H_γ SPECTRAL LINE

Row No.	r_{plate} mm	$\Delta\lambda$-A											
		0	0.5	1.0	1.5	2.0	2.5	3.0	3.5	4.0	4.5	5.0	5.5
1	0.125	4.145	2.939	1.886	1.303	.875	.763	.640	.584	.598	.546	.416	.506
2	0.375	4.193	2.898	1.854	1.260	.902	.687	.674	.573	.612	.588	.620	.520
3	0.625	3.896	2.510	1.618	1.107	.814	.699	.615	.580	.542	.496	.410	.134
4	0.875	3.640	2.224	1.397	1.021	,773	.663	.628	.555	.456	.383	.249	.276
5	1.125	3.396	1.923	1.267	.927	.713	.633	.593	.523	.368	.248	.126	
6	1.375	3.077	1.747	1.118	.839	.660	.554	.504	.405	.258	.173	.022	
7	1.625	2.708	1.510	.973	.767	.606	.529	.385	.311	.188	.065		
8	1.875	2.406	1.373	.862	.660	.567	.467	.335	.204	.127	.019		
9	2.125	2.135	1.191	.763	.610	.511	.357	.243	.128	.072			
10	2.375	1.895	1.039	.655	.524	.449	.290	.163	.088				
11	2.625	1.671	.834	.570	.442	.325	.193	.103	.016				
12	2.875	1.406	.685	.474	.339	.185	.101	.031					
13	3.125	1.171	.555	.384	.238	.097	.045						
14	3.375	.927	.450	.282	.141	.043							
15	3.625	.724	.353	.179	.069								
16	3.875	.562	.261	.112									
17	4.125	.406	.155	.026									
18	4.375	.296	.105										
19	4.625	.183	.025										
20	4.875	.106											
21	5.125	.058											
22	5.375												
23	5.625												
24	5.875												
25	6.125												

TABLE XXXII

COMPUTER PROGRAM OUTPUT DATA, i_r ($\Delta\lambda$)

PLATE NO. 12-19-60A EXPOSURE NO. 4 H_β SPECTRAL LINE

Row No.	r_{plate} mm	$\Delta\lambda$ -A								
		0	0.5	1.0	1.5	2.0	2.5	3.0	3.5	4.0
1	0.125	2.657	1.882	1.249	.708	.494	.302	.185	.120	.059
2	0.375	2.665	1.898	1.123	.717	.490	.293	.167	.115	.062
3	0.625	2.594	1.843	1.092	.693	.489	.292	.177	.114	.032
4	0.875	2.516	1.791	1.129	.667	.466	.290	.167	.079	
5	1.125	2.354	1.665	1.040	.640	.450	.288	.146	.051	
6	1.375	2.211	1.584	.975	.619	.413	.258	.112	.020	
7	1.625	1.999	1.496	.865	.569	.365	.193	.066	.002	
8	1.875	1.848	1.389	.767	.520	.276	.129	.028		
9	2.125	1.658	1.166	.622	.400	.189	.076	.005		
10	2.375	1.511	1.011	.526	.273	.120	.032			
11	2.625	1.362	.811	.388	.164	.064	.006			
12	2.875	1.189	.698	.274	.099	.028				
13	3.125	1.068	.569	.190	.047	.003				
14	3.375	.910	.426	.136	.022					
15	3.625	.769	.310	.077	.004					
16	3.875	.622	.178	.060						
17	4.125	.452	.114	.039						
18	4.375	.267	.069							
19	4.625	.153	.037							
20	4.875	.086								
21	5.125	.012								
22	5.375									
23	5.625									
24	5.875									
25	6.125									

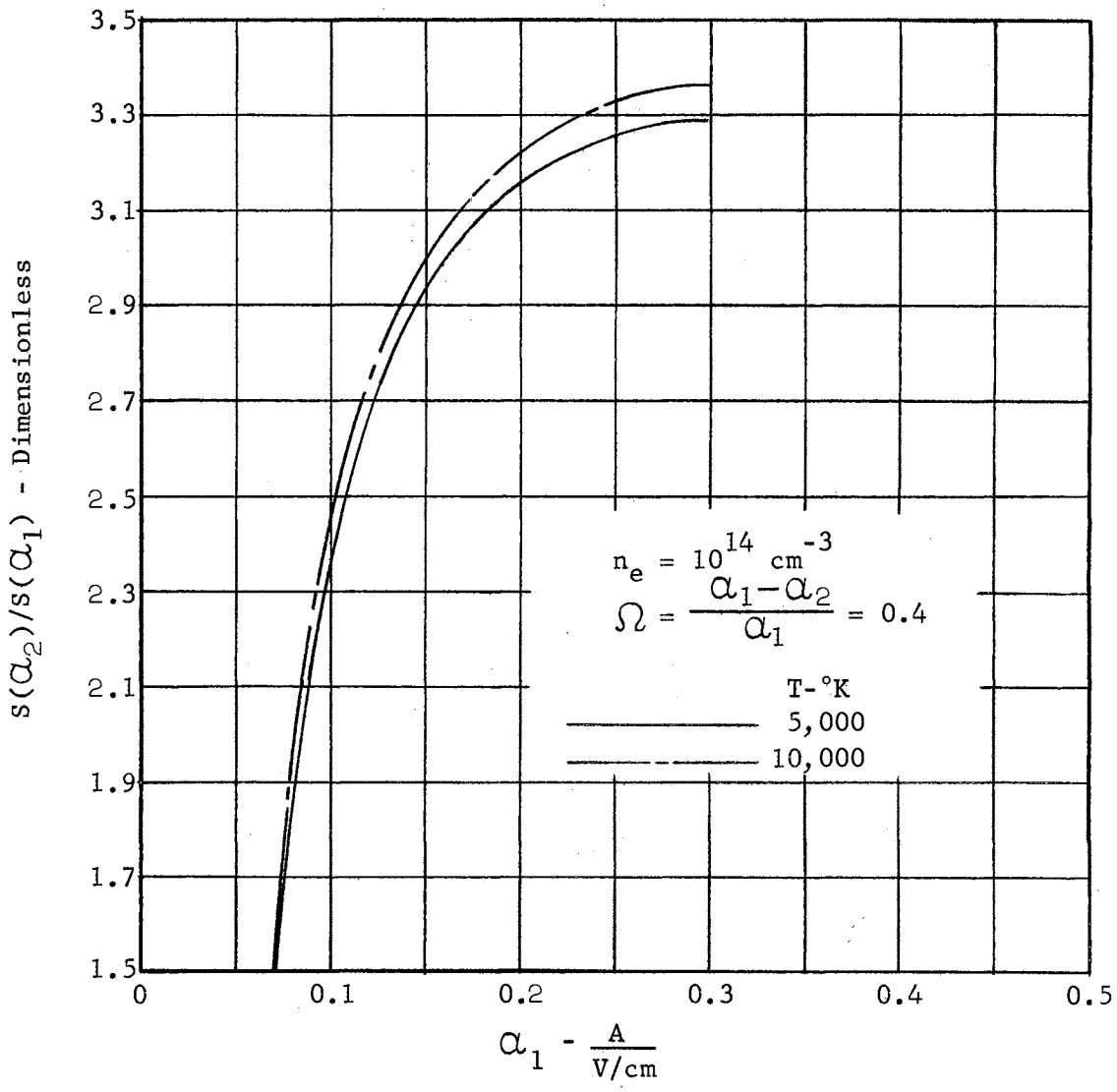

Figure 40a. Theoretical Relative Intensity Ratio for H_β (38)

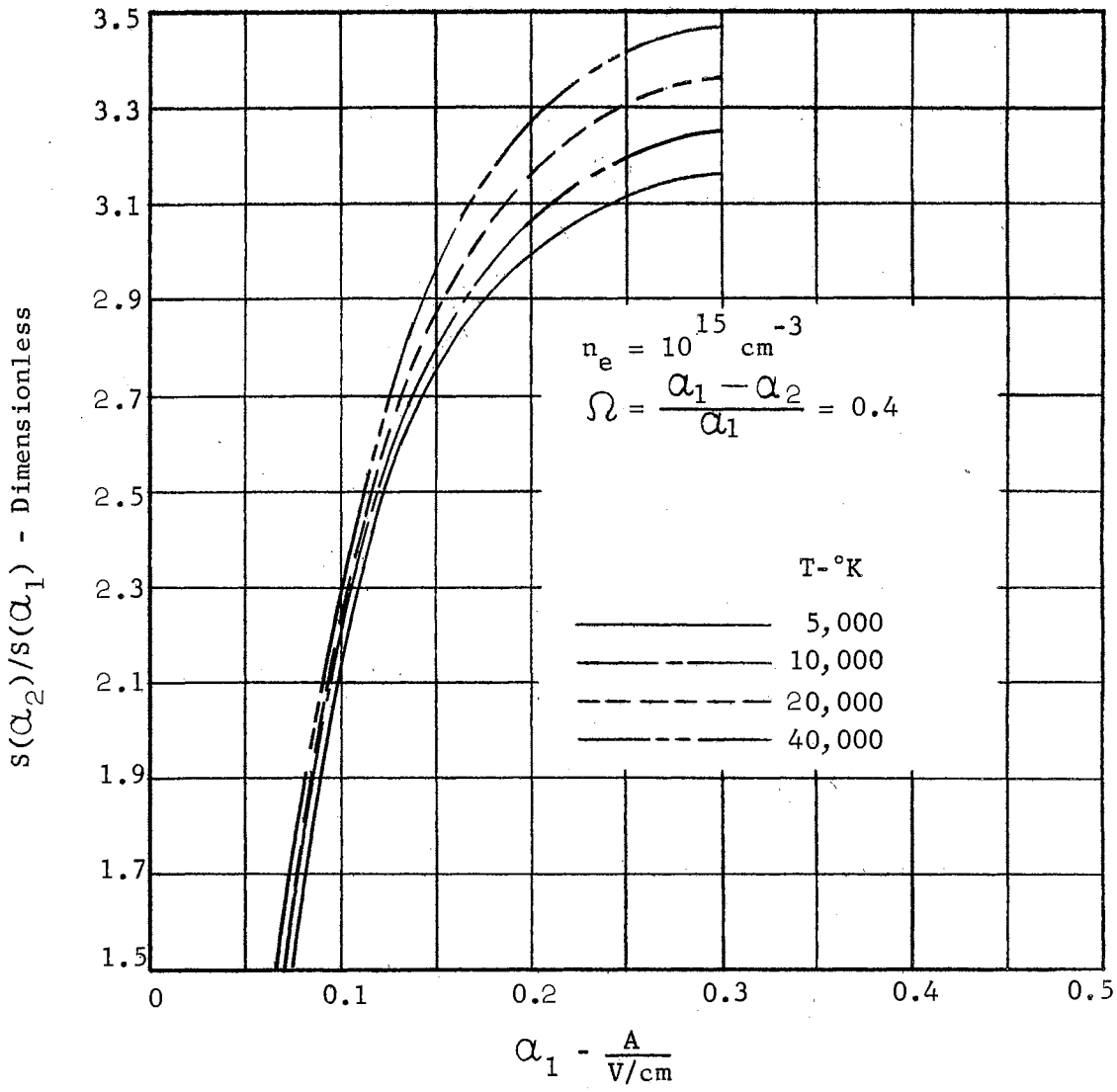

Figure 40b. Theoretical Relative Intensity Ratio for H_β (38)

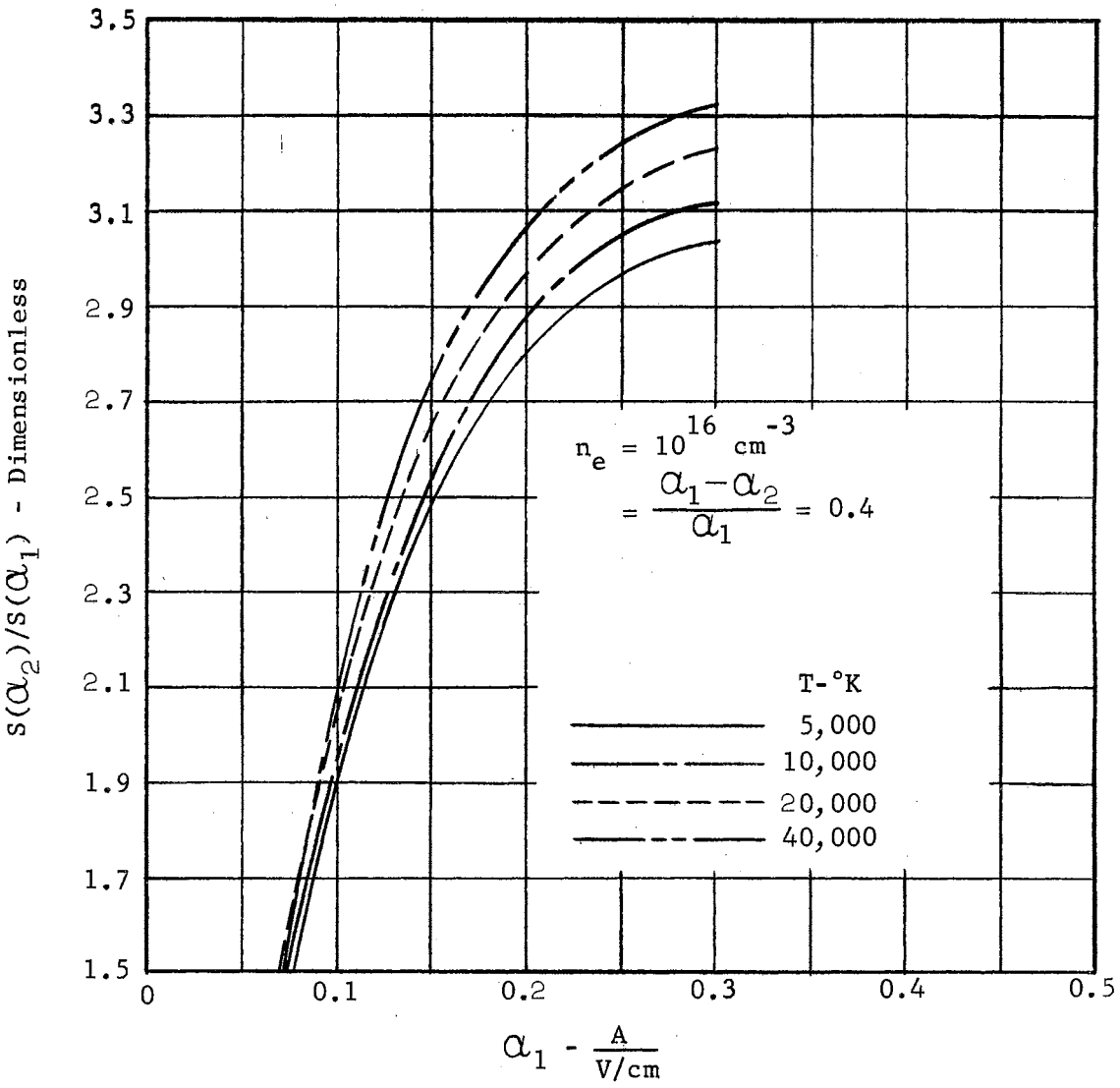

Figure 40c. Theoretical Relative Intensity Ratio for H_β (38)

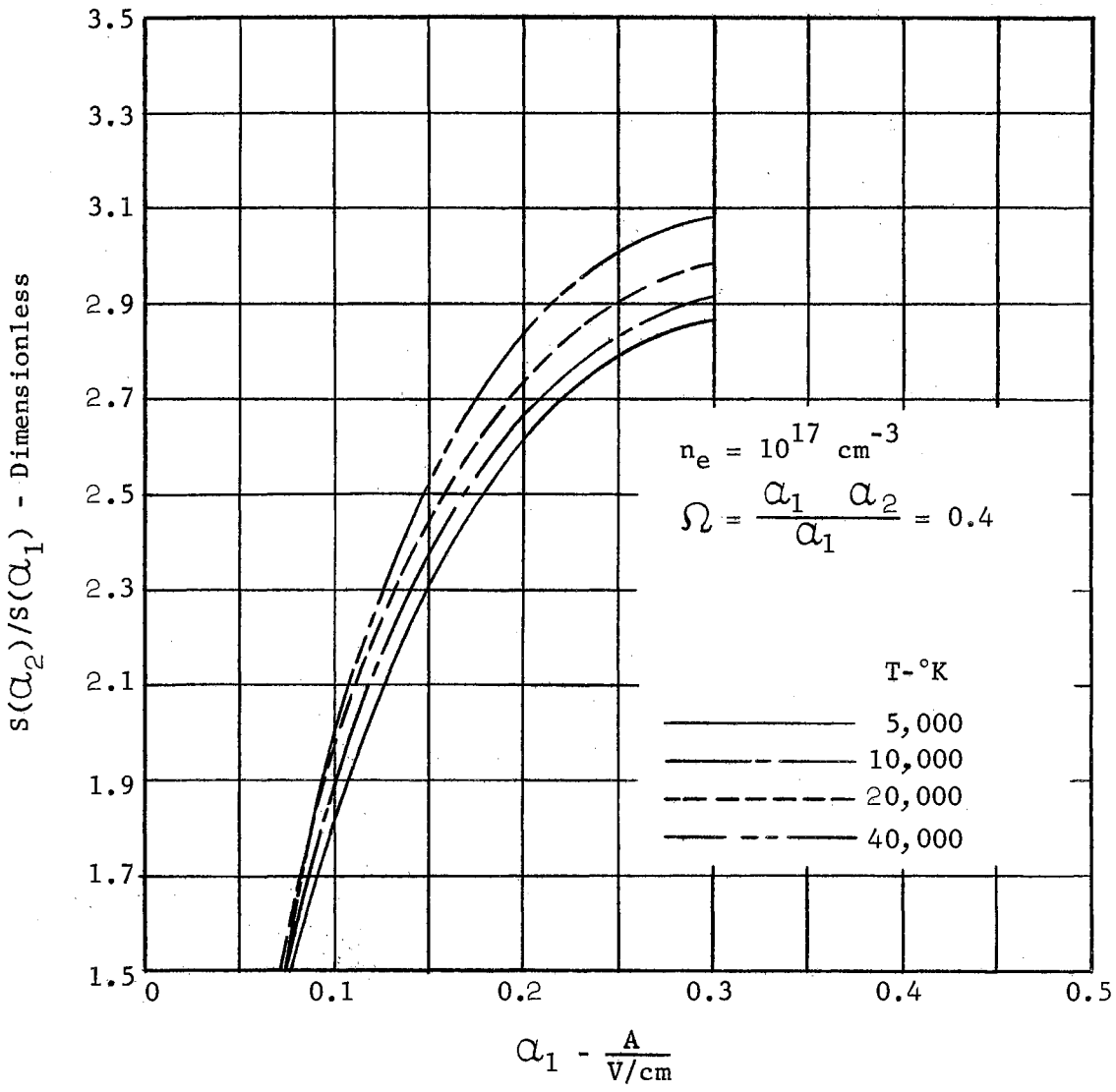

Figure 40d. Theoretical Relative Intensity Ratio for H_β (38)

APPENDIX C

PLASMA TEMPERATURE CALCULATION TABLES FOR CVRC SPECTROGRAPHIC PLATE NO. 12-19-60A

TABLE XXXIII

PLASMA TEMPERATURE CALCULATION

PLATE NO. 12-19-60A EXPOSURE NO. 2 H_γ SPECTRAL LINE

$\Omega = \frac{\Delta\lambda_1 - \Delta\lambda_2}{\Delta\lambda_1} = 0.4$ $\log_{10} P/P_o = -1.606$

$\Delta\lambda_1$ - A	$\Delta\lambda_2$ - A	$i_r(\Delta\lambda_1)$	$i_r(\Delta\lambda_2)$	$\frac{i_r(\Delta\lambda_2)}{i_r(\Delta\lambda_1)}$	$\alpha_1 = \frac{A}{V/cm}$	Eo -V/cm	T - °K
r_{plate} = 0.125 mm (r_{jet} = 0.29 mm)		Assumed: $n_e = 10^{15}$ cm^{-3};		T = 10,000°K			
1.5	0.9	1.530	2.280	1.490	0.116	12.94	9220
2.0	1.2	1.100	1.880	1.710	0.133	15.04	9460
2.5	1.5	0.810	1.530	1.890	0.158	15.82	9520
3.0	1.8	0.610	1.260	2.065	0.178	16.90	9630
					Average Temperature = 9460 °K		
					$n_e = 1.30 \cdot 10^{15}$		
r_{plate} = 0.625 mm (r_{jet} = 1.46 mm)		Assumed: $n_e = 10^{15}$ cm^{-3};		T = 10,000°K			
1.5	0.9	1.390	2.030	1.460	0.113	13.29	9280
2.0	1.2	1.000	1.680	1.680	0.135	14.81	9430
2.5	1.5	0.730	1.390	1.905	0.160	15.63	9510
3.0	1.8	0.545	1.140	2.090	0.176	17.04	9650
					Average Temperature = 9470 °K		
					$n_e = 1.30 \cdot 10^{15}$		
r_{plate} = 1.125 mm (r_{jet} = 2.63 mm)		Assumed: $n_e = 10^{15}$ cm^{-3};		T = 10,000°K			
1.5	0.9	1.200	1.760	1.468	0.114	13.16	9260
2.0	1.2	0.880	1.460	1.659	0.133	15.04	9460
2.5	1.5	0.640	1.200	1.875	0.156	16.03	9570
3.0	1.8	0.470	1.000	2.130	0.186	16.12	9570
					Average Temperature = 9460 °K		
					$n_e = 1.30 \cdot 10^{15}$		
r_{plate} = 1.625 mm (r_{jet} = 3.80 mm)		Assumed: $n_e = 10^{15}$ cm^{-3};		T = 10,000°K			
1.5	0.9	0.950	1.360	1.433	0.110	13.65	9310
2.0	1.2	0.705	1.150	1.632	0.130	15.40	9500
2.5	1.5	0.515	0.950	1.844	0.153	16.35	9580
3.0	1.8	0.384	0.800	2.350	0.215	13.95	9340
					Average Temperature = 9430 °K		
					$n_e = 1.25 \cdot 10^{15}$		
r_{plate} = 2.125 mm (r_{jet} = 4.96 mm)		Assumed: $n_e = 10^{15}$ cm^{-3};		T = 10,000°K			
1.5	0.9	0.725	1.100	1.517	0.120	12.50	9180
2.0	1.2	0.505	0.900	1.781	0.146	13.70	9320
2.5	1.5	0.355	0.725	2.040	0.175	14.30	9380
3.0	1.8	0.252	0.580	2.300	0.208	14.42	9400
					Average Temperature = 9320 °K		
					$n_e = 1.14 \cdot 10^{15}$		
r_{plate} = 2.625 mm (r_{jet} = 6.13 mm)		Assumed: $n_e = 10^{15}$ cm^{-3};		T = 10,000°K			
1.5	0.9	0.490	0.775	1.581	0.125	12.00	9120
2.0	1.2	0.340	0.620	1.822	0.150	13.35	9280
2.5	1.5	0.235	0.490	2.083	0.181	13.80	9320
3.0	1.8	0.160	0.395	2.468	0.231	13.00	9240
					Average Temperature = 9240 °K		
					$n_e = 1.04 \cdot 10^{15}$		
r_{plate} = 3.125 mm (r_{jet} = 7.30 mm)		Assumed: $n_e = 10^{15}$ cm^{-3};		T = 10,000°K			
1.5	0.9	0.288	0.530	1.840	0.153	9.80	8870
2.0	1.2	0.174	0.390	2.240	0.200	10.00	8900
2.5	1.5	0.105	0.288	2.744	0.276	9.06	8730
3.0	1.8	0.065	0.212	3.260	--	--	--
					Average Temperature = 8830 °K		
					$n_e = 0.70 \cdot 10^{15}$		
r_{plate} = 3.625 mm (r_{jet} = 8.47 mm)		Assumed: $n_e = 0.5 \cdot 10^{15}$ cm^{-3};		T = 7,500°K			
1.00	0.60	0.240	0.410	1.708	0.128	7.82	8590
1.25	0.75	0.170	0.338	1.987	0.154	8.12	8620
1.50	0.90	0.118	0.275	2.330	0.190	7.90	8600
1.75	1.05	0.079	0.225	2.850	0.258	6.78	8400
					Average Temperature = 8550 °K		
					$n_e = 0.50 \cdot 10^{15}$		

TABLE XXXIV

PLASMA TEMPERATURE CALCULATION

PLATE NO. 12-19-60A EXPOSURE NO. 3 H_γ SPECTRAL LINE

$\Omega = \frac{\Delta\lambda_1 - \Delta\lambda_2}{\Delta\lambda_1} = 0.4$ $\log_{10} P/P_o = -1.606$

$\Delta\lambda_1$ - A	$\Delta\lambda_2$ - A	$i_r(\Delta\lambda_1)$	$i_r(\Delta\lambda_2)$	$\frac{i_r(\Delta\lambda_2)}{i_r(\Delta\lambda_1)}$	$\alpha_1 = \frac{A}{V/cm}$	E_o -V/cm	T - °K
r_{plate} = 0.125 mm (r_{jet} = 0.29 mm)		Assumed: $n_e = 10^{15}$ cm^{-3}; T = 10,000°K					
1.5	0.9	1.425	2.040	1.432	0.110	13.65	9300
2.0	1.2	1.050	1.700	1.620	0.129	15.50	9510
2.5	1.5	0.790	1.425	1.805	0.149	16.79	9630
3.0	1.8	0.610	1.180	1.935	0.162	18.52	9790
					Average Temperature = 9560 °K		
					$n_e = 1.43 \cdot 10^{15}$		
r_{plate} = 0.625 mm (r_{jet} = 1.46 mm)		Assumed: $n_e = 10^{15}$ cm^{-3}; T = 10,000°K					
1.5	0.9	1.210	1.700	1.405	0.107	14.03	9350
2.0	1.2	0.905	1.440	1.590	0.125	16.00	9550
2.5	1.5	0.680	1.210	1.780	0.146	17.12	9660
3.0	1.8	0.515	1.020	1.980	0.168	17.85	9730
					Average Temperature = 9570 °K		
					$n_e = 1.43 \cdot 10^{15}$		
r_{plate} = 1.125 mm (r_{jet} = 2.63 mm)		Assumed: $n_e = 10^{15}$ cm^{-3}; T = 10,000°K					
1.5	0.9	1.020	1.420	1.394	0.106	14.15	9370
2.0	1.2	0.770	1.210	1.571	0.124	16.14	9570
2.5	1.5	0.585	1.020	1.743	0.142	17.60	9700
3.0	1.8	0.455	0.865	1.900	0.159	18.86	9820
					Average Temperature = 9620 °K		
					$n_e = 1.47 \cdot 10^{15}$		
r_{plate} = 1.625 mm (r_{jet} = 3.80 mm)		Assumed: $n_e = 10^{15}$ cm^{-3}; T = 10,000°K					
1.5	0.9	0.845	1.140	1.350	0.102	14.71	9410
2.0	1.2	0.638	1.000	1.567	0.124	16.14	9570
2.5	1.5	0.480	0.845	1.760	0.144	17.37	9680
3.0	1.8	0.356	0.715	2.010	0.172	17.45	9690
					Average Temperature = 9590 °K		
					$n_e = 1.45 \cdot 10^{15}$		
r_{plate} = 2.125 mm (r_{jet} = 4.96 mm)		Assumed: $n_e = 10^{15}$ cm^{-3}; T = 10,000°K					
1.5	0.9	0.640	0.900	1.406	0.107	14.03	9350
2.0	1.2	0.460	0.770	1.673	0.134	14.92	9430
2.5	1.5	0.333	0.640	1.920	0.161	15.53	9510
3.0	1.8	0.240	0.525	2.186	0.192	15.61	9520
					Average Temperature = 9450 °K		
					$n_e = 1.27 \cdot 10^{15}$		
r_{plate} = 2.625 mm (r_{jet} = 6.13 mm)		Assumed: $n_e = 10^{15}$ cm^{-3}; T = 10,000°K					
1.5	0.9	0.415	0.640	1.540	0.121	12.40	9180
2.0	1.2	0.285	0.520	1.824	0.151	13.25	9260
2.5	1.5	0.198	0.415	2.097	0.182	13.74	9320
3.0	1.8	0.134	0.330	2.462	0.231	13.00	9240
					Average Temperature = 9250 °K		
					$n_e = 1.04 \cdot 10^{15}$		
r_{plate} = 3.125 mm (r_{jet} = 7.30 mm)		Assumed: $n_e = 0.5 \cdot 10^{15}$ cm^{-3}; T = 7,500°K					
1.0	0.60	0.360	0.535	1.485	0.109	9.18	8790
1.4	0.84	0.230	0.425	1.846	0.142	9.86	8870
1.8	1.08	0.142	0.330	2.328	0.190	9.48	8820
2.2	1.32	0.083	0.252	3.040	0.308	7.14	8500
					Average Temperature = 8750 °K		
					$n_e = 0.66 \cdot 10^{15}$		
r_{plate} = 3.625 mm (r_{jet} = 8.47 mm)		Assumed: $n_e = 0.5 \cdot 10^{15}$ cm^{-3}; T = 7,500°K					
0.9	0.54	0.200	0.330	1.650	0.123	7.32	8500
1.0	0.60	0.172	0.305	1.774	0.133	7.52	8520
1.25	0.75	0.114	0.250	2.195	0.174	7.18	8480
1.50	0.90	0.072	0.200	2.760	0.247	6.08	8300
					Average Temperature = 8450 °K		
					$n_e = 0.45 \cdot 10^{15}$		

TABLE XXXV

PLASMA TEMPERATURE CALCULATION

PLATE NO. 12-19-60A EXPOSURE NO. 4 H_γ SPECTRAL LINE

$\Omega = \frac{\lambda\lambda_1 - \lambda\lambda_2}{\lambda\lambda_1} = 0.4$ $\log_{10} P/P_o = -1.606$

$\Delta\lambda_1$ - A	$\Delta\lambda_2$ - A	$i_r(\Delta\lambda_1)$	$i_r(\Delta\lambda_2)$	$\frac{i_r(\Delta\lambda_2)}{i_r(\Delta\lambda_1)}$	$\alpha_1 = \frac{A}{V/cm}$	E_o -V/cm	T - °K
r_{plate} = 0.125 mm (r_{jet} = 0.29 mm)		Assumed: $n_e = 10^{15}$ cm^{-3}; T = 10,000°K					
1.5	0.9	1.910	2.500	1.310	.097	15.46	9510
2.0	1.2	1.420	2.320	1.635	.130	15.40	9500
2.5	1.5	1.080	1.910	1.770	.145	17.25	9730
3.0	1.8	0.820	1.600	1.952	.165	18.20	9820
					Average Temperature = 9640 °K		
					$n_e = 1.51 \cdot 10^{15}$		
r_{plate} = 0.625 mm (r_{jet} = 1.46 mm)		Assumed: $n_e = 10^{15}$ cm^{-3}; T = 10,000°K					
1.5	0.9	1.720	2.500	1.455	.112	13.40	9280
2.0	1.2	1.270	2.070	1.630	.130	15.40	9500
2.5	1.5	0.960	1.720	1.793	.147	17.00	9690
3.0	1.8	0.720	1.430	1.986	.170	17.65	9770
					Average Temperature = 9560 °K		
					$n_e = 1.43 \cdot 10^{15}$		
r_{plate} = 1.125 mm (r_{jet} = 2.63 mm)		Assumed: $n_e = 10^{15}$ cm^{-3}; T = 10,000°K					
1.5	0.9	1.350	2.030	1.505	.117	12.83	9210
2.0	1.2	0.990	1.660	1.677	.135	14.81	9420
2.5	1.5	0.735	1.350	1.836	.152	16.45	9610
3.0	1.8	0.555	1.120	2.018	.173	17.35	9720
					Average Temperature = 9490 °K		
					$n_e = 1.34 \cdot 10^{15}$		
r_{plate} = 1.625 mm (r_{jet} = 3.80 mm)		Assumed: $n_e = 10^{15}$ cm^{-3}; T = 10,000°K					
1.5	0.9	1.200	1.620	1.350	.103	14.55	9400
2.0	1.2	0.780	1.350	1.730	.140	14.30	9380
2.5	1.5	0.545	1.200	2.200	.195	12.83	9210
3.0	1.8	0.394	0.900	2.280	.206	14.55	9400
					Average Temperature = 9350 °K		
					$n_e = 1.18 \cdot 10^{15}$		
r_{plate} = 2.125 mm (r_{jet} = 4.96 mm)		Assumed: $n_e = 10^{15}$ cm^{-3}; T = 10,000°K					
1.5	0.9	0.770	1.220	1.585	.125	12.00	9120
2.0	1.2	0.530	0.960	1.810	.149	13.43	9280
2.5	1.5	0.370	0.770	2.080	.181	13.81	9320
3.0	1.8	0.265	0.625	2.355	.215	13.95	9340
					Average Temperature = 9260 °K		
					$n_e = 1.07 \cdot 10^{15}$		
r_{plate} = 2.625 mm (r_{jet} = 6.13 mm)		Assumed: $n_e = 10^{15}$ cm^{-3}; T = 10,000°K					
1.5	0.9	0.445	0.730	1.640	.131	11.45	9090
2.0	1.2	0.296	0.572	1.932	.162	12.35	9190
2.5	1.5	0.200	0.445	2.223	.197	12.70	9200
3 0	1.8	0.138	0.340	2.465	.231	13.00	9250
					Average Temperature = 9180 °K		
					$n_e = 0.98 \cdot 10^{15}$		
r_{plate} = 3.125 mm (r_{jet} = 7.30 mm)		Assumed: $n_e = 10^{15}$ cm^{-3}; T = 10,000°K					
1.5	0.9	0.213	0.385	1.807	.150	10.00	8860
2.0	1.2	0.131	0.285	2.177	.191	10.48	8900
2.5	1.5	0.082	0.213	2.600	.252	9.93	8850
3.0	1.8	0.052	0.159	3.060	.356	8.42	8650
					Average Temperature = 8820 °K		
					$n_e = 0.70 \cdot 10^{15}$		
r_{plate} = 3.625 mm (r_{jet} = 8.47 mm)		Assumed: $n_e = 0.5 \cdot 10^{15}$ cm^{-3}; T = 7,500°K					
1.00	0.60	0.171	0.300	1.755	.130	7.70	8550
1.25	0.75	0.120	0.245	2.040	.160	7.81	8560
1.50	0.90	0.810	0.198	2.445	.204	7.35	8500
1.75	1.05	0.540	0.160	2.962	.285	6.14	8300
					Average Temperature = 8480 °K		
					$n_e = 0.45 \cdot 10^{15}$		

TABLE XXXVI

PLASMA TEMPERATURE CALCULATION

PLATE NO. 12-19-60A EXPOSURE NO. 4 H_β SPECTRAL LINE

$\Omega = \frac{\Delta\lambda_1 - \Delta\lambda_2}{\Delta\lambda_1} = 0.4$ $\log_{10} P/P_o = -1.606$

$\Delta\lambda_1$ - A	$\Delta\lambda_2$ - A	$i_r(\Delta\lambda_1)$	$i_r(\Delta\lambda_2)$	$\frac{i_r(\Delta\lambda_2)}{i_r(\Delta\lambda_1)}$	$\alpha_1 = \frac{A}{V/cm}$	E_o -V/cm	T - °K
r_{plate} = 0.125 mm (r_{jet} = 0.29 mm)		Assumed: $n_e = 10^{15}$ cm^{-3};		T = 10,000°K			
1.0	0.6	1.240	1.800	1.452	0.070	14.29	9400
1.5	0.9	0.750	1.370	1.825	0.084	17.85	9730
2.0	1.2	0.460	1.020	2.218	0.103	19.40	9880
2.5	1.5	0.305	0.750	2.455	0.116	21.56	10700
					Average Temperature = 9930 °K		
					$n_e = 1.87 \cdot 10^{15}$		
r_{plate} = 0.625 mm (r_{jet} = 1.46 mm)		Assumed: $n_e = 10^{15}$ cm^{-3};		T = 10,000°K			
1.0	0.6	1.170	1.680	1.437	0.070	14.29	9400
1.5	0.9	0.710	1.270	1.790	0.082	18.30	9780
2.0	1.2	0.435	0.950	2.180	0.102	19.60	9890
2.5	1.5	0.280	0.710	2.535	0.123	20.32	9960
					Average Temperature = 9760 °K		
					$n_e = 1.66 \cdot 10^{15}$		
r_{plate} = 1.125 mm (r_{jet} = 2.63 mm)		Assumed: $n_e = 10^{15}$ cm^{-3};		T = 10,000°K			
1.0	0.6	1.070	1.530	1.435	0.070	14.29	9400
1.5	0.9	0.635	1.170	1.843	0.084	17.85	9730
2.0	1.2	0.390	0.860	2.203	0.103	19.40	9880
2.5	1.5	0.245	0.635	2.590	0.127	19.70	9890
					Average Temperature = 9720 °K		
					$n_e = 1.64 \cdot 10^{15}$		
r_{plate} = 1.625 mm (r_{jet} = 3.80 mm)		Assumed: $n_e = 10^{15}$ cm^{-3};		T = 10,000°K			
1.0	0.6	0.940	0.137	1.456	0.070	14.29	9400
1.5	0.9	0.540	0.104	1.925	0.087	17.25	9680
2.0	1.2	0.320	0.750	2.340	0.109	18.35	9770
2.5	1.5	0.195	0.540	2.770	0.146	17.14	9690
					Average Temperature = 9630 °K		
					$n_e = 1.50 \cdot 10^{15}$		
r_{plate} = 2.125 mm (r_{jet} = 4.96 mm)		Assumed: $n_e = 10^{15}$ cm^{-3};		T = 10,000°K			
1.0	0.6	0.640	1.120	1.750	0.081	12.35	9170
1.5	0.9	0.330	0.740	2.240	0.103	14.56	9410
2.0	1.2	0.180	0.490	2.720	0.140	14.29	9380
2.5	1.5	0.107	0.330	3.085	0.206	12.15	9150
					Average Temperature = 9270 °K		
					$n_e = 1.07 \cdot 10^{15}$		
r_{plate} = 2.625 mm (r_{jet} = 6.13 mm)		Assumed: $n_e = 10^{15}$ cm^{-3};		T = 10,000°K			
0.8	0.48	0.530	0.880	1.660	0.076	10.54	8960
1.0	0.60	0.380	0.740	1.946	0.090	11.10	9010
1.2	0.72	0.265	0.600	2.262	0.105	11.44	9050
1.4	0.84	0.190	0.490	2.580	0.126	11.12	9020
					Average Temperature = 9010 °K		
					$n_e = 0.81 \cdot 10^{15}$		
r_{plate} = 3.125 mm (r_{jet} = 7.30 mm)		Assumed: $n_e = 0.5 \cdot 10^{15}$ cm^{-3};		T = 10,000°K			
0.8	0.48	0.300	0.590	1.965	0.087	9.22	8790
1.0	0.60	0.196	0.460	2.343	0.104	9.62	8830
1.2	0.72	0.126	0.360	2.858	0.149	8.06	8620
1.4	0.84	0.082	0.274	3.340	--	--	--
					Average Temperature = 8750 °K		
					$n_e = 0.65 \cdot 10^{15}$		
r_{plate} = 3.625 mm (r_{jet} = 8.47 mm)		Assumed: $n_e = 0.5 \cdot 10^{15}$ cm^{-3};		T = 7,500°K			
0.6	0.36	0.243	0.422	1.736	0.079	7.60	8550
0.8	0.48	0.148	0.322	2.177	0.095	8.43	8670
1.0	0.60	0.086	0.243	2.826	0.144	6.94	8450
1.2	0.72	0.050	0.183	3.660	--	--	--
					Average Temperature = 8560 °K		
					$n_e = 0.50 \cdot 10^{15}$		

APPENDIX D

IBM 650 FLOATING POINT MATRIX INVERSION PROGRAM

MA INV III

(5.2.011)

1. General: This program can invert a square matrix n x n, where $n(n+1) \leq 1999$. The matrix can be augmented on the right by m column vectors and the simultaneous equation solutions obtained where $(n+1) \cdot (n+m) \leq 1999$. The calculation is made with floating decimal numbers and the output elements are in floating decimal. The solution vectors will be on the left.

The entire drum, except 0000, can be used for the storage of matrix elements. Immediate access storage is used for the load routine, the inversion program, and the output routine. The time required is approximately . $.02n^3$ seconds.

2. Numbers: The numbers must be in 650 floating point normalized form or in the following form: 00xxxxxxxx with decimal the same for all elements.

3. Input: Cards do not have to be in a particular order. Program has zero routine so that only non-zero elements need be entered. The matrix is punched row wise, one element per card in the following format:

Word 1: Problem Number

Word 2: Matrix Element

Word 3: 00 00ii 0jjj where i represents the row of the element and j represents the column

Word 4-8: Zeros

The matrix element cards are non-load cards to be read in by the program. A control card which is also non-load must precede the input element deck. It is punched as follows:

Word 1: Problem Number

Word 2: x 000000 $\begin{matrix}8888\\9999\end{matrix}$ (control word)

Word 3: 00 $\underset{n}{xx}$ 000 $\underset{n+m}{xxx}$ where n is the number of rows in the matrix and n+m is the number of columns.

The control word, x 00000 $\begin{matrix}8888\\9999\end{matrix}$ is determined as follows:

1st Position:	8: print output on 407	9: don't print
2nd Position:	8: punch output from 533	9: don't punch
3rd Position:	8: count input cards and check for the correct number	9: count but don't check for the correct number
4th Position:	8: machine will float data	9: will not float.
10th Position:	Used only when 4th position is punched 8. The digit represents the number of integer places in the element card field.	

4. Output: Word 1 is the problem number, word 2 is the element in floating decimal, and word 3 is 00 00ii 0jjj.

Console Settings:

Console 70 1951 9999+

Programmed - Stop

Half Cycle - Run

Address Sel. - xxxx

Control - Run

Display - Program Register

Overflow - Stop

Error - Stop

Card Input -

Two load routines (12 cards)

Control Card

Matrix Elements

Inversion and Output (20 cards)

Program Description -

Uses index registers, floating decimal device, core and standard 8-10 control panel.

If no identification check is wanted, set console - 00 0000 9005 and Programmed-Run

Program Stops and Required Action -

D-Address	I-Address	
0001	8000	Element card problem number is not the same as that on the control card. If only control card is in error, transfer control to 9005.
0002	8000	Wrong number of elements entered. If only control card is in error, transfer control to 9000.
9999	9999	Job completed.

Division by zero will cause an automatic overflow stop. This can happen only when a_{11} or one of the elements which takes its place

during the reduction process is zero.

Machine exponent overflows or underflows will also stop the machine.

APPENDIX E

SAMPLE CALCULATIONS FOR OSU PLASMA FACILITY DATA

Sample calculations are given below for the recorded data of Table IV.

1. Power Input, P_{in}

$P_{in} = 3.413EI$

P_{in} = power input, Btu/hr

E = arc voltage, volts

I = arc current, amperes

Run No. 1 $P_{in} = (3.413)(36)(400) = 49,200$ Btu/hr

Run No. 2 $P_{in} = (3.413)(35)(500) = 59,800$ Btu/hr

Run No. 3 $P_{in} = (3.413)(33)(420) = 47,300$ Btu/hr

2. Cooling Water Flow Rates, $\dot{m}$ - lb_m/hr

The cooling water flow rates are determined from Figure 26.

Rear Electrode

Run No. 1 Manometer deflection = 6.6 in. $\dot{m} = 142$ lb_m/hr

Run No. 2 Manometer deflection = 7.0 in. $\dot{m} = 146$ lb_m/hr

Run No. 3 Manometer deflection = 7.0 in. $\dot{m} = 146$ lb_m/hr

Main Chamber

Run No. 1 Manometer deflection = 2.3 in. $\dot{m} = 80$ lb_m/hr

Run No. 2 Manometer deflection = 2.5 in. $\dot{m} = 84$ lb_m/hr

Run No. 3 Manometer deflection = 2.0 in. $\dot{m} = 75$ lb_m/hr

Converging Nozzle

Run No. 1 Manometer deflection = 17.0 in. $\dot{m}$ = 225 lb_m/hr

Run No. 2 Manometer deflection = 17.0 in. $\dot{m}$ = 225 lb_m/hr

Run No. 3 Manometer deflection = 17.0 in. m = 225 lb_m/hr

3. Power Loss to Cooling Water, P_L

$$P_L = \sum m\, c_p\, \Delta T$$

P_L = total power loss to cooling water, Btu/hr

$\dot{m}$ = cooling water flow rate for each circuit, lb_m/hr

c_p = specific heat for cooling water, 1.0 Btu/lb_m F

ΔT= cooling water temperature rise for each circuit, F

Rear Electrode

Run No. 1 $\dot{m}\, c_p \Delta T$ = (142)(1.0)(130-58) = 10,220 Btu/hr

Run No. 2 $\dot{m}\, c_p \Delta T$ = (146)(1.0)(147-58) = 13,000 Btu/hr

Run No. 3 $\dot{m}\, c_p \Delta T$ = (146)(1.0)(130-58) = 10,500 Btu/hr

Main Chamber

Run No. 1 $\dot{m}\, c_p \Delta T$ = (80)(1.0)(64-58) = 480 Btu/hr

Run No. 2 $\dot{m}\, c_p \Delta T$ = (84)(1.0)(64-58) = 504 Btu/hr

Run No. 3 $\dot{m}\, c_p \Delta T$ = (75)(1.0)(64-58) = 450 Btu/hr

Converging Nozzle

Run No. 1 $\dot{m}\, c_p \Delta T$ = (225)(1.0)(126-58) = 15,300 Btu/hr

Run No. 2 $\dot{m}\, c_p \Delta T$ = (225)(1.0)(144-58) = 19,400 Btu/hr

Run No. 3 $\dot{m}\, c_p \Delta T$ = (225)(1.0)(114-58) = 12,600 Btu/hr

Total Power Loss

Run No. 1 P_L = 10,220 + 480 + 15,300 = 26,000 Btu/hr

Run No. 2 P_L = 13,000 + 504 + 19,400 = 32,904 Btu/hr

Run No. 3 P_L = 10,500 + 450 + 12,600 = 23,550 Btu/hr

4. Net Power Input to Argon, P_{gas}

$$P_{gas} = P_{in} - P_L$$

Run No. 1 $P_{gas} = 49,200 - 26,000 = 23,200$ Btu/hr

Run No. 2 $P_{gas} = 59,800 - 32,904 = 26,896$ Btu/hr

Run No. 3 $P_{gas} = 47,300 - 23,550 = 23,750$ Btu/hr

5. Argon Flowmeter Upstream Pressure, P_A - psia

P_A = gage pressure + atmospheric pressure

atmospheric pressure = 29.14 in. Hg. $\times \frac{0.491 \text{ psi}}{\text{in. Hg.}} = 14.3$ psia.

$P_A = 18.0 + 14.3 = 32.3$ psia (each run)

6. Argon Flowmeter Pressure Differential, ΔP_A

Run No. 1 $\Delta P_A = 30.0 - 9.9 = 20.1$ in. H_2O

Run No. 2 $\Delta P_A = 30.0 - 9.9 = 20.1$ in. H_2O

Run No. 3 $\Delta P_A = 30.0 - 9.2 = 20.8$ in. H_2O

7. Argon Volumetric Flow Rate, $Q_{A,STP}$

$Q_{A,STP}$ - Read from Figure 24 for calculated values of ΔP_A and P_A, SCFH

Run No. 1 $Q_{A,STP} = 84$ SCFH

Run No. 2 $Q_{A,STP} = 84$ SCFH

Run No. 3 $Q_{A,STP} = 85$ SCFH

8. Argon Mass Flow Rate, $\dot{m}_A$

$$\dot{m} = [\rho Q]_{A,STP}$$

$\dot{m}_A$ = argon mass flow rate, lb_m/hr

$\rho_{A,STP}$ = density of argon at 14.7 psia and 70°F = 0.1034 lb_m/ft^3

$Q_{A,STP}$ = argon volumetric flow rate based on 14.7 psia and 70°F, SCFH

Run No. 1 $\dot{m}_A = (0.1034)(84) = 8.68\ lb_m/hr$

Run No. 2 $\dot{m}_A = (0.1034)(84) = 8.68\ lb_m/hr$

Run No. 3 $\dot{m}_A = (0.1034)(85) = 8.78\ lb_m/hr$

9. Hydrogen Flowmeter Upstream Pressure, P_H - psia

P_H = gage pressure + atmospheric pressure

Run No. 1 $P_H = 18.2 + 14.3 = 32.5$ psia

Run No. 2 $P_H = 18.2 + 14.3 = 32.5$ psia

Run No. 3 $P_H = 18.0 + 14.3 = 32.3$ psia

10. Hydrogen Volumetric Flow Rate, $Q_{H,STP}$

$Q_{H,STP}$ - Read from Figure 25 for recorded values of flowmeter reading and the calculated flowmeter upstream pressure, SCFH

Run No. 1 $Q_{H,STP} = 2.21$ SCFH

Run No. 2 $Q_{H,STP} = 2.16$ SCFH

Run No. 3 $Q_{H,STP} = 0$

11. Hydrogen Mass Flow Rate, $\dot{m}_H$

$\dot{m}_H = [\rho Q]_{H,STP}$

$\dot{m}_H$ = hydrogen mass flow rate, lb_m/hr

$\rho_{H,STP}$ = density of hydrogen at 14.7 psia and 70°F = $0.00518\ lb_m/ft^3$

$Q_{H,STP}$ = hydrogen volumetric flow rate based on 14.7 psia and 70°F, SCFH

Run No. 1 $\dot{m}_H = (0.00518)(2.21) = 0.01145\ lb_m/hr$

Run No. 2 $\dot{m}_H = (0.00518)(2.16) = 0.0112\ lb_m/hr$

Run No. 3 $\dot{m}_H = 0$

12. Ratio of Hydrogen to Argon by Volume, H/A

$$H/A = \frac{Q_{H,STP}}{Q_{A,STP}}$$

Run No. 1 $H/A = \frac{2.21}{84} = 0.0263$

Run No. 1 $H/A = \frac{2.16}{84} = 0.0257$

Run No. 3 $H/A = 0$

13. Test Section Pressure, P_t - psia

P_t = atmospheric pressure - vacuum pressure

$P_t = (29.14\text{-}28.50)$ in. Hg. $(0.491) \frac{\text{psia}}{\text{in. Hg.}} = 0.314$ psia (each run)

$P_t/P_o = \frac{0.314}{14.7} = 0.0214$

$\log_{10} P_t/P_o = -1.67$

14. Average Argon Temperature at Nozzle Exit, T_{ave}

T_{ave} is determined from Reference 39 by calculating the enthalpy level, $\frac{h}{RT_o}$, per lb_m of argon at the nozzle exit.

$$\frac{h}{RT_o} = \frac{h_1}{RT_o} + \frac{\triangle h}{RT_o}$$

h = enthalpy at nozzle exit, Btu/lb_m

h_1 = enthalpy at inlet to plasma generator, Btu/lb_m

$\triangle h$ = energy added per lb_m of argon, Btu/lb_m

R = gas constant for argon = 0.0496 $Btu/lb_m{}^\circ R$

$T_o = 492^\circ R$

$RT_o = 24.4$ Btu/lb_m

For each run the argon temperature at the inlet to the plasma generator was 76° F. From Reference 39 for $T_1 = 536^\circ R$.

$$\frac{h_1}{RT_o} = 3$$

$$\triangle h = \frac{P_{gas}}{\dot{m}_A}$$

Run No. 1 $\triangle h = 23,200/8.68 = 2670$ Btu/lb_m

Run No. 2 $\triangle h = 26,896/8.68 = 3100$ Btu/lb_m

Run No. 3 $\triangle h = 23,750/8.78 = 2700$ Btu/lb_m

Run No. 1 $\triangle h/RT_o = 2670/24.4 = 109$

Run No. 2 $\triangle h/RT_o = 3100/24.4 = 127$

Run No. 3 $\triangle h/RT_o = 2700/24.4 = 111$

Run No. 1 $h/RT_o = 3 + 109 = 112$

Run No. 2 $h/RT_o = 3 + 127 = 130$

Run No. 3 $h/RT_o = 3 + 111 = 114$

From Reference 39 for h/RT_o values and for $\log_{10} P_t/P_o = -1.67$

Run No. 1 $T_{ave} = 8950°K$

Run No. 2 $T_{ave} = 9250°K$

Run No. 3 $T_{ave} = 9000°K$

VITA

Donald Robert Haworth

Candidate for the Degree of

Doctor of Philosophy

Thesis: DEVELOPMENT OF A PLASMA FACILITY AND SPECTROGRAPHIC DETERMINATION OF PLASMA TEMPERATURES

Major Field: Mechanical Engineering

Biographical:

Personal Data: Born in Steubenville, Ohio, January 26, 1928, the son of Lowell and Mary Etta Haworth.

Education: Attended the College of the Academy of the New Church, Bryn Athyn, Pennsylvania; received the Bachelor of Science degree from Purdue University, Lafayette, Indiana, with a major in Mechanical Engineering, in January, 1952; received the Master of Science degree from the Purdue University, with a major in Mechanical Engineering, in June, 1955; completed requirements for the Doctor of Philosophy degree in May, 1961.

Professional experience: Design Engineer with the Bell Helicopter Corporation, Fort Worth, Texas, from September, 1952 to September, 1954; Instructor at Purdue University from September, 1954 to June, 1956; Lead Engineer in Theoretical Propulsion Group at Chance Vought Corporation, Dallas, Texas, from June, 1956 to September, 1958; Assistant Professor in Mechanical Engineering at Oklahoma State University from September, 1958 to May, 1961.

Professional organizations: The author is a member of the following honorary, educational and professional organizations: Pi Tau Sigma, Tau Beta Pi, American Society of Mechanical Engineers and Institute of the Aerospace Sciences.